



**HAL**  
open science

# Noncovalent functionalization of carbon nanotubes with new conjugated aromatic ligands for selective detection of water pollutants

Aram Nasiri

► **To cite this version:**

Aram Nasiri. Noncovalent functionalization of carbon nanotubes with new conjugated aromatic ligands for selective detection of water pollutants. Materials. Institut Polytechnique de Paris, 2024. English. NNT: 2024IPPAX097. tel-04956870

**HAL Id: tel-04956870**

**<https://theses.hal.science/tel-04956870v1>**

Submitted on 19 Feb 2025

**HAL** is a multi-disciplinary open access archive for the deposit and dissemination of scientific research documents, whether they are published or not. The documents may come from teaching and research institutions in France or abroad, or from public or private research centers.

L'archive ouverte pluridisciplinaire **HAL**, est destinée au dépôt et à la diffusion de documents scientifiques de niveau recherche, publiés ou non, émanant des établissements d'enseignement et de recherche français ou étrangers, des laboratoires publics ou privés.

# Noncovalent functionalization of carbon nanotubes with conjugated molecules for selective detection of water pollutants

Thèse de doctorat de l'Institut Polytechnique de Paris  
Préparée à l'École Polytechnique  
École doctorale n°626 École doctorale de l'Institut Polytechnique de  
Paris (ED IP Paris)

Spécialité de doctorat : Chimie  
Thèse présentée et soutenue à Palaiseau, le 25/06/2024, par

**Aram NASIRI**

## Composition du Jury :

**Paolo Bondavalli**

*Ingénieur de recherche, Thales TRT*

**Président du Jury**

**Vincent Derycke**

*Directeur de recherche, CEA*

**Rapporteur**

**Benoit Piro**

*Professeur, Université Paris Cité*

**Rapporteur**

**Camilla Noé**

*Assistante professeure, Politecnico di Torino*

**Examinatrice**

**Cédric Tard**

*Directeur de recherche, École Polytechnique*

**Invité**

**Yvan Bonnassieux**

*Professeur, École Polytechnique*

**Directeur de thèse**



**Abstract:** Climate change accelerates water quality decline, necessitating innovative solutions. Nanotechnology has significantly addressed global issues, notably improving access to clean drinking water. Nanotech-driven sensors offer remote water quality analysis, crucial for decision-making in crisis management. These advancements aim to alleviate the ongoing drinking water scarcity worldwide, with potential long-term benefits.

The first part of this work explores carbon nanotubes (CNTs) as 2D nanomaterials for enhancing the reliability of resistive devices. It emphasizes the importance of understanding and treating CNTs in thin film to ensure electronic and chemical reliability. A new purification process is introduced to eliminate unwanted amorphous matter, enhancing the effectiveness of wet processes and solvent-based depositions of CNTs. This approach aims to restore trust in these cost-effective and scalable methods, addressing previous concerns about poor quality and high amorphous content.

In the second experimental chapter, CNTs underwent extensive studies for their parallel electronic and chemical capability to create nanohybrids with conjugated molecules, referred to as noncovalent  $\pi$ - $\pi$  functionalization. Different methods of noncovalent functionalization were thoroughly compared, and finally incubation method was chosen both for its more promising results in terms of functionalization and its perfect compatibility with the thin-film treatment method developed in the first part.

Thanks to a process development mindset, the resulting nanohybrids were accessible in thin-films and proven for their highly electronic and chemical performances. Finally, these prepared thin films were integrated into different resistive device concepts, and were characterized against different analytes in water. The results of the devices are preliminary but promising in the domain of water quality analysis to inspire more studies on the development of sensors.

## Résumé français

Le changement climatique aggrave la détérioration de la qualité de l'eau, ce qui nécessite des solutions innovantes. Les nanotechnologies permettent de proposer des solutions aux problèmes sociétaux actuels, notamment en améliorant potentiellement l'accès à une eau potable et propre. Ces capteurs pilotés offrent une analyse à distance de la qualité de l'eau, ce qui est crucial pour la prise de décision et la gestion de crise. Ces avancées visent à soulager la pénurie d'eau potable mondiale actuelle, avec des avantages potentiels à long terme.

Dans le premier chapitre de ce travail, nous avons discuté l'état de l'art concernant les nanotubes de carbone (CNTs), leur fonctionnalisation, et les capteurs basés sur les CNTs. Les résultats de cette étude nous ont permis de faire progresser le projet sous différents aspects, notamment en nous aidant à comprendre que :

- Les propriétés électroniques et chimiques des CNT peuvent être exploitées pour créer des dispositifs électroniques avec des fonctionnalités simples. Elles sont intéressantes dans le développement de capteurs, en raison de l'interaction chimique avec leur environnement.
- La fonctionnalisation non-covalente des CNT est un moyen de contrôler leurs interactions, de les canaliser vers des interactions désirées spécifiques, et de bénéficier de leurs propriétés électroniques.
- Les capteurs jouent un rôle important dans nos vies, et ils sont nécessaires pour lutter contre les changements écologiques, notamment la détérioration de la qualité de l'eau potable.

Des capteurs basés sur les CNT ont été développés par différents groupes pour aborder la qualité de l'eau, et notamment les capteurs chimio résistifs qui ont un mécanisme simple et une polyvalence intéressante. Cependant, sur la base de l'étude de l'état de l'art, les limitations suivantes pourraient être énumérées :

- Une des limitations importantes des CNT est leur tendance à former des faisceaux. L'hybridation  $sp^2$  des CNT (résultant de la présence d'orbitales  $\pi$  abondantes) est



responsable de l'interaction avec les espèces de leur environnement. Principalement, ces interactions fortes aboutissent à la création d'agrégats de CNT, ce qui diminue leurs propriétés particulières.

- D'autre part, malgré de nombreuses études sur l'intérêt et les applications de la fonctionnalisation non-covalente des CNT, il existe des limitations en termes de compatibilité du processus avec des méthodes de dépôt simples, contournant les impacts de la dispersion assistée par sonication des CNT. Il y a également des perspectives de recherche sur le type de molécules conjuguées et leurs interactions spécifiques avec les CNT.
- Enfin, le développement d'un dispositif de détection basé sur les CNT doit être adapté aux méthodes de dépôt et de fonctionnalisation utilisés. Il existe un vaste domaine de recherche sur les dispositifs de fabrication spécifiques à la détection des analytes dans l'eau.

Le deuxième chapitre explore l'aspect important de la préparation des CNT avant de débiter le processus de fonctionnalisation. Dans certaines applications où les propriétés électroniques des CNT sont d'une importance capitale, l'exploration des voies de fonctionnalisation sont prometteuses, même en présence de matière amorphe. Grâce à la fonctionnalisation, un mélange de modifications mécaniques, thermiques et chimiques peut être induit dans le comportement des CNT, indépendamment de leur qualité initiale.<sup>1-3</sup> Cependant, lorsque les échanges électroniques à l'interface entre les CNT et les groupes fonctionnels sont importants, une attention particulière doit être accordée à la qualité de surface des CNT. Cela garantit l'efficacité et la fiabilité des interactions électroniques, améliorant ainsi les performances des systèmes basés sur les CNT dans les applications électroniques. L'objectif du deuxième chapitre était d'étudier la nécessité de procédures de post-traitement pour garantir la qualité de surface des CNT avant de progresser vers le développement de dispositifs de détection, et les résultats suivants ont été obtenus :

- Les méthodes de dépôt des CNT basées sur des solutions sont choisies pour leur polyvalence, leur faible coût et leur grande évolutivité.

- La morphologie du dépôt et la dispersion homogène des CNT dans un réseau homogène sont importantes pour la fiabilité du capteur. Ainsi, un réseau homogène de CNT peut être produit à partir d'une encre contenant des nanotubes hautement dispersés.
- Les CNT reçus du fournisseur ont subi un processus de purification pour éliminer la majorité de leur matière amorphe. Cependant, ce processus ne garantit pas l'élimination totale de la matière amorphe.
- Le oDCB et le NMP sont des solvants qui peuvent disperser les CNT en utilisant la sonication. Les dispersions sous forme d'encres avec le NMP comme solvant offrent une durée de vie 50 fois plus longue que celles basées sur le oDCB.
- L'impression jet d'encre a été particulièrement étudiée, et un processus avec l'imprimante Dimatix a été optimisé qui utilise une buse, une vitesse de goutte de 6 m/s et une distance par rapport au substrat de 500  $\mu\text{m}$ .
- La sonication a montré qu'elle fournissait suffisamment d'énergie pour initier une ouverture de cycle des solvants oDCB et NMP, entraînant la dégradation de ces solvants et la création des dits "sonochimiques". Ces sonochimiques peuvent induire encore plus de matière amorphe sur les parois des CNT.
- Une étape de post-traitement est nécessaire pour purifier les CNT en éliminant la matière amorphe qui vient de la matière amorphe issue de la récupération des CNTs de la surface après la synthèse en poudre commerciale, et plus important encore, les sonochimiques qui occupent les parois des CNT.
- Un processus a été développé qui consiste à chauffer des films minces de CNT à 650  $^{\circ}\text{C}$  et 1 mbar. Cette procédure a été caractérisée et s'est avérée efficace pour améliorer la qualité des CNT.

Dans le chapitre suivant, il a été discuté que le développement d'une fonctionnalisation efficace pour les SWCNTs implique un processus nuancé et complexe. Trois méthodes de fonctionnalisation distinctes ont été explorées. Dans le cas de la méthode de mélange, la présence claire de la molécule dans l'encre de CNT a éliminé le besoin de caractérisations spécifiques. En revanche, avec l'approche de fonctionnalisation en une étape, où il existait une

incertitude quant à la présence de la molécule à l'état solide aux côtés des CNTs, diverses techniques spectroscopiques ont été utilisées pour étayer la fonctionnalisation.

En tenant compte de l'impact observé de la sonication sur la qualité des CNT et de l'occupation de la surface par la matière amorphe, il est devenu évident que la simple présence de matière amorphe pourrait ne pas impliquer un échange électronique entre les molécules aromatiques et les CNT. Par conséquent, une enquête sur la méthode d'incubation a été initiée après le processus de nettoyage. Cette analyse exhaustive a révélé que la méthode de fonctionnalisation induisait des altérations structurelles, influençait l'occupation des parois et modifiait la morphologie des CNT. Ayant réussi à assembler un autre élément de ce puzzle complexe, on peut affirmer qu'un matériau à l'état solide a été créé, capable de servir de capteur. Cette réalisation fait avancer la recherche, préparant le terrain pour la discussion à venir dans le chapitre suivant.

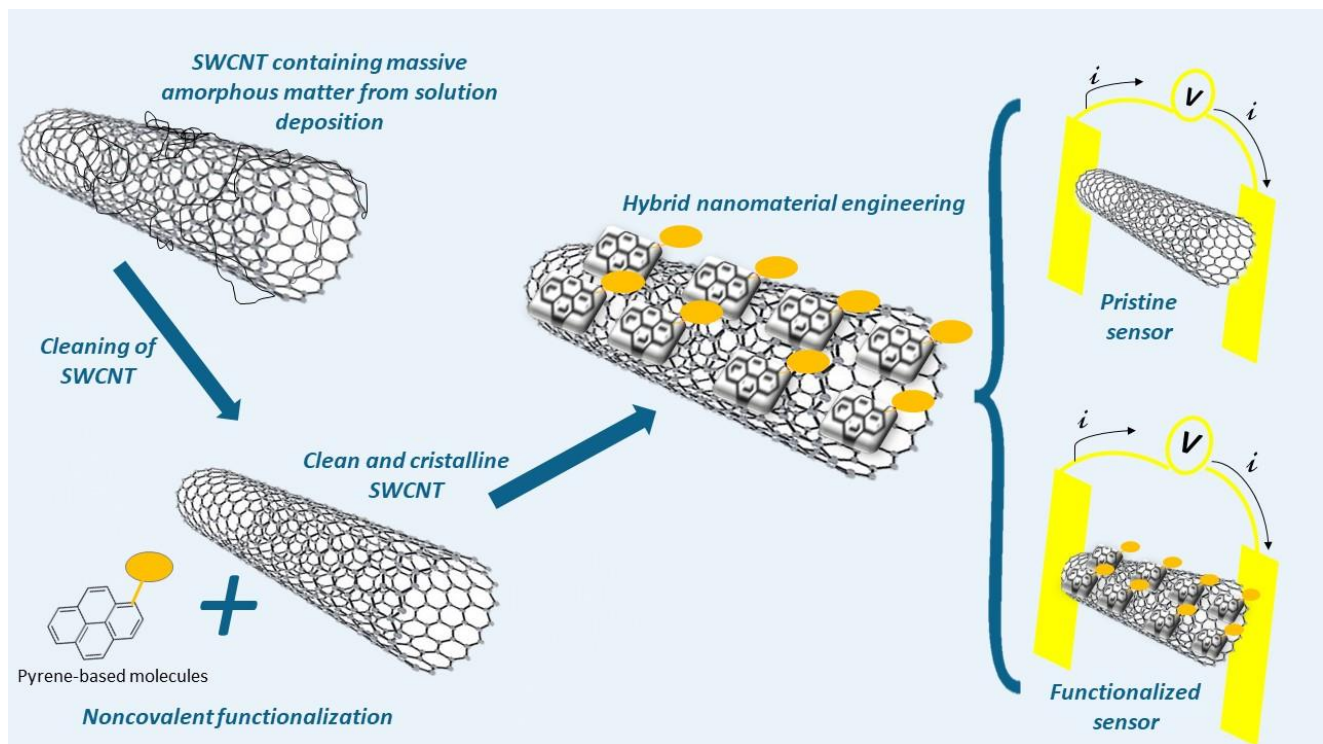
Après avoir développé un chemin de fonctionnalisation efficace pour les SWCNTs, il était temps de passer à l'objectif ultime du travail présent et d'appliquer les CNT fonctionnalisées dans le développement de dispositifs de détection capables d'interagir avec les analytes dans l'eau. Le dernier chapitre s'est penché sur les tests des efforts visant à purifier et à fonctionnaliser les nanotubes de carbone (CNT) pour leur application potentielle dans les dispositifs de détection.

Les résultats sont multifacettes, chaque caractérisation offrant des perspectives spécifiques sur divers facteurs qui influent sur l'efficacité opérationnelle des capteurs chimiorésistifs utilisant des CNT. Par conséquent, des enseignements ont été tirés de chaque caractérisation, informant sur les optimisations dans le traitement des CNT (en particulier le processus de chauffage), les techniques de fonctionnalisation des CNT, et la conception et la fabrication des dispositifs de détection.

Ce processus itératif a conduit à une évolution dans la caractérisation des dispositifs de détection, des dispositifs haut de gamme (IDEs) utilisant des CNT non traitées et insuffisamment fonctionnalisées, à des dispositifs plus fondamentaux ( $\mu$ CQs) utilisant des matériaux soigneusement caractérisés. Notamment, une sensibilité accrue des CNT aux

variations de pH a été observée pour donner suite à une fonctionnalisation réussie avec la molécule M3.

De plus, il a été démontré que la fonctionnalisation des CNT avec la molécule M2 conférait une sélectivité à l'égard de la concentration d'eau dissoute. Enfin, l'utilisation de  $\mu$ CQs a permis l'examen sélectif de la réponse de la molécule M5 au glyphosate. Bien que les résultats présentés dans ce chapitre ne soient peut-être pas révolutionnaires dans le domaine de la technologie des capteurs, ils offrent des perspectives précieuses et novatrices qui peuvent être explorées davantage pour faire progresser les capteurs chimiorésistifs basés sur les CNT.



## Acknowledgment

Doing a PhD is a long way and requires a high amount of mental strength and perseverance. Even though every PhD game is unique, and the main player is one person with a unique story, it is impossible to reach the end, without, help, support, and acts of kindness from others. I would like to express my most profound thanks to the people listed here and tell them how much I appreciate them.

- My family including my parents, my sisters Shaghayegh and Kolaleh, my dear cousin Navid, and more particularly, my lovely wife, my soulmate, my friend, and my companion, Kosar for all her support, love, understanding and patience. Unlucky for her, I went through many difficult times and without her by my side, it would have not been possible to do it.
- My supervisor, Dr. Yvan Bonnassieux, for all his help as a director, as a mentor and as a friendly figure during 4 years of working in LPICM, and to his courage and his great personality in taking responsibilities in particular at the end of my PhD.
- Dr. Cédric Tard, the responsible of the Chemistry department, an amazing human being, a great leader, and a formidable supporter, as well as his valuable insights about my manuscript.
- Dr. Iliana Florea, Dr. Jean-Luc Maurice, and Dr. Kassioyé Dembélé for their exceptional and great work as experts of TEM, and their patience in running measurements on my samples that were very difficult and particular.
- Jean-Charles Vanel for all his support, presence, and kindness throughout the times that we worked together,
- Marc Malvaux, and Jonathan Meot, the friendly and nice support team of LPICM, without whose help, patience, and kind manners for the design and fabrication of different tools and support elements, this work would have not been finished.
- Jacqueline Tran for her patience and hard work in AFM and SEM training and measurements.



## Institut Polytechnique de Paris

- Caroline Frot for her kind guidance in the design and fabrication of microfluidic systems.
- Clémence Herissey and Nicolas Moysan, the professionals on mental health that helped me through different types of traumas during my PhD. Their help and support were as important as anyone else mentioned here to reach the end of this work.
- My dearest friend, a great support and an amazing human being, Amir Habibi for his kind and uncensored knowledge-sharing and support.
- My former colleagues and friends that taught me many things on different characterization methods, procedures, and know-hows. Among them, I must mention Dr. Fatima Bouanis, Dr. Denis Tondelier, Eva Grinerval, Sawsen El Hadj, Issoufou Ibrahim Zamkoye, Manel Hanana, Pavel Bulkin, Christian Murga, Arghyadeep Bhattacharyya, and others who taught me and helped me grow as a person and professional.
- All dear friends from LPICM who made my life easier with their love and friendship, and I share many sweet moments and memories with:
  - o Martina, Mbaye, Camilla, Andrea, Guili, Xinley, Aymeric, Hindia, Sami, Shenming, Pingping, Michel, and more.
- My dear friends outside of LPICM who were supportive, positive, and kind:
  - o Mohammad, Erfan, Omid, Selim, Armita, Sina, Mehrasa, Amir, Fateme, Kimia, Mojtaba, Saman, Maryam Kadkhodaei, Maryam Asadi, Afshin, Armin, Hojjat, Farzaneh, Thomas, Marion, Thibaut Dirand, Thibaut Sallum, Wenxin, Emna, and more.

## List of abbreviation

AFE	Analogue Front End
BV	Benzyl Viologen
ChemFET	Chemical Field Effect Transistor
CFME	Carbon-Fiber Microelectrode
CMOS	Complementary metal–oxide–semiconductor
CNT	Carbon nanotube
CV	Cyclic voltammetry
CVD	Chemical Vapor Deposition
DCM	Dichloromethane
DI	Deionized
DMF	Dimethylformamide
DO	Dissolved Oxygen
DOD	Drop-On-Demand
EIS	Electrochemical impedance spectroscopy
FET	Field Effect Transistor
FTIR	Fourier transform infrared
HRTEM	High resolution transmission electron microscopy
IDE	Interdigitated Electrodes
IJP	Inkjet Printing
MAC	Maximum Acceptable Concentration
MALA	Material-assisted laser ablation
MWCNT	Multi-Walled Carbon nanotube
NMP	N-Methyl-2-pyrrolidone
NR	Natural Rubber



oDCB	<i>ortho</i> -Dichlorobenzene
OTS SAM	Octadecyltrichlorosilane self-assembled monolayers
PCB	Printed Circuit Board
PDMS	Polydimethylsiloxane
PEI	Polyethyleneimine
PMMA	Polymethylmethacrylate
PTFE	Polytetrafluoroethylene
RBM	Radial Breathing Mode
SEM	Scanning Electron Microscopy
SIN	Silicon + Silicon nitride (Si/Si <sub>3</sub> N <sub>4</sub> )
SoC	System-on-Chip
SWCNT	Single-Walled Carbon nanotube
TEM	Transmission Electron Microscopy
THF	Tetrahydrofuran
TLM	Transfer Length Method
UVO	Ultra-Violet Ozone
WHO	World Health Organization
μCQ	Quartz Substrates integrated with a MicroChannel



# Table of content

Résumé français .....	3
Acknowledgment .....	8
List of abbreviation .....	10
Table of content .....	12
Table of figures .....	15
Table of tables .....	21
Introduction.....	24
1. Introduction to the state of the art .....	27
1.1. Carbon nanotubes (CNTs).....	27
1.1.1. Structure of CNTs.....	28
1.1.2. Applications of CNTs .....	30
1.1.3. Synthesis of CNTs .....	33
1.2. Functionalization of CNTs .....	37
1.3. Characterization of noncovalent functionalized CNTs .....	42
1.3.1. Raman spectroscopy to study noncovalent functionalization.....	42
1.3.2. Transmission Electron Microscopy (TEM).....	45
1.4. Sensors based on CNTs.....	46
1.4.1. Electrical transduction sensors .....	48
1.4.1.1. Electrochemical sensors .....	48
1.4.1.2. Field Effect Transistor (FET) .....	51
1.4.1.3. Chemiresistive sensor .....	52
1.5. Drinking water analytes and sensors .....	54
1.5.1. Drinking water analytes.....	54
1.5.2. Sensing devices design and preparation .....	58
1.5.2.1. Inkjet Printing .....	59
1.5.2.2. State of the art on CNT-based chemiresistive sensors for water quality analysis ...	63
1.6. Conclusion on the state of the art and project objectives .....	68
1.6.1. Objectives of this project .....	69
2. Processing of CNTs.....	72
2.1. CNTs used in this work.....	73
2.2. Dispersion of CNTs.....	75
2.2.1. Ink preparation.....	77

2.2.2.	Ink concentration estimation .....	78
2.3.	Solvent-based deposition.....	80
2.3.1.	Drop casting.....	81
2.3.2.	Spin coating .....	81
2.3.3.	Spray coating .....	83
2.3.4.	Inkjet printing .....	84
2.3.4.1.	Optimization of the printing process with Dimatix .....	86
2.4.	Impact of sonication on CNTs .....	90
2.5.	CNT deposition with reduced amorphous matter .....	93
2.5.1.	CNT quality enhancement proof of concept.....	95
2.5.2.	Optimization of the Heating Process .....	97
2.5.2.1.	Temperature profile of the Heating Process .....	97
2.5.3.	Characterization of the Heating Process.....	100
2.5.3.1.	RAMAN spectroscopy .....	100
2.5.3.2.	TEM analysis of the effect of the Heating Process .....	104
2.5.4.	Going beyond the heating process.....	105
2.5.4.1.	Effect of the temperature and pressure on the Heating Process on .....	106
2.6.	Conclusion on the processing of CNTs.....	109
3.	Functionalization of CNTs.....	114
3.1.	Conjugated molecules for noncovalent functionalization of CNTs.....	114
3.1.1.	Choice of conjugated molecules.....	115
3.1.2.	Description of molecules .....	116
3.1.3.	Emission spectroscopy of CNT-molecule interactions .....	118
3.2.	Methods of functionalization .....	123
3.2.1.	Mixing functionalization .....	123
3.2.2.	One-pot functionalization .....	125
3.2.2.1.	Rate of one-pot functionalization .....	127
3.2.2.1.	One-pot functionalization validation by Fourier transform Infrared (FTIR) .....	130
3.2.2.2.	One-pot functionalization validation by Raman.....	131
3.2.2.3.	One-pot functionalization validation by UV-Vis absorption .....	132
3.2.3.	Functionalization by incubation .....	133
3.2.4.	Compare the success of functionalization methods by Raman .....	136
3.3.	Characterization of the chosen method for functionalization .....	147
3.3.1.	Raman scattering .....	148



3.3.2.	TEM analysis.....	151
3.4.	Conclusion on the functionalization of CNTs.....	152
4.	Sensing devices based on CNTs.....	156
4.1.	Components of electrical resistance.....	156
4.1.1.	Transfer Length Method (TLM).....	157
4.2.	Design of sensing devices and characterization procedures.....	161
4.2.1.	InterDigitated Electrodes on Si/SiO <sub>2</sub> (IDE).....	161
4.2.1.1.	Protection layer fabrication for CNT deposition in IDEs.....	162
4.2.1.2.	Wirebonding, waterproofing and characterization method for IDEs.....	166
4.2.2.	Simple electrodes on Si/Si <sub>3</sub> N <sub>4</sub> (SiN).....	167
4.2.3.	Simple electrodes on Quartz integrated with a MicroChannel (μCQ).....	168
4.2.3.1.	Metal evaporation using RIBER.....	168
4.2.3.2.	Design and fabrication of microfluidic channel.....	169
4.2.3.3.	Resistance study in μCQ.....	170
4.3.	Characterization of the sensing devices.....	173
4.3.1.	MWCNT IDE devices to detect free chlorine.....	173
4.3.2.	Detection of pH.....	178
4.3.2.1.	MWCNT IDE devices to detect pH.....	179
4.3.2.2.	SWCNT SiN devices to detect pH.....	182
4.3.3.	MWCNT SiN devices to detect pH, Dissolved oxygen, and Cu (II).....	184
4.3.3.1.	Detection of pH.....	185
4.3.3.2.	Detection of DO.....	186
4.3.3.3.	Detection of Copper (II).....	189
4.3.4.	SWCNT μCQ devices to detect Glyphosate.....	190
4.4.	Conclusions on the sensing devices.....	193
5.	General Conclusion.....	195
6.	Perspectives.....	197
6.1.	Perspectives on the processing CNTs.....	197
6.2.	Perspectives on the functionalization of CNTs.....	198
6.3.	Perspectives on the sensors based on CNTs.....	198
	References.....	200

## Table of figures

Figure 1. Carbon nanotubes, Graphene and Graphite in correlation (from tuball.com).....	28
Figure 2. $sp$ , $sp^2$ and $sp^3$ types of hybridization (toppr.com).....	29
Figure 3. Two lattice vectors $a_1$ and $a_2$ on a graphene sheet <sup>22</sup> (with permission). ....	29
Figure 4. Carbon nanotubes are classified as armchair, chiral, or zigzag based upon their structure. Each type has differing electronic properties <sup>25</sup> (with permission) .....	30
Figure 5. Supposed mechanism of CNTs Antimicrobial activity. CNTs clustered against bacterial cells and then tear down them by penetration <sup>33</sup> (with permission).....	31
Figure 6. Schematic drawing of the insertion of protein into the bilayer of a lipid modified MWCNT (front view). (A) Covalent modification of a COOH–MWCNT after reaction with DPPE. (B) Lipid bilayer formation during sonication of lipid-modified MWCNT with DPPC molecules in phosphate buffer and (C) insertion of $\alpha$ -hemolysin in the lipid bilayer-coated MWCNT. Drawing not to scale <sup>37</sup> (with permission).....	32
Figure 7. Graphical breakdown of the major areas of research and development in the carbon nanotube–silicon solar cell literature <sup>40</sup> (with permission). ....	33
Figure 8. Schematic of CVD device <sup>47</sup> (with permission). ....	34
Figure 9. Schematic of a carbon arc discharge for the synthesis of nanoparticles <sup>58</sup> (with permission).....	35
Figure 10. Schematic diagram of an arc discharge system to synthesize CNTs <sup>65</sup> (with permission).....	36
Figure 11. Simplified schematic of a) covalent and b) noncovalent functionalization. ....	38
Figure 12. A molecular model of a SWCNT(6,6) noncovalently functionalized by an external group <sup>83</sup> (with permission). ....	39
Figure 13. a) Structure of porphyrins 1-3; b) i) hydroxylamine 50 wt. % in water, Et3N, 2h, RT; ii) O <sub>2</sub> , RT overnight; c) schematic representation of the different steps of functionalization: A) the nanotubes are dispersed and individualized in micelles; B) the porphyrins in an organic solvent are introduced on the nanotube surfaces; C) after solvent evaporation, the reaction to cross-link the porphyrin is performed leading to a stable organic shell around the nanotubes; D) the nanotube derivatives are purified via filtration and extensive washing to remove the surfactants, reagents and unbound porphyrins <sup>88</sup> (with permission).....	40
Figure 14. Raman spectra of (A) Carbon-fiber microelectrode, (B) CNT-P, and (C) CNT-F electrodes <sup>103</sup> (with permission). ....	43
Figure 15. Typical 2D-band Raman spectra of a strained CNT film and fiber. (a) Comparison of the Raman spectra for unstrained and max-strained film and fiber. (b) Raman shift of the 2D band as a function of applied strain. <sup>106</sup> .....	44
Figure 16. Raman spectral map of CNT–PMMA composite (a)indicating CNT aggregates (bright spots). The blue arrow denotes direction of the spectral line scan (b) starting in the	

aggregate and ending in the dispersed area. Each spectrum in (b) corresponds to one step scan of 1 mm. Spectra were collected at 1.96 eV photon excitation energy.<sup>108</sup> ..... 45

Figure 17. TEM images of the membrane samples after growing CNT forests for (a) 3 min, (b) 3.5 min, (c) 5 min, and (d) 10 min at 740 °C. (Note: each image has a different scale bar)<sup>115</sup> (with permission). ..... 46

Figure 18. The working mechanism of a CNT-based electrochemical sensor<sup>142</sup> (with permission). ..... 50

Figure 19. Simplified topology of a FET (CNT ChemFET) showcasing a bottom gate structure.<sup>145</sup> ..... 51

Figure 20. Schematic of a chemiresistive sensor based on CNT. .... 53

Figure 21. Topography maps of the SWCNTs networks obtained by c) one, d) three, and e) ten printing passes. Scale bars are 500 nm.<sup>185</sup> ..... 60

Figure 22. (a) An inkjet-printed flexible strain sensor. (b) An illustration of the tensile test coupon with applications of a strain gauge rosette and the CNT thin film. (c) The tensile test setup.<sup>187</sup> (With permission). ..... 61

Figure 23. (a), (b), and (c) SEM images of a cloth fabric with inkjet-printed SWNT films. (d) Schematic diagram of an inkjet-printed SWCNT supercapacitor using PVA/H3PO4 as solid electrolyte and separator. The inset shows a supercapacitor made of SWNT/cloth fabric electrodes rolled around a pencil. (e) Photograph of a PET substrate with nanotube films printed with different geometries and print numbers. The features on the background picture are clearly visible. (f) SEM image of inkjet-printed SWNT films on a PET substrate and a photograph of a supercapacitor built with SWNT/PET electrodes. (g) Variation of conductance and transmittance of printed SWNT films on PET substrates as a function of film thickness ..... 62

Figure 24. Sensor fabrication process. (a) Front and back views of three screen-printed contacts and copper tape connections, (b) air brushing CNT on the frosted part of the glass slide and SEM image of the resulting CNT film, (c) functionalizing the CNT film with 0.1 M of NaOH·15-crown-5 ether solution and SEM image of the resulting n-doped CNT film, (d) curing the sensor at 85 °C, (e) applying pre-cut clear PET sheet to cover the contacts and have specific openings, (f) drop-casting ISM solution into the openings and drying for 12 hours. . 64

Figure 25. Schematic diagrams showing the (a) complete fabrication process of CNT based sensor, wherein 1) a silver electrode is printed first using aerosol jet technology, 2) CNT sensing element is printed, 3) thermal sintering process is carried out for the printed inks and 4) external wires are connected for measurements. Diagram depicting (b) parameters affecting the aerosol jet printing process and (c) dimensions of the fabricated sensor<sup>194</sup> (with permission). ..... 65

Figure 26. (a) Schematic process flow of the flexible pH sensor based on nanocomposites of SWCNTs and Nafion having three channels, fabricated by a screen printing process in ambient air, (b) chemical structure of Nafion, and (c) an optical image of the flexible <sup>195</sup> (with permission). ..... 66

Figure 27. (a) Schematic of sensor geometry; the inset shows a SEM image of the CNT film. (b) Recorded sensor response as current (nA) over time for the different steps of the measurement. Solvent and molecule solution induces n-doping on the surface, while the oxidant (free chlorine) results in p-doping behavior. When exposed to ascorbic acid, the sensor showed a reset in the response due to analytes getting reduced by ascorbic acid.<sup>196</sup>.... 67

Figure 28. Typical Raman of SWCNT and MWCNT used in this project..... 74

Figure 29. Procedure of concentration estimation by precipitation..... 79

Figure 30. Spin coating method for thin film depositions. .... 82

Figure 31. Illustration of spray coating method for thin film depositions. .... 83

Figure 32. DMP-2800 Series, Fujifilm Dimatix printer. .... 84

Figure 33. Cartridge of the Dimatix printer. .... 85

Figure 34. The drop position 300  $\mu\text{m}$  below the nozzle, 50  $\mu\text{s}$  after release from the nozzle, is a good estimation of the average drop speed which is 6 m/s..... 86

Figure 35. Continuity of the CNT deposition from inkjet printing. .... 90

Figure 36. Sonication of pure solvent resulted in obvious color changes. .... 91

Figure 37. TEM images of a) a solid commercial MWCNT, b) MWCNT dispersed in oDCB. .... 92

Figure 38. HRTEM images of a pristine SWCNT ink in NMP. a represents the abundant amorphous matter around individual tubes, and b represents the excess of amorphous matter in the SWCNT network..... 94

Figure 39. TEM image of pristine SWCNT ink in NMP before (a,c) and after (b,d) Heating Process in the TEM chamber. .... 96

Figure 40. Temperature profile of the tubular furnace to a maximum of 950°C for cleaning of CNT depositions. .... 98

Figure 41. Optimal temperature profile compatible with lab processes and the best outcome. .... 100

Figure 42. Comparison between the Raman spectra of a SWCNT deposition, before and after the Heating Process..... 102

Figure 43. Heating Process impact, with the presence of random conjugated groups among the amorphous matter..... 103

Figure 44. Effect of the Heating Process on the Raman spectra of MWCNTs. .... 104

Figure 45. Effect of the Heating Process on the surface quality of SWCNT by TEM analysis. a) Usual SWCNT network before heating. b) Usual SWCNT network after heating by using a tiny tube. c) Usual SWCNT network after heating by scratching the surface and scrubbing the TEM grid..... 105

Figure 46. Effect of the heating temperature in air on SWCNT quality..... 106

Figure 47. Effect of the heating temperature under vacuum on SWCNT quality. .... 107

Figure 48. Effect of the temperature and oxygen content in the Heating Process on the quality of SWCNTs..... 108

Figure 49. SEM images of a SWCNT deposition A) before heating, B) after heating in air at 375°C, and C) after applying the Heating Process. .... 109

Figure 50. Left: Pyrene molecule, right: Porphyrin molecule. .... 115

Figure 51. Some of the molecules used in this project. .... 117

Figure 52. Dilution of M1 molecule with the solvent (left) and the CNT ink(right) ..... 119

Figure 53. Quenching of maximum emission for M1 molecule by adding solvent and the diluted CNT ink. .... 119

Figure 54. Dilution of M2 molecule with the solvent (left) and the CNT ink(right). .... 120

Figure 55. Quenching of maximum emission for M2 molecule by adding solvent and the diluted CNT ink. .... 121

Figure 56. Dilution of M5 molecule with the solvent (left) and the CNT ink(right). .... 122

Figure 57. Quenching of maximum emission for M5 molecule by adding solvent and the diluted CNT ink. .... 122

Figure 58. Emission of Molecule/CNT mixture supernatant at different ratios between the two materials. .... 124

Figure 59. UV-Vis and emission spectrum of the M5 molecule (excitation wavelength = 371nm). .... 128

Figure 60. Effect of initial weight ratio on the Raman spectra in One-pot functionalization. 130

Figure 61. IR spectra of functionalization of MWCNT with M5 molecule using one-pot approach. .... 131

Figure 62. Raman spectra of functionalized MWCNT with M1 using One-pot approach and the M2 molecule as a reference for porphyrin-based molecules. .... 132

Figure 63. UV-Vis absorption spectroscopy study of a M5 molecule and its trace in a functionalized (filtration) sample..... 133

Figure 64. Creation of crystals of a Porphyrin-based molecule due to slow solvent evaporation..... 135

Figure 65. molecules a) M4, b) M5, and solvents c) oDCB, d) DMF used to study the success rate of functionalization by Raman spectroscopy..... 136

Figure 66. Comparison of different functionalization methods for M5 molecule using oDCB as solvent..... 137

Figure 67. Comparison of different functionalization methods for M4 molecule using oDCB as solvent..... 137

Figure 68. Comparison of different functionalization methods for M5 molecule using DMF as solvent. .... 138

Figure 69. Comparison of different functionalization methods for M4 molecule using DMF as solvent. .... 139

Figure 70. Comparison of different solvents for M5 molecule in incubation method. .... 139

Figure 71. Comparison of different solvents for M5 molecule in Mixing method. .... 140

Figure 72. Comparison of different solvents for M4 molecule in Incubation method. .... 141

Figure 73. Comparison of different solvents for M4 molecule in Mixing method. .... 141

Figure 74. Comparison of Mixing functionalization for different molecule with oDCB as solvent. .... 142

Figure 75. Comparison of Incubation functionalization for different molecule with ODCB as solvent. .... 143

Figure 76. Comparison of One-pot functionalization for different molecule with oDCB as solvent. .... 143

Figure 77. Comparison of mixing functionalization for different molecule with DMF as solvent. .... 144

Figure 78. Comparison of Mixing functionalization for different molecule with DMF as solvent. .... 145

Figure 79. Evolution of the Raman spectra of SWCNT deposition after incubation with M2. .... 149

Figure 80. Raman spectra of a SWCNT deposition, before and after incubation with M5.... 150

Figure 81. TEM image of 4 samples: a) pristine clean SWCNT after heating, b) SWCNT incubated with M1 molecule, c) SWCNT incubated with M2 molecule, d) SWCNT incubated with M5 molecule. .... 152

Figure 82. Schematic of different resistance components in a CNT-based chemiresistive device. .... 157

Figure 83. Image of the CNT depositions, the electrodes, and their dimensions used for TLM measurements. .... 158

Figure 84. IDE substrates comprising of four different geometries of interdigitated electrodes. .... 162

Figure 85. 1  $\mu\text{m}^2$  AFM image showing grain boundary at the surface of the porous film.<sup>319</sup> 163

Figure 86. Image of (a). placement of the taped chip on the holder, and (b) the Ossila spin-coater. .... 165

Figure 87. The PCB used to connect the chips to the measurement system..... 166

Figure 88. Wire bonding machine and the connection between the chips and the PCB. .... 166

Figure 89. SIN substrates with four sections. Only the area at top left is used. .... 167

Figure 90. The design and fabrication process of  $\mu\text{CQ}$  sensing devices. .... 170

Figure 91. The evolution of resistance of devices with different steps of fabrication..... 172



Figure 92. Chemical structure of FF-UR polymer used for the detection of free chlorine. ... 174

Figure 93. Relationship Between HOCl and OCl<sup>-</sup> at Various pH Values. .... 175

Figure 94. Response of pristine (P1, P2, P3, and P4) and functionalized (F1 and F2) IDE devices to the concentration of free chlorine in water. .... 177

Figure 95. The relationship between the sensitivity and the baseline resistance for IDEs based on MWCNT. .... 178

Figure 96. Chemical structure of M3, a pyrene-based molecule for the detection of water acidity. .... 179

Figure 97. Chip used for the characterization of IDE device for the detection of pH. The device bordered in red was printed with Pristine ink, and the device in green with functionalized ink. .... 180

Figure 98. Result of the characterization of one IDE chip with only two printed devices. .... 181

Figure 99. The results of the cartelization of pristine and functionalized (with M3) SIN devices for responses against the changes in the pH of water. .... 183

Figure 100. Results of characterization of Pristine and Functionalized sensors with M2, M3, and M4 molecules against the changes in the water pH. .... 186

Figure 101. Results of characterization of Pristine and Functionalized sensors with M2, M3, and M4 molecules against the changes in the DO level in water. .... 188

Figure 102. Results of characterization of Pristine and Functionalized sensors with M2, M3, and M4 molecules against the concentration of Cu (II) in water. .... 189

Figure 103. Reminder of the chemical structure of M5 molecule and Glyphosate. .... 190

Figure 104. Results of characterization of Pristine and Functionalized with M5 molecule  $\mu$ CQ devices against the concentration of Glyphosate in water. .... 191

Figure 105. Results of characterization of Pristine and Functionalized with M5  $\mu$ CQ devices against the concentration of Zn(II) in water. .... 193

## Table of tables

Table 1. Critical chemical parameters in qualifying drinking water. <sup>8</sup> .....	55
Table 2. Results of the inkjet printing study to determine the effect of different parameters on the deposition shape. ....	87
Table 3. Comparison of the amorphous matter coverage of the two CNT samples. The value of variation coefficient among different images is reported. ....	93
Table 4. Impact of heating under vacuum at different temperatures on the resistance of SWCNT depositions .....	99
Table 5. Summary presentation of all Raman spectroscopy results, with calculated averages of important ratios. ....	101
Table 6. Parameters of One-pot functionalization for pyrene-based molecules in the literature (schemes taken with permission). ....	126
Table 7. Calculations of the linear relationship between concentration of M5 with UV-Vis and emission spectra. ....	128
Table 8. Calculations of the functionalization rate with One-pot method.....	129
Table 9. Parameters of Incubation functionalization in the literature (schemes taken with permission).....	134
Table 10. The comparative table of the success rate of functionalization with different methods using Raman spectroscopy. ....	146
Table 11. The values of the measured resistance for the four ink types.....	159
Table 12. Calculation of $R_s$ and $R_c$ in each approach to model the circuit.....	160
Table 13. Dimension details and Resistance values of IDE geometries.....	161
Table 14. Data of characterization of sensing devices based on functionalized MWCNTs with FFUR-14 polymer. ....	176
Table 15. The timeline of analyte addition to the SiN devices.....	182
Table 16. SiN devices for the characterization of multiple molecules and multiple analytes.....	184
Table 17. complementary information to Figure 104.. ....	192



**Institut Polytechnique de Paris**



قُلْ لَوْ كَانَ الْبَحْرُ مِدَادَ الْكَلِمَاتِ رَبِّي لَنَفَذَ الْبَحْرُ قَبْلَ أَنْ تَنْفَدَ كَلِمَاتُ

رَبِّي وَلَوْ جِئْنَا بِمِثْلِهِ مَدَدًا (الكهف 109)

Say, O Prophet, "If the ocean were ink to write the science belonging to of my Lord in words, it would certainly run out before the science of my Lord were finished, even if it was refilled with more ink".



## Introduction

Ecological changes have diverse impacts on human livelihood, with a pronounced challenge being the longstanding struggle for reliable sources of drinking water globally. Currently, this challenge is summarized by three primary factors. Firstly, climate change disrupts rainfall patterns, rendering historically arid regions even drier. Secondly, the irresponsible release of industrial waste contaminates water resources, posing threats to human and wildlife health. Lastly, the expanding population intensifies the demand for this essential life necessity amid decreasing availability.

According to the World Health Organization (WHO), approximately 2 billion people lack access to safe drinking water, resulting in around 1.8 million annual deaths, primarily due to water-borne diseases like diarrhea.<sup>4</sup> Additionally, poor water quality can lead to various health problems, including skin infections, respiratory issues, and even cancer.<sup>5</sup> Moreover, the ecological consequences of water pollution can result in the degradation of aquatic habitats and loss of biodiversity.<sup>6</sup>

Simultaneously, there is a growing need to assess water quality along pipelines and in local areas. Contaminants such as bacteria, viruses, protozoan parasites, pesticides, and heavy metals pose unique threats, necessitating their identification and removal before distribution to the public.<sup>7</sup> Continual monitoring and testing of water sources and distribution systems are imperative, especially in communities relying on surface water susceptible to contamination from various sources.<sup>8</sup>

Technological advancements, particularly in digital data collection and transmission, facilitate autonomous processes, providing rapid data for informed decision-making to combat the water crisis.<sup>9</sup> Electrical sensors with digital transduction, such as those measuring contamination as electrical resistance, prove effective in evaluating water quality across diverse locations, including remote areas.<sup>10</sup>

In the context of this project, the objective is to fabricate selective resistive sensors using carbon nanotubes (CNTs) functionalized with home-made conjugated molecules. This



approach aims to detect water pollutants efficiently. Deposition of nanomaterials from a solvent, particularly through inkjet printing, emerges as a cost-effective method for sensor fabrication.<sup>11</sup>

After a comprehensive literature review on the topic, employing a drill-down analysis approach, the report continues with the subject of CNT processing and explores a novel approach to enhance the quality of CNTs deposited from a solvent, crucial for sensor applications. Subsequently, the report delves into functionalization routes for developing nanohybrids that selectively interact with common water pollutants. Lastly, it details a novel design of sensing devices incorporating microfluidic systems for water pollutant detection. The conclusion offers perspectives for further exploration in drinking water sensor development.



# **First Chapter**

# **state of the art**



# 1. Introduction to the state of the art

In this chapter, a comprehensive bibliography review will be presented on the subjects of interest in a logical manner. First, the topic of carbon nanotubes, their structure, synthesis methods, and applications will be discussed opening the door to the next major topic on this thesis; functionalization. In the functionalization section, different methods will be discussed as well as their applications and their impact on the intrinsic properties of CNTs.

Later on, different methods in the literature will be discussed that are used for characterization of functionalization. Finally, the topic of water analytes and the state of the art on the CNT-based sensors for water quality analysis will be generally mentioned from the literature, sensors based on CNTs will be discussed, providing a general overview of different transduction methods, and the topic will be narrowed down to chemiresistive sensors, and more specifically those used for water quality analysis.

## 1.1. Carbon nanotubes (CNTs)

Carbon nanotubes (CNTs) were first identified in 1991 by Sumio Iijima a Japanese scientist, who observed these tiny tubes while examining the by-products of the arc discharge method used to produce carbon fibers.<sup>12</sup> Since then, they have been the subject of numerous studies and have gained interest in various fields of science and technology due to their unique properties. The global commercial interest in CNTs is evident in a production capacity that is several thousand tons annually.<sup>13</sup>

There are two types of CNTs; Single-Walled CNT (SWCNT) and Multi-Walled CNT (MWCNT). As the name suggests, SWCNT is one single tube-shaped by rolling one graphene layer, while in MWCNT multiple graphene layers are rolled and the smaller tubes are within larger tubes as depicted in Figure 1.



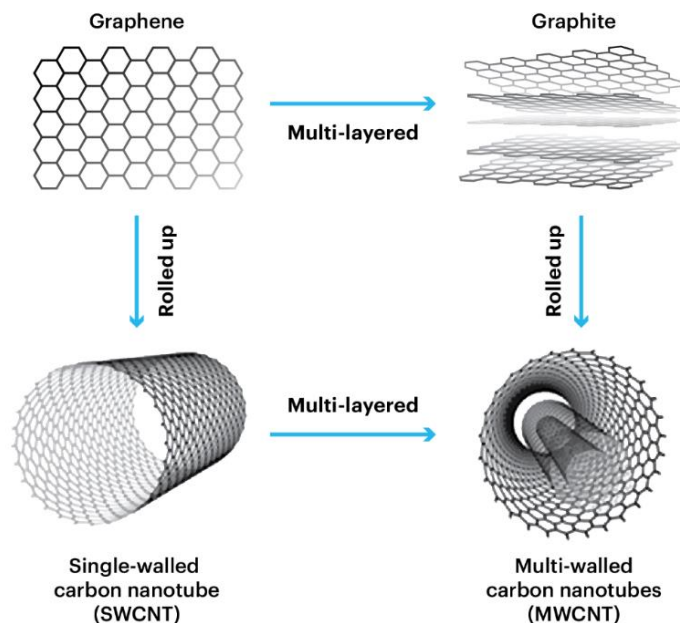


Figure 1. Carbon nanotubes, Graphene and Graphite in correlation (from tuball.com).

Beyond their structural and electronic characteristics, CNTs have been investigated for diverse applications in the realm of materials science.<sup>14</sup>

### 1.1.1. Structure of CNTs

Carbon nanotubes represent two-dimensional tubular structures formed by  $sp^2$  hybridized carbon atoms, presenting an enhanced iteration of sheet graphene.<sup>15</sup> In the honeycomb-like structure of CNTs, each carbon atom is bound to 3 other carbon atoms, leaving one free electron in the  $\pi$  orbital providing an  $sp^2$  structure.<sup>16</sup>

The  $sp^2$  hybridization of carbon atoms in CNTs has a foundational role in dictating their electrical conductivity. Variations in the electrical conductivity of cone-shaped CNTs have been linked to a reduction in charge carrier concentration, stemming from hydrogen localization on carbon  $\pi$ -orbitals, the shift from  $sp^2$  to  $sp^3$  hybridization affecting the band structure of CNTs, thus resulting in a metal-semiconductor-insulator transition.<sup>17</sup> Extensive

exploration into the  $sp^2$  hybridization of carbon nanomaterials has been conducted to tailor their electrocatalytic attributes through noncovalent functionalization with molecular doping, thereby influencing the electronic structure for exceptional properties.<sup>18</sup>

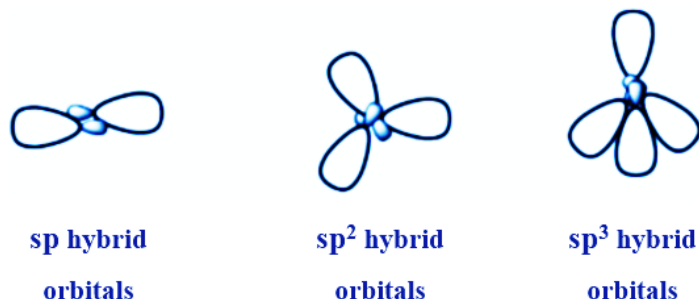


Figure 2.  $sp$ ,  $sp^2$  and  $sp^3$  types of hybridization (toppr.com).

The configuration of carbon atoms within CNTs, known as chirality, imparts diverse electronic characteristics, encompassing semiconducting, semi-metallic, or metallic behavior, alongside altered mechanical properties.<sup>19</sup>

The electronic traits of CNTs intricately hinge on their atomic makeup delineated by chirality, denoted by the chiral indices  $(a_1, a_2)$ <sup>20</sup> as shown in Figure 3. These chiral indices are important in elucidating the structure-property correlations essential in CNT studies.<sup>21</sup>

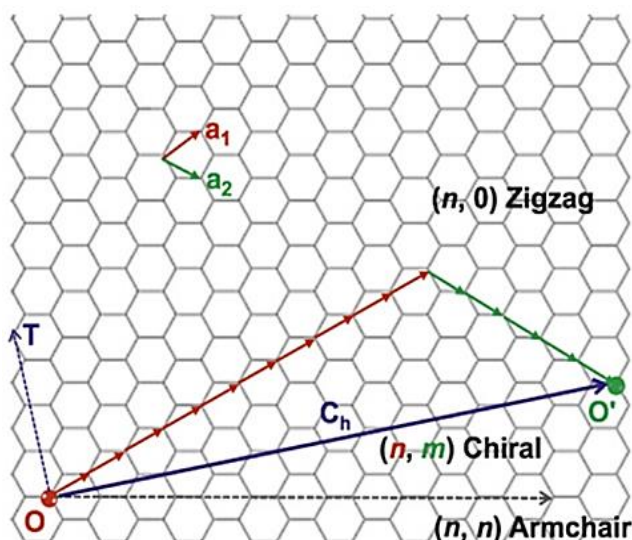


Figure 3. Two lattice vectors  $a_1$  and  $a_2$  on a graphene sheet<sup>22</sup> (with permission).

Chirality comes from the orientation of the graphene sheets to which they are rolled.<sup>23</sup> Figure 4 shows the different orientations of CNT when they are synthesized. The shape and diameter of a CNT are defined by a lattice vector as  $C = ma_1 + na_2$ , where  $a_1$  and  $a_2$  are related to the diameter, and  $m$  and  $n$  define the chirality. If  $m = n$ , the CNT is called armchair, and when  $m = 0$  or  $n = 0$ , the CNT is called zigzag. Metallic properties are always seen in armchair CNTs.<sup>24</sup>

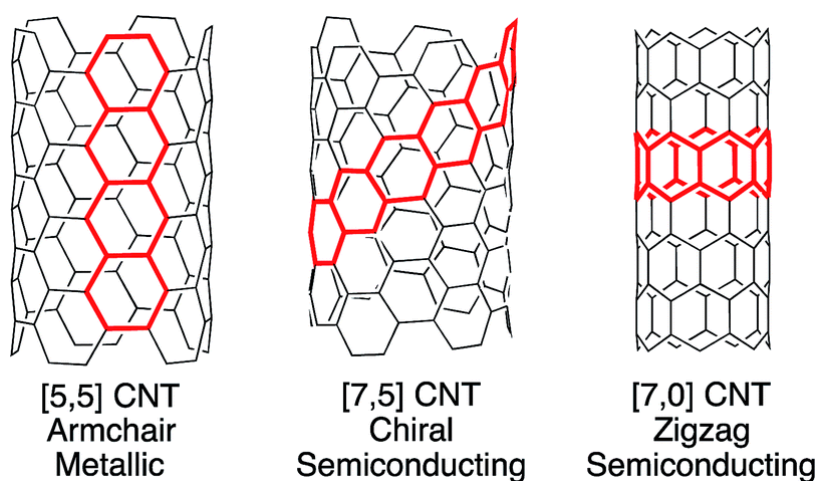


Figure 4. Carbon nanotubes are classified as armchair, chiral, or zigzag based upon their structure. Each type has differing electronic properties<sup>25</sup> (with permission)

### 1.1.2. Applications of CNTs

The extended system of  $\pi$  orbitals on the walls of CNT makes them a great candidate for electronic conductance.<sup>26</sup> On the other hand, this structure allows CNTs to adsorb chemicals in their surrounding environment, which alters their electronic conductance.<sup>27</sup>

CNTs have gained significant attention due to their exceptional properties, leading to a wide range of applications across various fields. They have been extensively utilized in diverse applications such as catalysts, water treatment absorbents, photo catalysis, conductive and high-strength composites, energy storage and conversion devices, sensors, field emission

displays, radiation sources, hydrogen storage media, semiconductor devices, probes, and interconnects.<sup>28,29</sup> Unique mechanical, chemical, and electrical properties of CNTs have made them valuable for electrochemical and optical biosensing, as well as for biomedical applications such as drug and vaccine delivery, scaffold materials, and biosensors.<sup>30–33</sup>

Figure 5 is an example of application of CNTs in exterminating bacteria, which is interesting in fighting bacteria diseases. They have also been explored for their biocompatibility and potential utilities in biological settings, which are crucial factors in determining their applications in medicine and biology.<sup>34</sup>

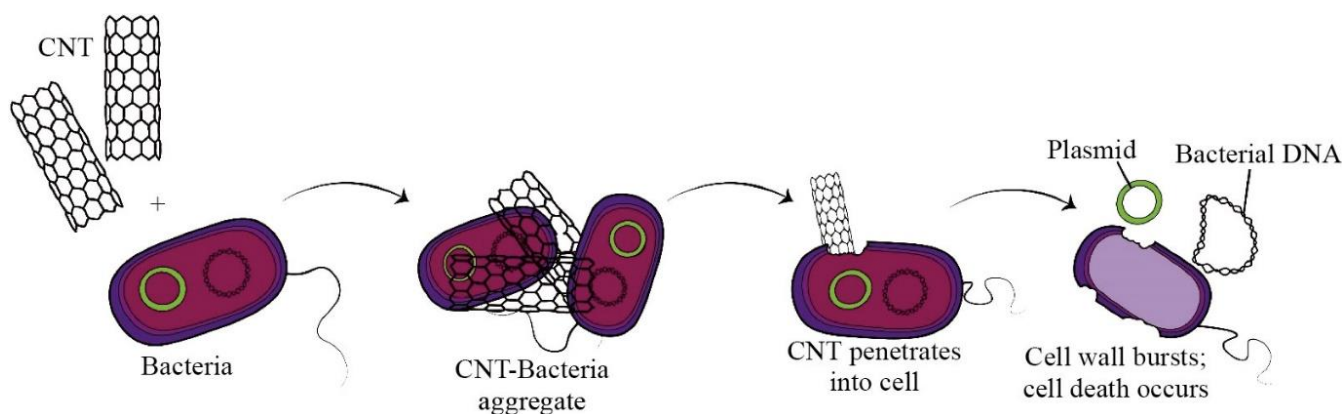


Figure 5. Supposed mechanism of CNTs Antimicrobial activity. CNTs clustered against bacterial cells and then tear down them by penetration<sup>33</sup> (with permission).

The potential applications of CNTs extend to the field of lightweight construction, where their outstanding mechanical properties make them promising materials for further development.<sup>35</sup> The exceptional electrical and mechanical properties of CNTs have led to their utilization in electronic applications, including the fabrication of nanocomposites with potential applications in electronics packaging as thermal interface materials.<sup>36</sup> CNTs have also attracted attention for their potential applications in lipid bilayers, as shown and explained in Figure 6.<sup>37</sup>

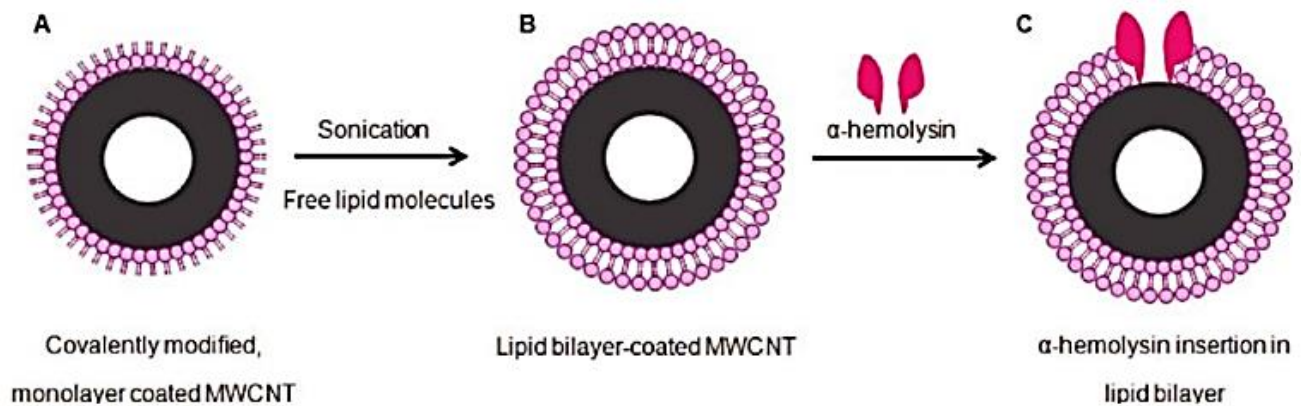


Figure 6. Schematic drawing of the insertion of protein into the bilayer of a lipid modified MWCNT (front view). (A) Covalent modification of a COOH–MWCNT after reaction with DPPE. (B) Lipid bilayer formation during sonication of lipid-modified MWCNT with DPPC molecules in phosphate buffer and (C) insertion of  $\alpha$ -hemolysin in the lipid bilayer-coated MWCNT. Drawing not to scale<sup>37</sup> (with permission).

The preparation of aligned and/or micro patterned CNTs has been identified as crucial for applications ranging from nanocomposites to field-emitting displays, further demonstrating the diverse applications of CNTs.<sup>38</sup> CNTs contribute to the creation of self-healing polymer nanocomposites, finding utility in diverse fields like sensors, actuators, coatings, microelectronics, adhesives, and biomedical applications.<sup>39</sup>

Figure 7 illustrates the potential of CNTs is underscored in the energy sector, with advancements in carbon nanotube–silicon heterojunction solar cells achieving power conversion efficiency and active area records exceeding 17% and 2 cm<sup>2</sup>, respectively.<sup>40</sup>

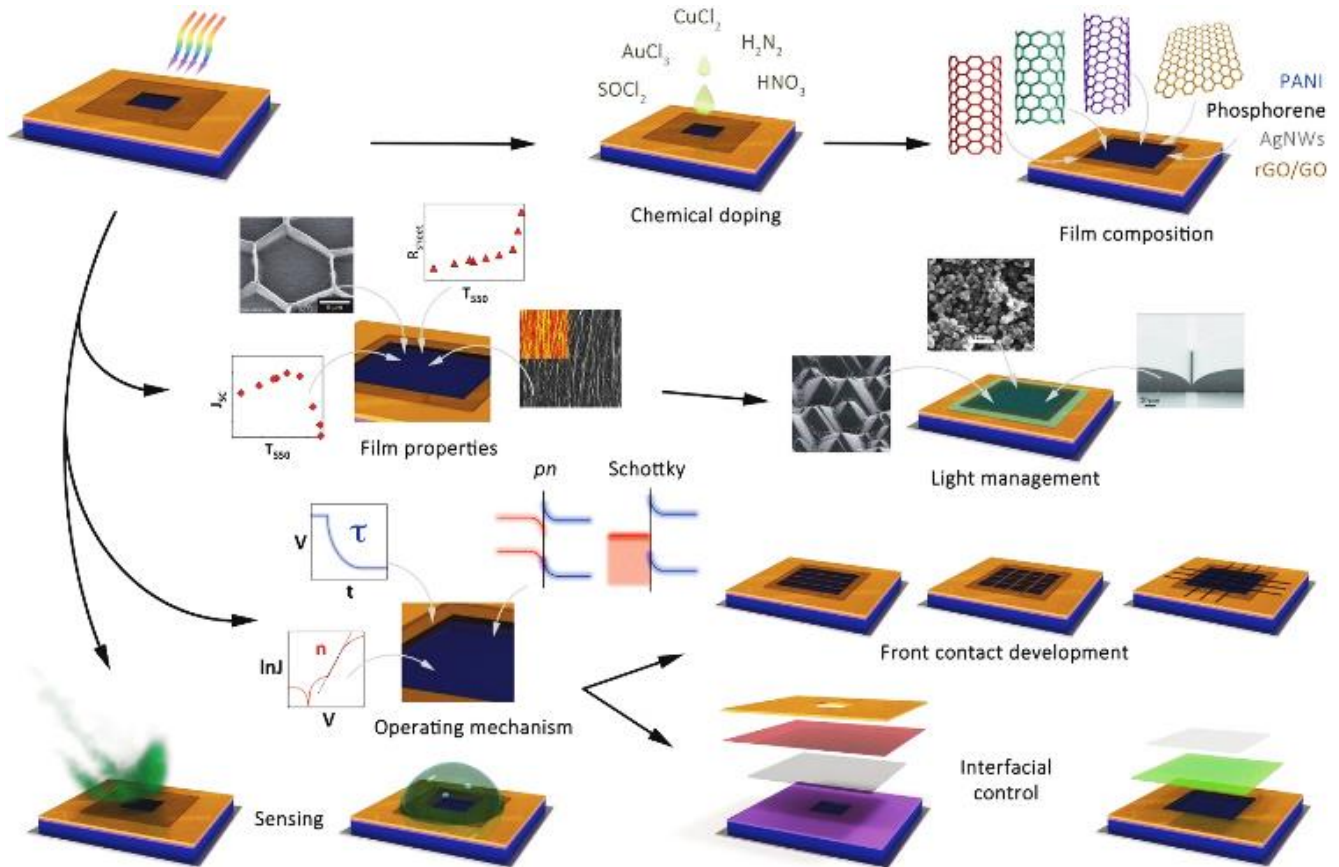


Figure 7. Graphical breakdown of the major areas of research and development in the carbon nanotube–silicon solar cell literature<sup>40</sup> (with permission).

### 1.1.3. Synthesis of CNTs

The synthesis, of CNTs have been the focus of extensive research, highlighting the significance of CNTs in materials science and their potential impact on various technological fields.<sup>41,42</sup> Various growth techniques, including plasma-enhanced chemical vapor deposition and laser-assisted growth, have been examined to control the growth and properties of CNTs.<sup>43,44</sup> Challenges persist in the orientation and direction of CNTs, posing hurdles for commercial purposes.<sup>45</sup>



Among CNT synthesis methods, chemical vapor deposition (CVD) has emerged as a promising approach for large-scale production. CVD involves the use of catalysts such as Ni, Fe, Fe-Ni, and Ni-Mo to facilitate the growth of CNTs.<sup>46</sup>

Figure 8 depicts a schematic representation of a standard thermal chemical vapor deposition (CVD) apparatus. Effectively managing the flow of source gases, adjusting pressure, and controlling temperature are crucial aspects of the CVD apparatus. It's worth noting that the apparatus is not restricted to a horizontal furnace configuration, as shown in Figure 8; vertical or cold-wall types are also prevalent. Within CVD techniques, the selective growth of SWCNTs can be achieved by manipulating catalyst particle size. Additionally, by regulating catalyst particle distribution or utilizing suitable substrates, the growth direction of individual SWCNTs can be precisely controlled.<sup>47</sup>

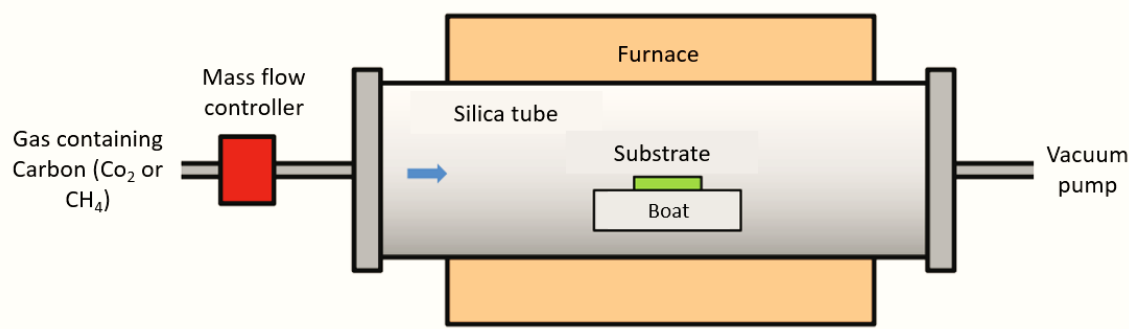


Figure 8. Schematic of CVD device<sup>47</sup> (with permission).

The diameter of CNTs is regulated by employing nearly monodisperse iron nanoclusters, defining the dimensions of CNTs synthesized through chemical vapor deposition (CVD).<sup>48</sup>

The arc discharge method is another a widely used technique for the synthesis of CNTs due to its simplicity and cost-effectiveness. This method involves creating an electric arc between two carbon electrodes in an inert atmosphere or liquid medium, resulting in the formation of CNTs. The arc discharge method has several variations, such as using hydrogen gas<sup>49</sup>,

deionized water and NaCl solution<sup>50</sup>, and even in open air.<sup>51</sup> The resulting CNTs exhibit good crystallinity, high thermal stability, and electrical conductivity.<sup>49</sup> The arc discharge method allows for the synthesis of not only CNTs but also other carbon nanostructures, such as carbon onions and fullerene tubes.<sup>52,53</sup>

The use of different catalysts and conditions in the arc discharge method can influence the properties of the synthesized CNTs. For example, the addition of metal powders to the anode can lead to the synthesis of CNTs containing metal.<sup>54</sup> Furthermore, the synthesis of metal-CNT network hybrids has been achieved using the hydrogen arc discharge method.<sup>55</sup> The arc discharge method has also been employed for the synthesis of CNTs from polymer waste and high-density polyethylene waste, demonstrating its potential for sustainable and environmentally friendly CNT production.<sup>56,57</sup>

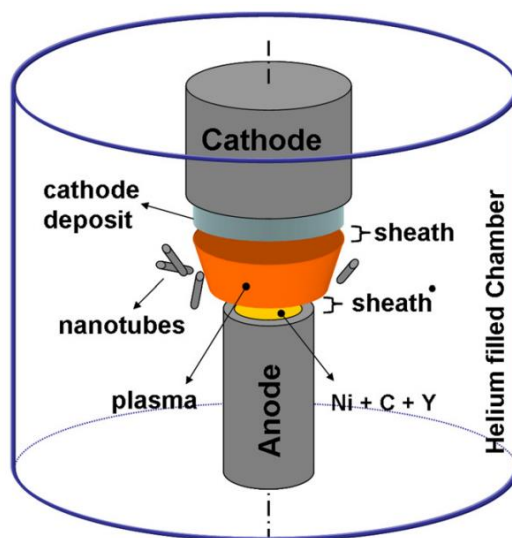


Figure 9. Schematic of a carbon arc discharge for the synthesis of nanoparticles<sup>58</sup> (with permission).

Although the arc discharge method offers simplicity and cost advantages, it introduces challenges concerning controllability and the optimization of synthesis conditions. Consequently, alternative methods, like chemical vapor deposition and laser ablation, have been devised to overcome these limitations.<sup>58</sup> Nonetheless, the arc discharge method remains a



valuable approach for the large-scale production of CNTs due to its scalability and potential for recycling waste materials.<sup>56,57</sup>

The synthesis of CNTs through the laser ablation method has established itself as a well-established technique. This approach entails laser vaporizing a graphite rod within an oven, utilizing Co and Ni as catalysts.<sup>59</sup> Recognized as a distinct and well-developed synthesis method for CNTs, laser ablation has found widespread application in the synthesis of nanoparticles, especially single-wall carbon nanotubes and C<sub>60</sub> molecules.<sup>60</sup> It has proven instrumental in growing both single and multi-walled carbon nanotubes, catering to diverse technological applications.<sup>61</sup>

In the laser ablation process, a femtosecond laser with varying parameters is employed for the ablation and patterning of CNT films.<sup>62</sup> This method extends its utility to determining the helicity population in a SWCNT sample.<sup>63</sup> Moreover, a novel patterning approach, termed material-assisted laser ablation (MALA), has been introduced for the precise patterning of carbon nanotubes and other nanowires, meeting the demands of high-volume production applications.<sup>64</sup>

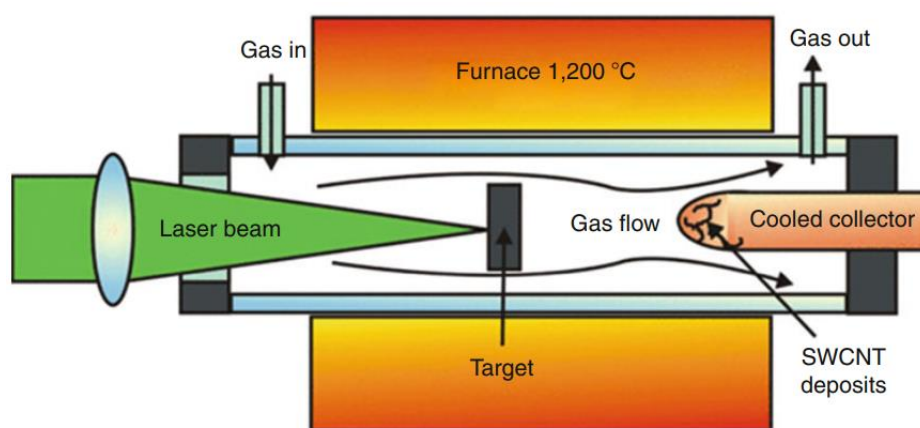


Figure 10. Schematic diagram of an arc discharge system to synthesize CNTs<sup>65</sup> (with permission).

Comparative studies with other synthesis techniques, such as arc discharge and chemical vapor deposition (CVD), highlight laser ablation as a commonly employed method for CNT

synthesis.<sup>66</sup> It has been observed that laser ablation, along with arc discharge and thermal chemical vapor deposition methods, is frequently chosen for CNT synthesis.<sup>67</sup> Additionally, laser ablation has been explored in conjunction with excimer laser irradiation to examine the surface morphology transformation of carbon nanotube thin films.<sup>68</sup>

The incorporation of boron impurity atoms into CNTs has demonstrated the ability to modify their physical, chemical, mechanical, and electrical properties, opening up new possibilities for diverse applications.<sup>69</sup> Additionally, the directed assembly of single-walled carbon nanotubes onto patterned surfaces showcases their versatility for potential use in sensors, flexible electronics, and photovoltaics.<sup>70</sup>

## 1.2. Functionalization of CNTs

Due to the presence of an abundant quantity of electrons in the  $\pi$  orbitals of carbon atoms, CNTs are among very reactive nanomaterials acting like sponges and interacting with most of the chemical groups in their surroundings.<sup>71</sup> Although this behavior of CNTs is the foundation of the interest in their use in chemical sensing applications<sup>72–74</sup>, at the same time it is a complexing issue. One of the most important parameters of a sensing device is their ability to distinguish between the analytes.<sup>75</sup> The term analyte is more general than pollutant and refers to something to be analyzed and reported or what it is expected from a sensor to respond to. An analyte could also be environmental parameters i.e. pressure, temperature, sound, chemicals, etc.

Functionalization is the process of adding a chemical group onto CNTs that can interact only with one or limited types of species. Although functionalization is useful for many applications, the main goal in sensor fabrication is adding selectivity. The functionalization of carbon nanotubes can be achieved through two major methods: covalent and noncovalent functionalization that are simplified in Figure 11.

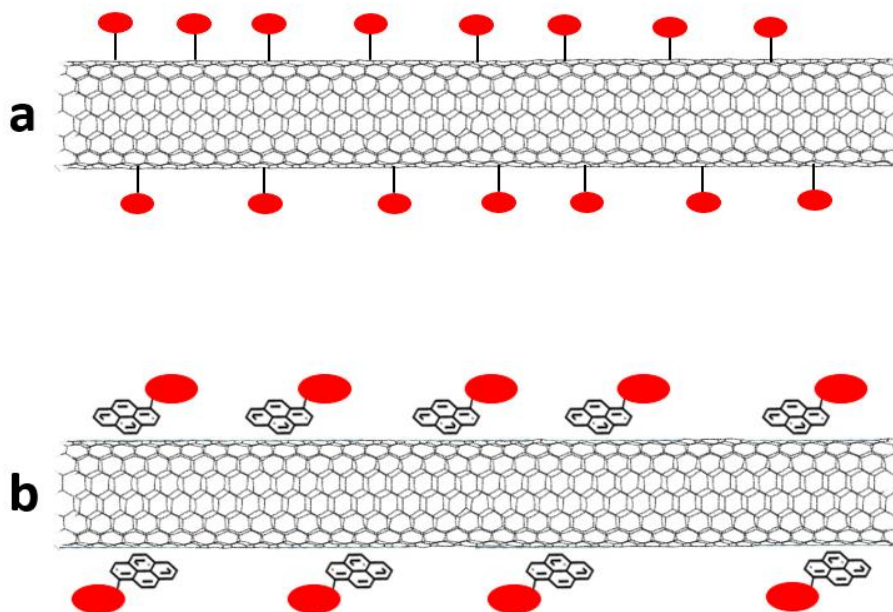


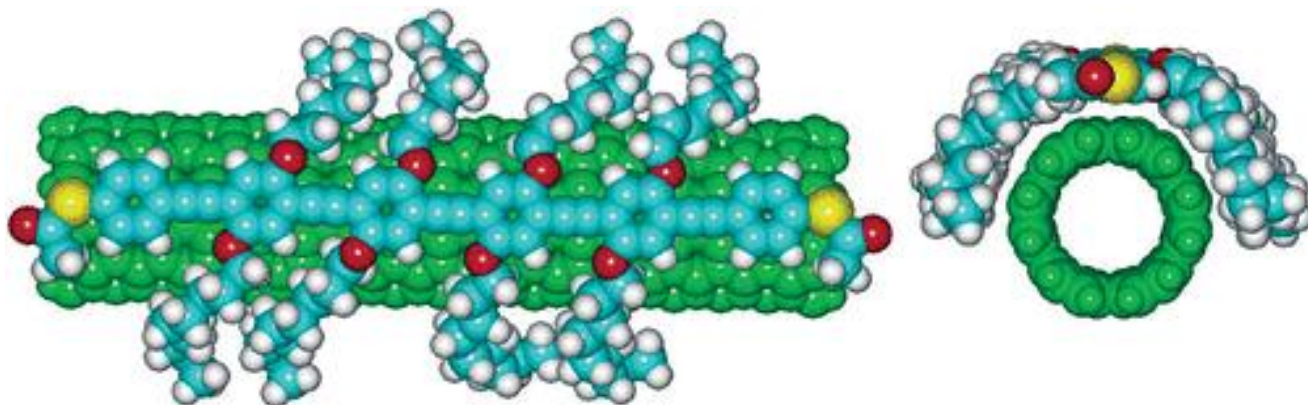
Figure 11. Simplified schematic of a) covalent and b) noncovalent functionalization.

Covalent functionalization involves the formation of a covalent bond between the nanotube wall and an external group, leading to the local disruption of the  $sp^2$  structure and alteration of the electronic properties of the CNT. Therefore, it has been shown to result in an increased degree of defects in the structure of carbon nanotubes, as well as the destruction of the delocalized  $\pi$  electron system of the graphite layers.<sup>76</sup>

This method has been widely used for attaching various organic or polymeric molecules onto carbon nanotubes, primarily focusing on dispersion or dissolution properties.<sup>77</sup> Additionally, covalent functionalization has been explored for applications in photovoltaics and biology, demonstrating its versatility and potential in various fields. For instance, covalent functionalization of carbon nanotubes with matrix polymers has been shown to be an effective approach for producing high-quality polymeric carbon nanocomposite materials.<sup>78–82</sup>

On the other hand, noncovalent functionalization involves the bonding of external groups to the graphitic structure of CNTs through extended  $\pi$  orbital systems, such as  $\pi$ - $\pi$  interactions, without significantly disrupting the electronic structure of the CNT.<sup>77</sup> This method has been

recognized as a nondestructive process for property engineering of carbon nanostructures.<sup>80</sup> Figure 12 schematically shows the creation of new nanohybrids through this method.



*Figure 12. A molecular model of a SWCNT(6,6) noncovalently functionalized by an external group<sup>83</sup> (with permission).*

Noncovalent functionalization offers advantages such as high solubility of small-diameter SWCNTs and superior control of the relative placement of functionalities on the nanotube surface.<sup>81</sup> Furthermore, noncovalent functionalization has been utilized to impart water solubility and chemical functionalities to carbon nanotubes, making them suitable for a wide range of applications.<sup>82</sup>

Through noncovalent functionalization techniques, various types of CNTs can be dispersed in organic solvents, introducing neutral and ionic functional groups onto their surfaces, and enhancing adsorption affinity for specific nanotube species with certain surfactants.<sup>83,84</sup> This approach has played a crucial role in the development of highly specific electronic biosensors, glucose biosensors, and the immobilization of diverse biological molecules on nanotube sidewalls.<sup>85,86</sup>

Noncovalent functionalization of SWCNT sidewalls has been successfully achieved for the immobilization of diverse biological molecules.<sup>87</sup> As shown in Figure 13, another innovative

method involves noncovalent functionalization through polymerization in micelles, combining the advantages of both covalent and noncovalent methods without their principal drawbacks.<sup>88</sup>

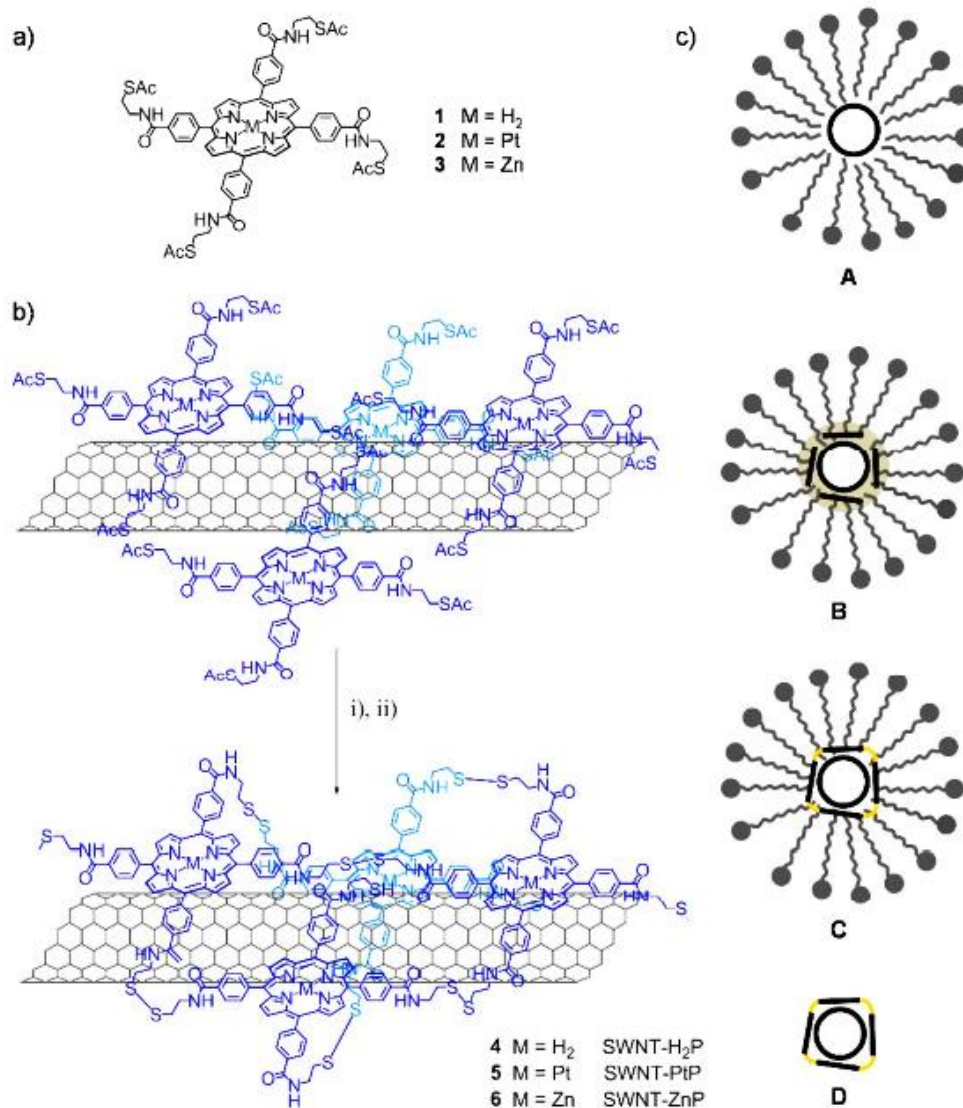


Figure 13. a) Structure of porphyrins 1-3; b) i) hydroxylamine 50 wt. % in water, Et<sub>3</sub>N, 2h, RT; ii) O<sub>2</sub>, RT overnight; c) schematic representation of the different steps of functionalization: A) the nanotubes are dispersed and individualized in micelles; B) the porphyrins in an organic solvent are introduced on the nanotube surfaces; C) after solvent evaporation, the reaction to cross-link the porphyrin is performed leading to a stable organic shell around the nanotubes; D) the nanotube derivatives are purified via filtration and extensive washing to remove the surfactants, reagents and unbound porphyrins<sup>88</sup> (with permission).

Moreover, noncovalent functionalization can result in enhancing the conductivity of polymer/SWCNT composites compared to untreated SWCNTs, underscoring its impact on the electrical characteristics of SWCNT-based materials.<sup>89</sup>

In optical SWCNT-based devices, noncovalent functionalization proves indispensable, given that covalent methods risk compromising the intrinsic fluorescence of SWCNTs, making the noncovalent route imperative for preserving optical qualities.<sup>90</sup> Additionally, the strategic use of semiconducting oxides in noncovalent functionalization stands out as a sought-after technique, introducing a synergistic effect for efficient heterostructure charge transfer and influencing the band structure and doping of SWCNTs.<sup>91</sup>

The conversion of SWCNTs into an air-stable n-type form has been achieved through noncovalent functionalization using organic nitrogen-containing electron donors such as polyethyleneimine (PEI) and reduced benzyl viologen (BV).<sup>92</sup> Various methods, including noncovalent modification with organic compounds, have been employed to achieve ammonia plasma-induced n-type doping of semiconducting carbon nanotube films.<sup>93</sup> A study on the n-type doping of SWCNTs with the reducing agent sodium borohydride ( $\text{NaBH}_4$ ) has suggested the potential for creating simple salt-coordinated n-type nanocarbon materials that are stable in air.<sup>94</sup>

Beyond noncovalent functionalization, the literature delves into the influence of doping on the electronic properties of SWCNTs. Notably, N-doped pristine SWCNTs have been suggested as potential candidates for sensing the presence of formaldehyde.<sup>95</sup> Furthermore, the controlled formation of carbon nanotube junctions in aqueous solution through linker-induced assembly has been explored, indicating the possibility of achieving controlled doping through specific assembly methods.<sup>96</sup>

### 1.3. Characterization of noncovalent functionalized CNTs

Characterization of functionalization is an important part of this project and is a necessary step toward the development of sensors. In this project, a combination of different microscopic and spectroscopic methods was used to characterize the efficient functionalization method, and compare different methods.

In this section, Raman spectroscopy and Transmission Electron Microscopy (TEM) will be discussed as tools to characterize the physics and chemistry of noncovalent functionalization of CNTs.

Composite materials resulting from noncovalent functionalization have been studied using different characterization methods.<sup>97-99</sup> Spectroscopic and microscopic methods are important in comprehensively characterizing the noncovalent functionalization of carbon nanotubes, providing essential insights into the structural and chemical changes inherent in the process.

#### 1.3.1. Raman spectroscopy to study noncovalent functionalization

Raman spectroscopy has been widely used as a powerful and nondestructive technique for characterizing the structural properties and local environment of CNTs.<sup>100</sup> The Raman spectra of CNTs are affected by noncovalent functionalization, leading to changes in various bands such as the radial breathing mode (RBM), tangential mode (G-band), and disordered mode (D-band).<sup>101</sup> These changes are attributed to the chemical oxidation of CNTs and the introduction of functional groups on the CNTs' surface.<sup>102</sup>

Raman spectroscopy has been employed to validate the surface integrity of CNTs after noncovalent functionalization. In Figure 14, a higher D/G ratio indicates increased surface defects or  $sp^3$  hybridized carbon. Carbon fibers typically exhibit high D/G ratios due to numerous  $sp^3$  sites on their surface. Spectral traces for carbon-fiber microelectrodes (CFMEs), CNT-P, and CNT-F electrodes showed variations in the average D/G ratio. While CFME and



CNT-F had significantly higher ratios than CNT-P, suggesting more defect sites, CFME and CNT-F exhibited similar degrees of defect sites. CNT-P electrodes displayed a higher degree of  $sp^2$  hybridization compared to CFME and CNT-F, attributed to their few-walled nature. Raman analysis of unpolished CNT-P electrodes validated that the polishing procedure did not significantly alter the surface. Additionally, a  $G'$  peak observed at  $2800\text{ cm}^{-1}$  for CNT fibers represents graphene or graphite layers, but its correlation to disorder degree is not straightforward.<sup>103</sup>

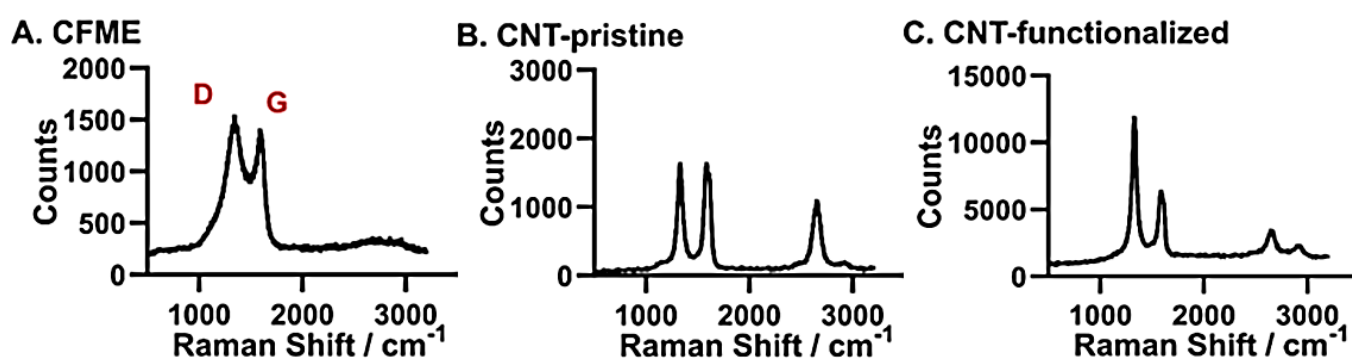


Figure 14. Raman spectra of (A) Carbon-fiber microelectrode, (B) CNT-P, and (C) CNT-F electrodes<sup>103</sup> (with permission).

The use of Raman spectroscopy in characterizing noncovalent functionalization of CNTs is further supported by its ability to provide information regarding the microstructure of carbon-based materials without destructing the sample.<sup>104</sup> This technique has also been utilized to detect any charge transfer between CNTs and other materials, such as silver nanoparticles, indicating its effectiveness in studying the electronic properties of CNTs after functionalization.<sup>105</sup> Furthermore, Raman spectroscopy has been employed to study the interfacial properties between CNTs and polymer matrices, demonstrating its significance in characterizing the interactions between CNTs and different materials, as Figure 15 illustrates the impact of different applied strains on the positioning of the 2D band.<sup>106</sup>



Moreover, Raman spectroscopy has been used to evaluate the crystalline property of CNTs and to estimate the load-bearing capability and microstructural changes of macroscopic-scale CNT architectures during tensile deformation, highlighting its role in assessing the mechanical properties of functionalized CNTs.<sup>107</sup> Raman spectroscopy has also been employed to characterize the distribution of CNTs in polymer composites, providing valuable insights into the homogeneity and dispersion of CNTs within the composite materials.<sup>108</sup>

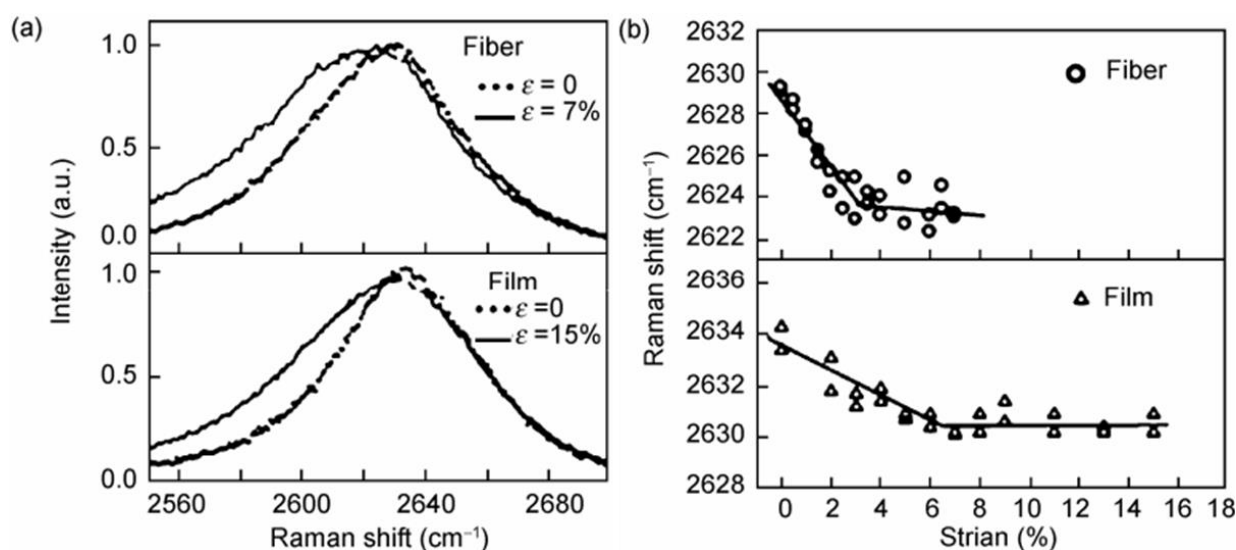


Figure 15. Typical 2D-band Raman spectra of a strained CNT film and fiber. (a) Comparison of the Raman spectra for unstrained and max-strained film and fiber. (b) Raman shift of the 2D band as a function of applied strain.<sup>106</sup>

As shown in Figure 16.a, using 2D spectral imaging helped find large clumps of CNTs for detailed study later on. Raman line scans were conducted, starting from these clumps and moving into the area where the CNTs were spread out, to study the border region. Figure 16.b shows one of these scans, with a set of Raman spectra spaced out in sequence. A piezo scanner was utilized to move in steps of 1  $\mu\text{m}$ , ensuring accuracy during the examination.

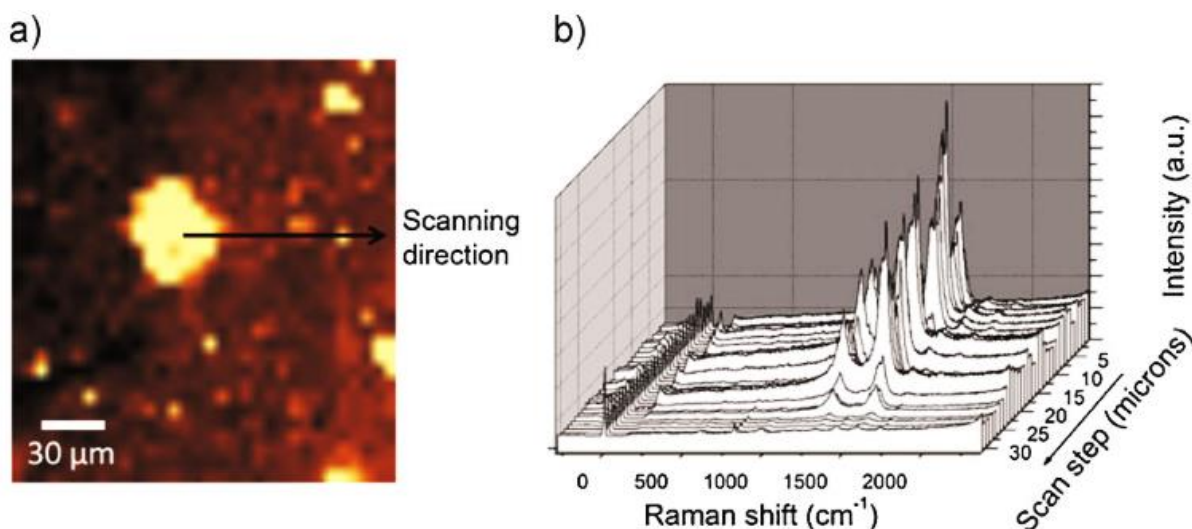


Figure 16. Raman spectral map of CNT-PMMA composite (a) indicating CNT aggregates (bright spots). The blue arrow denotes direction of the spectral line scan (b) starting in the aggregate and ending in the dispersed area. Each spectrum in (b) corresponds to one step scan of 1 mm. Spectra were collected at 1.96 eV photon excitation energy.<sup>108</sup>

### 1.3.2. Transmission Electron Microscopy (TEM)

Transmission Electron Microscopy (TEM) is a powerful tool for characterizing the noncovalent functionalization of CNTs. Cryogenic TEM is particularly useful for determining the morphology of dilute phases of CNT-laden fluids.<sup>109</sup> TEM can be used to characterize conducting composites based on CNTs and discuss the role of noncovalent functionalization on their properties.<sup>110</sup> TEM images reveal the dispersion of silicon nanoparticles inside the hollow core of CNTs, demonstrating its capability to visualize the internal structure of CNT composites.<sup>111</sup> Furthermore, TEM has been employed to visualize single CNTs inside cells and investigate the CNT-cell interaction over time.<sup>112</sup>

Moreover, TEM has been used to measure CNT diameter and length, showing its effectiveness in studying CNT length distribution.<sup>113</sup> TEM has been utilized to image CNTs after noncovalent functionalization for siRNA delivery, demonstrating its applicability in visualizing functionalized CNTs.<sup>114</sup>

TEM has also been used to investigate the interface between CNT arrays and catalyst/support layers, providing new insights into CNT forest growth<sup>115</sup> as shown in Figure 17.

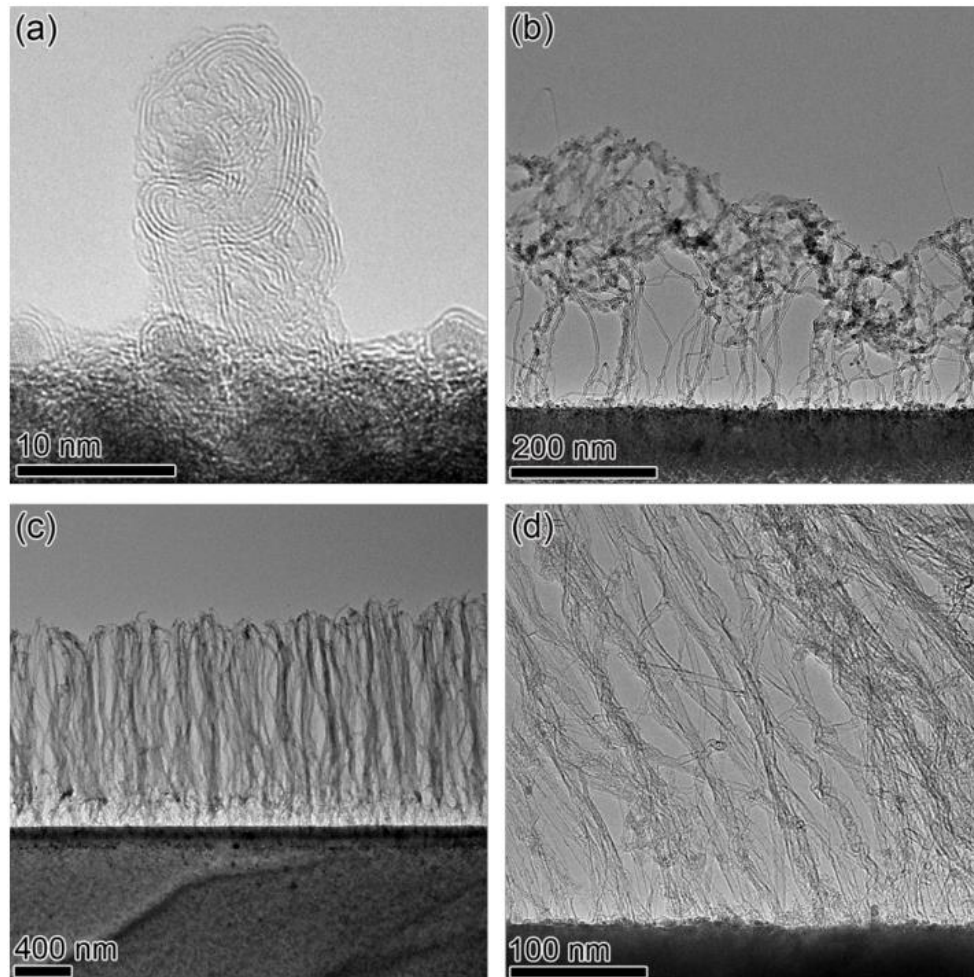


Figure 17. TEM images of the membrane samples after growing CNT forests for (a) 3 min, (b) 3.5 min, (c) 5 min, and (d) 10 min at 740 °C. (Note: each image has a different scale bar)<sup>115</sup> (with permission).

## 1.4. Sensors based on CNTs

Sensors, essential devices for detecting and responding to specific inputs from the physical environment, are composed of three primary components: the receptor, the transducer, and the

signal processor. The receptor's role is to identify the stimulus, as seen in chemical sensors, where it recognizes chemical compounds.<sup>116</sup> The transducer converts the detected stimulus into an electrical signal, facilitating further processing and analysis.

CNTs have been used in the creation of diverse sensor types, including strain, gas, humidity, ionization, temperature, and biosensors. These sensors have consistently exhibited remarkable capabilities, including high sensitivity, flexibility, and multifunctionality.<sup>117-123</sup> Leveraging the high surface area of CNTs facilitates efficient adsorption of gas molecules, resulting in heightened sensitivity and selectivity in gas sensing applications.<sup>124</sup> Moreover, the integration of CNT-based sensors into flexible and stretchable substrates has enabled the creation of wearable and conformable sensor devices, particularly for characterizing human joints and detecting motion.<sup>125,126</sup>

CNTs are also well-suited for piezoresistive strain sensors, where they demonstrate both high sensitivity and resistance to hysteresis under cyclic loading.<sup>126,127</sup> Furthermore, exploration of CNT-based sensors has extended to potential biomedical applications, including neurotransmitter detection and characterization of human joint motion.<sup>122,125</sup>

Despite their numerous advantages, challenges confront CNT-based sensors. A notable limitation is the presence of flicker noise, which can impact the resolution of these sensors.<sup>128,129</sup> Endeavors have been undertaken to alleviate this noise and enhance the overall performance of CNT-based sensor systems.<sup>129</sup> Additionally, the integration of CNT-based sensors with conventional microelectronics has presented challenges due to unpredictable device characteristics, impeding their reliable and widespread deployment.<sup>122</sup>

In this section two transduction mechanisms will be discussed in more details due to their relevance to the goal of this project. Electrochemical transduction is utilized in different benchmark sensors and the research on CNT-based electrochemical sensor for detection of water analytes is advanced. On the other hand, due to some limitation in the preparation, cost, and remote applications of electrochemical sensors, electrical transduction becomes more interesting and is the focus of the last chapter of this work.

### 1.4.1. Electrical transduction sensors

There are a variety of electrical sensors designed for diverse applications, each employing electrical or electronic principles to convert physical stimuli into understandable signals. Among these sensors are electrochemical sensors, chemiresistive sensors, field-effect transistors, piezoresistive sensors, capacitive sensors, piezoelectric sensors, and several specialized variants.

Piezoresistive sensors operate by translating changes in resistance resulting from external pressure into an electrical signal.<sup>130</sup> Widely used in pressure sensing applications, they boast high sensitivity and rapid response times.

Capacitive sensors, on the other hand, detect and measure physical quantities like pressure, humidity, and fluid levels through alterations in capacitance. Renowned for their high resolution and low power consumption, capacitive sensors serve a broad range of functions. Piezoelectric sensors generate an electrical charge when subjected to mechanical stress, making them ideal for monitoring vibrations and acceleration.<sup>130</sup> There are also strain sensors utilizing CNTs and Bucky paper, showcasing isotropic and anisotropic electrical behaviors, respectively.<sup>131</sup> These sensors are invaluable for measuring mechanical deformation and conducting structural health monitoring.

Due to their importance in the development of sensors for environmental and health-related analysis, three types of electrical sensors will be explained, highlighting their working function and different use cases. These sensor types are electrochemical sensors, field-effect transistors, and chemiresistive sensors.

#### 1.4.1.1. Electrochemical sensors

CNT-based electrochemical sensors offer various transduction options, including electrochemical, resistive, field-effect-based, and electromechanical, making them versatile

for monitoring a wide range of chemicals in water. When modified with inorganic nanomaterials, CNTs have been extensively studied for their application in electrochemical sensors.<sup>132</sup> These sensors are based on the principle of electrochemical transduction, where the interaction between the analyte and the modified CNTs leads to a measurable electrical signal. The functionalization of CNTs with various transduction materials has enabled the development of both nonaligned and aligned CNT electrodes for electrochemical sensors.<sup>133</sup>

The applications of CNT-based electrochemical sensors extend to the analysis of biological substances and drugs, as well as the construction of enzyme-based electrochemical biosensors.<sup>134</sup> These sensors have also been explored for their potential use in wearable or implantable biomedical sensor applications due to the excellent mechanical flexibility and biocompatibility of CNTs.<sup>135</sup> Functionalization of CNTs provides control over their surface reactivity, dispersion, and active sites, which is crucial for efficient electrochemical redox response in sensors.<sup>136</sup>

CNT-based electrochemical sensors have been employed for the detection of various compounds, including glucose, phenolic compounds, and toxic chemicals, showcasing their high sensitivity, stability, and cost-effectiveness.<sup>137–139</sup> The modification of electrodes with CNTs has been shown to enhance the electrocatalytic activity, enabling the simultaneous determination of multiple analytes.<sup>140</sup> Additionally, the fabrication of inexpensive and flexible electronic and electrochemical sensors using CNTs is in high demand for a wide range of biochemical and biomedical applications.<sup>141</sup>

As Figure 18 shows, a composite structure, comprising Cu nanoparticles (NPs) deposited onto carbon nanotubes and modified with ferrocene-branched chitosan, was developed to create a nonenzymatic electrochemical glucose biosensor (Fc-CHIT/CNT@Cu). The composition, morphology, and structure of the carbon nanohybrids were characterized using various techniques. Electrochemical impedance spectroscopy (EIS), cyclic voltammetry (CV), and chronoamperometry methods were employed to evaluate the biosensing properties of glucose. The electrode exhibited significant glucose sensitivity, with a wide linear detection range (0.2 mM to 22 mM), low detection limit (13.52  $\mu\text{M}$ ), and high sensitivity (1.256  $\mu\text{A mM}^{-1}\text{cm}^{-2}$ ), attributed to the synergistic effect of Cu NPs and ferrocene. Additionally, the modified

electrode demonstrated long-term stability and selectivity in the presence of interfering substances. The electrode's low cost and robust performance suggest its potential for practical application in non-enzymatic electrochemical glucose detection.

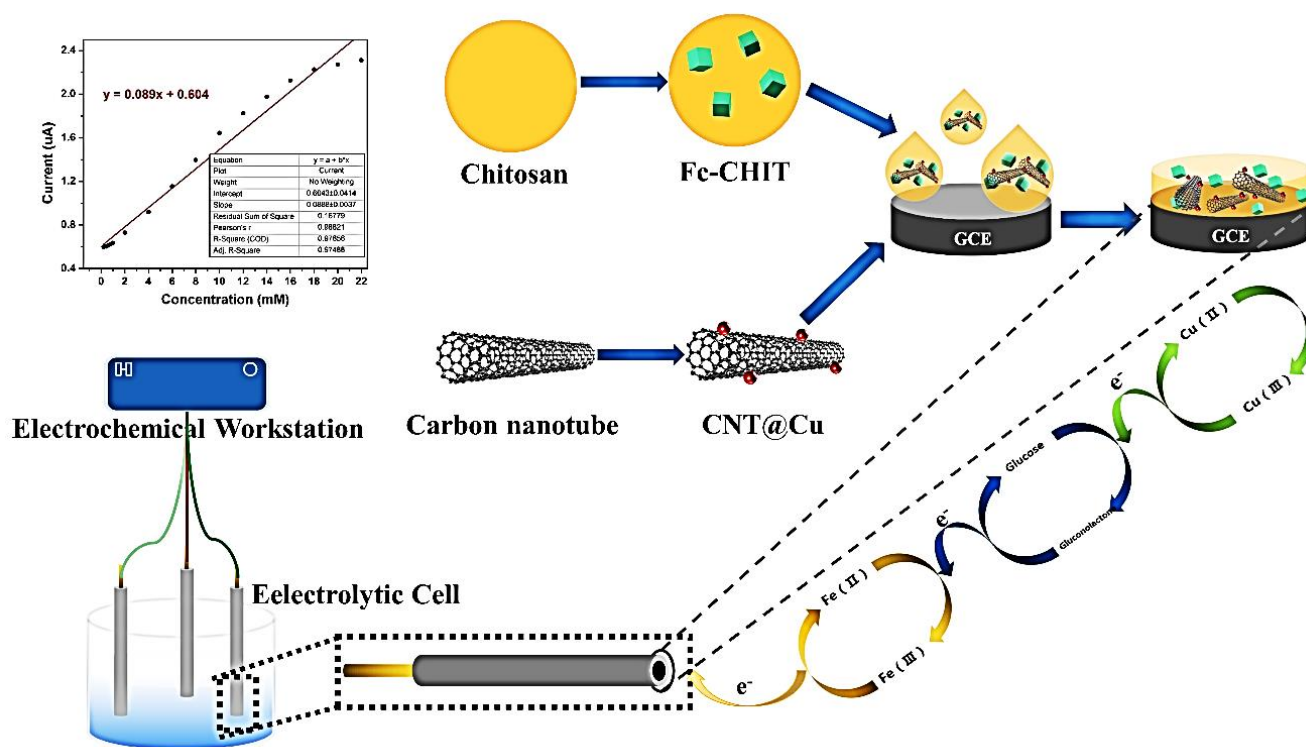


Figure 18. The working mechanism of a CNT-based electrochemical sensor<sup>142</sup> (with permission).

The exceptional material properties of CNTs, such as unique electrical/thermal conductivity, biocompatibility, and high quenching efficiency, make them well-suited for both electrical/electrochemical and optical sensors/biosensors.<sup>143</sup> CNTs have also been widely used in electrochemical sensors and thermocells due to their excellent electrochemical, mechanical, chemical, electrical, and thermal properties.<sup>144</sup>



### 1.4.1.2. Field Effect Transistor (FET)

A field-effect transistor (FET) is an electronic device comprising a semiconducting layer, known as the channel, that connects a source and a drain electrode. A simplified schematic of FETs is illustrated in Figure 19. The density of electronic carriers flowing between the source and drain electrodes is controlled by the potential of a third electrode, the gate electrode, insulated from the active layer by a dielectric material.

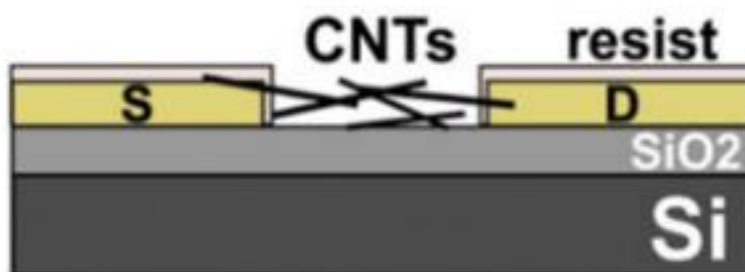


Figure 19. Simplified topology of a FET (CNT ChemFET) showcasing a bottom gate structure.<sup>145</sup>

When this setup is used for chemical sensing, it's termed a chemical FET (chemFET), where the conduction characteristics are influenced by the presence and concentration of surrounding electrolytes. While the semiconducting channel is typically the primary chemically sensitive layer, the electrodes and dielectric layer can also contribute to sensitivity. In electrolyte-gated chemFETs, the target liquid itself acts as the gate and dielectric layer.

ChemFETs detect chemicals through short-range interactions between the analyte and the active layer.<sup>146</sup> However, chemFETs offer a broader range of parameters for analysis, including current, resistance, transconductance, threshold voltage, and hysteresis during gate voltage sweeps. This makes chemFETs more sensitive and selective than chemistors but also necessitates a more complex fabrication procedure and operating electronics.<sup>147,148</sup>

CNT-FETs utilize a CNT layer as the channel, with SWCNTs preferred for their semiconducting properties. SWCNTs may require pre-processing or post-processing to ensure



semiconductor behavior.<sup>149</sup> CNT-FET channels can consist of a single SWCNT or a network of them. While single SWCNT devices offer remarkable electrical performance, random networks of SWCNTs are favored for sensing applications due to their larger sensing area, simpler fabrication, and better scalability, despite slightly inferior electrical performance.<sup>150</sup>

There are four architectures for CNT-FET chemical sensors: top gate, bottom gate, liquid gate, and hybrid structures. Bottom gate structures require high gate voltages leading to water hydrolysis in water quality monitoring applications. Top gate structures, although requiring lower operating gate voltages, are less common due to insulation of the sensitive channel. Liquid gate structures, applying the gate voltage through surrounding electrolyte, offer lower-voltage operation and simplified fabrication. Hybrid structures combine various gating strategies for enhanced performance. Dielectric materials like  $\text{SiO}_2$ ,  $\text{Al}_2\text{O}_3$ , or  $\text{Si}_3\text{N}_4$  are commonly used between the semiconducting channel and the substrate or gate electrode, with different materials offering trade-offs in thickness, homogeneity, and durability.

### 1.4.1.3. Chemiresistive sensor

A resistor functions based on the Ohm's Law, where  $V = I \cdot R$ ,  $V$  being the voltage across the conductor in volts (v),  $I$  being the current flowing through the conductor in amperes (A), and  $R$  being the resistance of the conductor in ohms ( $\Omega$ ).

In a resistive sensor, a conductive material fills the space between two electrodes to create a full circuit. The resistance of the sensor changes when a change to the properties of the material happens. If the changes have a chemical nature (exchange of electrons and energy), the resistive sensor is called a chemiresistive sensor or a chemistor.

The unique electrical conductivity and one-dimensional structure of CNTs make them ideal for constructing chemiresistive sensors with rapid response times and exceptional performance in different sensing applications.<sup>151</sup> Figure 20 shows the simplified structure of a chemiresistive sensor based on CNT. The random network of CNTs act as a conductor with a

specific resistance. If a chemical interaction happens between the CNT network and analytes in the environment, the resistance of the network changes, and therefore, the measured current changes proportionally, according to the Ohm's Law.

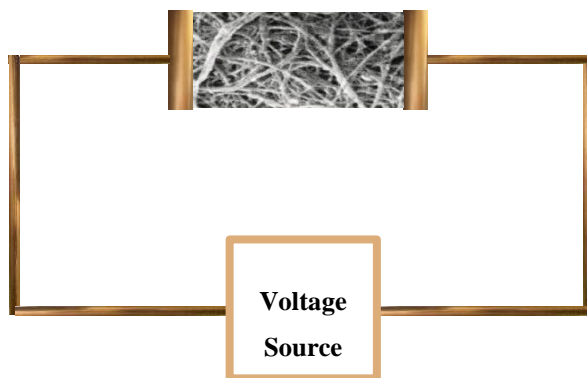


Figure 20. Schematic of a chemiresistive sensor based on CNT.

CNT-based chemiresistive sensors are valued for their ease of fabrication, compact size, and remarkable sensitivity, rendering them adept at detecting a wide array of analytes.<sup>152</sup> Chemiresistive sensor arrays employing SWCNTs functionalized with metalloporphyrins complexes have exhibited interesting performance in volatile organic compounds and amine detection.<sup>153,154</sup> Moreover, chemiresistive sensors leveraging CNTs have proven effective in detecting nerve agents, glucose, and a variety of toxic gases.<sup>155–157</sup> CNTs have been employed in the detection of specific analytes such as methane, ammonia, and hydrogen peroxide as well.<sup>158–160</sup> Additionally, integrating CNTs with other materials like metal oxides and polymers has led to the development of hybrid sensors with heightened sensitivity and selectivity.<sup>161,162</sup>

CNT-based chemiresistive sensors offer numerous advantages, including high sensitivity, low detection limits, and the ability to integrate multisensory arrays for simultaneous detection of multiple analytes.<sup>163</sup> They have also been instrumental in the creation of wireless and wearable devices for real-time monitoring of hazardous gases and environmental pollutants.<sup>164</sup>

In addition to their sensing capabilities, research has focused on optimizing the electrode structures of CNT-based chemiresistive sensors to enhance sensitivity and gas sensing performance.<sup>165</sup> Furthermore, exploring the functionalization of CNTs with specific molecules and polymers has been instrumental in tailoring their sensing properties for the detection of target analytes such as hydrogen peroxide and toxic chemicals.<sup>160,166</sup>

## 1.5. Drinking water analytes and sensors

### 1.5.1. Drinking water analytes

Chemical contaminants, including heavy metals, pesticides, and organic compounds are the most dominant water pollutants. They can originate from industrial activities, agricultural practices, and urban runoff.<sup>167</sup> Nutrients such as nitrogen and phosphorus are other common nonpoint source pollutants that can lead to eutrophication and harmful algal blooms in water bodies.<sup>168</sup> Furthermore, microbial pollutants, including bacteria and pathogens from sewage and agricultural runoff, pose significant risks to water quality and human health.<sup>169</sup>

Measuring the pH and the level of dissolved oxygen in water is crucial for assessing water quality and understanding the health of aquatic ecosystems. Dissolved oxygen is a critical parameter that serves as an indicator of water quality and is essential for the survival of aquatic organisms. The concentration of dissolved oxygen directly impacts the metabolic processes of aquatic organisms and is a key factor in the self-purification capacity of water bodies.<sup>170</sup> It is of great significance in various fields such as industrial production, environmental monitoring, aquaculture, and food production.<sup>171</sup> Additionally, the measurement of dissolved oxygen is a primary parameter in pollution studies and is used to assess the strength of pollutants in natural and waste waters.<sup>172</sup>

Furthermore, the pH of water is a fundamental parameter that influences chemical and biological processes in aquatic environments. It is an important factor in determining the suitability of water for various uses, including drinking water, irrigation, and industrial

processes.<sup>173</sup> The pH level affects the solubility of nutrients and heavy metals, as well as the biological availability of various chemical species in water.<sup>174</sup> Moreover, pH is a critical factor in the growth and survival of aquatic organisms, as it can impact their physiological functions and overall health.<sup>175</sup>

Table 1 summarizes the common drinking water analytes that require constant monitoring. In this table the Maximum Acceptable Concentration (MAC) of each analyte based on the regulations from Canadian government, US government, European union, and the World Health Organization (WHO) is presented.

*Table 1. Critical chemical parameters in qualifying drinking water.<sup>8</sup>*

<b>Maximum acceptable concentration (MAC)</b>				
<b>Parameter</b>	<b>Canada</b>	<b>USA</b>	<b>Europe</b>	<b>WHO</b>
<b>pH</b>	<b>Range 7~10.5</b>	<b>Range 6.5~8.5</b>	<b>Range 6.5~9.5</b>	<b>Range 6.5~8.5</b>
<b>Water hardness &amp; Micronutrients</b>				
<b>Boron</b>	<b>5 ppm</b>	<b>-</b>	<b>1 ppm</b>	<b>500 ppb</b>
<b>Cadmium</b>	<b>5 ppb</b>	<b>5 ppb</b>	<b>5 ppb</b>	<b>3 ppb</b>
<b>Copper</b>	<b>1 ppm</b>	<b>1.3 ppm</b>	<b>2 ppm</b>	<b>2 ppm</b>
<b>Iron</b>	<b>300 ppb</b>	<b>300 ppb</b>	<b>200 ppb</b>	<b>-</b>
<b>Manganese</b>	<b>50 ppb</b>	<b>50 ppb</b>	<b>50 ppb</b>	<b>400 ppb</b>
<b>Zinc</b>	<b>5 ppm</b>	<b>5 ppm</b>	<b>-</b>	<b>-</b>
<b>Disinfectants &amp; Chlorine</b>				
<b>Chloramines</b>	<b>3 ppm</b>	<b>4 ppm</b>	<b>-</b>	<b>3 ppm</b>
<b>Free chlorine</b>	<b>-</b>	<b>4 ppm</b>	<b>-</b>	<b>0.5~5 ppm</b>
<b>Chlorine dioxide</b>	<b>-</b>	<b>800 ppb</b>	<b>-</b>	<b>-</b>

<b>Chlorate</b>	<b>1 ppm</b>	<b>1 ppm</b>	<b>-</b>	<b>700 ppb</b>
<b>Chloride</b>	<b>250 ppm</b>	<b>250 ppm</b>	<b>250 ppm</b>	<b>-</b>
<b>Chlorite</b>	<b>1 ppm</b>	<b>1 ppm</b>	<b>-</b>	<b>700 ppb</b>
<b>Nitrogen</b>				
<b>Ammonia/ammonium</b>	<b>-</b>	<b>-</b>	<b>500 ppb</b>	<b>-</b>
<b>Nitrate</b>	<b>45 ppm</b>	<b>45 ppm</b>	<b>50 ppm</b>	<b>50 ppm</b>
<b>Nitrite</b>	<b>3 ppm</b>	<b>3 ppm</b>	<b>500 ppb</b>	<b>3 ppm</b>
<b>Sulfur</b>				
<b>Sulfate</b>	<b>500 ppm</b>	<b>250 ppm</b>	<b>250 ppm</b>	<b>-</b>
<b>Sulfide</b>	<b>50 ppb</b>	<b>-</b>	<b>-</b>	<b>-</b>
<b>Heavy metals, other contaminants</b>				
<b>Aluminum</b>	<b>200 ppb</b>	<b>200 ppb</b>	<b>200 ppb</b>	<b>-</b>
<b>Antimony</b>	<b>6 ppb</b>	<b>6 ppb</b>	<b>5 ppb</b>	<b>20 ppb</b>
<b>Arsenic</b>	<b>10 ppb</b>	<b>10 ppb</b>	<b>10 ppb</b>	<b>10 ppb</b>
<b>Barium</b>	<b>1 ppm</b>	<b>2 ppm</b>	<b>-</b>	<b>700 ppb</b>
<b>Beryllium</b>	<b>-</b>	<b>4 ppb</b>	<b>-</b>	<b>-</b>
<b>Bromate</b>	<b>10 ppb</b>	<b>10 ppb</b>	<b>10 ppb</b>	<b>10 ppb</b>
<b>Chromium</b>	<b>50 ppb</b>	<b>100 ppb</b>	<b>50 ppb</b>	<b>50 ppb</b>
<b>Cyanide</b>	<b>200 ppb</b>	<b>200 ppb</b>	<b>50 ppb</b>	<b>70 ppb</b>
<b>Fluoride</b>	<b>1.5 ppm</b>	<b>4 ppm</b>	<b>1.5 ppm</b>	<b>1.5 ppm</b>
<b>Lead</b>	<b>10 ppb</b>	<b>15 ppb</b>	<b>10 ppb</b>	<b>10 ppb</b>
<b>Mercury</b>	<b>1 ppb</b>	<b>2 ppb</b>	<b>1 ppb</b>	<b>1 ppb</b>
<b>Molybdenum</b>	<b>-</b>	<b>-</b>	<b>-</b>	<b>70 ppb</b>
<b>Nickel</b>	<b>-</b>	<b>-</b>	<b>20 ppb</b>	<b>20 ppb</b>

<b>Selenium</b>	<b>50 ppb</b>	<b>50 ppb</b>	<b>10 ppb</b>	<b>10 ppb</b>
<b>Silver</b>	-	<b>100 ppb</b>	-	-
<b>Thallium</b>	-	<b>2 ppb</b>	-	-
<b>Uranium</b>	<b>20 ppb</b>	-	-	<b>15 ppb</b>
<b>Small organic molecules</b>				
<b>Acrylamide</b>	-	-	<b>0.1 ppb</b>	<b>0.5 ppb</b>
<b>Benzene</b>	<b>5 ppb</b>	<b>5 ppb</b>	<b>1 ppb</b>	<b>10 ppb</b>
<b>Benzo(a)pyrene</b>	<b>0.04 ppb</b>	<b>0.2 ppb</b>	<b>0.01 ppb</b>	<b>0.7 ppb</b>
<b>Formaldehyde</b>	-	-	-	<b>900 ppb</b>
<b>Styrene</b>	-	<b>100 ppb</b>	-	<b>20 ppb</b>
<b>Toluene</b>	<b>60 ppb</b>	<b>1 ppm</b>	-	<b>700 ppb</b>
<b>Xylenes</b>	<b>90 ppb</b>	<b>10 ppm</b>	-	<b>500 ppb</b>
<b>Halogenated organic molecules</b>				
<b>Carbon tetrachloride</b>	<b>2 ppb</b>	<b>5 ppb</b>	-	<b>4 ppb</b>
<b>Chlorobenzene</b>	-	<b>100 ppb</b>	-	-
<b>1,2-Dichlorobenzene</b>	<b>200 ppb</b>	<b>600 ppb</b>	-	<b>1 ppm</b>
<b>1,4-Dichlorobenzene</b>	<b>5 ppb</b>	<b>75 ppb</b>	-	<b>300 ppm</b>
<b>1,2-Dichloroethane</b>	<b>5 ppb</b>	<b>5 ppb</b>	<b>3 ppb</b>	<b>30 ppb</b>
<b>Haloacetic acids</b>	<b>80 ppb</b>	<b>60 ppb</b>	-	-
<b>Tetrachlorophenol</b>	<b>10 ppb</b>	<b>5 ppb</b>	<b>10 ppb</b>	<b>40 ppb</b>
<b>Trihalomethanes</b>	<b>100 ppb</b>	<b>80 ppb</b>	<b>100 ppb</b>	-
<b>Vinyl chloride</b>	<b>2 ppb</b>	<b>2 ppb</b>	<b>0.5 ppb</b>	<b>0.3 ppb</b>
<b>Polycyclic aromatic hydrocarbons</b>	-	-	<b>0.1 ppb</b>	-

<b>Pesticides</b>				
<b>Pesticides (total)</b>	-	-	<b>0.5 ppb</b>	-
<b>Altrazine</b>	<b>5 ppb</b>	<b>3 ppm</b>	<b>0.1 ppb</b>	<b>100 ppb</b>
<b>Carbaryl</b>	<b>90 ppb</b>	-	<b>0.1 ppb</b>	-
<b>Carbofuran</b>	<b>90 ppb</b>	<b>40 ppm</b>	<b>0.1 ppb</b>	<b>7 ppb</b>
<b>Chlorpyrifos</b>	<b>90 ppb</b>	-	<b>0.1 ppb</b>	<b>30 ppb</b>
<b>DDT</b>	-	-	<b>0.1 ppb</b>	<b>1 ppb</b>
<b>Glyphosate</b>	<b>280 ppb</b>	<b>700 ppb</b>	<b>0.1 ppb</b>	-
<b>Picloram</b>	<b>190 ppb</b>	<b>500 ppb</b>	<b>0.1 ppb</b>	-
<b>Simazine</b>	<b>10 ppb</b>	<b>4 ppb</b>	<b>0.1 ppb</b>	<b>2 ppb</b>
<b>Triafuralin</b>	<b>45 ppb</b>	-	<b>0.1 ppb</b>	<b>20 ppb</b>

### 1.5.2. Sensing devices design and preparation

Efforts to address water pollution encompass various approaches, including regulatory measures, technological interventions, and sustainable land management practices. For instance, the implementation of water quality standards and pollution control measures is essential for reducing the discharge of contaminants into water bodies.<sup>176</sup> In this final section, first the use of inkjet printing in depositing CNT thin films will be discussed, since it is the primary deposition method for the preparation of sensing devices, and later the most recent CNT-based sensors used for the purpose of water quality analysis will be discussed.

### 1.5.2.1. Inkjet Printing

Inkjet printing has emerged as a versatile and efficient technology for various applications, particularly in the fields of electronics, biosensing, and materials science. This method involves the precise deposition of ink droplets onto a substrate, allowing for the creation of intricate patterns and structures with minimal waste. The advantages of inkjet printing include its cost-effectiveness, scalability, and ability to handle a wide range of materials, including conductive inks, polymers, and biological substances.<sup>177,178</sup> The technology has been widely adopted for the production of printed electronics, such as sensors, antennas, and circuit boards, due to its capacity for high-resolution patterning and rapid prototyping.<sup>179–181</sup>

The ability to print nanoscale materials enables the fabrication of devices with enhanced functionalities and performance. For instance, the integration of CNTs into inkjet printing processes has been explored in the review from Tortorich and Choi.<sup>182</sup> The use of inkjet printing allows for the controlled deposition of CNTs, facilitating the creation of thin films that can be tailored for specific applications in nanoelectronics and beyond.<sup>183</sup>

One of the primary benefits of inkjet printing CNTs is its ability to produce conductive patterns with low sheet resistance. For instance, demonstrated that inkjet-printed SWCNT electrodes achieved a remarkably low sheet resistance of  $132 \Omega/\square$ , which is critical for applications in electrochemical sensors. This low resistance is essential for enhancing the performance of devices, as it allows for efficient charge transport. Additionally, the stability of the printed films over time, provided they are not mechanically damaged, further underscores the reliability of this printing technique.<sup>184</sup>

The formulation of CNT inks is crucial for successful inkjet printing. highlighted the use of ortho-dichlorobenzene as a solvent for redispersing CNTs, which facilitates the creation of high-performance FETs.<sup>185</sup> Deposition density is an important factor that controls different properties of devices based on CNTs, particularly in the case of chemiresistive devices, where the resistance of the device (directly controlled by the CNT thin film density) can be tuned by the number of printing passes. Figure 21 shows images of CNT depositions prepared by different printing passes. The number of CNT connections increase with more printing passes



illustrating the capabilities of inkjet printing in controlling electrical properties of CNT depositions.

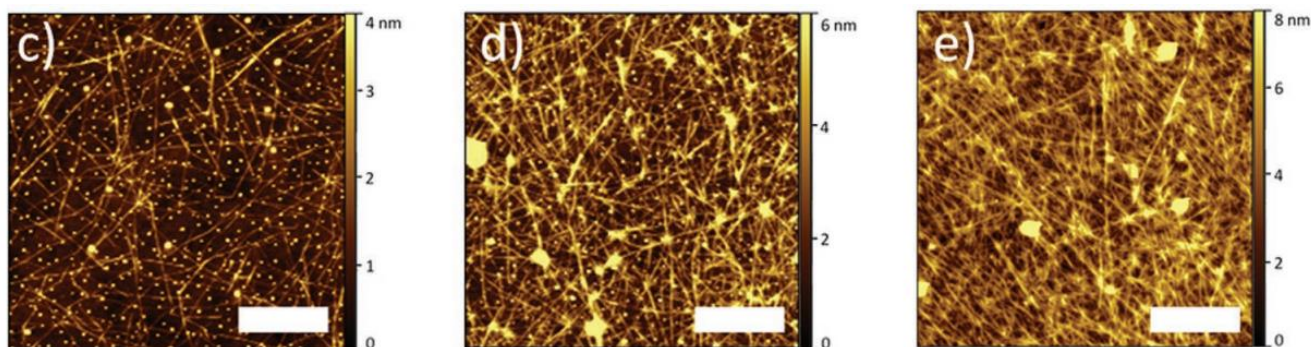


Figure 21. Topography maps of the SWCNTs networks obtained by c) one, d) three, and e) ten printing passes. Scale bars are 500 nm.<sup>185</sup>

The choice of solvent impacts the viscosity and stability of the ink, which are critical parameters for achieving uniform deposition during printing. Moreover, the incorporation of surfactants can enhance the dispersion of CNTs in the ink, preventing issues such as nozzle blockage and ensuring consistent print quality.<sup>186</sup>

Inkjet printing also allows for the fabrication of complex structures and devices. For example, Zhao *et al.* developed a strain distribution sensor using inkjet-printed CNTs, demonstrating the versatility of this technique in creating functional sensors for real-time monitoring applications.<sup>187</sup> The ability to print on various substrates, including flexible materials, expands the potential applications of CNT-based devices in wearable technology and other innovative fields.<sup>188</sup> Figure 22 shows a use case of inkjet printing in preparing complex devices, for the specific case of strain sensors.

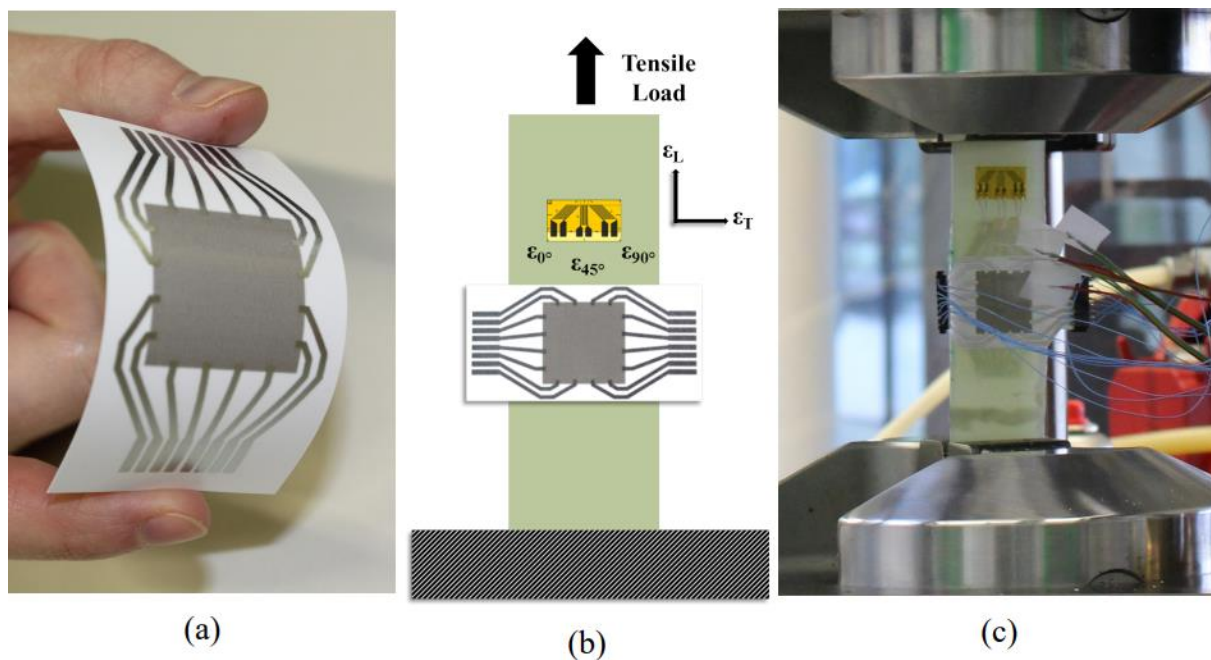


Figure 22. (a) An inkjet-printed flexible strain sensor. (b) An illustration of the tensile test coupon with applications of a strain gauge rosette and the CNT thin film. (c) The tensile test setup.<sup>187</sup> (With permission).

Furthermore, the integration of CNTs into supercapacitors has been explored extensively. reported on the successful inkjet printing of SWCNT/RuO<sub>2</sub> nanowire supercapacitors on flexible substrates, showcasing the potential for energy storage applications.<sup>189</sup> The ability to print these materials directly onto cloth fabrics and other flexible substrates highlights the adaptability of inkjet printing for energy devices that require flexibility and lightweight characteristics.

Figure 23 illustrates the process and characteristics of inkjet-printed SWCNT films on various substrates, such as cloth fabric and PET. It highlights how multiple layers of SWNT ink form dense, tangled networks on these surfaces, which can be used to create thin-film electrodes for supercapacitors without further treatment. The figure also emphasizes the trade-off between electrical conductivity and optical transparency with increased film thickness, showcasing the versatility and potential of this method for fabricating wearable electronics and other applications.

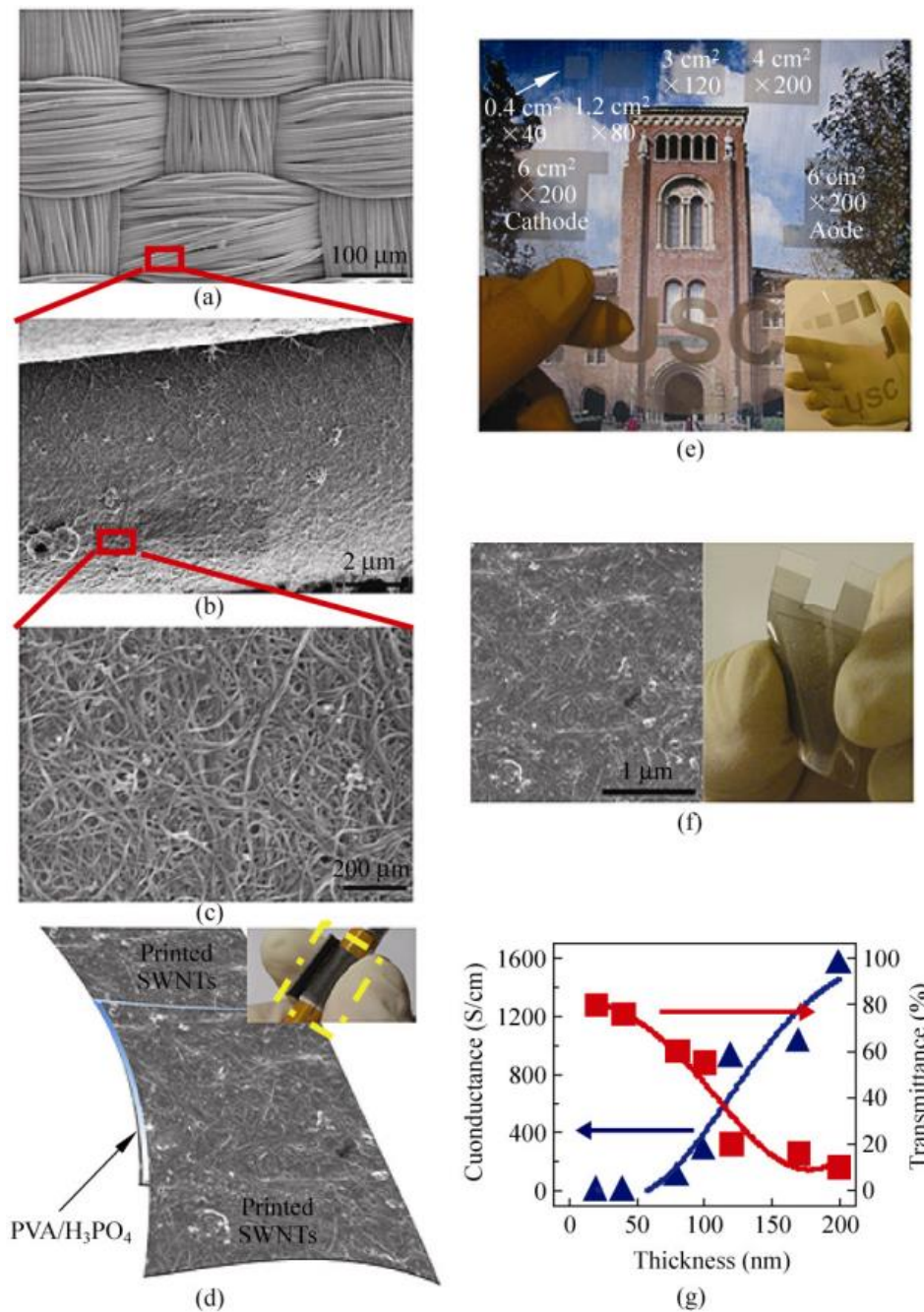


Figure 23. (a), (b), and (c) SEM images of a cloth fabric with inkjet-printed SWNT films. (d) Schematic diagram of an inkjet-printed SWCNT supercapacitor using PVA/H<sub>3</sub>PO<sub>4</sub> as solid electrolyte and separator. The inset shows a supercapacitor made of SWNT/cloth fabric electrodes rolled around a pencil. (e) Photograph of a PET substrate with nanotube films printed with different geometries and print numbers. The features on the background picture are clearly visible. (f) SEM image of inkjet-printed SWNT films on a PET substrate and a photograph of a supercapacitor built with SWNT/PET electrodes. (g) Variation of conductance and transmittance of printed SWNT films on PET substrates as a function of film thickness

In summary, inkjet printing of CNTs presents a promising avenue for the development of advanced electronic devices, sensors, and energy storage systems. The technique's ability to produce low-resistance conductive patterns, combined with the flexibility of substrate choices and the potential for complex device fabrication, positions it as a key method in the field of printed electronics.

#### **1.5.2.2. State of the art on CNT-based chemiresistive sensors for water quality analysis**

Chemiresistive sensors are used for the detection of analytes in water and the analysis of drinking water quality continuously monitoring the quality of drinking water, particularly in terms of heavy metals, toxic substances, and microbial contamination.<sup>190</sup> The assessment and monitoring of drinking water quality are essential to identify and address water quality issues promptly.<sup>191</sup>

In their interesting work, Liao et al. synthesized composite nanofibers comprising SWCNTs and polyaniline, with an initiator, offer highly tunable conductivities ( $10^{-4}$  to  $10^2$  S/cm) at up to 5.0wt % SWCNT loadings. Chemiresistive sensors made from these nanofibers, particularly those with 1.0 wt % SWCNT loading, exhibit faster responses to low concentrations (100 ppb) of HCl and NH<sub>3</sub> vapors compared to pure polyaniline nanofibers (120s vs 1000s). These SWCNT/polyaniline composite nanostructures show promise for use in low-cost disposable sensors and electrodes due to their adjustable conductivities.<sup>192</sup>

Darestani-Farahani *et al.* proposed the use of a lead-selective membrane integrated with a chemiresistive device for continuous, real-time monitoring of Pb<sup>2+</sup> ion concentrations (Figure 24). The detection limit was enhanced by stabilizing the resistive film surface along with optimizing the sensor geometry to maximize the effective surface area. The detection mechanism of their chemiresistive device relies on the complexation of Pb<sup>2+</sup> ions by lead ionophores within the membrane, which in turn modulates the interactions between the ionophores and the chemiresistive film. The fabricated devices demonstrated a reliable



detection limit below  $2 \mu\text{g/L}$ , with concentrations extending up to  $3 \text{ mg/L}$  across multiple measurement cycles. These chemiresistive sensors were able to achieve lower detection limits compared to potentiometric devices, while also being more robust and easier to fabricate due to the absence of a reference electrode. Consequently, ion-selective membrane-covered chemiresistors offer a viable solution for the continuous monitoring of drinking water sources, enabling the real-time detection of harmful lead levels.<sup>193</sup>

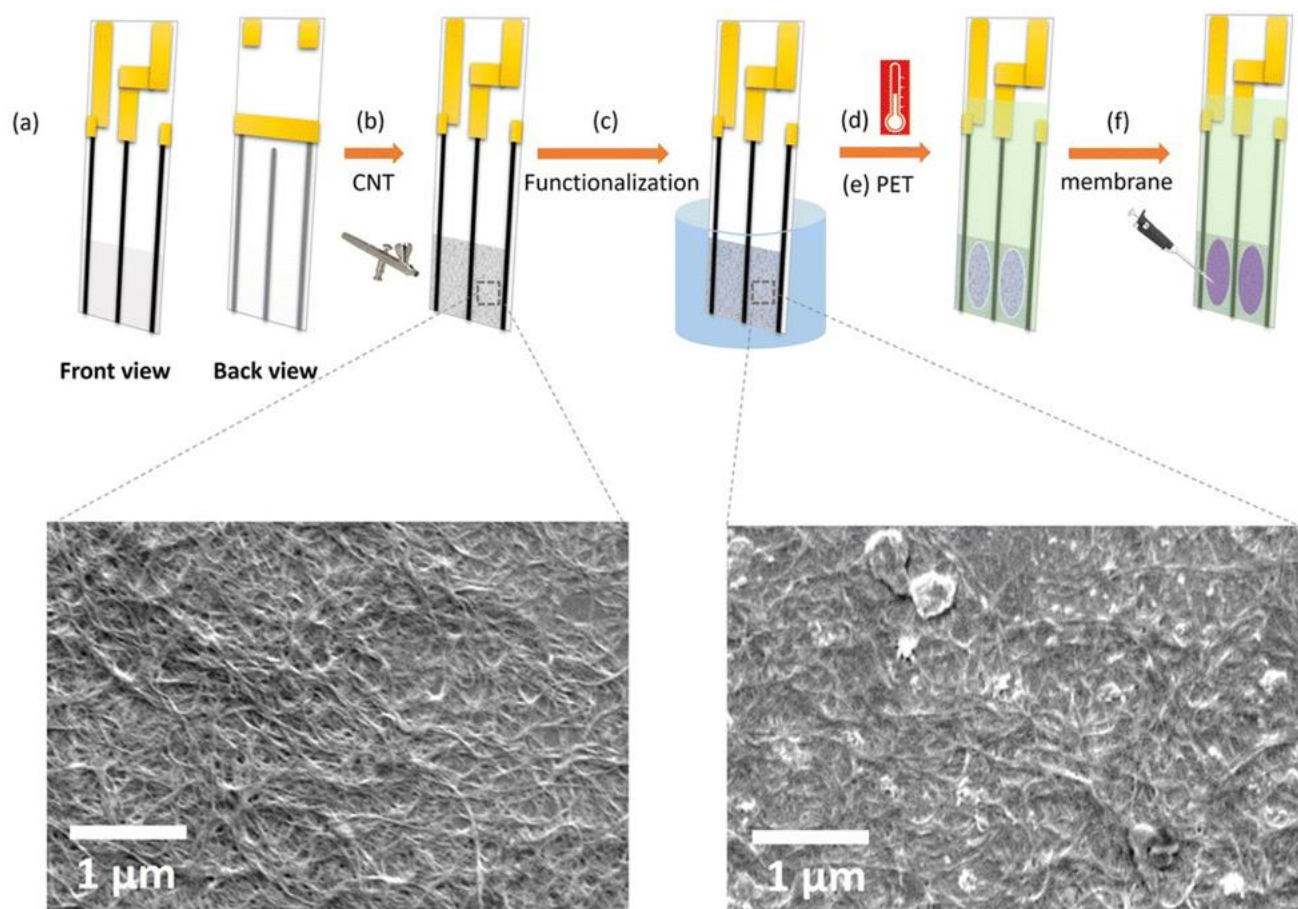


Figure 24. Sensor fabrication process. (a) Front and back views of three screen-printed contacts and copper tape connections, (b) air brushing CNT on the frosted part of the glass slide and SEM image of the resulting CNT film, (c) functionalizing the CNT film with 0.1 M of NaOH-15-crown-5 ether solution and SEM image of the resulting n-doped CNT film, (d) curing the sensor at  $85 \text{ }^\circ\text{C}$ , (e) applying pre-cut clear PET sheet to cover the contacts and have specific openings, (f) drop-casting ISM solution into the openings and drying for 12 hours.

Using Aerosol jet printing, Gou *et al.* fabricated a low-cost, flexible CNT pH sensor the schematic procedure of which is shown in Figure 25. The chemiresistive sensor features a CNT-based miniaturized serpentine sensing element atop silver electrodes, with trace width accurately controlled. Parameters are optimized for high-resolution printing (20  $\mu\text{m}$ ). The sensor exhibits good sensitivity (up to 59  $\text{k}\Omega/\text{pH}$ ), repeatability (<1.15% coefficient of variance), and excellent biocompatibility for live cell applications.<sup>194</sup>

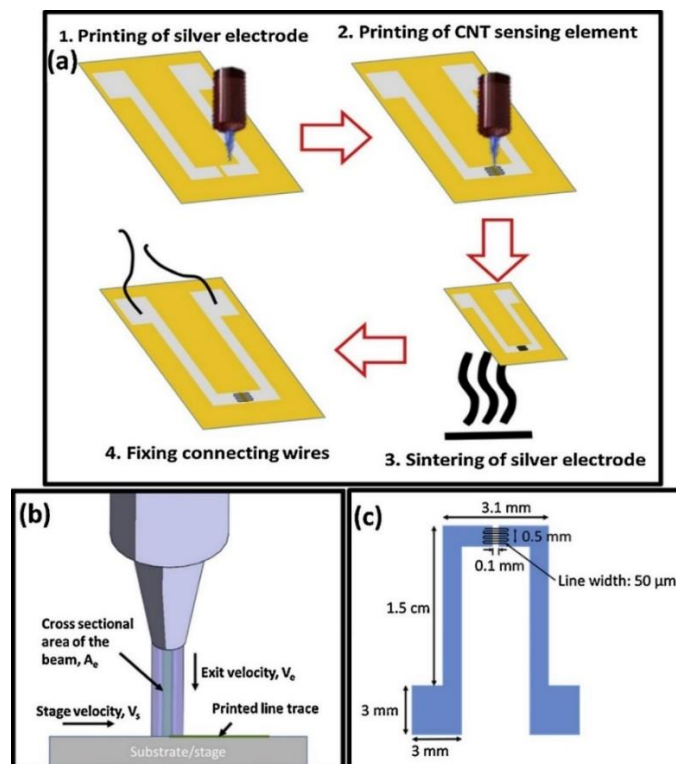


Figure 25. Schematic diagrams showing the (a) complete fabrication process of CNT based sensor, wherein 1) a silver electrode is printed first using aerosol jet technology, 2) CNT sensing element is printed, 3) thermal sintering process is carried out for the printed inks and 4) external wires are connected for measurements. Diagram depicting (b) parameters affecting the aerosol jet printing process and (c) dimensions of the fabricated sensor<sup>194</sup> (with permission).

Jeon *et al.* fabricated high-performance flexible pH sensors, from SWCNTs and Nafion, via screen printing on flexible substrates (Figure 26). The sensors monitor pH changes from 1 to

12 by measuring resistance in printed nanocomposite films. Operational stability remains after 200 bending cycles, crucial for wearable electronics integration. Sensing mechanism involves chemical reactions with hydrogen or hydroxide ions. Integration with a drone-based system enables real-time data visualization and remote target detection on smartphones.<sup>195</sup>

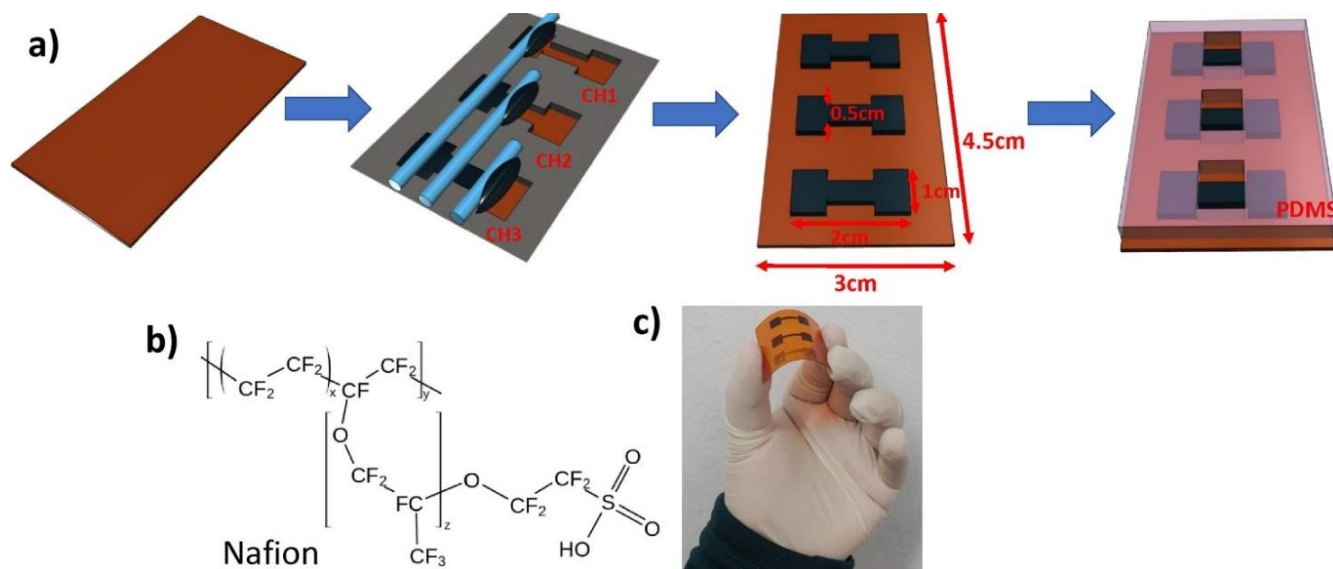


Figure 26. (a) Schematic process flow of the flexible pH sensor based on nanocomposites of SWCNTs and Nafion having three channels, fabricated by a screen printing process in ambient air, (b) chemical structure of Nafion, and (c) an optical image of the flexible<sup>195</sup> (with permission).

Ali Akbar *et al.* presented an effective method to identify and quantify multiple disinfectants (specifically free chlorine and potassium permanganate) in water using SWCNT-based reagent-free chemiresistive sensing arrays. The sensing array included both functionalized and pristine SWCNT sensors to differentiate between the disinfectants. Pristine and functionalized sensors exhibit different response mechanisms, resulting in responses that depend on both concentration and pH. They revealed excellent separation of the analytes across five pH levels (5.5, 6.5, 7.5, 8.5, and 9.5), as well as high separability and predictability, with a  $Q^2$  of 94.26% and an  $R^2$  of 95.67% for the five pH ranges of the two analytes. This proof-of-concept solid-state chemiresistive sensing array can be adapted for specific disinfectants commonly used in

water treatment plants and deployed in water distribution and monitoring systems.<sup>196</sup> The schematic of the sensor and the characterization is shown in Figure 27

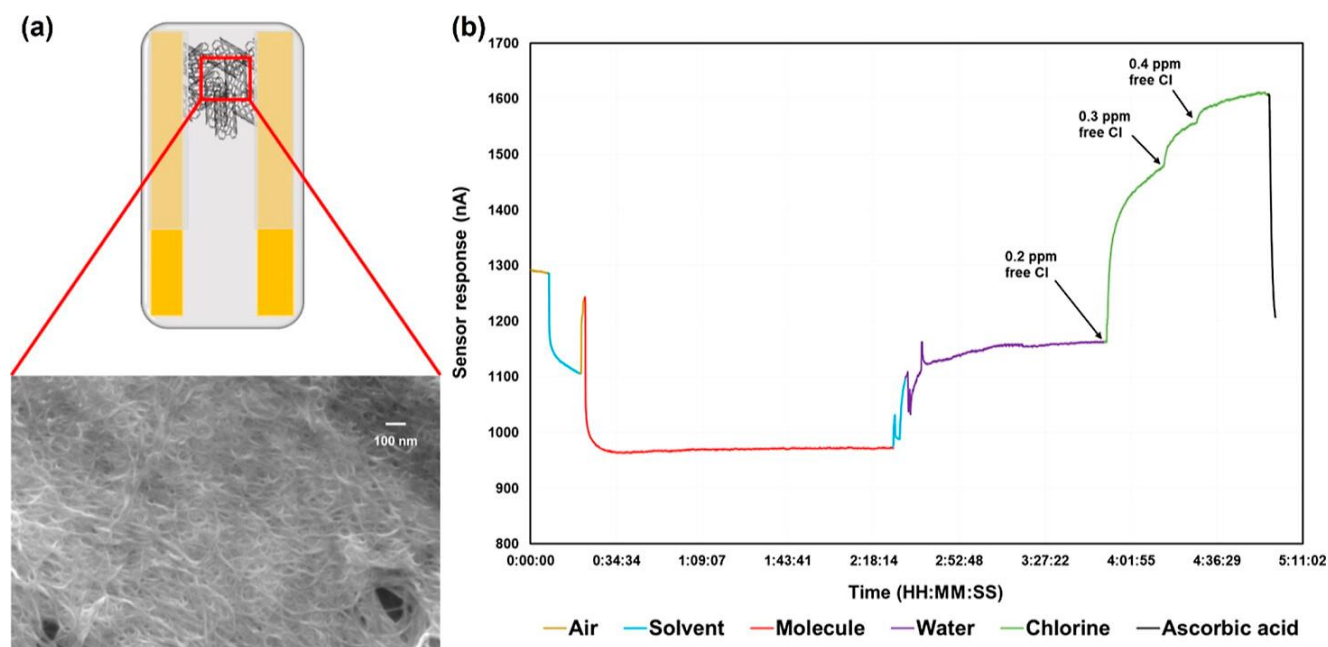


Figure 27. (a) Schematic of sensor geometry; the inset shows a SEM image of the CNT film. (b) Recorded sensor response as current (nA) over time for the different steps of the measurement. Solvent and molecule solution induces *n*-doping on the surface, while the oxidant (free chlorine) results in *p*-doping behavior. When exposed to ascorbic acid, the sensor showed a reset in the response due to analytes getting reduced by ascorbic acid.<sup>196</sup>

Heavy metal pollution poses a significant health risk to living organisms, prompting extensive research into their detection. In their study, Martinez Jimenez *et al.* developed a sensor platform for the selective detection of lead(II) acetate. The sensor utilizes self-assembled polyethyleneimine-functionalized carbon nanotubes (PEI-CNTs) and graphene oxide films deposited onto gold interdigitated electrodes. The graphene-based nanostructure exhibited resistive behavior, and the layer-by-layer fabricated film was employed to detect  $\text{Pb}^{2+}$  acetate



in aqueous solutions using three electrochemical techniques: impedance spectroscopy, amperometry, and potentiometric stripping analysis. Across these methods, the sensor demonstrated a detection limit as low as 36 pmol/L and a sensitivity of up to 4.3  $\mu\text{A}\cdot\text{L}/\mu\text{mol}$ , along with excellent repeatability. The detection mechanism is attributed to the high affinity of heavy metal ions for the functional groups in the PEI-CNTs and graphene oxide, which facilitates high performance and sensitivity. These findings are crucial for advancing integrated monitoring and sensing platforms for  $\text{Pb}^{2+}$  contamination in drinking water.

## 1.6. Conclusion on the state of the art and project objectives

In this first chapter, the state of the art on the topics of carbon nanotubes, functionalization of carbon nanotubes, and sensors based on carbon nanotubes were discussed. Based on the information of this chapter, and the general objective of the project (developing sensors for water quality analysis) the following conclusions could be listed:

- The electronic properties of CNTs can be exploited to create electronic devices with simple functionalities. They are interesting in the development of sensors, because of their chemical interaction with their surroundings.
- Noncovalent functionalization of CNTs is a way to control their interactions, channel them down to specific desired interactions, and benefit from their electronic properties.
- Sensors have an important role in our lives, and they are necessary for a battle against ecological changes, among them the distress in drinking water quality. CNT-based sensors have been developed by different groups to address water quality, among them chemiresistive sensors, have a simple mechanism and interesting versatility.

However, based on the investigation of the state of the art, the following limitations could be listed, that are case-specific to this project and its objectives:

- One of the important limitations of CNTs, is their desire to create bundles. The  $\text{sp}^2$  hybridization of CNTs (resulting from the extended system of  $\pi$  orbitals) is responsible

for interaction with the species in their surroundings. Primarily, these strong interactions result in the creation of CNT aggregates, disarming their properties.

- On the other hand, despite numerous studies on the interest and applications of noncovalent functionalization of CNTs, there are limitations in terms of the process compatibility with simple deposition methods, bypassing the impacts of sonication-assisted dispersion of CNTs. There is also room for research on the type of conjugated molecules and their specific interactions with CNTs.
- Finally, the development of a sensing device based on CNTs need to be specific to the case of deposition and functionalization methods, and there is a large area for research on the fabrication devices, specific for the detection of common water analytes.

### **1.6.1. Objectives of this project**

Although, there are approaches to create homogenous and high crystalline depositions of CNTs, in this work, this issue is targeted by dispersing CNTs in solvents and depositing them using simple solution-based deposition methods. This method has a high scalability potential and low cost but can deteriorate the interesting properties of CNTs. The focus of the first chapter will be to develop processes to maintain the choice of using solution-based deposition methods, while benefiting from the properties of CNTs.

In the second chapter, based on the described approaches in the literature, the functionalization of CNTs with specific molecules will be discussed and characterized. An essay to optimize the functionalization process will be discussed that is compatible with the deposition method.

Finally, in the last main chapter, the development of sensors compatible with the deposition and the functionalization methods will be discussed and the devices functionalized with specific molecules will be characterized to detect different analytes especially glyphosate as a danger to the soil and water resources.



**Institut Polytechnique de Paris**



## **Second Chapter**

# **Processing of CNTs**

## 2. Processing of CNTs

Processing CNTs refers to different steps of experimentation that provides CNTs for a designated application. As discussed in the previous chapter, CNTs have interesting properties that theoretically makes them candidates for different domains of application. However, the widespread application of CNTs faces practical limitations that present significant challenges. Although CNT yarns and sheets exhibit promising performance in certain applications, such as supercapacitors and lightweight electromagnetic shields, their overall mechanical and electrical properties still fall short for many practical uses.<sup>13</sup>

Moreover, the challenges extend to the difficulty of isolating single-chirality nanotube preparations with desired functionalities, restricting the applications of SWCNTs in bioimaging and biosensing.<sup>197</sup> The insolubility of carbon nanotubes in most solvents adds another layer of complexity, posing challenges in their controlled attachment to electric circuits and impeding their practical use as electrode materials.<sup>198</sup>

The closed or capped tips of aligned CNTs prepared by most chemical vapor deposition (CVD) methods also impose limitations on their potential applications.<sup>199</sup> Additionally, despite the high aspect ratio, flexibility, and low mass density of CNTs making them attractive as reinforcing fillers for polymer matrices, achieving uniform dispersion and alignment within the polymer matrix remains a practical challenge, hindering their effective reinforcement.<sup>200</sup>

In the realm of biomedicine, CNTs show promise for biological and biomedical applications like drug delivery systems and tissue regeneration. However, concerns about their biocompatibility and potential toxicity limit their practical use in these applications.<sup>201</sup> Furthermore, the unique properties of CNTs, such as their high Young's modulus and low density, make them appealing for strain sensing applications. Still, challenges in achieving large-area application and practical demonstration hinder their widespread use in this area.<sup>202,203</sup>

Several factors limit the practical use of CNTs in sensor applications, leading to challenges in their widespread adoption. A primary constraint stems from the inherent irregularity and

unpredictability of individual CNT devices, resulting in highly erratic behavior of CNT-based sensors. This irregularity poses significant challenges in achieving reproducibility and reliability in sensor performance, impeding their practical applications and commercialization.<sup>204</sup>

Moreover, for CNT-based sensors to be viable in diverse applications, such as chemical warfare agent detection and disease diagnostics, their sensitivity, selectivity, and stability are paramount. However, these sensors face limitations in terms of low sensitivity, restricting their ability to detect subtle variations like micro-pressure changes.<sup>205</sup> The manufacturing process itself presents challenges, with the weak binding of CNT arrays to substrates making them prone to detachment, thereby affecting sensor performance and reliability.<sup>206</sup>

Additionally, the integration of CNT-based sensors with conventional microelectronics encounters fundamental limitations, including unpredictable device characteristics.<sup>122</sup> This integration challenge further complicates the practical use of CNTs in sensor applications, especially in achieving seamless compatibility with existing electronic systems. Addressing these issues is crucial for unlocking the full potential of CNTs in sensor technologies.

Understanding the limitations of CNTs is important to make suitable choices for each application. In this chapter, CNTs will be experimented thoroughly to draw a full picture of their dispersion, deposition, and post deposition treatments.

## 2.1. CNTs used in this work

Two samples of commercial CNT powder were utilized for the experiments:

- First sample: MWCNT with a purity of 70%, purchased from Sigma Aldrich.
- Second sample: HiPCo SWCNT, with a purity exceeding 95%, average diameter from 0.8 to 1.2 nm, and an average length from 100 to 1000 nm. This sample has a semiconducting composition of 70% and was purchased from Nanointegris™.

The experiments were initiated with the utilization of MWCNTs. However, later, alternation between MWSNTs and SWCNTs was implemented for comparative purposes.

Compared to SWCNTs, MWCNTs have more surface defects that can impact their sensing capabilities.<sup>207</sup> It is possible to get more reproducible and meaningful results by using SWCNTs for functionalization and sensing application. Also, due to their high conductance, it is difficult to distinguish the changes that are chemically induced on MWCNTs, because their stronger conductance could dominate the chemiresistive results.<sup>208</sup> Therefore, more focus will be on SWCNTs, keeping the results on MWCNTs as a comparative measure.

As depicted in Figure 28, the main difference between the samples of CNT used in this project lies in the ratio of D-band peak to G-band peak. While MWCNTs have an  $I_d/I_g$  larger than 1, this ratio is smaller than 1 for SWCNTs. This is related to the fact that MWCNTs have more layers and the probability of defects in the crystalline  $sp^2$  structure is higher which reflects in Raman spectroscopy.<sup>209</sup> Any mechanical and chemical handling of MWCNTs can cause modification of the surface, while this effect is weaker in SWCNTs and the surface remains more neutral to the surrounding.<sup>85</sup> This is an interesting property for sensor development.

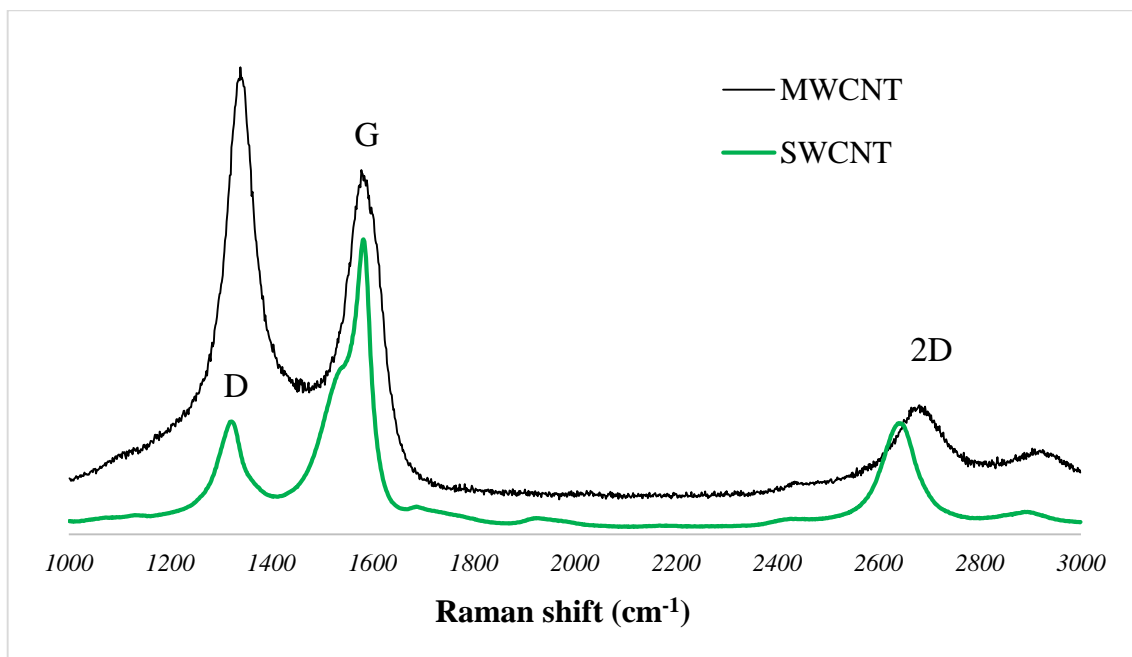


Figure 28. Typical Raman of SWCNT and MWCNT used in this project.

Also, by looking at the 2D band peak, the effect of the number of layers is clear, where a larger and more narrow 2D peak signifies a lower number of graphitic layers.<sup>210</sup> The other difference between the two spectra lies in the peak at  $2900\text{ cm}^{-1}$ , which is related to the presence of amorphous carbon in the structure.<sup>211</sup> This is more sample specific and shows that the SWCNT sample is purer than the MWCNT sample.

Looking at Figure 28, a shift in the 2D peak can also be noticed. Doping effects can result in the shift of the 2D peak in Raman spectra. Studies have shown that shifts in the G and 2D peak positions indicate n-type doping by metals nanoparticles like NP-Pt, while p-type doping effects have been linked to edge oxidation.<sup>212,213</sup> It is important to note that Figure 28 illustrates the Raman spectra of pure CNT samples as received from the provider and the Raman spectra will be thoroughly studied in the coming sections after applying different purification processes.

## 2.2. Dispersion of CNTs

Carbon nanotubes tend to create strong aggregates due the presence strong  $\pi$ - $\pi$  interactions.<sup>214</sup> Dissociating these aggregates requires a great amount of energy that no solvent can provide.<sup>215</sup> Therefore, preparing a solution of CNTs in known solvents is rather impossible. However, there are different methods to provide the necessary energy to dissociate bundles of CNT, among which using ultrasonic waves is the most common.<sup>216</sup> In this section details about the dispersion process of CNTs in solvents will be provided. This procedure will be called ink preparation, and an ink is a dispersion of CNTs in a solvent. This name comes from the use of CNT dispersions in the inkjet printing deposition method (will be explained later in this chapter).

Before ink preparation, in this project, an acidic treatment was applied to the CNTs, which is an effective way to eliminate the amorphous matter in a bulk of CNT powder. The effects of various chemical surface treatments on the electro oxidative filter performance of CNTs were explored by Gao & Vecitis.<sup>217</sup> It was determined that acid treatment proved effective in



removing internal residual metal oxide and amorphous carbon, resulting in improved filter performance. A significant reduction in the weight of ash residue, indicating the removal of impurities and amorphous carbon, was demonstrated by Liu et al.<sup>218</sup> through acid treatment of CNTs. Additionally, Rinaldi et al.<sup>219</sup> observed that mild HNO<sub>3</sub> treatment oxidatively removed amorphous carbon and extensively oxidized the CNT surface, leading to the elimination of functionalized polyaromatic fragments. The collective findings from these studies endorse the use of acidic treatment for the elimination of amorphous matter from CNT powder, emphasizing its effectiveness in enhancing the purity and performance of CNTs.

The acidic treatment procedure to clean 100 mg of SWCNTs or MWCNTs in this project is detailed as the following:

1. Addition of the CNT powder to 150 ml of nitric acid (25% vol),
2. Sonication of the mixture in bath for 30 minutes (uncontrolled temperature),
3. Heating the dispersion at 100°C with water reflux cooling and magnetic agitation for 5 hours,
4. Filtration of the dispersion on a Polytetrafluoroethylene (PTFE) membrane (0.2 μm) and wash with water until the water is colorless,
5. Drying the CNT powder on the filter until no solvent is visible,
6. Recuperation of the solid CNT (with or without the filter),
7. immersing the solid SWCNT (with or without the filter) in 100 ml of NaOH (2 M),
8. Sonication in bath for 10 min (uncontrolled temperature),
9. Filtration of the dispersion on a PTFE 0.2 μm membrane and wash with water until the pH of the leaking water is neutral,
10. Recuperation of the solid SWCNT (with or without the filter),
11. immersing the solid SWCNT (with or without the filter) in 100 ml of HCl (1 M),
12. Sonication in bath for 10 min (uncontrolled temperature),
13. Filtration of the dispersion on a PTFE 0.2 μm membrane and wash with water until the pH of the leaking water is neutral,
14. Washing with acetone and ether to eliminate water and detach the CNTs from the membrane,

15. Heating the CNT powder at 50°C for one night under vacuum.

### **2.2.1. Ink preparation.**

An important parameter to take into consideration in the ink preparation process is the aging of an ink. To fabricate homogenous thin films on CNT, it is necessary to have a stable ink without aggregates.<sup>220</sup>

The controlled deposition of large area highly conducting CNT films with high homogeneity required for applications remains elusive.<sup>221</sup> Experimental results suggest a consistent trend between CNT concentrations and strain sensor sensitivity, indicating the importance of homogeneity in CNT thin films for sensing applications.<sup>222</sup> Additionally, the electrical resistivity of CNT thin films increases linearly with strain, making them ideal materials for piezoresistive strain sensors, highlighting the significance of film homogeneity in achieving reliable sensing performance.<sup>127</sup> Below, the ink preparation steps is described:

1. Mixing 10 mg of CNT with 30 ml of the solvent,
2. 1-hour tip sonication with alternating pulses of 15s "On" + 15s "Off" (30 min effective),
3. Balancing the mixture into centrifuge tubes,
4. Centrifugation for 30 minutes at 10000 xG force,
5. Collecting the supernatant and balance into new centrifuge tubes,
6. Centrifugation for 5 hours at 12000 xG force,
7. Collecting the supernatant and storage under the name stable CNT ink.

The role of sonication is to provide the energy to dissociate CNT bundles, and centrifugation is an effective method to sediment larger and more heavy particles at the bottom of the tube.<sup>223</sup> The higher the rotation speed of the centrifugation step, the lighter the CNT colonies remaining in the dispersion and lower the possibility of CNT ink aging.<sup>224</sup>

### 2.2.2. Ink concentration estimation

The estimation of CNT ink concentration can be carried out through the precipitation of CNT ink. The following procedure was applied to determine the concentration of an ink with N-Methyl-2-pyrrolidone (NMP) as solvent. With a high boiling point (202°C) and a low vapor pressure (0.345 mmHg), NMP is a highly stable solvent with a very low volatility. These properties are interesting for the development of inks based on CNTs with long lifetime and better homogeneity of depositions.

1. Taking 10 ml of the CNT ink in a vial,
2. Magnetic stirring at 100°C for one day until the formation of agglomerates is observed,
3. Drying a glass centrifuge tube at 110°C for 1 h,
4. Measuring the weight of the empty tube,
5. Transferring 2 ml of the heated ink into the tube,
6. Adding 1 ml Ethanol as agglomerating agent to accelerate the precipitation and leave for 1 h,
7. Centrifugation at 10000 rpm for 5 h,
8. Collection of the supernatant (NMP + Ethanol) and leave the CNT at the bottom of the tube,

The process is repeated 4 more times, by adding 2 ml of the ink in the same tube each time to gather enough CNT, and reduce the error in the weight measurement. Finally, the tube is heated at 150°C for 2 days to evaporate residual solvent. After drying the tube and the containing CNT, the weight of the tube is measure. This way, the weight of the gathered CNT is calculated and by dividing over the initial volume (10 ml in total of 5 repetitions), the concentration is estimated.

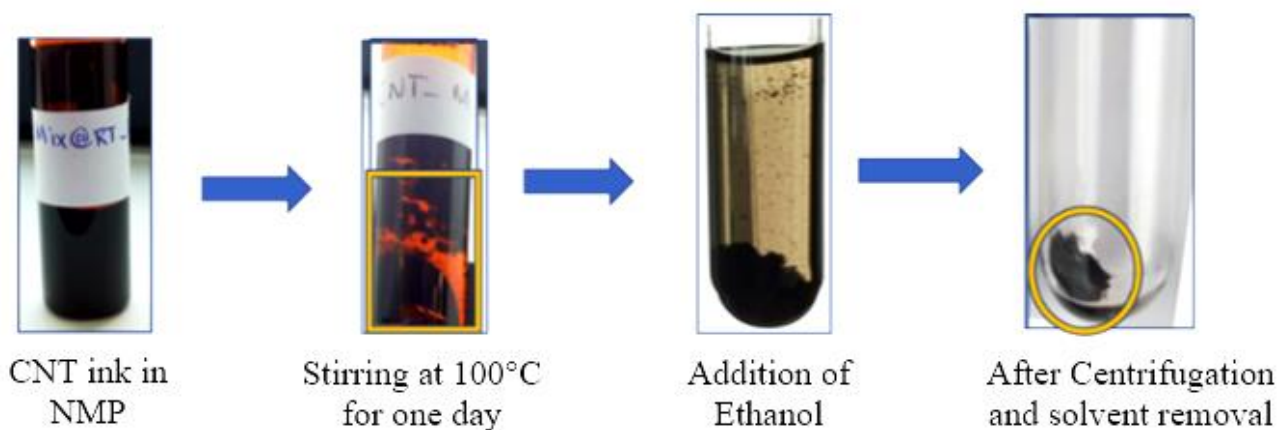


Figure 29. Procedure of concentration estimation by precipitation.<sup>1</sup>

This estimation was carried out only once by inspiring from the internship work of Suriya Venkatesan, using different solvent and different initial quantities. The value obtained as the estimated concentration is 75 mg/L. In certain cases throughout the next sections and chapters of this report, a value as the concentration of CNT inks is necessary, where this value (0.075 mg/ml) will be used. This estimation is only valid under the specified initial conditions (10 mg SWCNT + 30 ml NMP).

It is important to note that this value is an estimation, subject to variation due to different parameters, such as the positioning of initial CNT bundles to the sonication tip or minor variations in tube weight during centrifugation. To streamline the process and avoid duplicating the procedure for each ink, in instances where any parameters differ (such as initial mass and/or volume, the type of CNT, and/or the solvent), these results are extrapolated to estimate the CNT ink concentration.

---

<sup>1</sup> Image from the internship report of Suriya Venkatesan

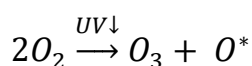
### 2.3. Solvent-based deposition

Deposition of thin layers of nanomaterial from a solvent is more preferable than other methods, due to its versatility, low costs, and easy processing.<sup>225–228</sup> Commercially available in powder form, carbon nanotubes can harness their pristine properties through adequate dispersion, deposition, and surface treatment. In the following sections, various deposition methods will be discussed.

Before CNT deposition, a treatment of the substrate surface is necessary to eliminate impurities on the surface that can affect the performance of thin films, particularly in the case of sensors<sup>229</sup>. In this work different substrates (Si/SiO<sub>2</sub>, glass, and quartz) were used for different application that will be disclosed in respective sections, However, the surface treatment for all substrates is similar. Here are the steps to treat the substrate surface before deposition:

1. Immersion of the substrate in DI water face up,
2. Bath sonication for 5 minutes to eliminate water-soluble agents from the surface,
3. Immersion of the substrate in Acetone face up,
4. Bath sonication for 15 minutes to eliminate greasy agents from the surface,
5. Immersion of the substrate in Isopropanol face up,
6. Bath sonication for 15 minutes to eliminate remaining agents from the surface.
7. UV/Ozone (UVO) treatment for 15 minutes:

For UVO treatment the substrate is encapsulated inside a chamber with a UV lamp bearing a wavelength as low as 184.9 nm that can turn oxygen in the air into ozone and radical oxygen:



Radical oxygen is a highly reactive agent that can interact with different types of agents on the surface and gasify them.<sup>230</sup> The UVO device has a suction pump to eliminate Ozone and the gas content in the chamber. At the end of the process, most of the polluting agents are eliminated, and the pure surface of the substrate remains.

### 2.3.1. Drop casting

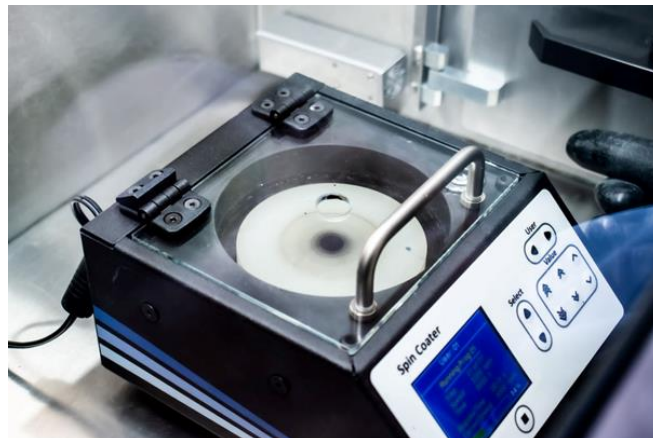
Drop casting is a straightforward technique that involves transferring a solution of the material onto a surface using a syringe or a pipette. In the context of this project, this method was employed to meticulously fabricate sensors by delicately depositing the ink onto the designated surface. The key to achieving optimal results lies in ensuring a superior dispersion, which, in turn, contributes to an enhanced quality of the thin film.<sup>220</sup>

It is noteworthy that the efficacy of the process can be influenced by the choice of solvent<sup>231</sup>, necessitating substrate heating to 130% of the solvent's boiling point to mitigate the formation of undesirable bundles. The process of drop casting is important in the fabrication of sensors, capitalizing on its simplicity and effectiveness.<sup>232–234</sup>

In this work, drop casting method was largely used for the deposition of CNT inks on one type of the sensing devices, the structure of which will be thoroughly discussed in the fourth chapter. The advantages of this deposition method in that specific case are the simplicity and the lower required time of deposition. However, in terms of the morphology, drop casting method results in high coffee ring effect<sup>235</sup> that reduces the reproducibility of electronic properties of the deposition.

### 2.3.2. Spin coating

Spin coating is another method of preparing homogenous thin films of materials. It consists of preparing a solution of the material and injecting it on the substrate, which is fixed on a rotating plate as shown in Figure 30. The important parameters that play a role in the thickness of the thin film include, concentration and viscosity of the solution, rotational speed of the substrate, and rotation time.



*Figure 30. Spin coating method for thin film depositions.*

The solution can be injected on the surface, before or after starting the rotation. The first case is normally referred to as spin casting, and the latter as spin coating. Another important parameter that controls the thickness of the film is the moment of solution injection (before or after rotation).

One of the drawbacks of the spin coating process is the loss of material due to the rotation. In the spin coating method, a high solution concentration is necessary to ensure the surface's coverage with the material.<sup>236</sup>

In this project, spin coating method was tried for the deposition of CNT inks on different substrates. As discussed earlier, the ink concentration is estimated to be as small as 0.075 mg/ml. Such a low concentration is important to guarantee the stability of the ink, however, after multiple trials to deposit CNT inks by spin coating, no film formed on the substrates, since CNTs have a lower affinity to attach to the substrate surface rather than staying in aggregates inside the ejected solution.

It is also possible to prepare inks with higher concentration, however, the higher the ink concentration, less stable they are, and there will be a continuous need for ink preparation, which results in the utilization of higher quantities of CNT powder and solvent, and is more

time consuming. Apart from that, inks with higher concentration give less homogenous deposition, since they contain larger aggregates.

Spin coating method was used for the deposition of a porous Polymethylmethacrylate (PMMA) layer on one type of sensing devices, which will be discussed thoroughly in the fourth chapter.

### 2.3.3. Spray coating

In this method of deposition, the CNT ink is kept in a reservoir and by using a pump, small droplets of the ink are sprayed onto the surface. Figure 31, illustrates the basics of spray coating. Spray coating has the advantage of simplicity and low deposition time; however, it needs a larger ink volume compared to other deposition methods, and in the specific case of our sensor development, the lack of control over the position of deposition. This method is mentioned in this section for the sake of a more complete introduction to the deposition methods.

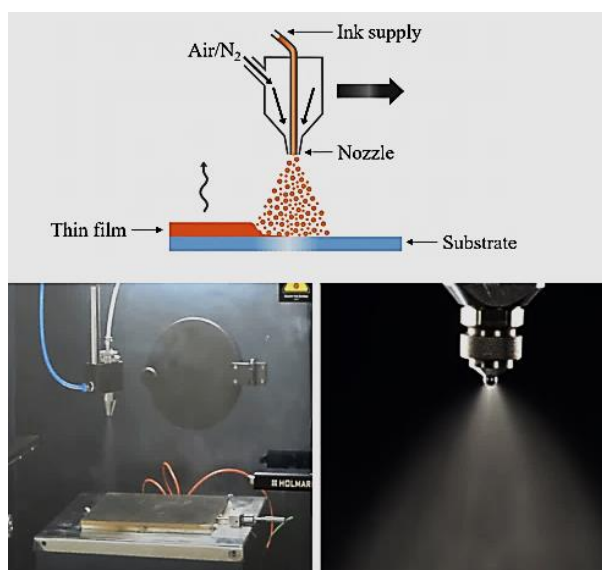


Figure 31. Illustration of spray coating method for thin film depositions.



### 2.3.4. Inkjet printing

This process requires no prefabrication of templates, allows a rapid printing process at low cost, does not require post-printing steps over the deposit, and one can precisely control the amount of deposited material.<sup>11</sup> The superior advantages of inkjet printing such as simplicity, flexibility, speed, high resolution, suitable efficiency for mass production in certain application, low cost, and possibility to extend the capabilities of devices beyond other manufacturing technologies, has led to a rise in depositing thin layers with this technology.<sup>237</sup> In IJP, the thickness and morphology of the deposition can be optimized by the amount of ink deposited per unit length and the time lag between the droplets, respectively.<sup>238</sup> For this project, a Dimatix printer of DMP-2800 Series from Fujifilm<sup>2</sup> was used, which is shown in Figure 32.

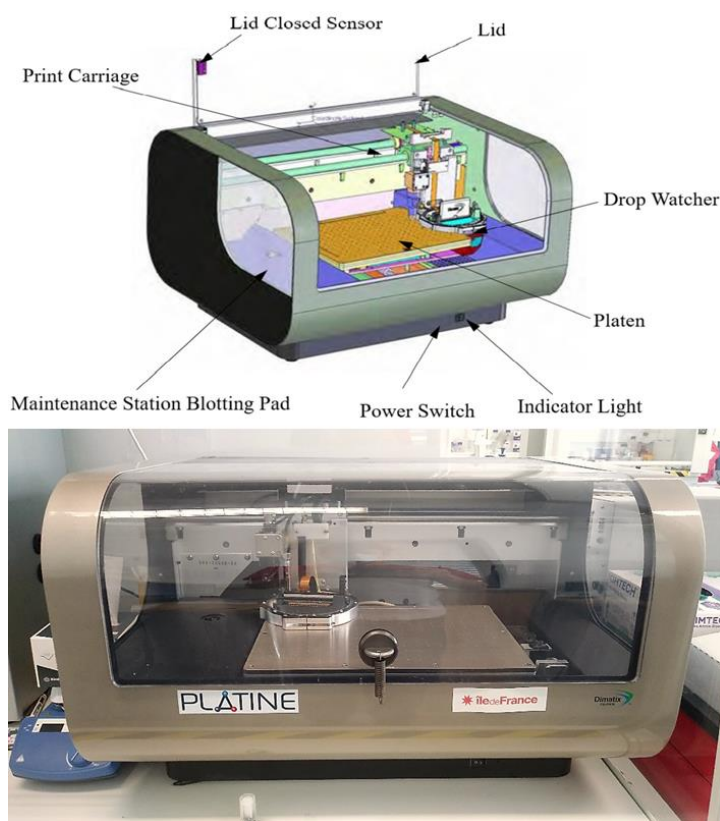
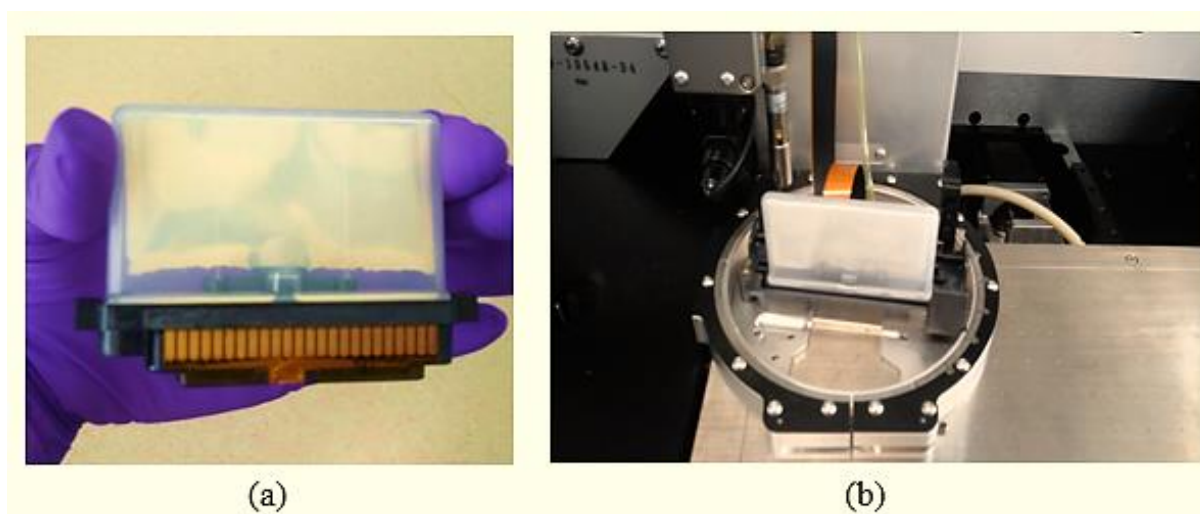


Figure 32. DMP-2800 Series, Fujifilm Dimatix printer.

<sup>2</sup> <https://www.fujifilm.com/us/en/business/inkjet-solutions/deposition-products/dmp-2850/support>

This machine works based on a piezoelectric effect and is among the Drop-On-Demand (DOD) type of inkjet printers.<sup>239</sup> As Figure 33 shows, the ink is filled into the reservoir of a cartridge and installed on the printhead. Dimatix cartridges have 16 nozzles and to create a drop from each nozzle, a voltage should be applied to the nozzle channel inducing pressure waves that results in the creation of a drop through the piezoelectric effect.



*Figure 33. Cartridge of the Dimatix printer.*

The printer is controlled by a computer software and different printing parameters like the nozzle configuration, number of layers, the arrangement of printing sections, and placement of the deposition are controlled through the software.

Since the jet diameter is in the order of a few micrometers,<sup>239</sup> aggregations of a few carbon nanotubes can easily obstruct it. There are options to prevent this; by checking the functionality of the nozzle after depositing every layer it is possible to avoid nozzle clogging. With Dimatix printer it is also possible to develop a plan consisting of cleaning cycles in between the printing process. Dimatix printer offers a solution to run a cleaning cycle after a certain time, during which the jets are cleaned by pushing the ink on a pad. Although this

method is simple, it increases the printing time and it does not allow controlling of the nozzles in the middle of the process.

For the deposition of CNT inks utilizing the Dimatix inkjet printer, an average drop velocity of 6 m/s was selected. This average velocity is to make sure that the drop does not spread around at the moment of collision, and instead spreads smoothly on the substrate.

The verification of this velocity involves the utilization of the drop watcher tool, as illustrated in Figure 34. To ensure an average velocity of 6 m/s, the drop position is captured precisely at 50  $\mu$ s following the release of the drop. By the adjustments of the nozzle voltage, the speed can be tuned in a way that at 50  $\mu$ s, the ink drop reaches the level 300  $\mu$ m. This meticulous process guarantees the desired deposition conditions for CNT inks through the inkjet printer.

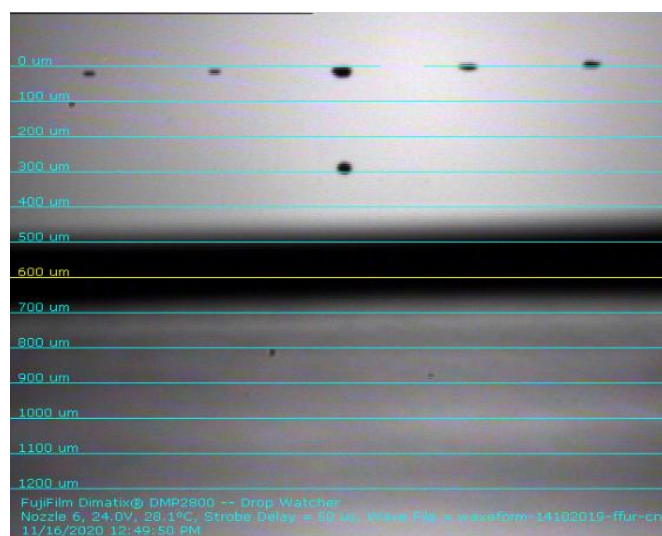


Figure 34. The drop position 300  $\mu$ m below the nozzle, 50  $\mu$ s after release from the nozzle, is a good estimation of the average drop speed which is 6 m/s.




#### 2.3.4.1. Optimization of the printing process with Dimatix

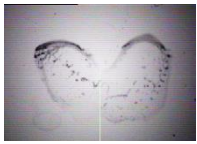
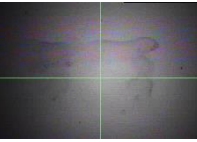

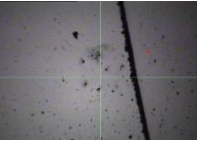

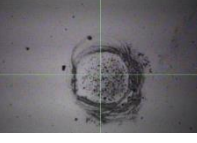
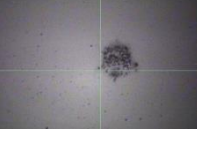
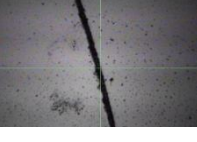
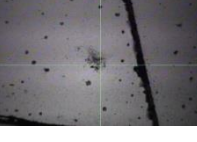
The importance of thin film morphology is evident in various sensor applications, including gas sensors, strain sensors, and humidity sensors. For instance, the morphology and

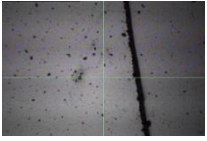

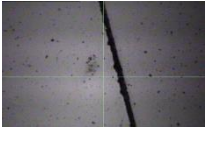
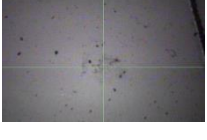


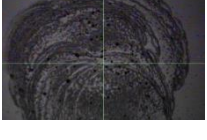
microstructure of  $\text{WO}_3$  thin films have been shown to affect their sensitivity to  $\text{NO}_2$ .<sup>240</sup> Moreover, the surface manipulation of precursor carbazole dendron polymer thin films has been explored for sensor applications, emphasizing the role of thin film morphology in sensor development.<sup>241</sup> The morphology of thin films also influences their electrical and optical properties, which are essential for sensor functionality.<sup>242,243</sup> Additionally, the utilization of nanomaterial-based thin films in gas sensors has been found to offer high response and short response and recovery times, further emphasizing the significance of thin film morphology in sensor applications.<sup>244</sup> Therefore, to create sensing devices with long lifetime and good reproducibility, it is important to control the deposition morphology.

A campaign of printing optimization was conducted to find the best deposition continuity. Table 2 summarizes the impact of changing different parameters on the deposition time and shape of the drops.

*Table 2. Results of the inkjet printing study to determine the effect of different parameters on the deposition shape.*

Drop spacing ( $\mu\text{m}$ )	Angle ( $^\circ$ )	Number of nozzles	Number of layers	Required time (min)	Speed ( $\text{mm}^2/\text{min}$ )	Shape of drops
5	1.1	1	2	15.78	79	
		2	2	8.25	41	
		3	2	5.58	28	

		7	4	5.38	13	
10	2.3	1	2	5.25	26	
		2	3	4.03	13	
		3	2	1.87	9	
		7	4	1.95	5	
15	3.4	1	2	2.67	13	
		2	3	2.1	7	
		3	4	2.13	5	
20	4.5	1	2	1.67	8	

		2	3	1.4	5	
		3	4	1.48	4	
25	5.6	1	3	1.92	6	
		2	4	1.53	4	
		3	5	1.48	3	
30	6.8	1	4	2.08	5	
		3	6	1.45	2	

The angle of the cartridge positioning with respect to the printer surface (equivalent to the drop spacing) which is mentioned in Table 2. By adding the drop spacing, and the number of working nozzles, the required time of printing decreases. However, as the images in the table show, the quality of the deposition also decreases with this reduction in the resolution. This reflects one of the main issues of inkjet printing which is the time required to print.

Finally, based on the presented table, using one nozzle and a drop spacing of 10  $\mu\text{m}$ , which is obtained by an angle of  $2.3^\circ$  (Figure 35), and using only one nozzle gives an acceptable deposition quality and duration.



Figure 35. Continuity of the CNT deposition from inkjet printing.

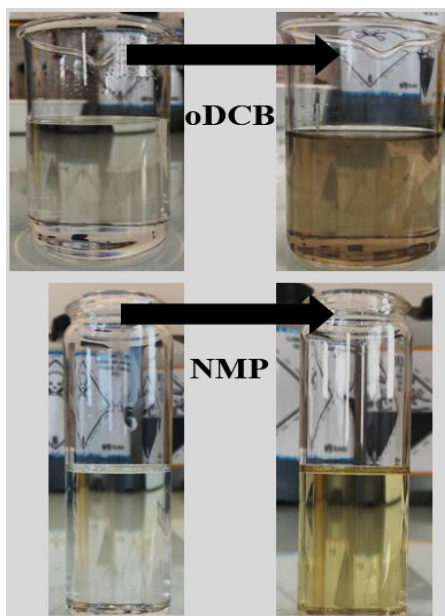
## 2.4. Impact of sonication on CNTs

The preparation of carbon nanotube (CNT) ink involves the use of solvents and dispersants, which are susceptible to degradation under the influence of sonication. Sonication, a process involving the application of sound energy to agitate particles in a solvent, has been found to have both physical and chemical effects on the solvent and dispersants used in CNT ink preparation.<sup>245–247</sup> It has been reported that sonication can lead to the physical and chemical degradation of solvents and dispersants, affecting their stability and properties.<sup>248</sup> Furthermore, the application of sonication during the dispersion of CNTs in solvents can damage CNTs, resulting in the formation of defects and cutting them into shorter pieces, which significantly degrades their electrical properties.<sup>249</sup>

The effect of sonication on solvents and dispersants used in CNT ink preparation has also been studied in the context of other nanomaterials and composites. For instance, it has been observed that sonication can lead to the generation of toxic degradation products, as well as the splitting of water into reactive oxygen species, initiating free radical pathways of polymer



degradation.<sup>250</sup> These findings underscore the significant impact of sonication on solvent degradation and its implications for the preparation of CNT inks. Figure 36 shows the impact of sonication of two main solvents used in this project for ink preparation.



*Figure 36. Sonication of pure solvent resulted in obvious color changes.*

To further study the effect of sonication on the quality of carbon nanotubes, Transmission Electron Microscopy (TEM) analysis was done to compare the surface coverage of CNTs before and after the ink preparation.

For the sample before ink preparation, a few drops of DI water was dropped on commercial MWCNT powder on clean paper and contact with the TEM grid was made simply by passing the grid over the wet samples. To take the sample after ink preparation, a drop of an ink based on MWCNT in *ortho*-Dichlorobenzene (oDCB) was casted on the TEM grid. Both samples were subjected to 10 minutes of annealing at 200°C to ensure the elimination of any solvent.

For each sample, at least 20 images were taken at the Nanomax infrastructure at the École Polytechnique. From each sample, one example is shown in Figure 37.



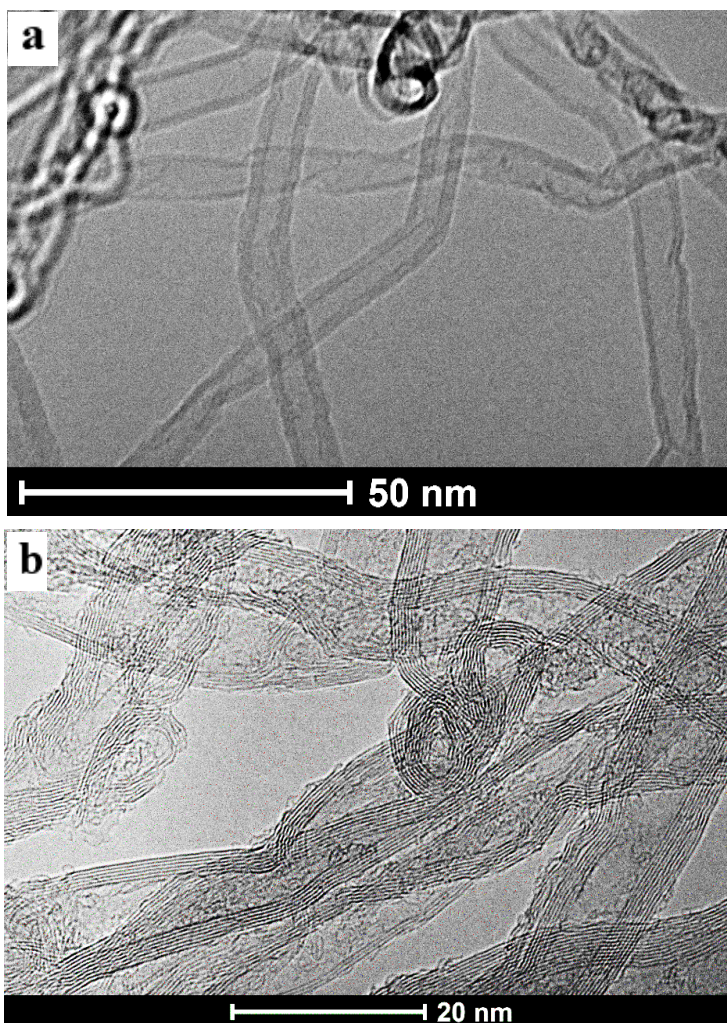


Figure 37. TEM images of a) a solid commercial MWCNT, b) MWCNT dispersed in oDCB.

The total CNT surface in each image was calculated using ImageJ software. Subsequently, for each image, the total surface of CNTs were roughly calculated. In the next step, for each image, the area covered by irregular amorphous matter were calculated by bordering those irregularities with ImageJ. Finally, the surface coverage of CNTs in every image was calculated simply by dividing the surface of amorphous matter to the total surface of CNTs, and listed as a percentage. It is important to note that the term surface does not represent the real surface of the CNTs, and it is equivalent to the projection of the 3D networks on the image after the acquisition of TEM.

Table 3 summarizes the values of average amorphous matter coverage for each sample. As it can be seen from the table, the value of amorphous matter coverage increases from a value of 12% for the sample before ink preparation to 35% after the ink preparation, suggesting a decreased CNT surface quality.

*Table 3. Comparison of the amorphous matter coverage of the two CNT samples. The value of variation coefficient among different images is reported.*

<b>Sample</b>	<b>MWCNT commercial Powder</b>	<b>MWCNT ink in oDCB</b>
Average amorphous coverage in %	12	35
<b>Coefficient of Variation among 20 images (%)</b>	69.7	47.7

The increase in the amorphous matter coverage of the CNTs after ink preparation, suggests that the solvent and the process have an important role on the quality of CNTs. A low CNT quality starts a chain of low success rate in noncovalent functionalization and sensor response. Since the choice of solvent-based deposition is an important factor in this project, instead of using other deposition methods like CVD to fabricate CNT thin-films, in the rest of the chapter the post processing methods will be discussed to enhance the surface quality of CNTs by reducing the quantity of amorphous matter.

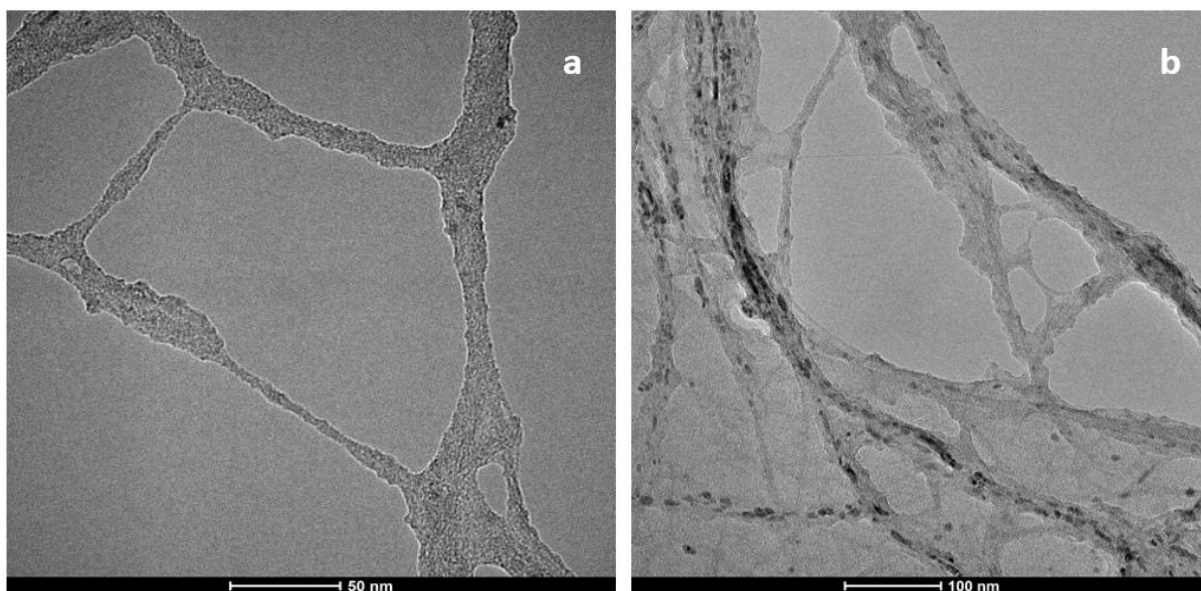
## **2.5. CNT deposition with reduced amorphous matter**

High resolution transmission electron microscopy (HRTEM) experiments were done to address the question of under which conditions the unwanted amorphous matter surrounding

CNTs can be eliminated. With a high boiling point (202°C) and a low vapor pressure (0.345 mmHg) NMP is among the solvents with the most difficult evaporation. However, NMP is the best candidate for a stable SWCNT ink for this research work. In literature, NMP is also known to degrade into sonochemicals that can wrap around nanotubes and hinder their  $\pi$  orbitals from interacting with other planar groups.<sup>246</sup>

In the rest of the chapter, the experiments done on SWCNTs will be discussed, because for different reasons that will be explained in next chapters, using MWCNTs were stopped in this work.

After the deposition the ink on the TEM grids, to eliminate the remaining solvent from the SWCNT network, TEM grid was annealed at 260°C for 15 minutes before entering the TEM chamber. Figure 38 shows two TEM images with different magnitudes, of SWCNTs deposited from a usual ink, and as it is clear from the images in Figure 38, the walls of SWCNT are covered by an excess of amorphous matter originated from the degradation of the solvent, due to the sonication.



*Figure 38. HRTEM images of a pristine SWCNT ink in NMP. a represents the abundant amorphous matter around individual tubes, and b represents the excess of amorphous matter in the SWCNT network.*

Despite the successful ink formulation and solvent-based deposition, CNT depositions have a high amorphous matter content and their surface is covered with a notable amount of amorphous matter. There are abundant  $\pi$  orbitals on CNTs that can attract different chemical groups from their surroundings.<sup>71</sup> These groups can be from different sources, for instance from the synthesis process by the provider. Also, unwanted sonochemicals that result from sonication, can irreversibly attach to CNTs. Apart from that, different gaseous groups can interact with the abundant electrons on the CNT surface and impact their purity.<sup>251</sup>

Functionalization of CNTs is an important objective in this project and is essential for the further applications, including sensors. The presence of amorphous matter from different sources can impact the functionalization in two ways:

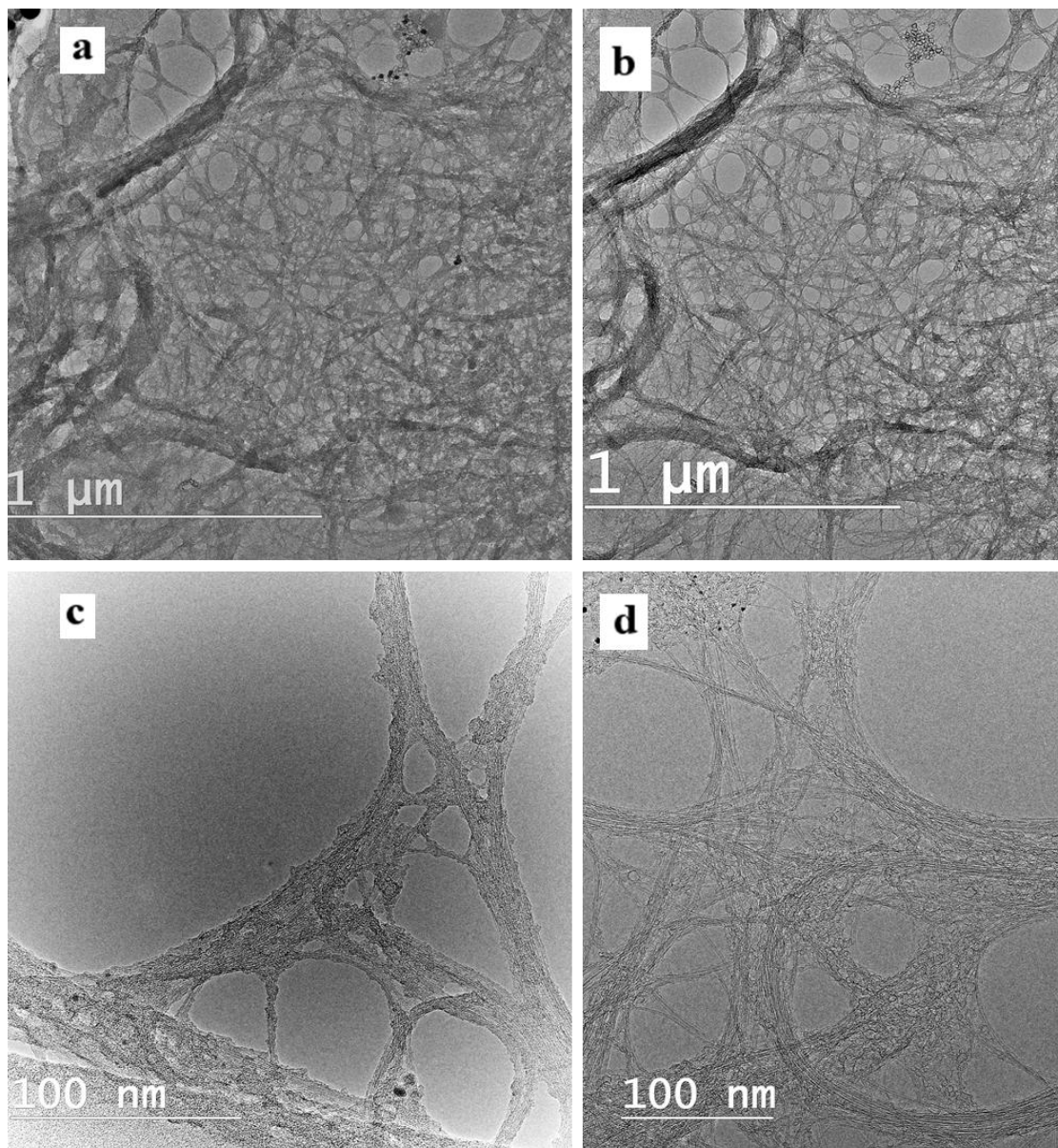
- (i) Amorphous materials covering CNTs completely block the attachment of conjugated functional groups on CNTs, and any post treatment, mechanical handling or exposure to water flow can result in the elimination of conjugated functional groups,<sup>252</sup>
- (ii) The  $\pi$ - $\pi$  forces between conjugated functional groups and CNTs can result in some level of attachment despite the presence of amorphous matter, but they interrupt efficient electronic exchange, which is essential for selective sensor response.<sup>16</sup>

### **2.5.1. CNT quality enhancement proof of concept**

A TEM chip has a SiC base and two gold electrodes deposited on top. By deposition of the CNTs on the chip, a high current can pass through the metallic CNTs (30 percent in the SWCNT sample). The high current heats up the CNTs, while the temperature is recorded. This process results in the degradation of any amorphous organic matter around the tubes in a high vacuum of  $10^{-6}$  torr.

A drop of the SWCNT ink was deposited on a chip and it was heated at  $1100^{\circ}\text{C}$  for 1 hour. Figure 39 shows the images of the tubes before and after the Heating Process. Figure 39.a

shows a large view and Figure 39.c shows a closer view of the SWCNT network before heating. On the other hand, Figure 39.b and Figure 39.d, show the SWCNT network of the same places after heating, respectively. By comparing the images before and after heating under vacuum, a significant decrease in the amorphous matter coverage can be seen, which is evidence of effectiveness of burning amorphous matter under vacuum.



*Figure 39. TEM image of pristine SWCNT ink in NMP before (a,c) and after (b,d) Heating Process in the TEM chamber.*

As resilient as CNTs are toward temperature, a thin film of a few hundreds of nanometers of CNT can degrade by a small oxygen content in their surroundings <sup>253</sup>. A high vacuum that gives a pressure of nearly  $10^{-6}$  torr, guarantees that amorphous matter degrades and evaporate, while the CNT network remains on the surface.

## 2.5.2. Optimization of the Heating Process

Cleaning CNTs with at super vacuum ( $10^{-6}$  torr) and high temperature ( $1100^{\circ}\text{C}$ ) consumes large amounts of energy and poses challenges when applied on a lab scale and for multiple devices. Therefore, an effort was made to optimize the energy consumption of the process and render it feasible for simultaneously apply to multiple devices. In these experiments quartz substrates were utilized, since handling silicon substrates for customized sensing devices can be challenging, and glass substrates cannot withstand the high temperatures of the Heating Process.

### 2.5.2.1. Temperature profile of the Heating Process

For the attempts to apply the Heating Process in a lab scale, a primary vacuum of 1 mbar was chosen, which can be more accessible and portable. This pressure is considerably higher than the pressure used in the TEM chamber ( $10^{-6}$  torr). Therefore, the temperature at which the SWCNTs would degrade decreases due to higher oxidation effect <sup>253</sup>.

In a series of experiments, SWCNTs were deposited on quartz substrates with two gold electrodes and were subject to heating under vacuum. The use of quartz substrates with gold electrodes, allows the verification of the presence of SWCNT network, by measuring their electrical conductivity (or its reciprocal, the resistance). To apply the temperature, the substrate was placed in a customized quartz tube and then inserted into a tubular furnace capable of heating up to  $3000^{\circ}\text{C}$ .



At the beginning, a temperature of 950°C was chosen and the furnace was heated with the profile presented in Figure 40. After waiting for 20 minutes for the furnace to reach 950°C, the heat source was stopped at once, but the cooling down took 6 hours to reach 50°C.

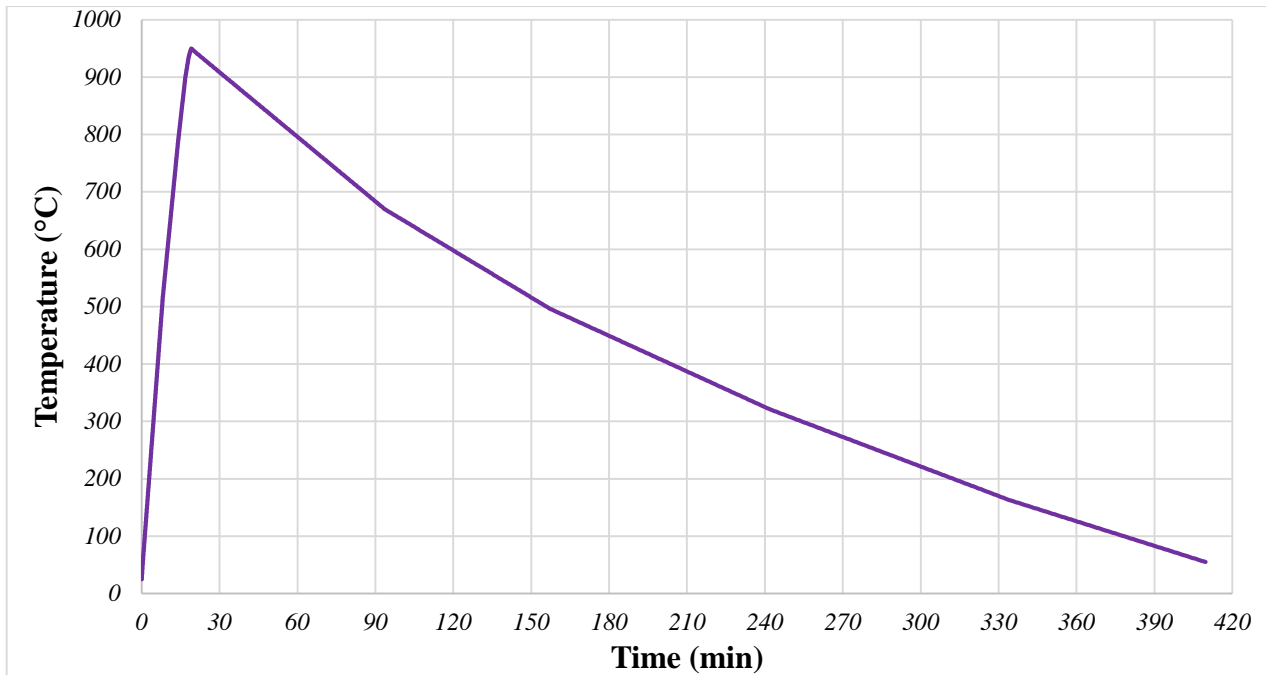


Figure 40. Temperature profile of the tubular furnace to a maximum of 950°C for cleaning of CNT depositions.

After collecting the quartz substrate, the characteristic black color of the CNT deposition disappeared. The resistance of the deposition was measured using the electrodes on the substrate, and a resistance out of range was observed indicating the absence of any conductivity between the electrodes. The resistance of the deposition before heating in the furnace was 53 kΩ.

The procedure was continued by reducing the maximum temperature in each experiment until a measurable and acceptable resistance was identified. As shown in Table 4, at 650°C, the increase in the deposition resistance is acceptable and this confirms the presence of the SWCNT network on the quartz surface.

Table 4. Impact of heating under vacuum at different temperatures on the resistance of SWCNT depositions

Resistance before heating (kΩ)	Heating temperature (°C)	Resistance after heating (kΩ)
53	950	100000
48	900	100000
56	850	100000
54	800	50000
50	750	10000
47	700	1000
52	650	120

To ensure the stability of pressure within the tube, the optimal Heating Process was planned, wherein the samples were kept at 200°C for 2.5 hours, the temperature was then raised to 650°C, and after one hour, the heat source was switched off, allowing for a gradual cooling over several hours. The temperature profile is depicted in Figure 41. Based on this figure the optimal Heating Process can be break down to the following steps:

1. 3 minutes to reach the of 200°C,
2. 150 minutes (2.5 hours) at 200°C to ensure the stability of the vacuum,
3. 16 minutes to increase the temperature from 200°C to 650°C,
4. Keeping the temperature at 650°C for exactly one hour,
5. Stopping the furnace and let it cool down to room temperature, which takes 10.5 hours.



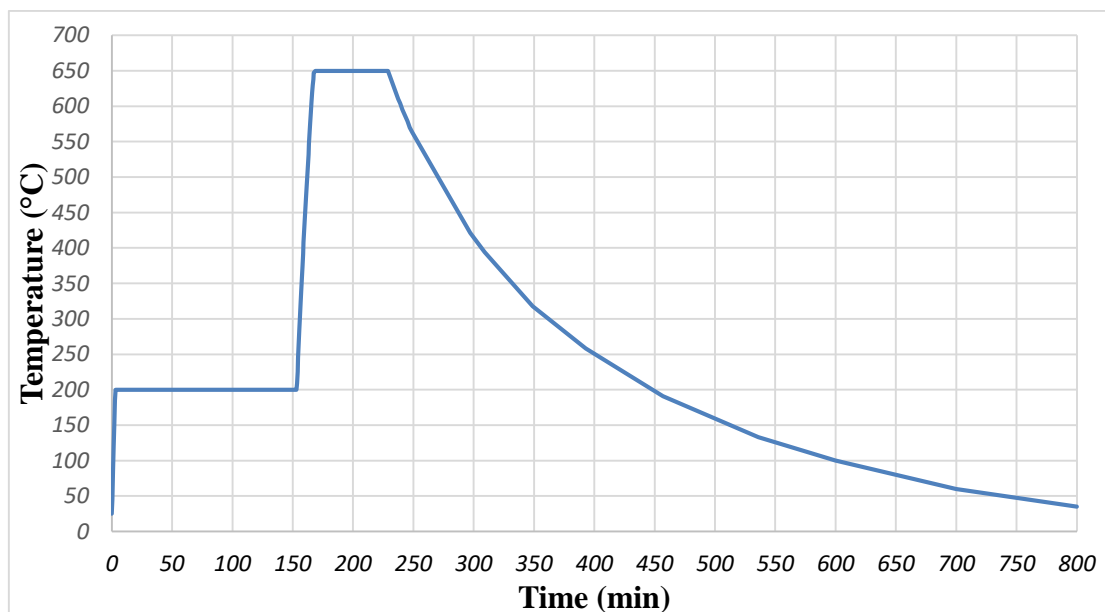


Figure 41. Optimal temperature profile compatible with lab processes and the best outcome.

### 2.5.3. Characterization of the Heating Process

To characterize the effect of the Heating Process on the quality of SWCNT depositions, RAMAN spectroscopy and TEM methods were investigated and will be discussed in this section. To make firm comparisons of the effect of the Heating Process, these characterization methods were applied to the same samples before and after heating, and the same area on the substrate was targeted.

#### 2.5.3.1. RAMAN spectroscopy

Over the duration of the present work, in multiple occasions throughout different campaigns of characterization, the Raman spectra of a SWCNT depositions before and after the Heating Process were obtained using the 100x objective and the 532 nm laser of a HORIBA Raman spectrometer. Table 5 summarizes the values of  $I_D$ ,  $I_G$ , and  $I_{2D}$  for all the measurements ever done on different samples. These measurements were done with different motivations that will

be discussed in the rest of the chapter or in the next chapter. In Table 5, the ratios of  $I_D/I_G$  and  $I_D/I_{2D}$  have also been calculated, and completed with the statistical data.

Table 5. Summary presentation of all Raman spectroscopy results, with calculated averages of important ratios.

Before heating					After heating				
$I_D$	$I_G$	$I_{2D}$	$I_D/I_G$	$I_D/I_{2D}$	$I_D$	$I_G$	$I_{2D}$	$I_D/I_G$	$I_D/I_{2D}$
1122	2713	338	0.41	3.32	1534	12459	3030	0.12	0.51
3401	9920	2427	0.34	1.40	6536	50223	22366	0.13	0.29
4780	10125	2496	0.47	1.92	6944	49753	22254	0.14	0.31
6650	9509	2311	0.70	2.88	7078	49265	21949	0.14	0.32
6837	9402	2267	0.73	3.02	7669	49935	21694	0.15	0.35
7320	9095	2165	0.80	3.38	7689	41345	14809	0.19	0.52
7506	8979	2125	0.84	3.53	7988	48526	21405	0.16	0.37
7547	8982	2124	0.84	3.55	8339	48243	21310	0.17	0.39
<b>Average</b>			<b>0.64</b>	<b>2.87</b>	8061	48927	21065	0.16	0.38
<b>St.dev</b>			<b>0.20</b>	<b>0.80</b>	10008	47112	19399	0.21	0.52
<b>CV%</b>			<b>31</b>	<b>28</b>	9092	47165	21704	0.19	0.42
					9348	46636	20310	0.20	0.46
					9520	46261	20120	0.21	0.47
					9662	43916	19935	0.22	0.48
					9875	45485	19651	0.22	0.50
					<b>Average</b>			<b>0.18</b>	<b>0.42</b>
					<b>St.dev</b>			<b>0.03</b>	<b>0.08</b>
					<b>CV%</b>			<b>18</b>	<b>19</b>

The ratio of  $I_D/I_G$  before the Heating Process on average of eight different characterizations is 0.64, while it decreases to 0.18 (average of 15 different characterizations) after the process. The D band corresponds to defects or disorder in the carbon structure, while the G band represents the graphitic carbon structure.<sup>254</sup> A smaller ratio of the intensity of the D band to G band in carbon nanotubes indicates a higher degree of graphitization and lower defect density, which is often associated with higher quality carbon nanotubes.<sup>255</sup> This ratio is a key indicator

of the structural quality and purity of carbon nanotubes, as it reflects the level of disorder and defects in the graphitic  $sp^2$  network of the nanotubes.<sup>256</sup>

However, since the sample is SWCNT, a degradation of an outer layer could not explain the decrease in the ratio. The ratio of  $I_D/I_{2D}$  can be studied to obtain more information and explain the physical events that result from the Heating Process. This ratio has decreased from 2.87 to 0.42 after the Heating Process. The  $I_D/I_{2D}$  ratio depends on the amount of graphitic flakes (stacked  $\pi$ -rich groups) deposited on the nanotube surface, and Raman spectroscopy provides a nondestructive control of structural and electronic characteristics of carbon materials, including the 2D band.<sup>257</sup>

Figure 42 shows the Raman spectra of SWCNT before and after the Heating Process.

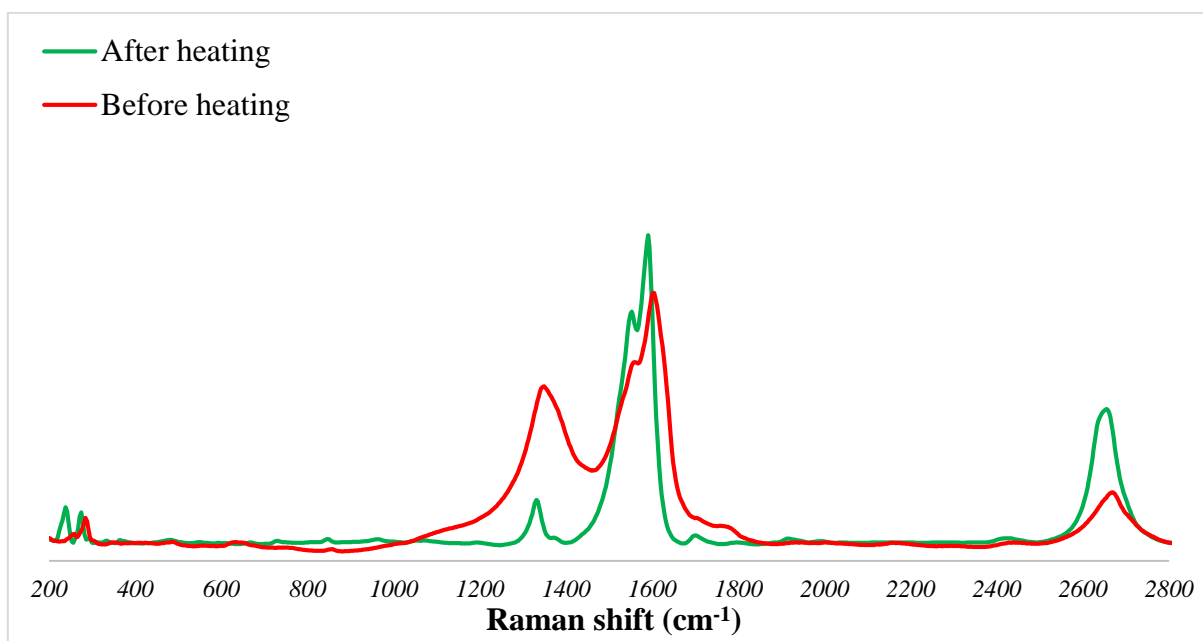
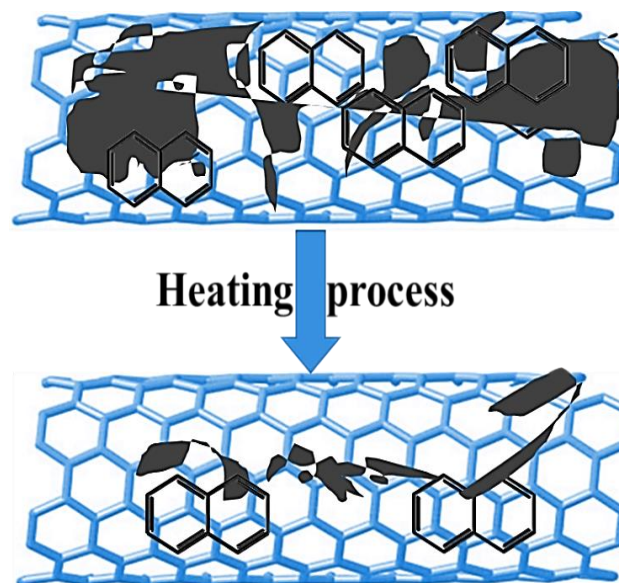


Figure 42. Comparison between the Raman spectra of a SWCNT deposition, before and after the Heating Process.

Based on the information derived from  $I_D/I_G$  and  $I_D/I_{2D}$ , it is observed that the number of graphitic layers detected by the Raman laser has diminished, along with a reduction in the

intensity of defective zones. This phenomenon signifies that a form of  $\pi$ - $\pi$  interaction is established between the SWCNT surface and the amorphous matter covering it. However, owing to their high edge effect, these interactions also contribute to the formation of additional defective zones. Consequently, the elimination of a significant portion of the amorphous matter results in a decrease in the number of stacked conjugated groups, along with a reduction in their edge effect, which, in turn, mitigates the occurrence of a prominent D peak. Figure 43 serves as an illustration of this model, supported by the results of Raman scattering.



*Figure 43. Heating Process impact, with the presence of random conjugated groups among the amorphous matter.*

Raman scattering was conducted on MWCNT only one time to observe the impact of the Heating Process. Figure 44 demonstrates a decrease in the  $I_D/I_G$  ratio from 1.38 to 1.22 and a decrease in the  $I_D/I_{2D}$  ratio from 3.66 to 2.28. Despite indicating an enhancement in the quality of MWCNTs, these results also highlight the persistent prevalence of defects within the MWCNT structure, even after the application of the heating process.

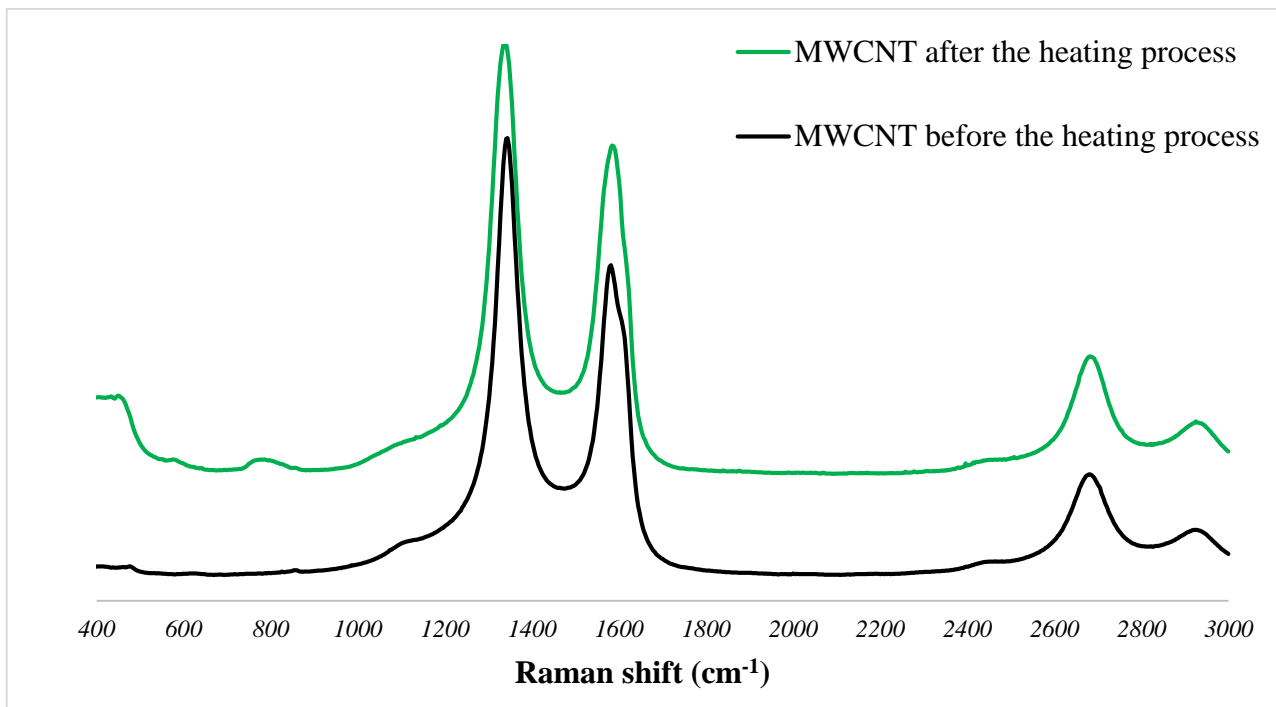
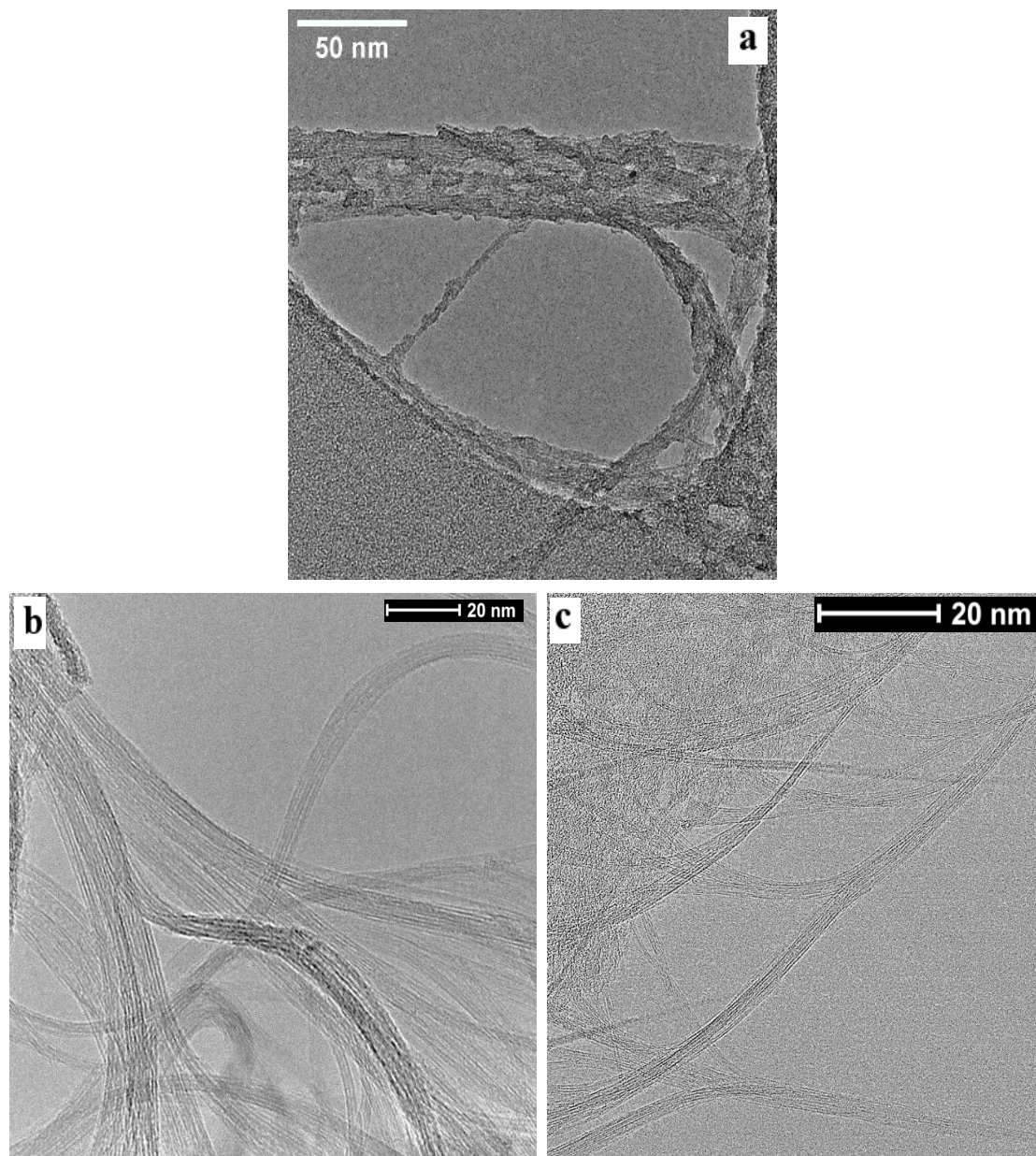


Figure 44. Effect of the Heating Process on the Raman spectra of MWCNTs.

### 2.5.3.2. TEM analysis of the effect of the Heating Process

For the TEM analysis, a thin and fragile grid is used to scan the surface and handling this grid can be challenging. Two methods were followed to ensure sample collection. In the first method, quartz substrates were used for the ink deposition and the Heating Process was applied to the substrate. Afterwards, the surface of the CNT deposition was scratched using a sharp object and the TEM grid was scrubbed against the scratched area to collect the sample. In the second method, the ink was deposited onto the TEM grid and to apply the Heating Process, the grid was placed in a tiny quartz tube, covered with aluminum foil and placed in the furnace tube for the Heating Process.





*Figure 45. Effect of the Heating Process on the surface quality of SWCNT by TEM analysis. a) Usual SWCNT network before heating. b) Usual SWCNT network after heating by using a tiny tube. c) Usual SWCNT network after heating by scratching the surface and scrubbing the TEM grid.*

#### **2.5.4. Going beyond the heating process**

The described Heating Process represents the maximum temperature at which CNTs can be heated without being burned under a primary vacuum. In two experiments, attempts were

made to explore alternative methods of cleaning the CNT surface while avoiding high temperatures. In one experiment, different temperatures were tested in both air and under vacuum conditions, while in the other experiment, UV-Ozone treatment was employed.

### 2.5.4.1. Effect of the temperature and pressure on the Heating Process on

Figure 46 presents the Raman spectra, comparing the effect of temperature annealing in air on the quality of SWCNT depositions. Each sample underwent annealing for 30 minutes. As indicated in the table, increasing the temperature from 250°C (deposition temperature) to 375°C resulted in improved quality of SWCNTs. Notably, at 400°C, the CNTs began to disappear from the surface, leading to a low CNT content and resulting in unusual Raman spectra with high  $I_D/I_G$  and  $I_D/I_{2D}$  ratios. It is worth mentioning that the temperature of 425°C was also tested; however, evidently, no SWCNTs remained on the surface.

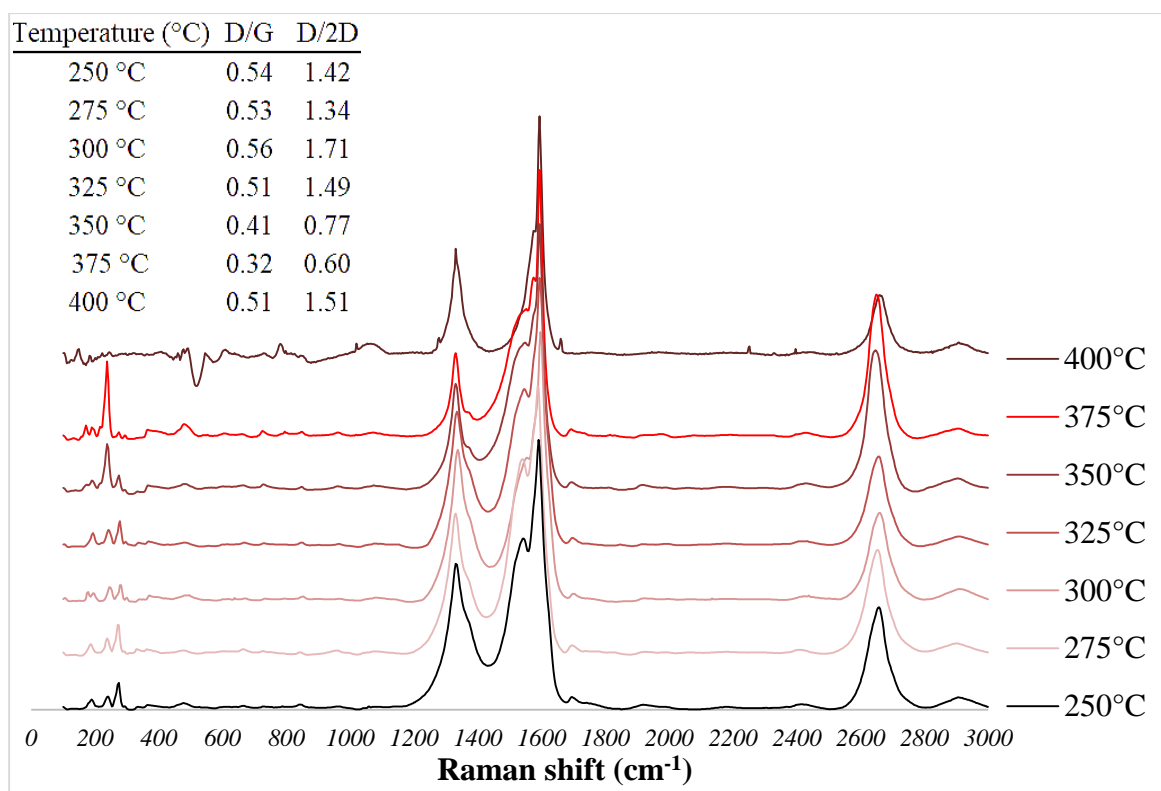


Figure 46. Effect of the heating temperature in air on SWCNT quality.

The Heating Process was additionally tested at maximum temperatures of 375°C and 500°C under primary vacuum to compare with the results of the heating temperature of 650°C. Figure 47 displays the outcomes of this experiment. It is evident that applying lower temperatures under vacuum does not yield the same results in terms of  $I_D/I_G$  and  $I_D/I_{2D}$  for the SWCNT deposition.

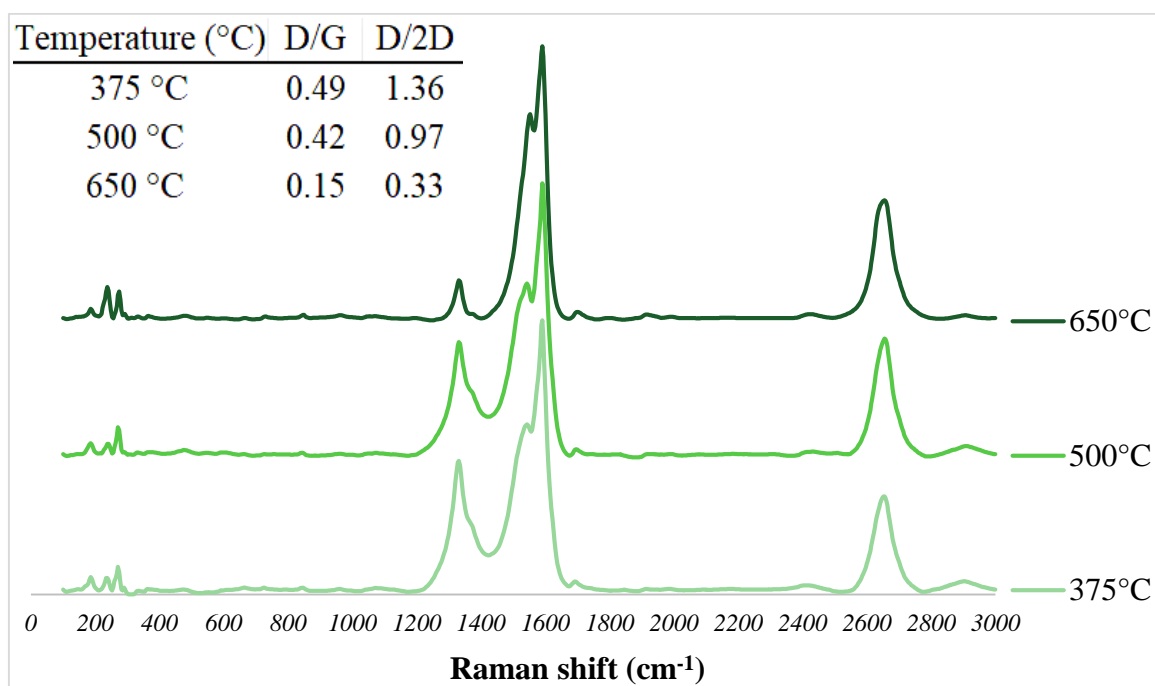


Figure 47. Effect of the heating temperature under vacuum on SWCNT quality.

It is noteworthy that at the same temperature of 375°C, the quality of SWCNTs is higher (considering  $I_D/I_G$  and  $I_D/I_{2D}$  ratios) when the heating is conducted in air compared to under vacuum. Even increasing the heating temperature under vacuum to 500°C does not result in better quality compared to heating in air at 375°C. This observation suggests that the amorphous matter has a high degradation temperature, primarily due to the interaction it creates with the surface of SWCNTs. Figure 48 summarizes the Raman results in terms of  $I_D/I_G$  and  $I_D/I_{2D}$  ratios for the explained heating conditions.



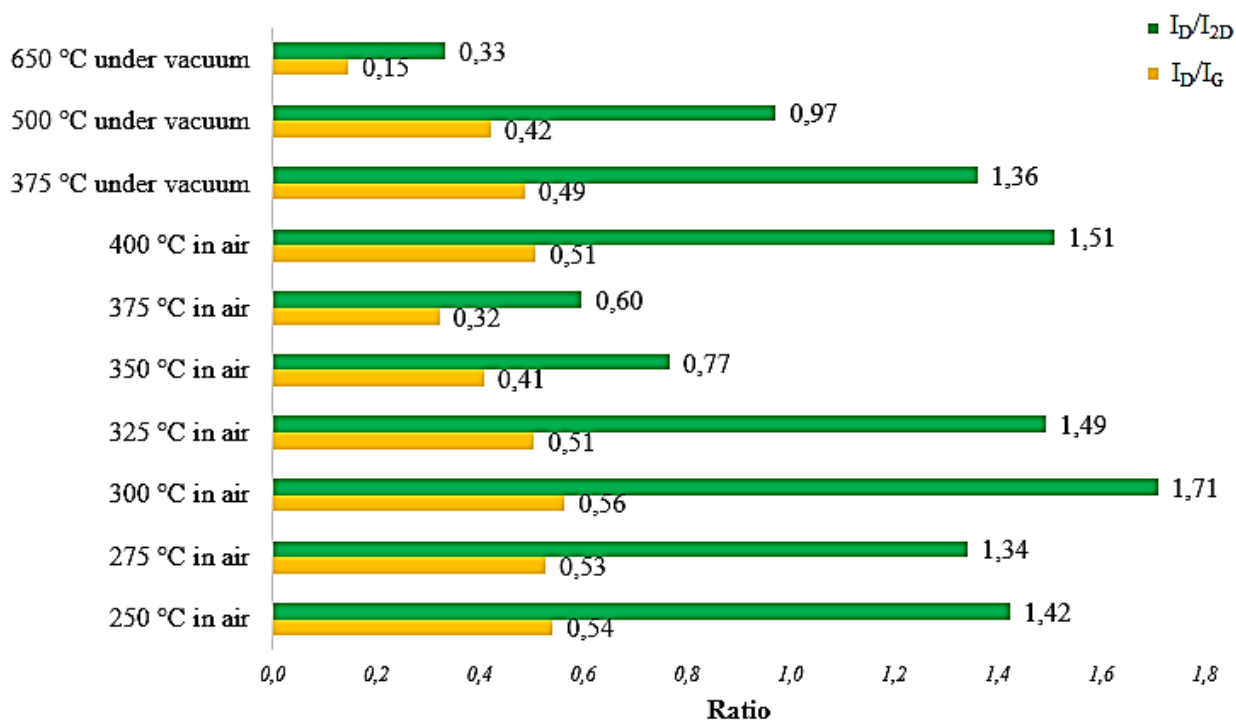


Figure 48. Effect of the temperature and oxygen content in the Heating Process on the quality of SWCNTs.

The Scanning Electron Microscopy (SEM) image in Figure 49 illustrates the varying impacts of heating in air at 375°C and under vacuum on the density of SWCNTs remaining on the surface. Due to heating in the presence of atmospheric pressure of oxygen, a thin film of CNTs degrades easily at 375°C. However, by reducing the oxygen pressure using a primary pump, applying a temperature as high as 650°C only leads to the degradation of the amorphous matter, leaving the CNT network intact. These SEM images were taken by Dr. Issoufou Ibrahim Zamkoye, during a mutual project on the study of the heating process.

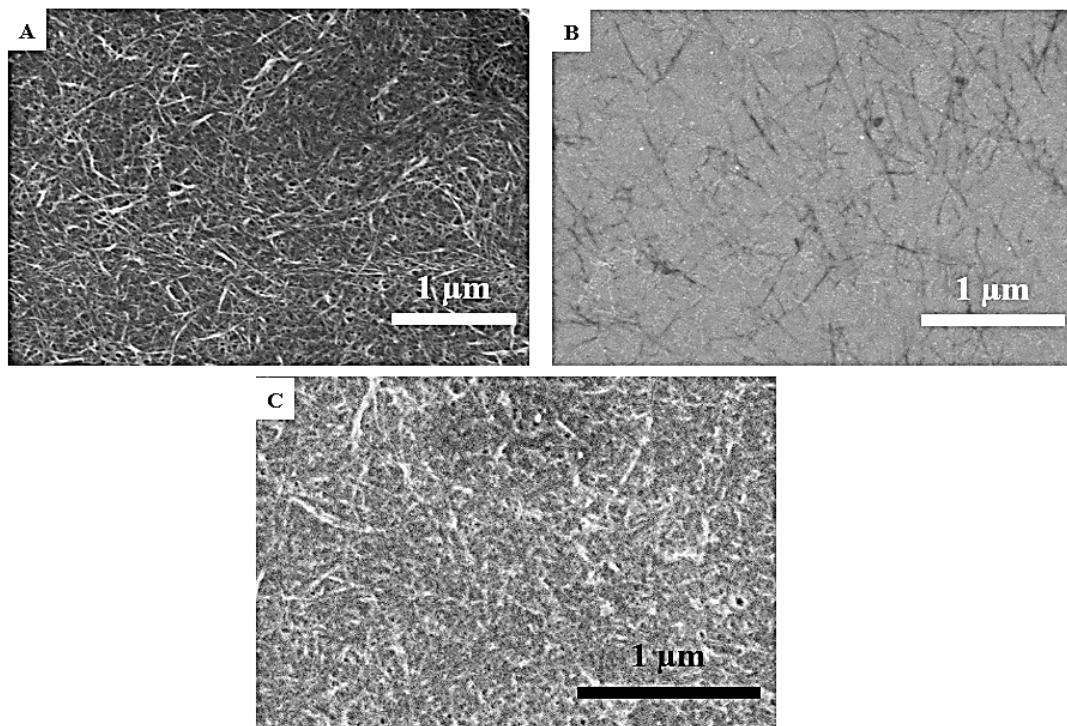


Figure 49. SEM images of a SWCNT deposition A) before heating, B) after heating in air at 375°C, and C) after applying the Heating Process.<sup>3</sup>

## 2.6. Conclusion on the processing of CNTs

This chapter delves into the critical aspect of preparing CNTs prior to embarking on functionalization processes. In certain applications where the electronic properties of CNTs are of utmost significance, exploring functionalization pathways holds promise, even in the presence of amorphous matter. Through functionalization, a mixture of mechanical, thermal, and chemical modifications can be induced in CNT behavior, irrespective of the initial quality of the CNTs.<sup>1-3</sup> However, when electronic exchanges at the interface of CNTs and functional groups are important, attention must be given to the surface quality of the CNTs. This ensures

---

<sup>3</sup> Credit: Dr. Issoufou Ibrahim Zamkoye

the effectiveness and reliability of electronic interactions, thereby enhancing the performance of CNT-based systems in electronic applications.

The aim of this chapter was to investigate the necessity of post-treatment procedures to guarantee the surface quality of CNTs before advancing towards the development of sensing devices. Here is a drill-down of what was presented in the present chapter, in a logical order:

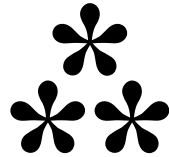
- 1- In the present work, solution-based deposition methods of CNTs are chosen for their versatility, low cost, and high scalability.**
- 2- In the realm of sensor development, the morphology of deposition and the well dispersion of CNTs in a homogenous network is important for sensor reliability.
- 3- A homogenous network of CNTs can only be produced from an ink with highly dispersed nanotubes.
- 4- CNTs received from the provider, underwent a purification process to eliminate the majority of their amorphous matter. However, this process, does not guarantee the total elimination of the amorphous matter.
- 5- oDCB and NMP are solvents that can disperse CNTs, using sonication. Dispersions (inks) with NMP as solvent offer 50 times longer lifetime than those based on oDCB.**
- 6- Inkjet printing was in particular was investigated and a process with Dimatix Printer was optimized that uses one nozzle, a drop speed of 6 m/s, and a distance from substrate of 500  $\mu\text{m}$ .**
- 7- Sonication is shown to provide enough energy to initiate a ring-opening of oDCB and NMP solvent, **resulting** in the degradation of these solvents and the creation of so-called “sonochemicals”. These sonochemicals can induce even more amorphous matter on the CNT walls.
- 8- A step of post treatment is necessary to purify CNTs to another level by eliminating the amorphous matter remaining from the powder form, and more importantly, the sonochemicals that occupy CNT walls.



- 9- **In the present work, a process was developed that consists of heating CNT thin films at 650°C and 1 mbar. This procedure was characterized in this chapter and was proven to be efficient in enhancing the quality of the CNTs.**



**Institut Polytechnique de Paris**



# Third Chapter

# Functionalization of CNTs

### 3. Functionalization of CNTs

In the previous chapter, the successful purification and treatment of the CNTs as thin films was discussed and the Heating Process that led to interesting results, was thoroughly characterized by different methods. This step was vital in the progression of this project, due to the choice of solvent-based deposition, and the functionalization in the next step.

Despite numerous references in the literature, functionalization of CNTs is still a subject of interest and can be adapted to different types of development projects and applications.

In this chapter, the functionalization of CNTs will be thoroughly studied. Three methods will be discussed to functionalize the walls of CNTs with different molecules. These methods are called mixing, one pot, and incubation.

In the following sections, the detailed steps of each method will be discussed and the superiority of incubation method to functionalize CNTs will be put into evidence.

#### 3.1. Conjugated molecules for noncovalent functionalization of CNTs

The exploration of noncovalent functionalization involving carbon nanotubes (CNTs) and conjugated molecules has attracted considerable attention within the realm of sensing applications. Conjugated molecules, distinguished by their delocalized  $\pi$ -electron systems, present distinctive electronic and structural properties. These properties enable effective interactions with the  $sp^2$  carbon network of CNTs, positioning them as promising contenders for optimizing the performance of sensors based on CNTs.<sup>83</sup> This method allows for the retention of the inherent properties of CNTs, simultaneously introducing supplementary functionalities through mechanisms such as  $\pi$ - $\pi$  stacking, van der Waals interactions, and other noncovalent bonding interactions.<sup>258</sup>

Leveraging conjugated molecules for the noncovalent functionalization of CNTs provides a versatile foundation for customizing the characteristics of materials based on CNTs, particularly for applications in sensing.<sup>259</sup> Utilizing the  $\pi$ -conjugated systems of organic molecules, scientists have investigated ways to improve the dispersion of CNTs in sensing matrices. Additionally, they have explored methods for modulating electronic properties and enhancing interfacial interactions within nanocomposites for sensors.<sup>260</sup>

### 3.1.1. Choice of conjugated molecules

The selection of chemical groups for noncovalent functionalization holds significance on two fronts. Firstly, the chosen chemical must be capable of establishing  $\pi$ - $\pi$  interactions with the CNT. Secondly, it should incorporate specific groups that can selectively interact with the desired analytes in a water environment<sup>261</sup>. In addition to their conjugated structure, which makes them good candidates for  $\pi$ - $\pi$  stacking on CNTs, pyrene and porphyrin molecules illustrated in Figure 50, exhibit fluorescent properties<sup>262,263</sup> that allows to make preliminary studies on their interactions with CNTs as well as the analytes of interest in water.

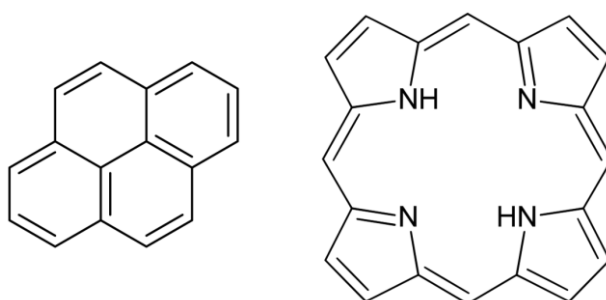


Figure 50. Left: Pyrene molecule, right: Porphyrin molecule.

Given their extensive aromaticity and conjugated system of  $\pi$  orbitals, pyrene derivatives stand out as top candidates for the functionalization of CNTs.<sup>264–267</sup> Pyrene derivatives are



largely studied as optical sensors.<sup>268</sup> Also, pyrene groups have been used to synthesize new molecules for different applications. They can be attached to other chemical groups like thiourea<sup>266</sup>, carboxylates,<sup>269</sup> esters,<sup>270</sup> etc. These attached groups interact with the analytes in the surrounding environment which involves electron exchange.

Porphyrin molecules, with their large aromaticity and conjugated system of  $\pi$  orbitals, are highly suitable for noncovalently functionalizing CNTs.<sup>271</sup> Porphyrin derivatives have been used in the preparation of optical sensors, showcasing substantial potential in this particular application.<sup>272</sup> They have been widely utilized to synthesize new molecules for various applications, often by attaching them to other chemical groups.<sup>273,274</sup>

The exploration of noncovalent binding between porphyrin molecules and CNTs has been established as a potent strategy to enhance the solubility of CNTs and introduce functionality without compromising the electronic structure.<sup>275,276</sup> Theoretical works have also been conducted to investigate the noncovalent adsorption of porphyrins and metalloporphyrins on CNT sidewalls, providing insights into  $\pi$ - $\pi$  interactions.<sup>277,278</sup>

Collectively, these studies show the diverse methods through which porphyrin molecules can noncovalently functionalize CNTs, highlighting their versatility and potential for a range of applications.

### 3.1.2. Description of molecules

In this project different molecules based on pyrene and porphyrin derivatives were studied for functionalization. Figure 51 shows the Four molecules that we studied extensively. All these molecules were designed, engineered, and synthesized in LPICM chemistry group by Dr. Christian Murga, Dr. Arghyadeep Bhattacharyya, and Dr. Qiqiao Lin under the supervision of Dr. Gael Zucchi.

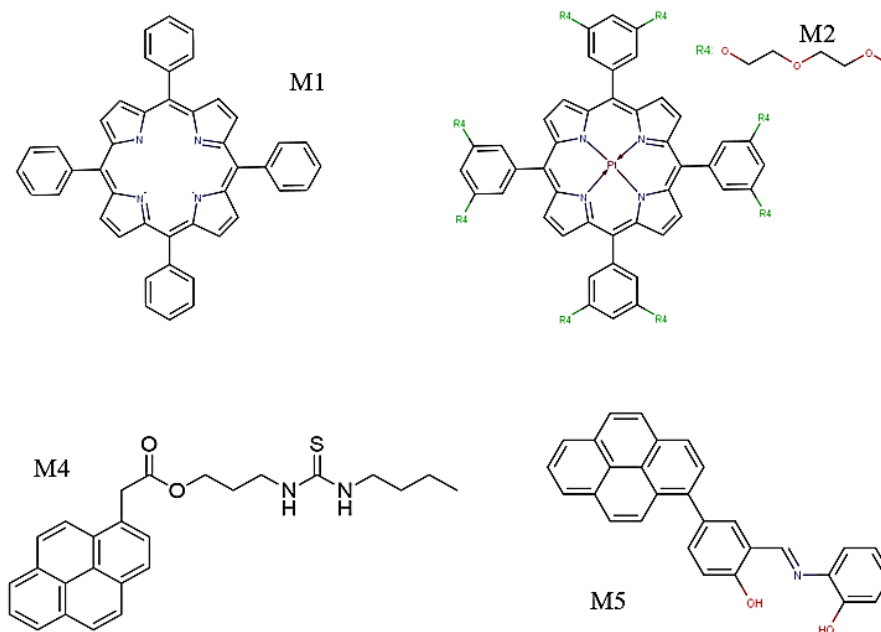


Figure 51. Some of the molecules used in this project.

Initial fluorescent studies on M5 reveal the sensitivity and selectivity of this molecule towards glyphosate, a widely used herbicide that has raised concerns regarding its impact on water quality due to the potential for leaching into ground and surface waters.<sup>279</sup> Studies have indicated that glyphosate can persist in the environment for long periods and has been found in surface and subsurface water sources, posing a threat to aquatic organisms.<sup>280–282</sup>

M2 is a molecule that was engineered and characterized by our chemistry group. This molecule has 8 ether chains that make the molecule less hydrophobic which is important for water analysis. The molecule is also complexing a platinum ion that can bind to dissolved oxygen in water.

Adequate levels of dissolved oxygen are essential for the sustainability of freshwater and marine environments, highlighting the importance of monitoring and maintaining appropriate dissolved oxygen concentrations in water bodies. Dissolved oxygen is a key indicator of stream water quality and ecosystem health.<sup>283,284</sup> Low levels of dissolved oxygen, often resulting from eutrophication and enhanced primary production, can lead to adverse effects on marine and freshwater ecosystems, impacting the biological health of rivers and the survival

of diverse aquatic life.<sup>285,286</sup> Additionally, the Dissolved Oxygen (DO) concentration in water is essential for aerobic communities living in aquatic systems and is involved in all metabolic processes, making it a critical factor for ecosystem sustainability.<sup>170</sup>

### 3.1.3. Emission spectroscopy of CNT-molecule interactions

In this section, we aim to characterize the interaction between CNTs and the molecules with emission spectroscopy studies. At low ranges of concentrations of pyrene<sup>287</sup> and porphyrin<sup>288</sup> molecules, their emission intensity decreases proportionally with their concentration in different solvents. On the other hand, several studies have investigated the photophysical interactions and energy transfer processes between pyrene<sup>289,290</sup> and porphyrin<sup>291,292</sup> molecules and carbon nanotubes. Emission spectroscopy studies were done on M1, M2, and M5 molecules to determine the impact of the presence of Single-Walled carbon nanotubes (SWCNTs).

For each molecule, fluorescent studies were done twice. In the first instance, the initial molecule solution was diluted by adding the pure solvent (NMP), and in the second instance, by adding a diluted SWCNT ink (estimated 2 mg/L). For each test, 35 spectra at different concentrations were collected. The chosen initial concentration for each molecule is the highest possible for the fluorescent device detector, before saturation, and it is different for each molecule studied here.

For the M1 molecule (porphyrin-based molecule), the initial concentration is 5  $\mu\text{M}$ . The left plot of Figure 52, shows the diluting of the initial solution from 5  $\mu\text{M}$  to 1.5  $\mu\text{M}$  in 35 steps with the pure solvent. As the black plot in Figure 53 shows, this dilution results in mild decrease in the maximum intensity of the spectra down to 3.5  $\mu\text{M}$ . However, further dilution from 3.5  $\mu\text{M}$  to 1.5  $\mu\text{M}$  happens with a higher rate with a seldom linear behavior.

On the other hand, the right plot of Figure 52, shows the diluting of the initial solution from 5  $\mu\text{M}$  to 1.5  $\mu\text{M}$  in 35 steps with a diluted SWCNT ink, instead of the pure solvent. As the red

plot in Figure 53 shows, contrary to the previous case, the decrease in the intensity happens at a higher rate, indicating the possible  $\pi$ - $\pi$  interactions of the M1 molecule with the SWCNTs.

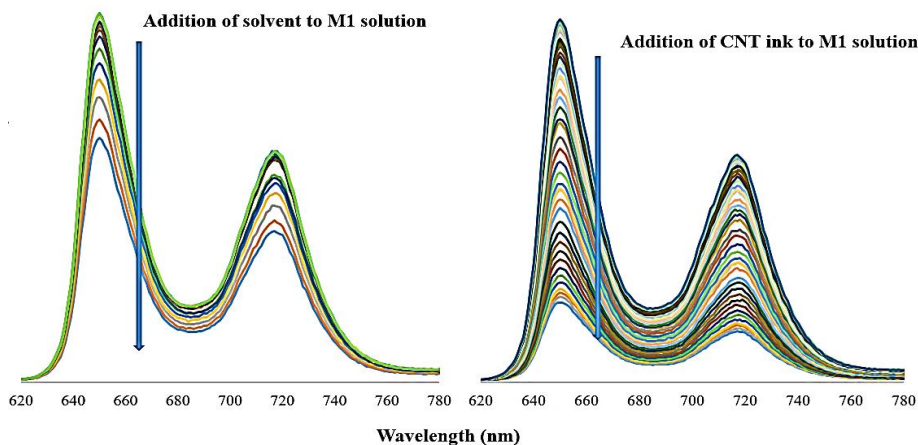


Figure 52. Dilution of M1 molecule with the solvent (left) and the CNT ink(right)

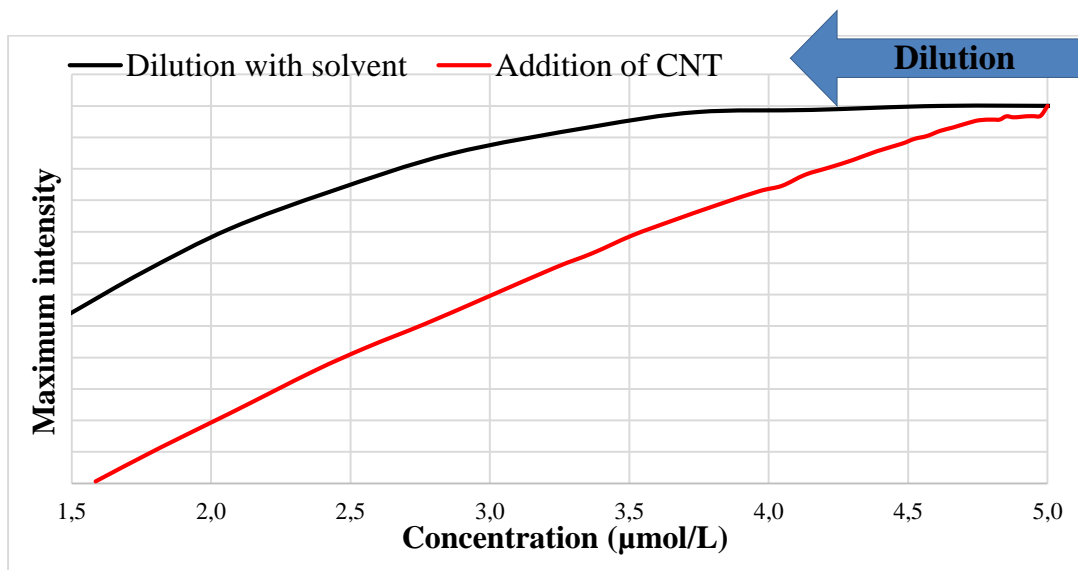


Figure 53. Quenching of maximum emission for M1 molecule by adding solvent and the diluted CNT ink.

These results indicate that aggregates of the M1 molecule begin to form around SWCNTs immediately upon the addition of the ink. As depicted in Figure 53, for solutions more diluted than 2.5  $\mu$ M, the emission intensity decreases with the same slope for both cases, suggesting that the impact of dilutions becomes significant at concentrations lower than 2.5  $\mu$ M.

For M2 molecule (porphyrin-based molecule), the initial concentration is 6.8  $\mu\text{M}$ . The left plot of Figure 54, shows the diluting of the initial solution from 6.8  $\mu\text{M}$  to 2.5  $\mu\text{M}$  in 35 steps with the pure solvent. As the black plot in Figure 55 shows, this dilution results in mild decrease in the maximum intensity of the spectra down to 6  $\mu\text{M}$ . However, further dilution from 6  $\mu\text{M}$  to 2.5  $\mu\text{M}$  happens with a higher rate with a linear behavior.

On the other hand, the right plot of Figure 54, shows the diluting of the initial solution from 6.8  $\mu\text{M}$  to 2.5  $\mu\text{M}$  in 35 steps with a diluted SWCNT ink, instead of the pure solvent. As the orange plot in Figure 55 shows, contrary to the previous case, a sharp decrease in the intensity happens at the first moment of adding the SWCNT ink, and then the rate of decreases becomes more similar to the case of dilution with the solvent. The sharp immediate decrease in the emission intensity shows a strong affinity of the M2 molecule to create  $\pi$ - $\pi$  interactions with the added SWCNTs.

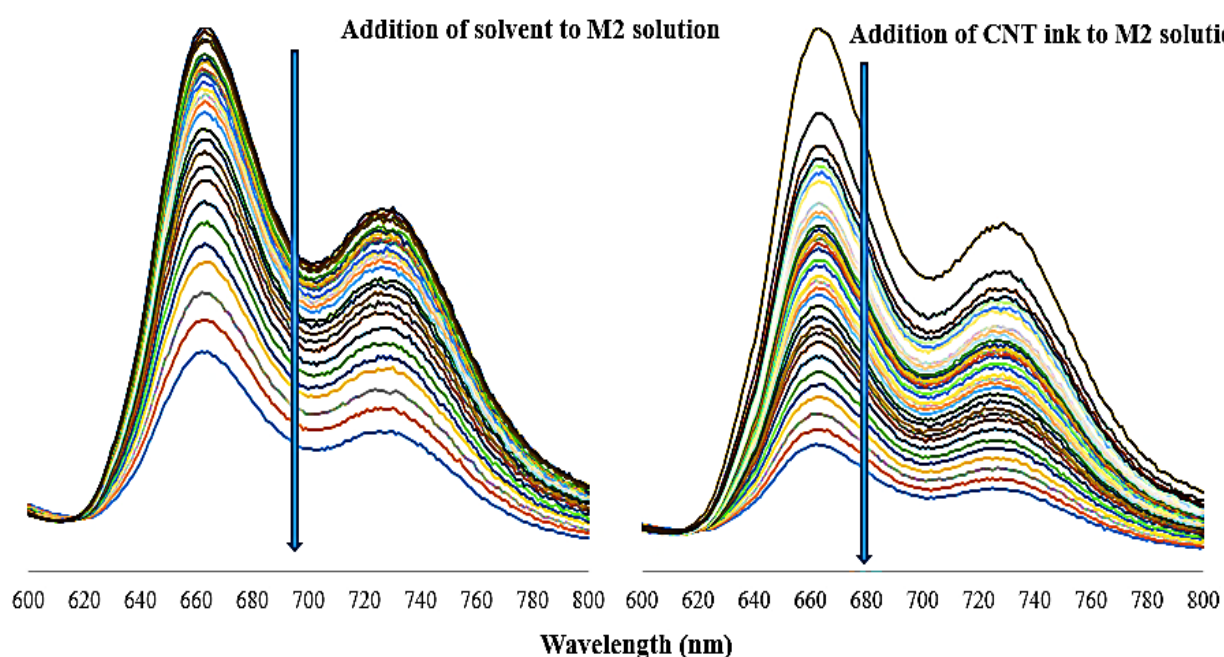


Figure 54. Dilution of M2 molecule with the solvent (left) and the CNT ink(right).

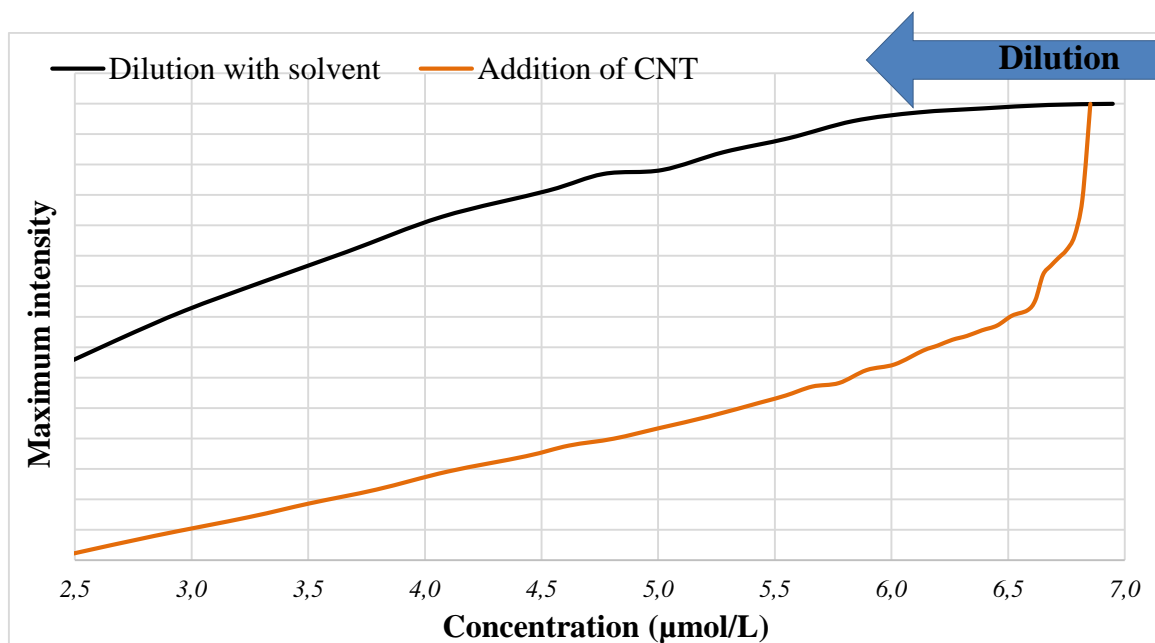


Figure 55. Quenching of maximum emission for M2 molecule by adding solvent and the diluted CNT ink.

Examining Figure 51, it's worth highlighting two significant distinctions between M2 and M1. Firstly, M2 forms a complex with a platinum ion, enhancing the interactions of porphyrin with SWCNTs through  $sp^2$ -d hybridization.<sup>293</sup> Secondly, the presence of larger 2s character in the hybrid orbitals within an ether strengthens the C–O bond, potentially influencing noncovalent interactions between ethers and CNTs due to the enhanced  $sp^2$  hybridization properties.<sup>294</sup>

For the M5 molecule (a pyrene-based molecule), the initial concentration is at 12.1  $\mu\text{M}$ . The left plot of Figure 56, shows the diluting of the initial solution from 12.1  $\mu\text{M}$  to 3.8  $\mu\text{M}$  in 35 steps with the pure solvent, and the right plot of Figure 56, shows the same dilution with a diluted SWCNT ink, instead of the pure solvent.

Illustrated in Figure 57, the introduction of SWCNTs leads to a swifter initial reduction in the emission spectra compared to the addition of the solvent. Nonetheless, it's crucial to emphasize that the effectiveness of the interaction between pyrene molecules and CNTs is comparatively lower than that of porphyrins, attributable to the size disparity in their conjugated systems.

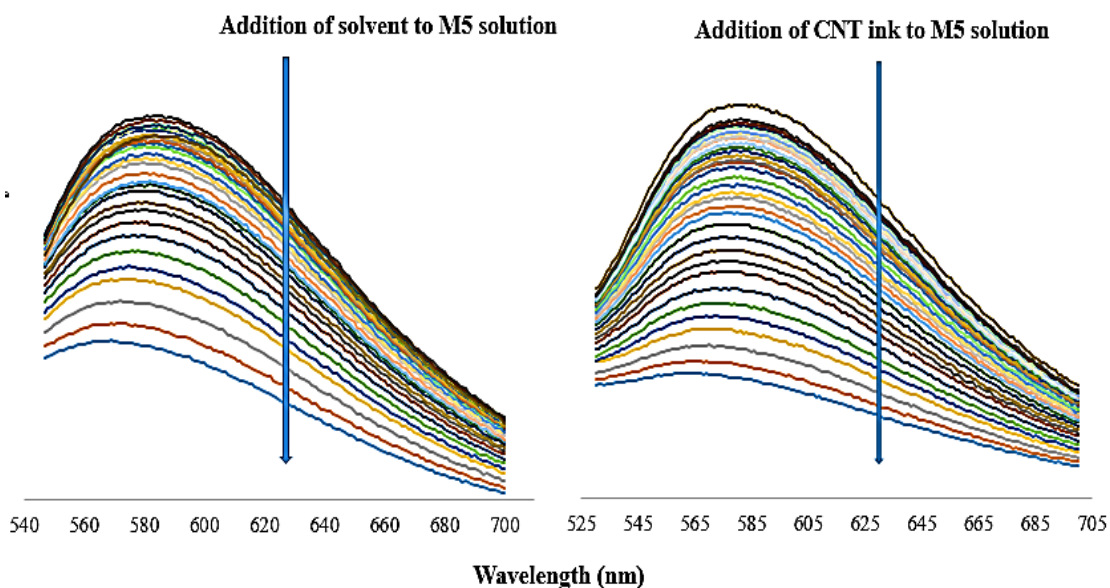


Figure 56. Dilution of M5 molecule with the solvent (left) and the CNT ink(right).

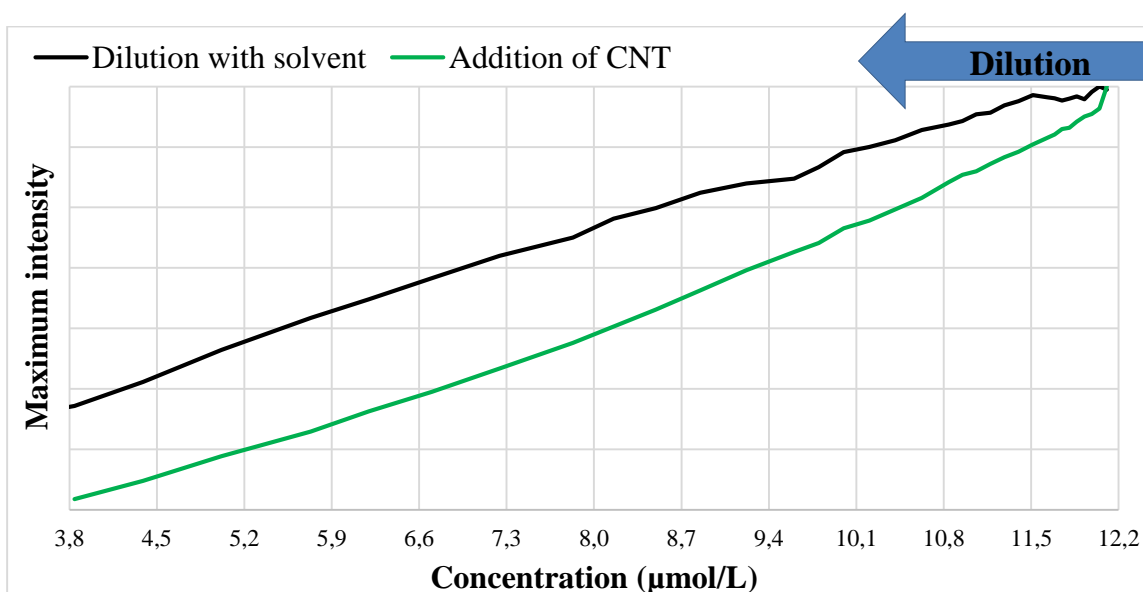


Figure 57. Quenching of maximum emission for M5 molecule by adding solvent and the diluted CNT ink.

Based on the results of emission spectroscopy, it can be concluded that, for the three mentioned molecules, certain interactions occur between the molecule and SWCNT when they

are introduced into the solution. The observation that the quenching of molecule emission is not as pronounced as when SWCNT is added suggests that, upon the addition of SWCNT ink to the molecule solution, a portion of the molecules attach to CNTs in a manner that prevents their emission. However, caution must be exercised in connecting these interactions to effective  $\pi$ - $\pi$  stacking, given that the SWCNTs have undergone the ink preparation process, and their surface has been contaminated with amorphous matter. Nevertheless, an affinity exists between SWCNTs and all these molecules, resulting in emission quenching for each molecule.

## **3.2. Methods of functionalization**

In this project, three different methods of functionalization were experimented with. For both mixing and one-pot methods, the functionalization is carried out in the liquid phase before the heating process. In the case of the incubation method, a film of CNT is deposited, and then this method is applied. In this section, each functionalization method will be explained and by further characterization their effectiveness is compared.

### **3.2.1. Mixing functionalization**

In this method, a solution of the molecule is mixed with the CNT ink and subjected to sonication for 30 minutes to immobilize the molecules on the CNT surface. The critical parameter in this method is the mass ratio of the molecule to CNT. To determine the optimal ratio for each molecule, 25 mixtures of CNT + molecule with varying ratios were prepared through sonication for 30 minutes. Subsequently, the samples are subjected to Ultracentrifugation at 100,000 rpm to facilitate the sedimentation of all functionalized CNTs at the bottom of the tube. The resulting supernatant of each sample constitutes a clear solution of the molecule.



Emission spectroscopy studies were done on the resulting supernatant solution to obtain insight about their comparative concentrations. Figure 58 illustrates the normalized intensity of each sample at their maximum emission for a pyrene-based molecule.

Initially, the emission intensity remains relatively stable with an increase in the ratio, as indicated by the red line. This observation suggests that the CNTs are possibly not saturated yet and can potentially absorb more molecules on their surface through  $\pi$ - $\pi$  interactions. The emission of the molecule begins to increase at a ratio of 1.5, demonstrating a relatively linear behavior with the increase in molecule mass, as depicted by the green line. This phase signifies that the CNT surface becomes saturated, further addition of the molecule does not result in any further interaction, and the emission of the extra molecules become more and more important. Finally, the addition of more mass of the molecule leads to the quenching of the emission spectra, indicating the formation of aggregates of the molecule due to solution saturation,<sup>295,296</sup> as denoted by the blue line.

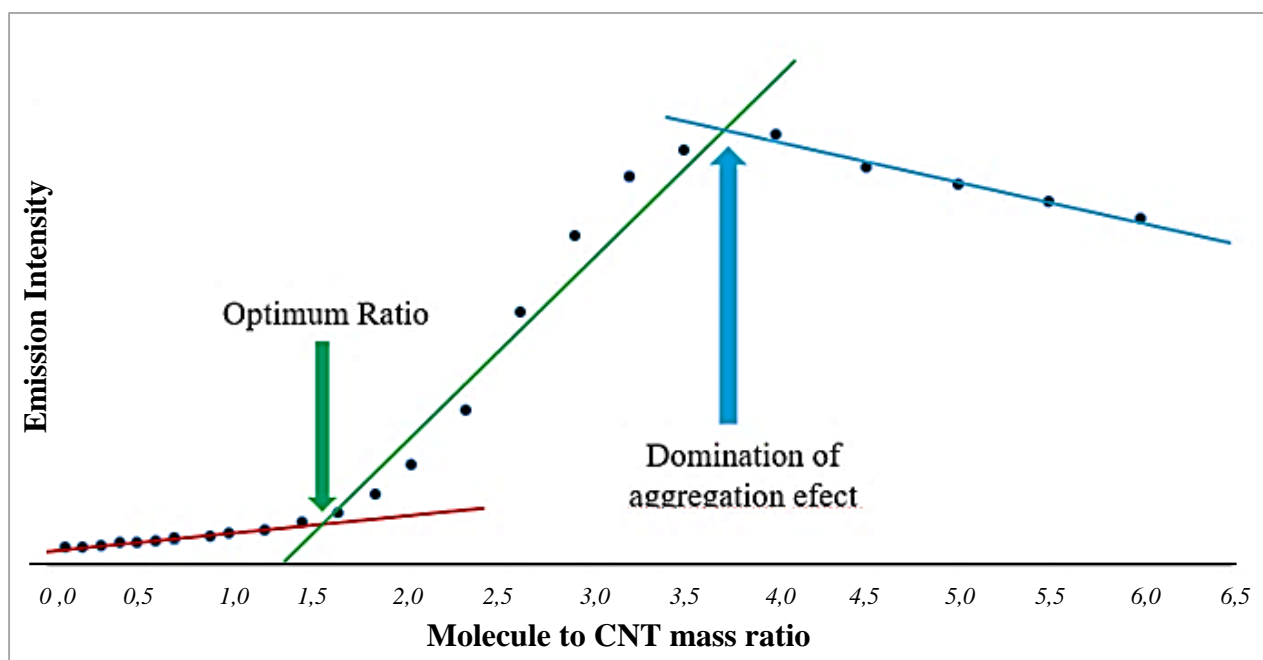


Figure 58. Emission of Molecule/CNT mixture supernatant at different ratios between the two materials.

It is important to note that Figure 58 serves as an illustrative example of the procedural approach that should be adopted for each molecule. Based on this methodology, the optimal ratio can be determined, which corresponds to the intersection of the red and green lines. The physical meaning of this intersection is the moment where the majority of CNT surfaces are covered with the molecule.

### 3.2.2. One-pot functionalization

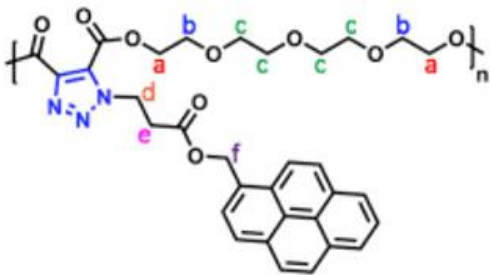
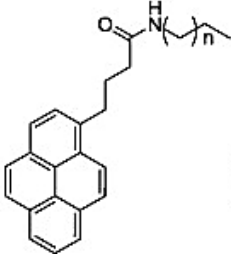
In chemistry, the term "one-pot" is utilized to describe a synthetic procedure in which all the required reagents are brought together in a single reaction vessel, enabling the sequential occurrence of multiple chemical transformations without the necessity of isolating intermediates.<sup>297</sup>

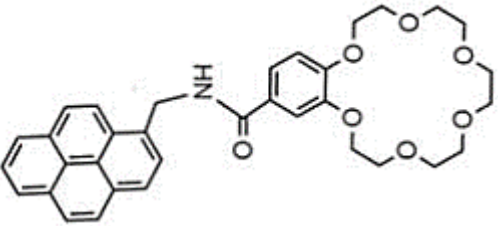
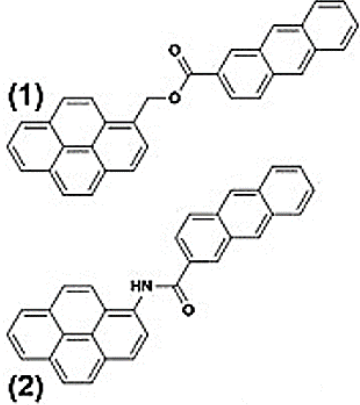
When applied to the functionalization of CNTs, the One-pot method involves combining CNTs, molecules, and the solvent in one vessel and conducting functionalization using sonication and magnetic stirring. Various parameters such as the mass ratio between CNTs and the molecule, solvent volume, temperature, and post-processing are manipulated. In the literature, different routes for one-pot functionalization of CNTs are documented, and Table 6 describes some examples. Molecules mentioned in this table are pyrene-based.

Based on the examples provided in literature, in this work the following process was applied:

- Mixing known mass of CNTs and the molecule, with a known volume of THF in one vessel,
- Sonication at 0 °C for 1 hour using a sonic bath (Fisherbrand, 37kHz, power 100%),
- Filtration on PTFE membrane with pore size of 0.2  $\mu\text{m}$ ,
- Washing the filtered solid with THF until the filtrate solvent is clear,
- Drain the solvent used for washing into a flask underneath the filter by applying vacuum in the flask,
- Drying the solid residue under vacuum over night at 50 °C.

Table 6. Parameters of One-pot functionalization for pyrene-based molecules in the literature (schemes taken with permission).

	CNT	Molecule	Solvent	Procedure details	Source
1	50 mg MWCNT	 <p style="text-align: center;">250 mg</p>	THF 150 mL	<p>Ultrasonic bath to disperse CNTs in THF for 20 min, → Addition of pyrene-functional polyester → Magnetic stirring at ambient temperature for ten days → Filtration through a PTFE membrane (pore size 0.2 μm) → Sonicated of the residual solid in excessive amount of fresh THF → Filtration until the elimination of all nonattached pyrene-functional polyester</p>	267
2	1 g MWCNT	 <p style="text-align: center;">1 g</p> <p style="text-align: center;">n=2, Amide like-1 n=6, Amide like-2 n=10, Amide like-3</p>	THF 300 mL	<p>Dispersion of the molecule and the CNT with 30 min of sonication using a typical bath-type sonicator → Filtration of the mixture → Washing with 3 L of THF → Drying under vacuum for 12 h.</p>	298

3	10 mg MWCNT	 <p style="text-align: center;">10 mg</p>	THF 10 mL	<p style="text-align: center;">Sonication of the using an ultrasonic bath (100 W) for 3 h at room temperature → Filtration PTFE membrane → Washing with excessively with THF, CH<sub>2</sub>Cl<sub>2</sub> and diethyl ether → Collection of a black solid the functionalized sample.</p>	299
4	260 mg MWCNT	 <p style="text-align: center;">57.5 mg</p>	N/A CH <sub>2</sub> Cl <sub>2</sub>	<p style="text-align: center;">sonication for 30 min → Stirring vigorously at room temperature for 24 h → Filtration and washing thoroughly with CH<sub>2</sub>Cl<sub>2</sub></p>	300

### 3.2.2.1. Rate of one-pot functionalization

The M5 molecule was studied by spectroscopic methods to investigate MWCNT functionalization with the molecule using one-pot approach. The emission and absorption spectra of the molecule in THF at six different concentrations are depicted in Figure 59 to identify the linearity domain of the molecule's solubility. The chosen concentrations are:

Sample	S <sub>1</sub>	S <sub>2</sub>	S <sub>3</sub>	S <sub>4</sub>	S <sub>5</sub>	S <sub>6</sub>
Concentration (M)	10 <sup>-6</sup>	2×10 <sup>-6</sup>	4×10 <sup>-6</sup>	6×10 <sup>-6</sup>	8×10 <sup>-6</sup>	10 <sup>-5</sup>

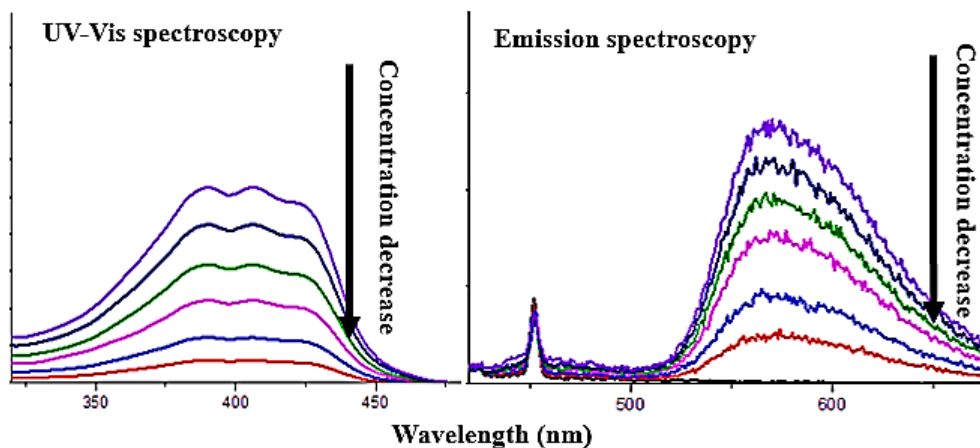


Figure 59. UV-Vis and emission spectrum of the M5 molecule (excitation wavelength = 371nm).

Based on the values of intensity for UV-Vis and emission spectra at 390 and 580 respectively, Table 7 presents the calculations of the linearity domains of luminescence for M5 with its concentration.

Table 7. Calculations of the linear relationship between concentration of M5 with UV-Vis and emission spectra.

[C] (M)	10 <sup>-5</sup>	8×10 <sup>-6</sup>	6×10 <sup>-6</sup>	4×10 <sup>-6</sup>	2×10 <sup>-6</sup>	10 <sup>-6</sup>	Linear relations
<b>I<sub>Abs</sub></b> At 390 nm	<b>0.527</b>	<b>0.429</b>	<b>0.318</b>	<b>0.233</b>	<b>0.124</b>	<b>0.059</b>	<b>Emi = 10<sup>9</sup>[C] + 2167.3</b> <b>→</b> <b>[C] = <math>\frac{Emi - 2167.3}{10^9}</math></b>
<b>I<sub>Emi</sub></b> At 580 nm	<b>13415.3</b>	<b>11513.0</b>	<b>9763.0</b>	<b>7784.6</b>	<b>4512.7</b>	<b>2534.4</b>	<b>Abs = 51436[C] + 0.0142</b> <b>→</b> <b>[C] = <math>\frac{Abs - 0.0142}{51436}</math></b>

To test the effectiveness of One-pot functionalization, the following samples were prepared, and the described procedure was applied.

- ❖ Sample 1: 1.9 mg M5 + 1.9 mg MWCNT + 10 mL THF
- ❖ Sample 2: 3.0 mg M5 + 2.0 mg MWCNT + 10 mL THF
- ❖ Sample 3: 5.6 mg M5 + 3.2 mg MWCNT + 19 mL THF

At the bottom of the flask, a solution of M5 in THF is collected, and the exact volume of THF was measured. Then, using the calibration relations introduced in Table 7, the concentration of the solution in the flask and subsequently the mass of recovered M5 for each sample is calculated. These calculations are summarized in Table 8. To take into consideration the quantity of spilled M5 in different stages including transferring from the vial to the PTFE membrane or the quantity trapped in the membrane, the calculated values were multiplied by a value of 1.2.

Table 8. Calculations of the functionalization rate with One-pot method.

Molecule to CNT weight ratio	Estimated recovered M5 mass (mg)		remaining M5 mass on CNT (mg)		Rate of functionalization (remaining M5/initial CNT)	
	Emi	Abs	Emi	Abs	Emi	Abs
1	1.4	1.3	0.5	0.6	0.26	0.31
1.5	2.3	2.2	0.7	0.8	0.35	0.40
1.8	3.8	3.9	1.8	1.7	0.56	0.53

Raman spectroscopy was conducted to compare the impact of different initial ratios in this functionalization method. As evidenced by Figure 60, a clear influence of the initial M5 quantity is observed. The band at  $1233\text{ cm}^{-1}$  is indicative of pyrene derivatives.<sup>301</sup>

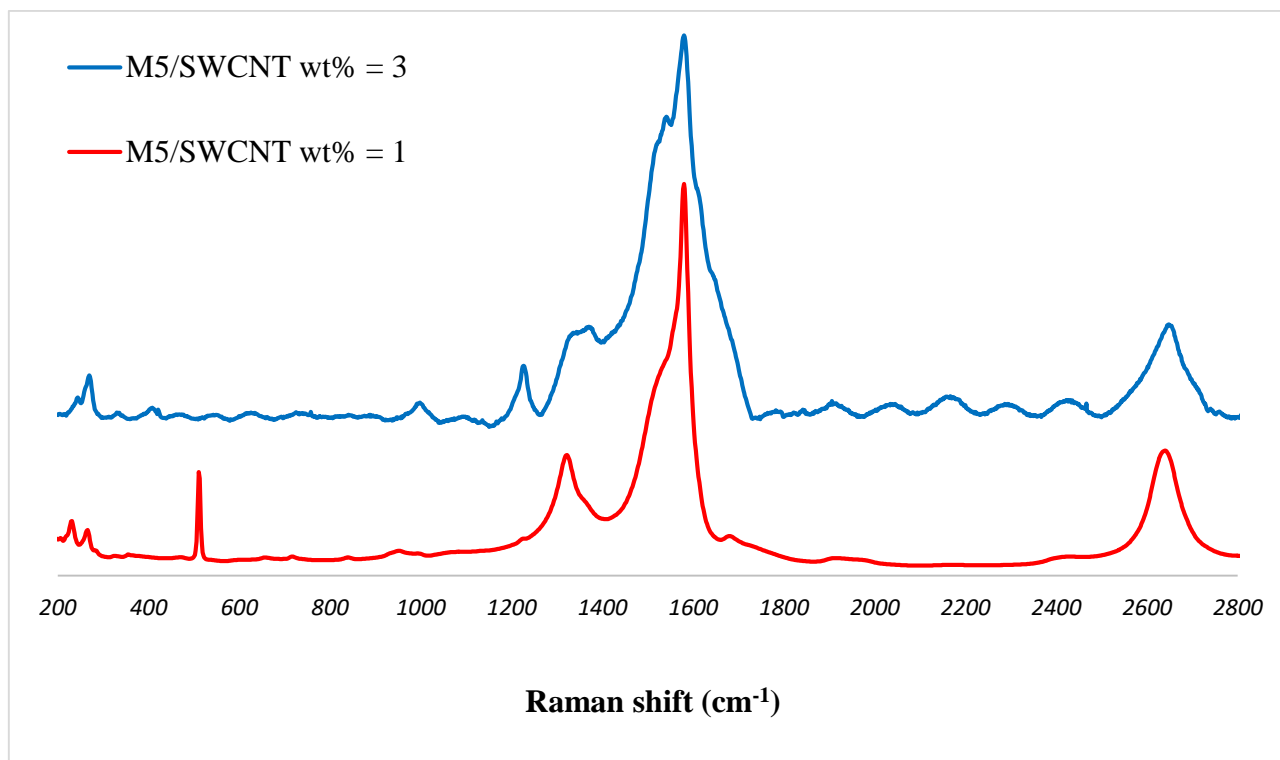


Figure 60. Effect of initial weight ratio on the Raman spectra in One-pot functionalization.

### 3.2.2.1. One-pot functionalization validation by Fourier transform Infrared (FTIR)

IR measurements were carried out on pristine multi-walled carbon nanotubes (MWCNT) ink, a solution of M5, and the functionalized solid with M5. For the measurements of the pristine MWCNT and the molecule, one drop of the ink or solution was placed on the plate of the IR device and the background was recorded in their respective solvents (NMP for the ink, and THF for the molecule). To record the IR spectra of the functionalized sample, the solid was placed on the plate and the background was recorded in air.

The results are shown in Figure 61. The two main characteristic bands that are seen on the molecule sample and have been transferred to the functionalized sample are at  $2850\text{ cm}^{-1}$  to  $3000\text{ cm}^{-1}$  and at  $3650\text{ cm}^{-1}$ . In the literature, the former is indicative a stretched C—H bond and the later reflect OH and C≡N bonds,<sup>302</sup> which are found in the molecule structure (Figure 51).

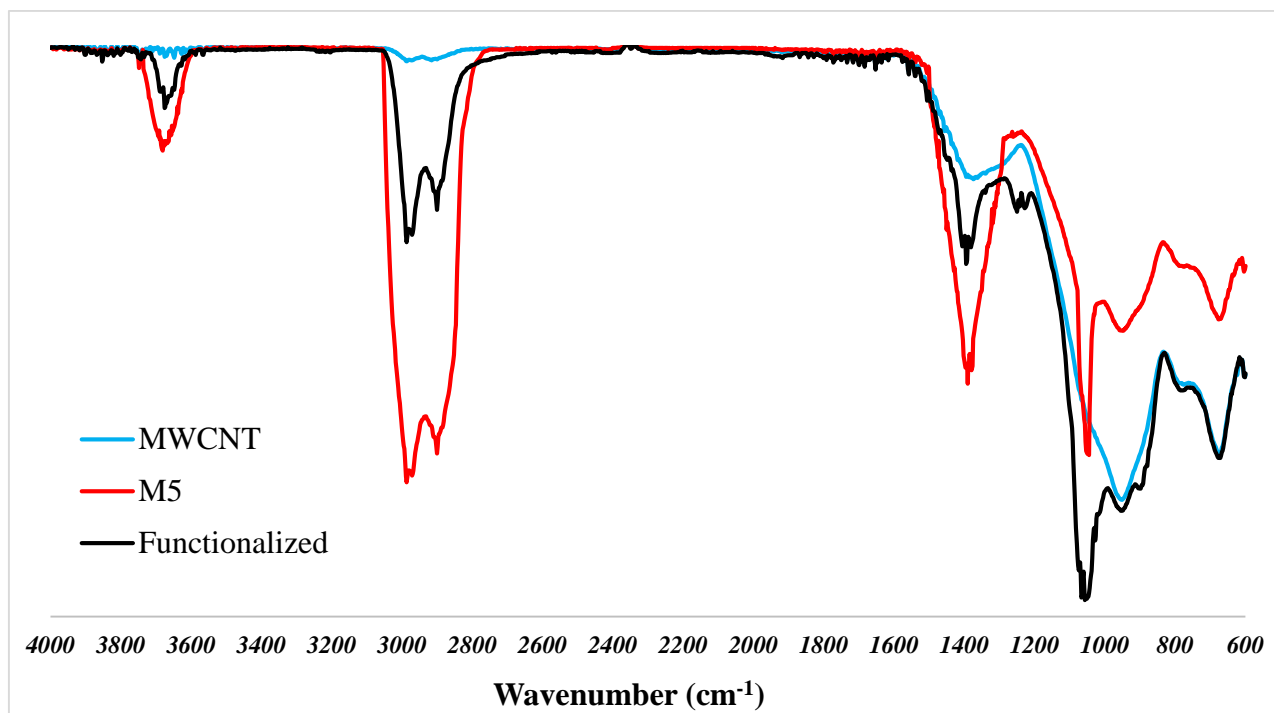


Figure 61. IR spectra of functionalization of MWCNT with M5 molecule using one-pot approach.

### 3.2.2.2. One-pot functionalization validation by Raman

Figure 62 shows the results of Raman spectroscopy to characterize one-pot functionalization method. In this method an initial mass ratio of 2:1 for M1 to MWCNT was chosen. As Figure 62 suggests, one-pot functionalization of MWCNTs with M1 as a porphyrin-based molecule results in an augmented level of graphitic structure. It is particularly important to note that the functionalization with M2 molecule could result in different spectra with more intense d band, since the M2 molecule has 8 ether chains that could affect the graphitic texture.

Raman study of porphyrins is explained in literature by numerical calculations and experimentation.<sup>303</sup> In this work the Raman spectra of M2 Molecule was collected as a reference for porphyrin-based molecules via crystalizing using a slow evaporation of solvent (DCM) on an SiO<sub>2</sub> substrate at room temperature.



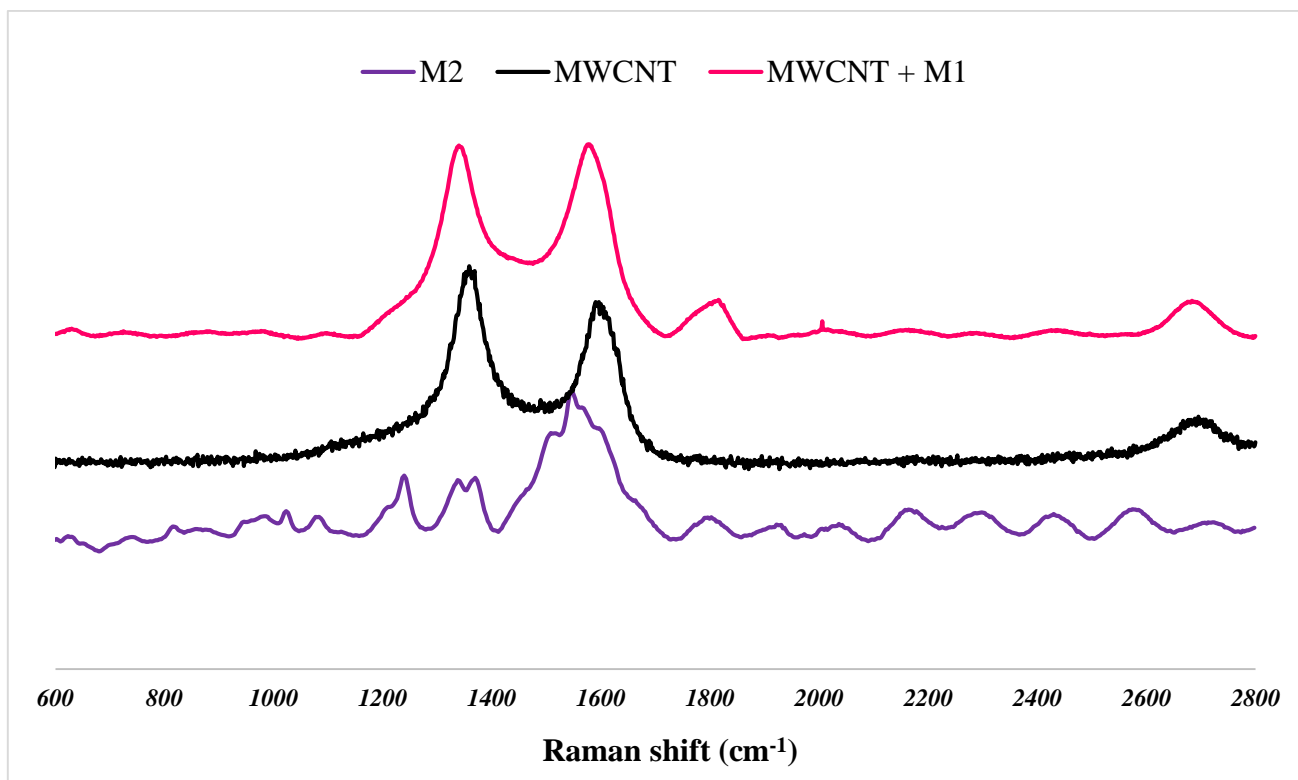


Figure 62. Raman spectra of functionalized MWCNT with M1 using One-pot approach and the M2 molecule as a reference for porphyrin-based molecules.

### 3.2.2.3. One-pot functionalization validation by UV-Vis absorption

To investigate one-pot method with UV-Vis absorption studies, an initial mass ratio of 4:1 of M4 to MWCNT was chosen. After performing the one-pot functionalization method, the filtered solid was used to prepare an ink in NMP solvent using the usual ink preparation method. Figure 63 shows the results of UV-Vis absorption. The absorption of MWCNT and the solvent were also collected.

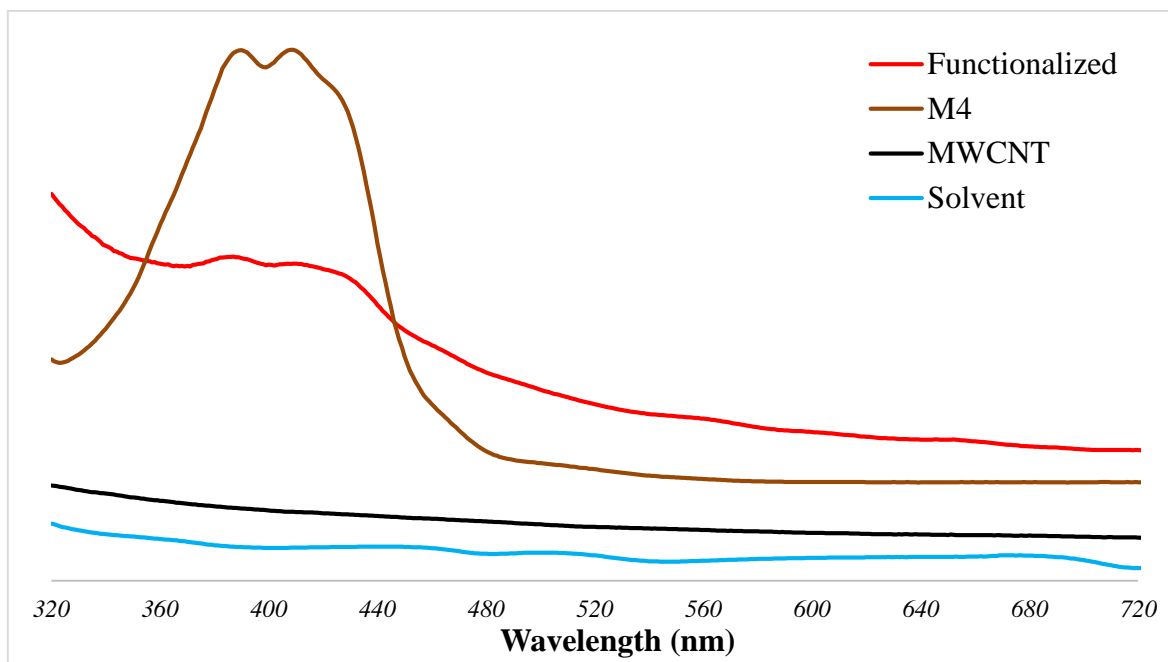


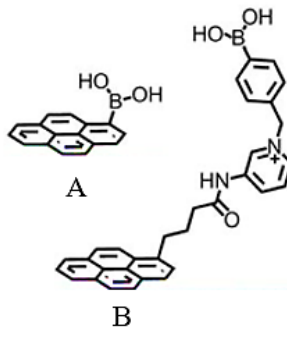
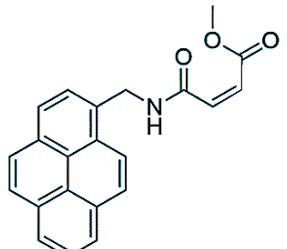
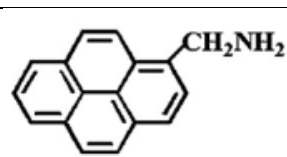
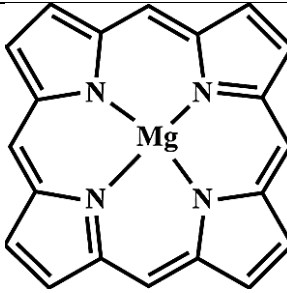
Figure 63. UV-Vis absorption spectroscopy study of a M5 molecule and its trace in a functionalized (filtration) sample.

The absorption of the M5 molecule shows two bands with the same intensity at 388 nm and 410 nm. On the functionalized sample, the same bands are seen in the spectra of CNT, which indicates the presence of the M5 molecule in the sample, despite extensive washing with THF. The results presented in Figure 63 are also indications of interaction between CNT and M4 as pyrene-based molecule.

### 3.2.3. Functionalization by incubation

Incubation method to functionalize CNTs means immersing a substrate on which CNTs are deposited or a bulky layer of CNTs into a solution containing the desired functional group. In the literature, this method has been described to be effective to functionalize CNTs with Pyrene and Porphyrin groups. Some examples from literature are presented in Table 9 by reporting parameters like incubation duration, temperature, and solution concentration.

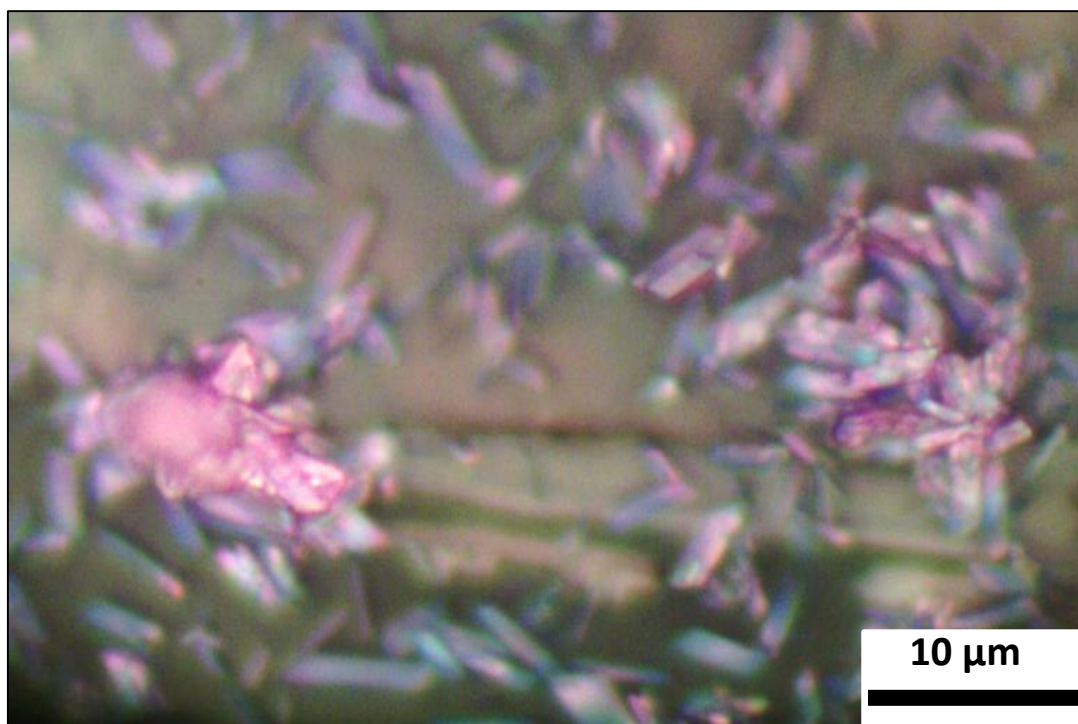
Table 9. Parameters of Incubation functionalization in the literature (schemes taken with permission).

	CNT	Molecule	Solvent	Concentration (mg/mL)	Temperature	Time	Source
1	MWCNT		DMF	A: 2.47 B: 3.96	Not reported	1 hour	304
2	SWCNT		CH <sub>3</sub> CN	0.173	-20 °C	1 hour.	264
3	SWCNT		PMA.HCl in Water 0.036% Triethylamine to remove HCl		Not reported	24 hours	27
4	SWCNT		Under vacuum	Putting 1 mg of the molecule with the CNT film under vacuum	215 °C	3 days	292

Based on the information in the literature, the parameters for incubation functionalization were optimized in this work. THF was used as the solvent for Pyrene-based molecules, and Dichloromethane (DCM) was used for Porphyrin-based molecules, to prepare solutions of 100 mg/L. After applying the heating process (discussed thoroughly in the previous chapter) to the CNT depositions, the substrates were immersed into the molecule solution. Then the vessel containing the substrate immersed into the solution was kept in -20 °C for at least 48 hours.

This time is enough to allow the contact between the CNT film and the molecules, while ensuring that the solvent does not evaporate.

After the incubation was completed, the substrates were removed from the remaining solution and annealed at 85 °C for 15 minutes. This temperature is more than the boiling point of the solvents (THF and DCM) allowing a fast evaporation of the solvent. In the event of a slow evaporation of DCM at room temperature for a porphyrin-based molecule, as shown in Figure 64, crystals of the molecule formed. This shows that when the solvent is evaporated slowly, the molecules are dragged from the CNT surface into formation of crystals up to 10  $\mu\text{m}$  in size.



*Figure 64. Creation of crystals of a Porphyrin-based molecule due to slow solvent evaporation.*

After the annealing, the substrates were subjected to rigorous rinsing with DI water to eliminate loosely attached molecules due to mechanical forces, and finally annealed at 95°C for 20 minutes to evaporate any remaining of solvent.

### 3.2.4. Compare the success of functionalization methods by Raman

The choice of functionalization methods, the effect of using different solvents, and the impact of molecule structure on the success of the functionalization was studied by Raman spectroscopy. In Figure 65, structure of the molecules and the solvents are presented. In this study MWCNT was used. The choice of solvent means using the solvent in the MWCNT ink as well as molecule solution preparation.

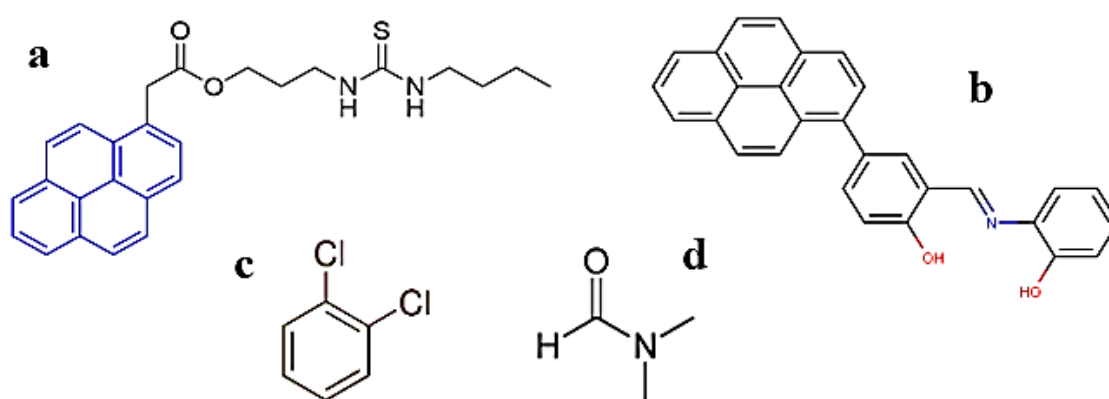


Figure 65. molecules a) M4, b) M5, and solvents c) oDCB, d) DMF used to study the success rate of functionalization by Raman spectroscopy.

Each of functionalization methods were applied following the procedures explained in detail in this section. For the case of mixing method, the substrates were rinsed by excessive amount of water after the deposition of the functionalized ink by inkjet printing.

As shown in Figure 66, for the case of using oDCB as solvent and functionalization with M5 molecule, the incubation method results in more changes to the Raman spectra.

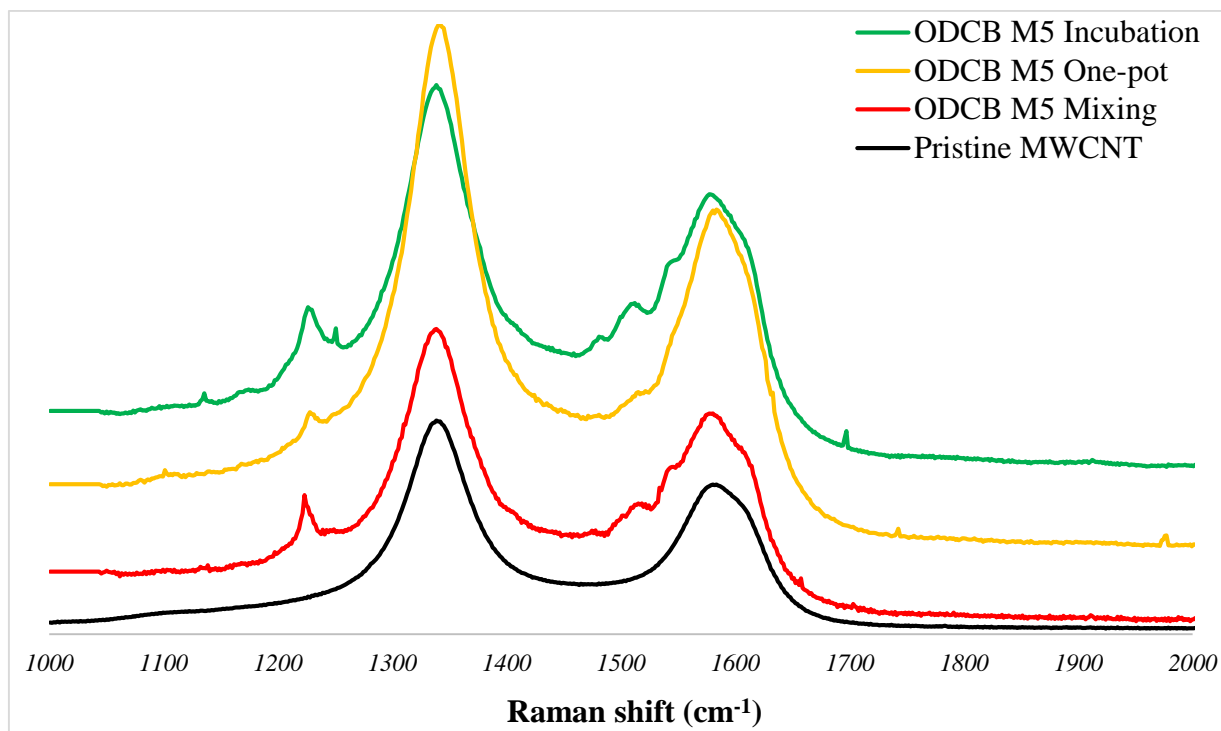


Figure 66. Comparison of different functionalization methods for M5 molecule using oDCB as solvent.

As Figure 67 suggests, neither of the approaches were successful for the case of using oDCB solvent to functionalize MWCNTs with M4 molecule.

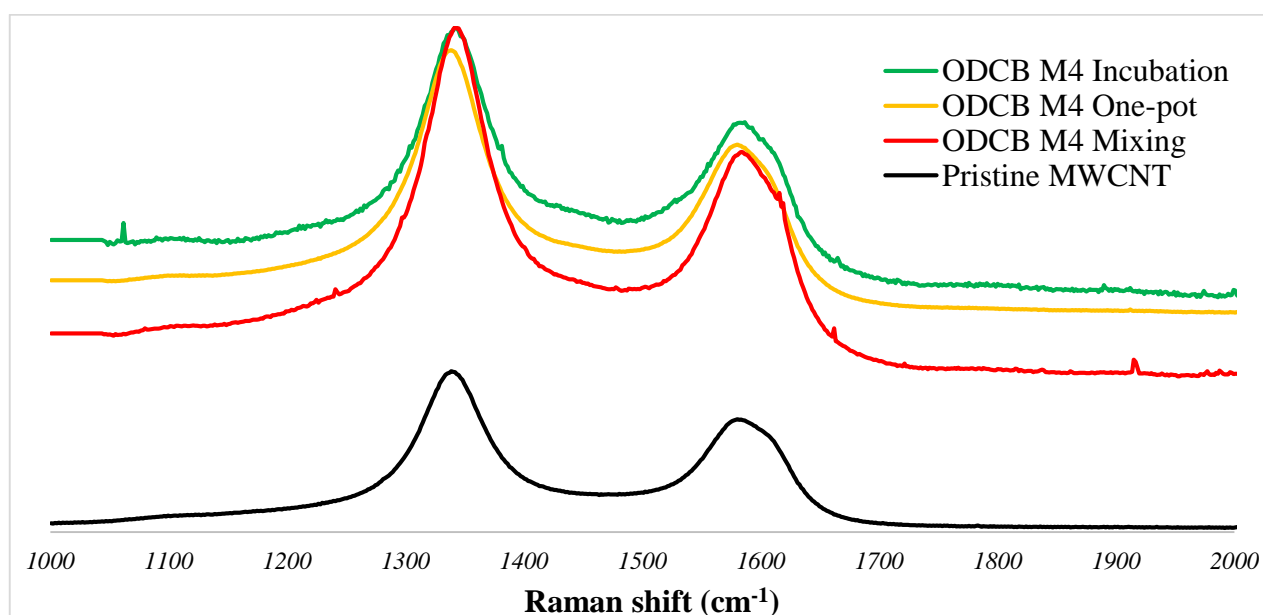


Figure 67. Comparison of different functionalization methods for M4 molecule using oDCB as solvent.

As depicted in Figure 68, for the case of using DMF as solvent, both mixing method and Incubation work properly to functionalize MWCNTs with M5 molecule, with the incubation giving better results.

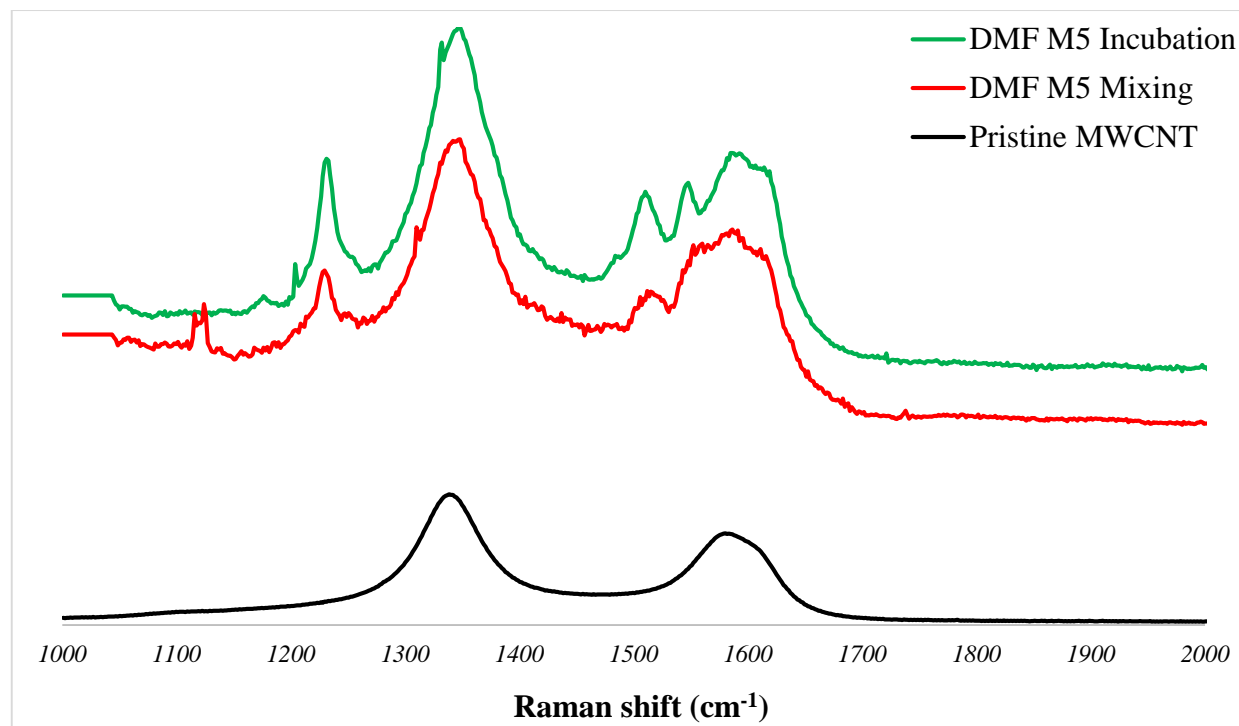


Figure 68. Comparison of different functionalization methods for M5 molecule using DMF as solvent.

As seen from Figure 69, functionalization of MWCNTs with M4 molecule in DMF is only successful with the mixing approach, but with lower intensity compared to M4 molecule depicted in Figure 68.

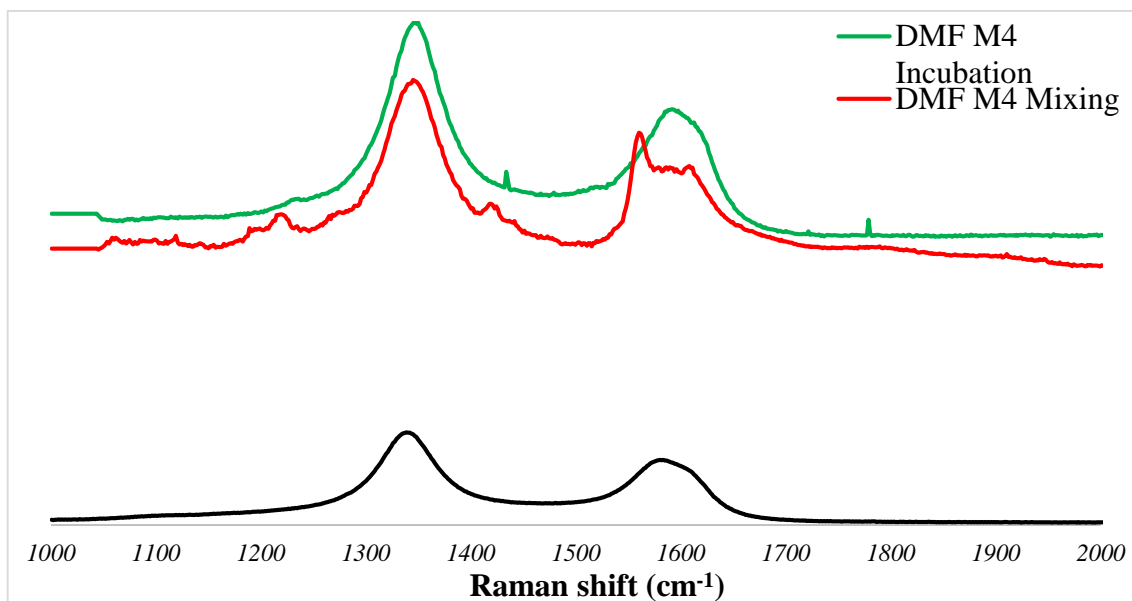


Figure 69. Comparison of different functionalization methods for M4 molecule using DMF as solvent.

It is also clear from Figure 70, that using DMF over oDCB as solvent results in better functionalization and larger changes to the Raman spectra, when the incubation method is applied to functionalize MWCNTs with M5.

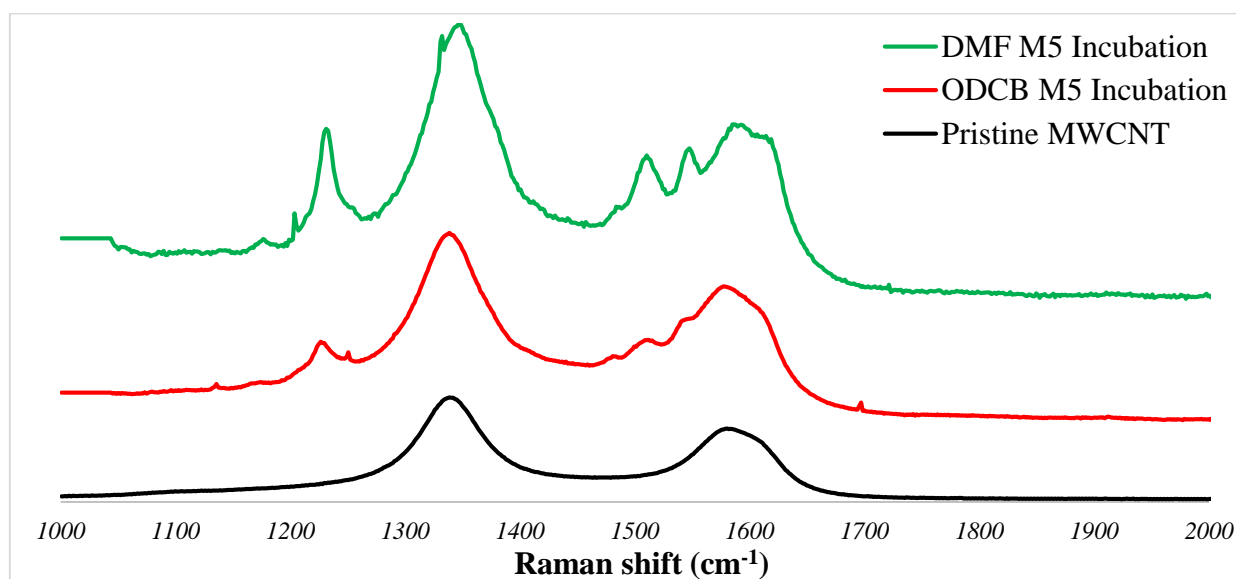


Figure 70. Comparison of different solvents for M5 molecule in incubation method.



By comparing the solvent effect to functionalize MWCNTs with M5 molecule in the mixing method, as Figure 71 suggests, DMF solvent gives better results.

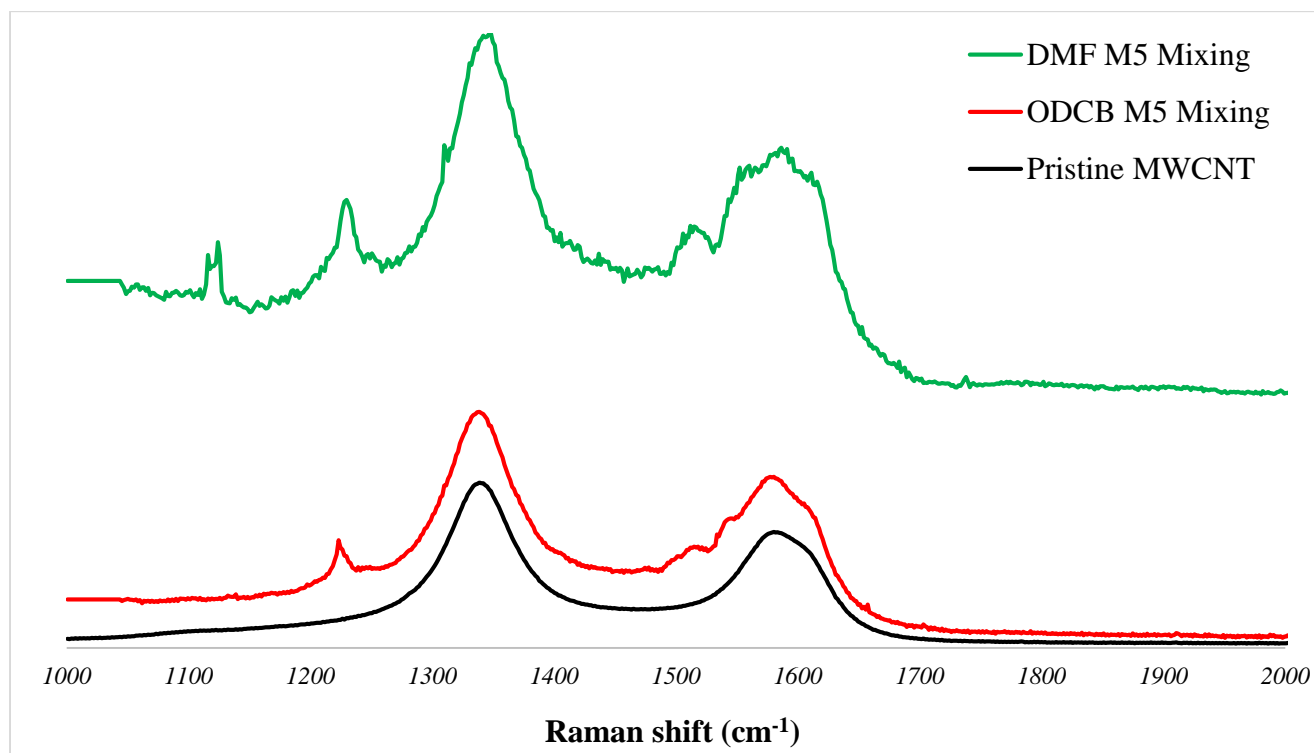


Figure 71. Comparison of different solvents for M5 molecule in Mixing method.

By looking at Raman spectra in Figure 72, it can be noted that using incubation method to functionalize MWCNTs with the M4 molecule, while using oDCB as solvent doesn't bring any evidence of functionalization, using DMF as solvent results in a minor appearance of the band at  $1233\text{cm}^{-1}$ .

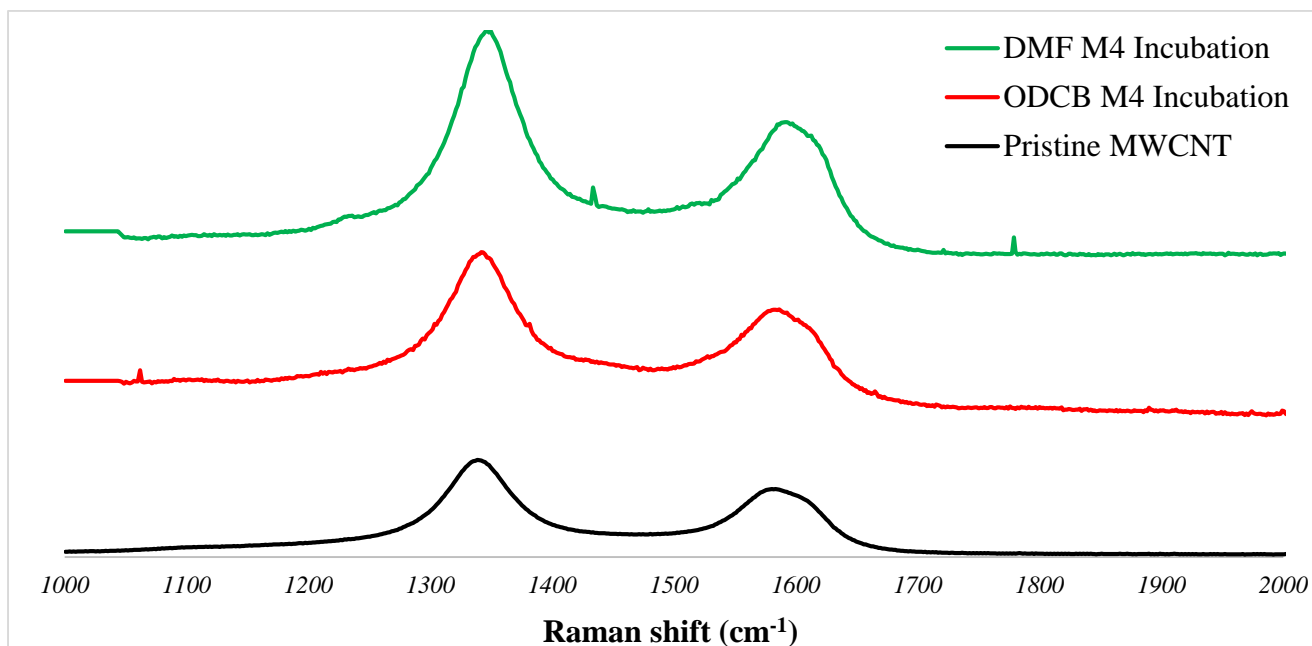


Figure 72. Comparison of different solvents for M4 molecule in Incubation method.

However, Figure 73 suggests that to functionalize MWCNTs with M4 molecule in the mixing method, using DMF as solvent results in the appearance of the characteristic peak of pyrene derivatives at 1233 cm<sup>-1</sup>.

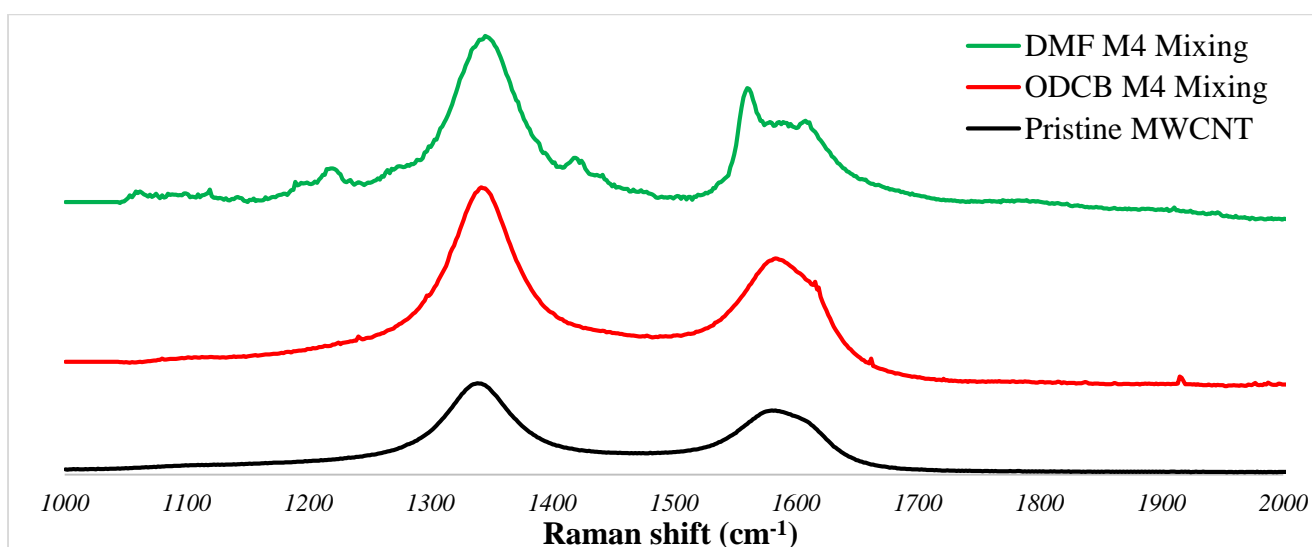


Figure 73. Comparison of different solvents for M4 molecule in Mixing method.

From Figure 74, it is also clear that using oDCB as solvent and the mixing method, M5 molecule changes the Raman spectra of MWCNTs, while no evidence of functionalization is seen by M4 molecule.

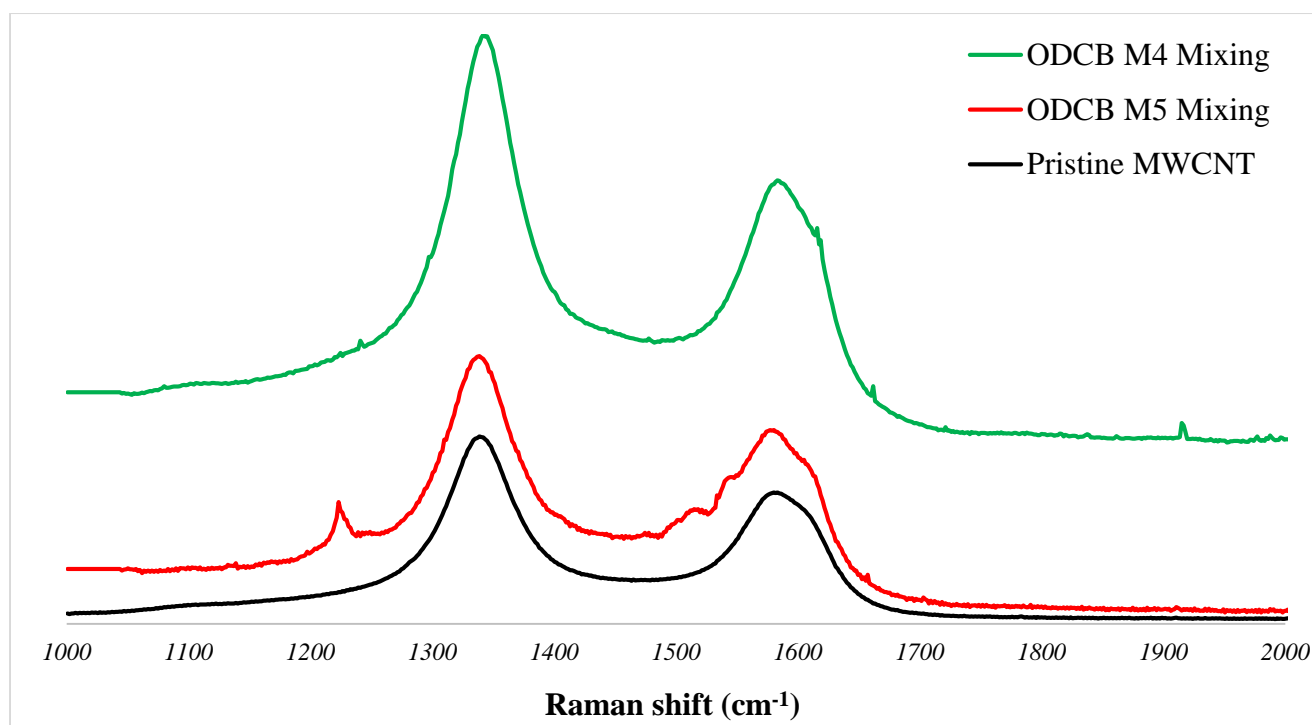


Figure 74. Comparison of Mixing functionalization for different molecule with oDCB as solvent.

The same analysis for the incubation method, using oDCB as solvent, reinforces the statement that functionalization with M4 doesn't happen, while with M5 molecule, the peak at  $1233\text{cm}^{-1}$  appears with a large intensity, as shown in Figure 75.

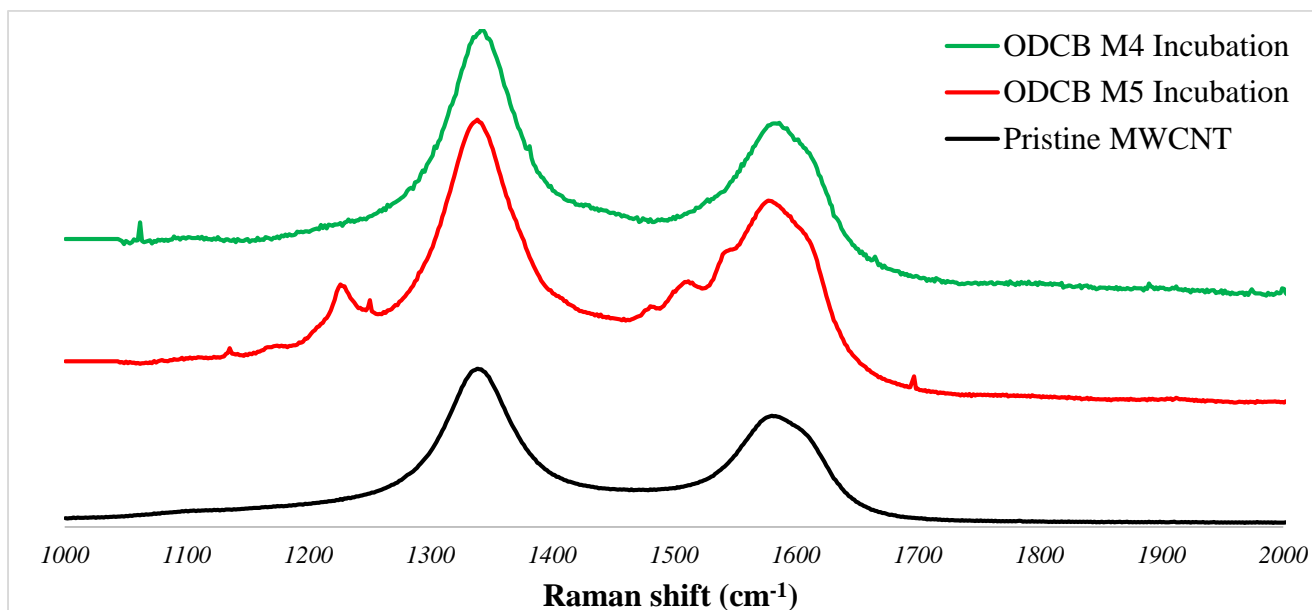


Figure 75. Comparison of Incubation functionalization for different molecule with ODCB as solvent.

Also, again in the case of using oDCB as the solvent, the results from one-pot approach in Figure 76 shows that functionalization of MWCNTs with M5 molecule is more effective than M4 molecule.

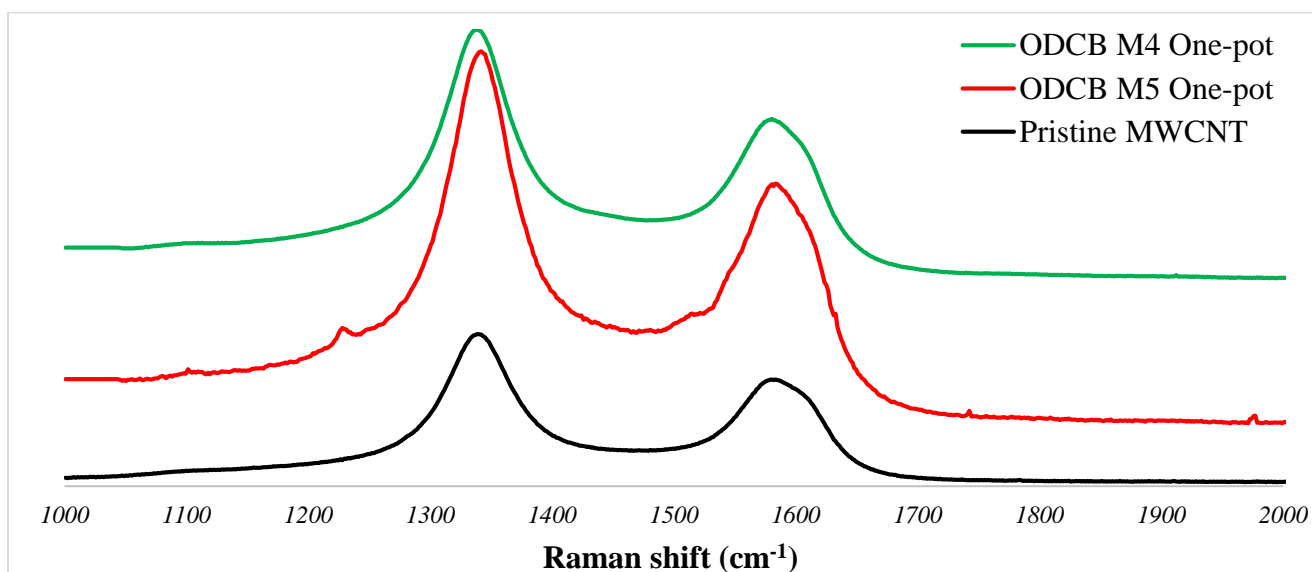


Figure 76. Comparison of One-pot functionalization for different molecule with oDCB as solvent.

In the case of using DMF as solvent and the mixing approach for functionalization, both molecules bring changes to the Raman spectra, while the spectra with M5 molecule has higher intensities according to Figure 77.

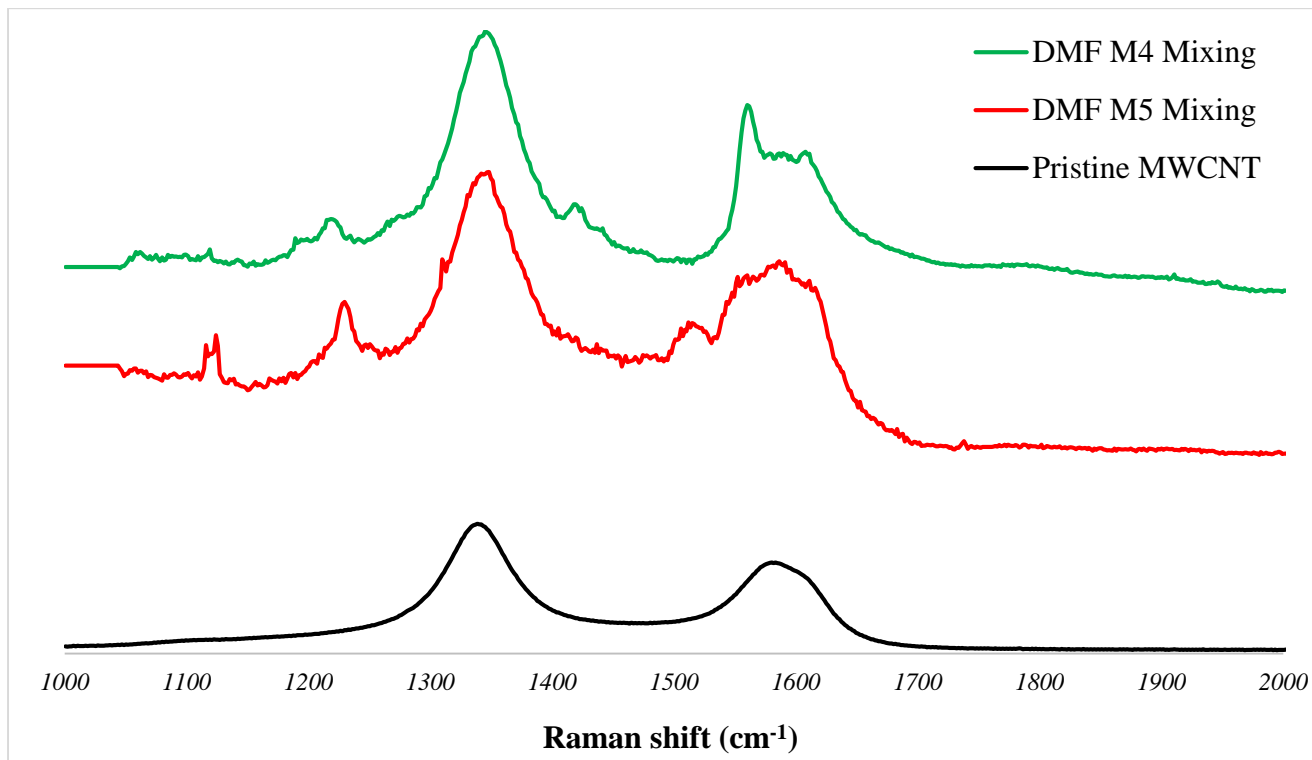


Figure 77. Comparison of mixing functionalization for different molecule with DMF as solvent.

Finally, by comparing the spectra in Figure 78, it is clear that using the incubation method and DMF solvent, M5 molecule functionalizes the MWCNTs, while M4 molecule barely brings any changes.

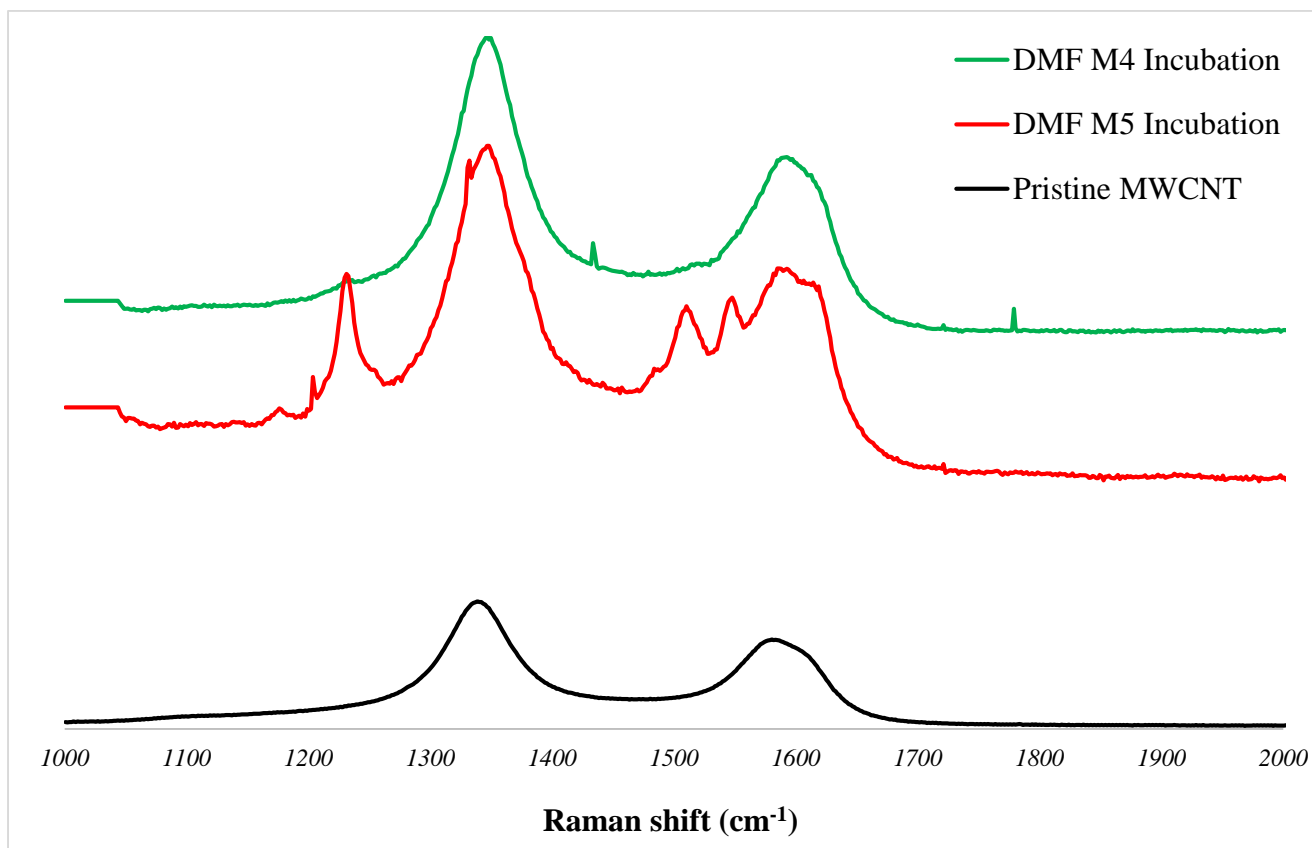


Figure 78. Comparison of Mixing functionalization for different molecule with DMF as solvent.

Table 10 summarizes the results of Raman study on 10 different samples based on the choice of solvent, molecule and functionalization method. In the last column of Table 10, a color code is introduced which presents the success rate of functionalization on a scale of 0 (no changes to the spectra) to 10 (most changes to spectra in terms of the intensity of the band at  $1233\text{ cm}^{-1}$ ), which happened for the case of using DMF as solvent and the incubation method for the functionalization of MWCNTs with M5 molecule.

Table 10. The comparative table of the success rate of functionalization with different methods using Raman spectroscopy.

Sample	Solvent	molecule	Functionalization method	Success rate in terms of the Intensity of the band at 1233 cm <sup>-1</sup>
1	oDCB	M4	Mixing	0
2			One-pot	0
3			Incubation	0
4		M5	Mixing	6
5			One-pot	3
6			Incubation	7
7	DMF	M4	Mixing	6
8			Incubation	1
9		M5	Mixing	8
10			Incubation	10

Results of this Raman campaign and Table 10 are important in understanding the impact of the structure of solvents and molecules in the noncovalent interactions between CNTs and pyrenes. It is clear that the incubation method has the best results simply due to the possibility of using clean surface of CNTs after the heating process.

On the other hand, in the case of using oDCB as solvent, the functionalization is less effective than the case of using DMF. Looking at Figure 65, this can be attributed to the impact of sonication on the degradation of oDCB, which results in the pollution of the CNT surface by the sonochemicals.<sup>245</sup> These sonochemicals hinder effective functionalization and the Raman results reinforce this.

Finally, by looking at Table 10, we can see that functionalization with M5 is more successful than M4. The reason for this can also be found in Figure 65 and the structure of the molecules. Apart from the pyrene base, M5 has two benzene rings sandwiching a thiourea group that can increase the conjugation size of the molecule and result in better mobilization on MWCNTs.<sup>305</sup>

### 3.3. Characterization of the chosen method for functionalization

The incubation method described in the last section of this chapter was chosen as the ultimate method to functionalize CNTs for the designated purpose of this research, sensors. There are three main reasons for this decision:

- First, other functionalization methods are not compatible with the heating process developed and discussed in the previous chapter, while the incubation method complies with the limitations posed by the Heating Process.
- Second, the primary characterization carried out by Raman spectroscopy indicates that the incubation method results in higher degree of functionalization.
- Third, the incubation method is compatible and easier than other methods for any sensor development process.

In this section the characterization of incubation method as the ultimate choice of functionalization will be discussed.

The functionalization of CNTs with pyrene and porphyrin molecules has been researched and techniques such as Raman spectroscopy and TEM have been employed to characterize the resulting composites.<sup>306</sup> Noncovalent functionalization of SWCNTs with aromatic small-molecule-based groups has been investigated, demonstrating the structural properties of the functional molecules on the SWCNTs. Raman scattering spectra have been used to characterize the coated layer on Si wafer surfaces, providing insights into the impact of functionalization on the materials.<sup>307</sup> High-resolution microscopy characterizations have



revealed the adsorption of porphyrin and phthalocyanine molecules on the surface of SWCNTs, highlighting the effectiveness of these techniques in studying the functionalization of CNTs with specific molecules.<sup>308</sup> The use of pyrene to introduce functionalities to CNTs via  $\pi$ - $\pi$  stacking has been well-established, underscoring the significance of noncovalent functionalization in modifying the properties of CNTs.<sup>309</sup>

These studies collectively demonstrate the diverse approaches and techniques utilized to characterize the functionalization of CNTs with pyrene and porphyrin molecules, providing valuable insights into the structural and optical properties of the resulting composites. Different techniques were used to characterize the functionalization of SWCNTs with pyrene and porphyrin-based molecules. They will be discussed here.

### 3.3.1. Raman scattering

The interaction of pyrene and porphyrin-based molecules with SWCNT was investigated through the examination of their Raman scattering. Figure 79 displays the Raman spectra of a SWCNT deposition subsequent to incubation with a M2 as a porphyrin-based molecule.

Each spectrum presented in Figure 79 are an average of a map over an area of  $10 \times 10 \mu\text{m}^2$  that comprises of 100 separate spectra. To obtain all spectra a laser of 532 nm was used. To prepare the M2 molecule sample for the Raman study, a solution of the molecule in DCM was casted on a  $\text{SiO}_2$  substrate and the solvent was evaporated at room temperature allowing the creation of crystals of the molecule.

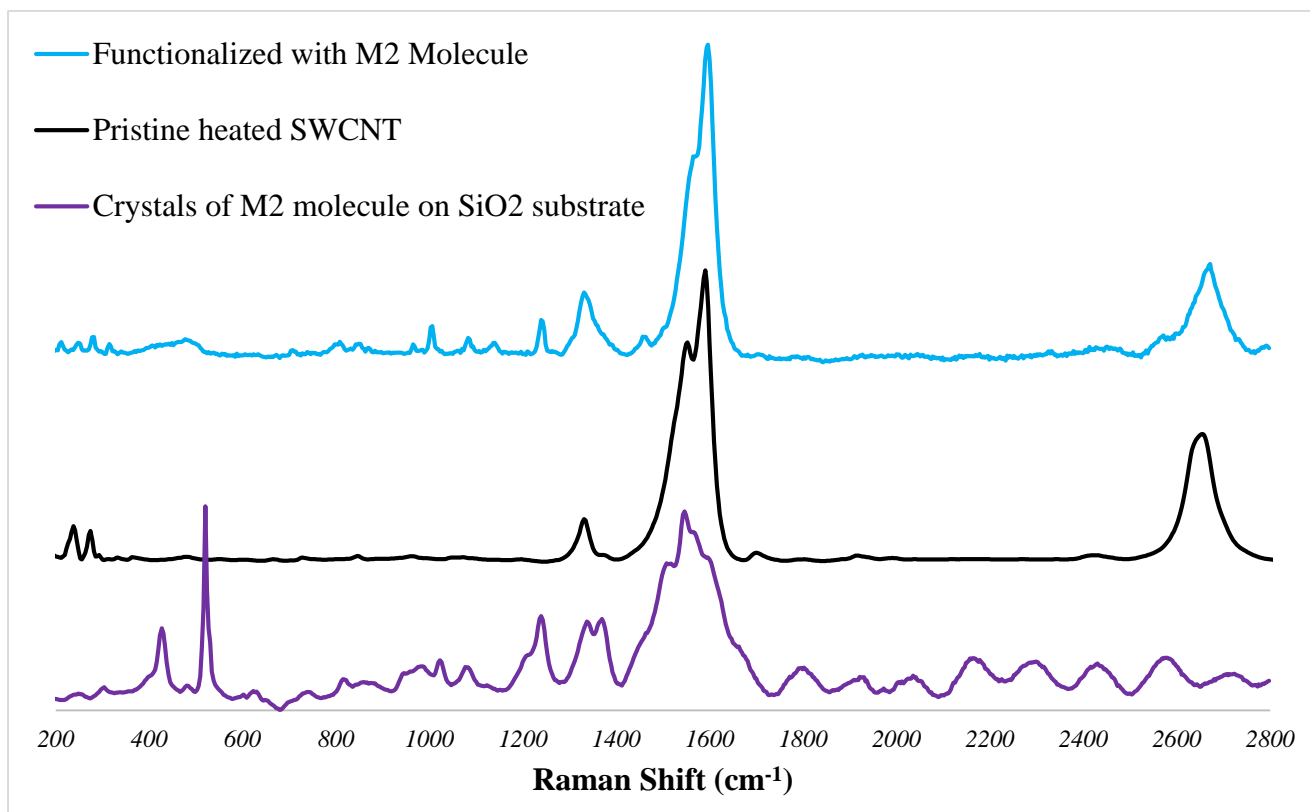


Figure 79. Evolution of the Raman spectra of SWCNT deposition after incubation with M2.

Observable changes are noted from the pristine SWCNT spectra (black) to the incubated sample (red), revealing the emergence of several peaks. The peaks appeared at 1006, 1090, and 1245  $\text{cm}^{-1}$  can be clearly found in the spectra of the molecule. The increase in the D peak and the decrease of the 2D peak are the direct result of the coverage of the surface of SWCNTs with the porphyrin-based molecule.

The increase in the D band is a result of the creation of anomalies on the graphitic surface of the CNT, while the decrease in the 2D band is evidence for the increased number of the conjugated layers stacked on one another. This argument is the reverse argument provided in the previous chapter regarding the destruction of the amorphous matter from the surface of the CNTs, which resulted in less intense D and more intense 2D peaks.

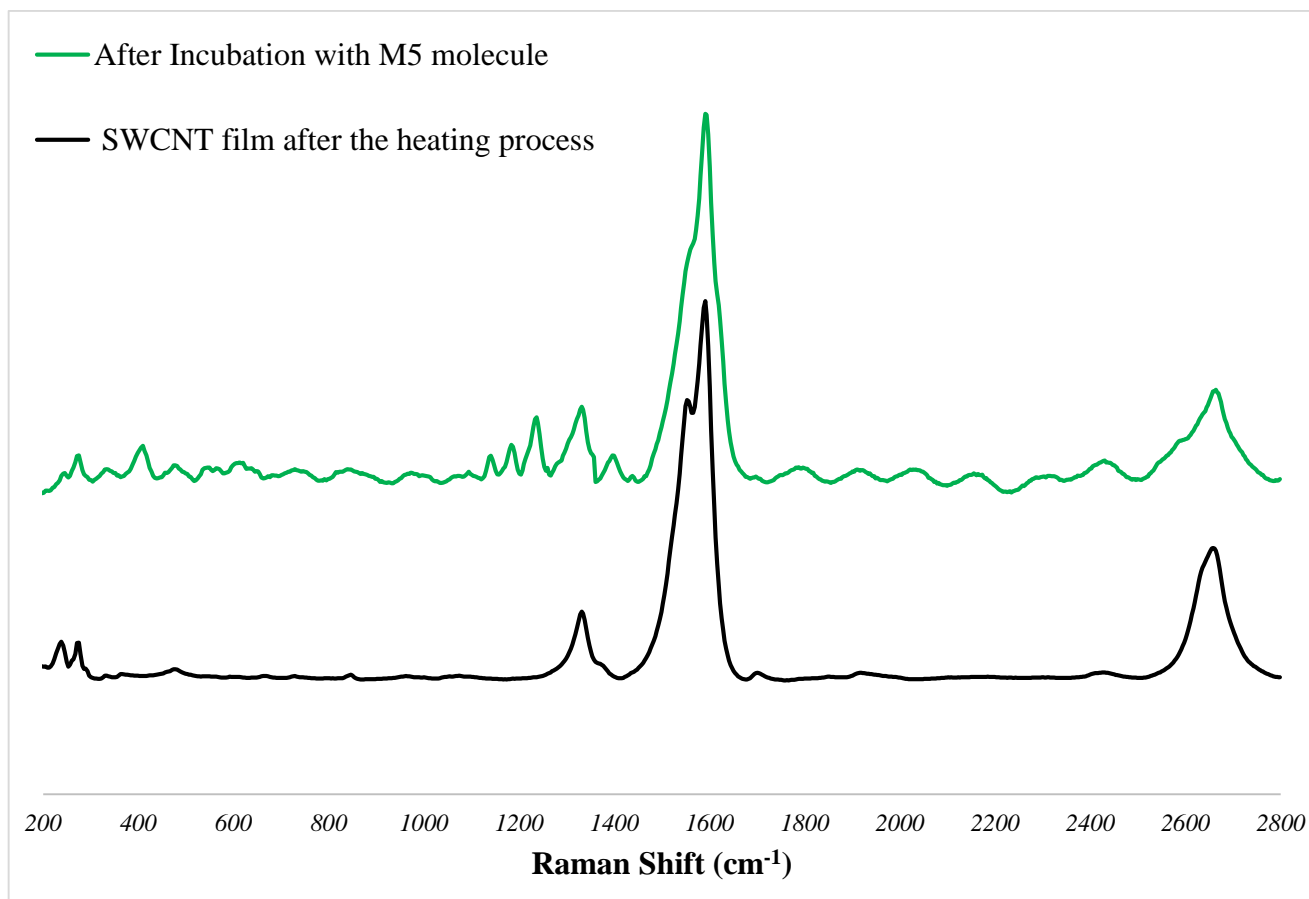


Figure 80. Raman spectra of a SWCNT deposition, before and after incubation with M5.

Figure 80 shows the Raman spectra of SWCNT deposition after the heating process and the same sample after incubation with M5 molecule. There are new bands that appear on the spectrum after functionalization including the usual band for pyrene derivatives at  $1233 \text{ cm}^{-1}$ . Other important changes that should be mentioned are the increase in the intensity ratio of D band to G band (increased anomalies of the surface due to the presence of pyrene molecules) and the decrease in the intensity ratio of 2D band to G band (immobilization of conjugated system and the increase of the number of  $\text{sp}^2$  layers).

### 3.3.2. TEM analysis

The TEM images of pristine SWCNT after the heating process are depicted in Figure 81.a. As discussed earlier, a noticeable decrease in the amorphous matter is observed in this sample after the heating process. However, upon incubation with each molecule, the SWCNT surface is found to be occupied by the respective molecule. The occupation of the SWCNT surface with porphyrin-based molecules is illustrated in Figure 81.b and Figure 81.c for M1 and M2 molecules, respectively. It is observed that the functionalization with M2 appears to be more efficient, homogeneously covering a larger surface, likely attributed to the longer chains of ether that facilitate enhanced functionalization.

Lastly, Figure 81.d presents the incubation of SWCNTs with M5, a pyrene-based molecule. The images clearly indicate that M5 molecules do not cover the entire CNT surface, indicating a lower yield of functionalization compared to porphyrin-based molecules. This observation aligns with the size of their conjugated system and is consistent with the results obtained from emission spectroscopy and Raman scattering.

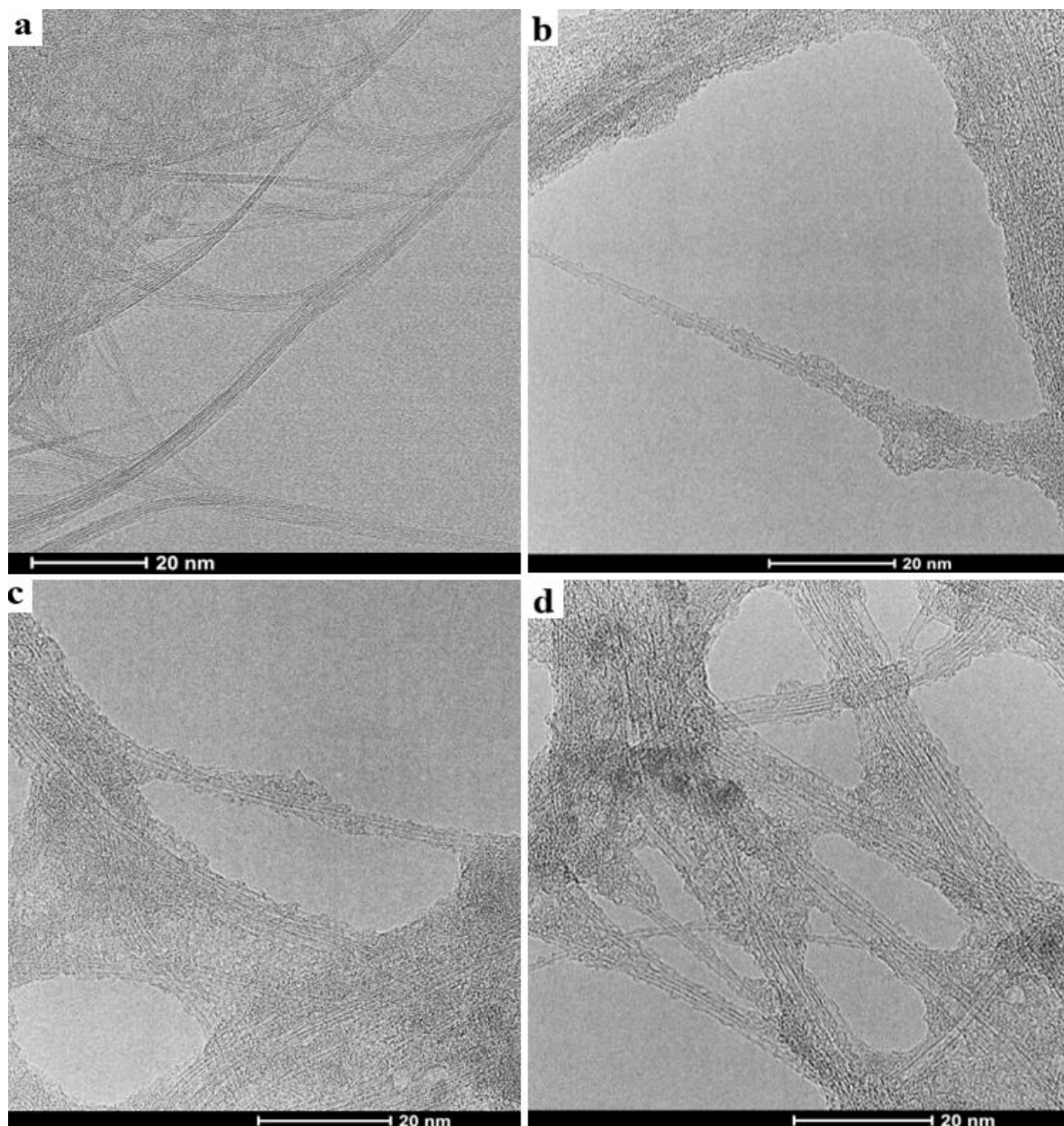


Figure 81. TEM image of 4 samples: a) pristine clean SWCNT after heating, b) SWCNT incubated with M1 molecule, c) SWCNT incubated with M2 molecule, d) SWCNT incubated with M5 molecule.

### 3.4. Conclusion on the functionalization of CNTs

The development of effective functionalization for SWCNTs involves a nuanced and intricate process. In this study, three distinct functionalization methods were explored. In the case of

the mixing method, the clear presence of the molecule in the CNT ink negated the need for specific characterizations. Conversely, with the one-pot functionalization approach, where uncertainty existed regarding the presence of the molecule in the solid state alongside the CNTs, various spectroscopic proofs were employed to substantiate the functionalization.

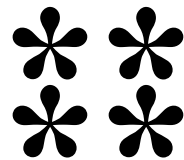
Considering the observed impact of sonication on the quality of CNTs and the surface occupation by amorphous matter, it became apparent that the mere presence might not imply electronic exchange between aromatic molecules and CNTs. Consequently, an investigation into the incubation method was initiated post the cleaning process. This comprehensive analysis revealed that the functionalization method induced structural alterations, influenced wall occupation, and altered the morphology of CNTs.

Having successfully assembled another piece of this intricate puzzle, it can be asserted that a material in the solid state has been created, capable of serving as a sensor. This achievement propels the research forward, setting the stage for the upcoming discussion in the subsequent chapter.

After developing an effective functionalization pathway for SWCNTs, it's time to proceed to the ultimate goal of this project and apply the functionalized CNTs in the development of sensing devices that can interact with analytes in water. The next chapter will discuss different types of sensing devices, and it will not be exclusive to the case of incubated SWCNTs, where the results of other types of functionalization and MWCNTs will also be discussed.



**Institut Polytechnique de Paris**



# Fourth Chapter

## Sensing devices based on CNTs



## 4. Sensing devices based on CNTs.

After discussing the process of CNT purification in the form of thin-films and their functionalization with conjugated bridges, in this chapter the design, fabrication, and sensing mechanism of functionalized CNTs will be discussed. Chemiresistive sensors have a simple mechanism that profit from the electronic properties of CNTs to transduce a chemical interaction.

### 4.1. Components of electrical resistance

In traditional resistors, the resistance is homogenous in the material and follows the Pouillet's law<sup>310</sup> as:

$$R = \frac{\rho * A}{l}$$

Where  $\rho$  is the resistivity of a homogenous material in  $\Omega/\text{mm}$ ,  $A$  is the surface in  $\text{mm}^2$  and  $l$  is the length of the resistor in  $\text{mm}$ . In the conventional resistors, the electronic properties of the metal govern the behavior of the device, and the role of wiring and the circuit is neglected in the performance of the device.

However, to create a chemiresistive sensor, by using solvent-based deposition methods, a random network of CNTs is created and there are two main differences with conventional resistors:

- First; a random CNT deposition is consisted of hundreds of thousands of tubes with different electronic and chemical properties, due to the difference in their shape, size, and chirality.<sup>311</sup> This component of resistance is more complicated since because apart from the importance of conductivity (resistance) of each tube in the network, every

contact between different CNTs has also a role in the resistance of the network, giving infinite number of possible small components.<sup>73</sup>

- Second; in the case of sensing devices, the resistance at the metallic contacts have an important role<sup>312</sup> and is referred to as Schottky barrier. This component governs the interactions at the contact of CNTs and the metallic electrodes.<sup>313</sup> It is a metal-semiconductor junction that exhibits rectifying behavior, acting like a diode with large currents flowing for forward bias and significantly smaller currents flowing for reverse bias.<sup>314</sup>

Based on these two fundamental differences, Figure 82 show a simplified schematic of a CNT network deposited between two gold electrodes.

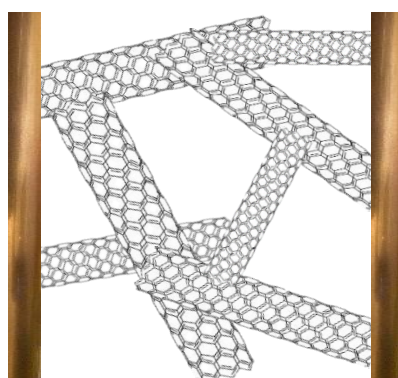


Figure 82. Schematic of different resistance components in a CNT-based chemiresistive device.

#### 4.1.1. Transfer Length Method (TLM)

The TLM method has been widely utilized to characterize the resistivity and contact resistance of CNT networks. Jiang *et al.* employed the TLM along with other methods to characterize the resistances of vertically aligned CNT forests with intrinsic bottom contacts.<sup>315</sup> The TLM method assumes a horizontal contact geometry, equipotential contact metallization, and identical resistivity underlying the contact.<sup>316</sup> This method has been crucial in providing insights into the resistive properties of CNT networks.

The details of the TLM measurements are depicted in Figure 83. On the left, the complete chip shape (captured by an optical Confocal microscope) is displayed, featuring multiple electrode systems. The system selected is indicated by the blue rectangle.

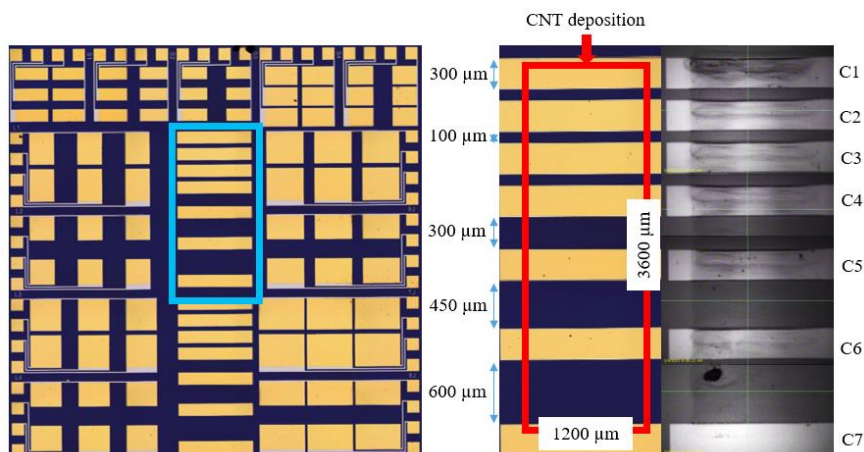


Figure 83. Image of the CNT depositions, the electrodes, and their dimensions used for TLM measurements.

The TLM system comprises of 7 gold electrodes with similar dimensions, albeit with varying spacing between them. The values of the spacing, along with the dimensions of the rectangles, are specified. The shape of the deposition is also depicted on the right side, captured by the camera of the Dimatix printer. Rectangles measuring  $1200 \mu\text{m} * 3600 \mu\text{m}$  were printed on the electrodes for each sample, as demonstrated by the red rectangle in the image in the middle.

Four inks were chosen for the TLM measurements: one-day old pristine MWCNT ink, nine-day old pristine MWCNT ink, 58-day old pristine MWCNT ink, and 11-day old pristine MWCNT ink after functionalized with M4 molecule. For each deposition, 6 resistance values were measured between every two neighboring electrodes and the values are reported in Table 11. The values of CNT deposition length are also reported in the table.

For developing models to characterize the TLM method, the following assumptions are considered:

- The relations provided are not general and are only applicable for the presented geometry of electrodes.
- The Resistance is proportional to the length, resistivity, and reverse of width. The effect of thickness is neglected since in all the depositions the same number of layers (five layers) were printed.

Table 11. The values of the measured resistance for the four ink types

Electrodes	L (µm)	Total Resistance (kΩ)			
		One-day old pristine ink	Nine-days old pristine ink	58-days old pristine ink	11-days old ink after functionalization
C1 - C2	100	10.2	4.2	6.1	28.7
C2 - C3	100	9.8	5.1	5.9	32.4
C3 - C4	100	8.9	4.5	7.0	23.3
C4 - C5	300	17.4	6.3	8.0	62.5
C5 - C6	450	21.0	9.1	9.3	87.7
C6 - C7	600	23.8	11.7	12.8	92.3

Based on the data of Table 11 and the assumptions listed, the model and the TLM system can be explained as:

$$R_t = R_c + R_{cnt} + R_c$$

where

$$R_{cnt} = \frac{\rho * L}{w * t}$$

In these equations,  $L$  is the effective length of the CNT deposition,  $W$  is the width of the deposition, which is equal to  $1200 \mu\text{m}$ ,  $\rho$  is the resistivity of CNT film, and  $t$  is the deposition thickness. The parameter of characteristic resistance ( $R_s$ ) which equals  $\frac{\rho}{t}$  is defined to avoid complexation of the model due to the thickness difference of the deposition. Also,  $R_c$  is the contact resistance between the CNT deposition and the gold electrodes.

Therefore, the relation in **Erreur ! Source du renvoi introuvable.** can be written as:

$$R_{cnt} = \frac{R_s * L}{1200}$$

Based on this simplified version, the resistance between every neighboring electrode will follow:

$$R_t = \left(\frac{R_s}{1200}\right) * L + 2R_c$$

This is a simple regression that can be written as  $y = ax + b$ , where  $a = \frac{R_s}{1200}$  and  $b = 2R_c$ . By using the data provided in Table 11, the values of  $a$  and  $b$ , and therefore the values of  $R_s$  and  $R_c$  can be calculated which are presented in Table 12.

*Table 12. Calculation of  $R_s$  and  $R_c$  in each approach to model the circuit.*

Parameters	One-day old pristine ink	Nine-days old pristine ink	58-days old pristine ink	11-days old ink after functionalization
<b><math>R_s</math> (k<math>\Omega</math>)</b>	<b>35.61</b>	<b>16.46</b>	<b>13.97</b>	<b>168.59</b>
<b>(error%)</b>	<b>(8)</b>	<b>(9)</b>	<b>(14)</b>	<b>(11)</b>
<b><math>R_c</math> (k<math>\Omega</math>)</b>	<b>3.51</b>	<b>1.52</b>	<b>2.49</b>	<b>7.92</b>
<b>(error%)</b>	<b>(11)</b>	<b>(14)</b>	<b>(11)</b>	<b>(32)</b>
<b><math>R^2</math> factor</b>	<b>0.967</b>	<b>0.967</b>	<b>0.924</b>	<b>0.956</b>

## 4.2. Design of sensing devices and characterization procedures

### 4.2.1. InterDigitated Electrodes on Si/SiO<sub>2</sub> (IDE)

Figure 84 on left shows the first type of chip used for characterizing the sensing properties of CNTs, fabricated at ESIEE as supplier. The substrate is silicon wafer with a layer of SiO<sub>2</sub> (450 nm). The chip is divided into four sections, each comprising of 10 interdigitated electrodes (IDE) and the metal used in platinum. On the right side of Figure 84 each geometry is shown. Details on the dimensions of their electrode fingers and their corresponding resistance for printing 5 layers of MWCNTs ink as a comparative measure is reported in Table 13.

*Table 13. Dimension details and Resistance values of IDE geometries.*

<b>Geometry</b>	<b>Electrode finger width (<math>\mu\text{m}</math>)</b>	<b>Electrode finger spacing (<math>\mu\text{m}</math>)</b>	<b>Electrode effective length (<math>\mu\text{m}</math>)</b>	<b>Resistance of device with 5 layers of MWCNT ink (<math>\Omega</math>)</b>
<b>A</b>	<b>30</b>	<b>100</b>	<b>5130</b>	<b>886</b>
<b>B</b>	<b>5</b>	<b>100</b>	<b>6100</b>	<b>1265</b>
<b>C</b>	<b>30</b>	<b>30</b>	<b>3720</b>	<b>242</b>
<b>D</b>	<b>30</b>	<b>100</b>	<b>19650</b>	<b>2380</b>

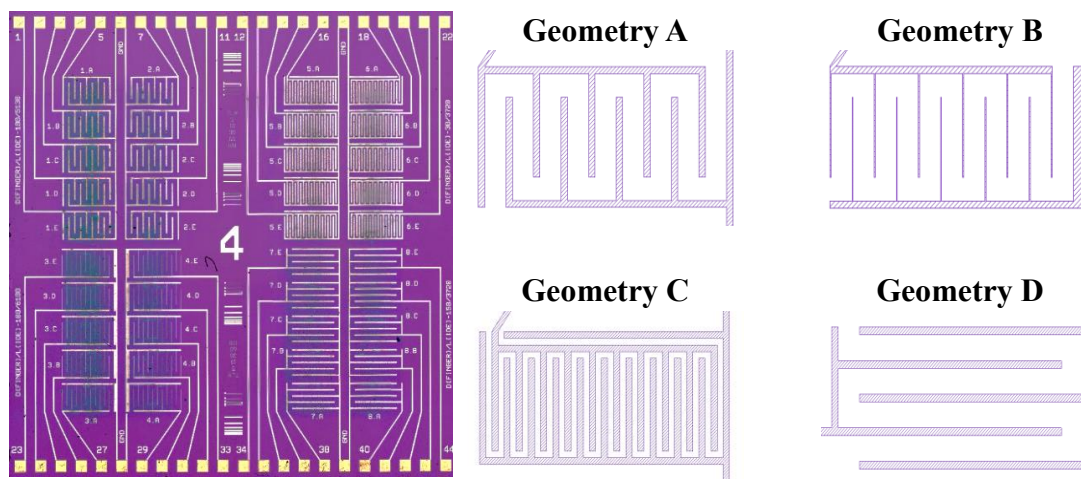


Figure 84. IDE substrates comprising of four different geometries of interdigitated electrodes.

It should be noted that the total dimension of each device is  $1200 * 600 \mu\text{m}$ , and the resistance values are average among 10 devices in one batch of printing. As it is clear from the values shown in Table 13, geometry C has a lower resistance for the same volume of CNT ink. For device fabrication, the entire surface of the device was printed with CNT ink.

#### 4.2.1.1. Protection layer fabrication for CNT deposition in IDEs

After depositing CNT ink, it is preferable to protect the deposition from release into water. Apart from protection of CNTs, limiting the access of water to the electrodes can result in more stability and durability of sensors by avoiding electrochemical impacts. Therefore, the deposition of a porous protective layer was studied. The material of protection must have the following characteristics:

- Compatible with thin-film deposition methods,
- Hydrophilic nature to allow the contact between water and the CNT layer,
- Pore size smaller than CNT length to limit the dissipation of CNTs in water.
- Insoluble in water,

- Inert to the changes of water pH (at least in the pH range of 6-8) and to the concentration of other common water analytes.

Block copolymers are a class of self-assembled materials that are composed of macromolecules with covalently connected segments of two or more different repeating units. These hybrid molecules can form ordered structures with nanometric heterogeneities. Nano porous membranes derived from block copolymers are being pursued as desirable materials for controlled separations due to their pore size tunability, narrow pore size distributions, and the ability for selective functionalization.<sup>317</sup>

Nguyen *et al.* in 2018 deposited a mixture of polystyrene-block-Polymethylmethacrylate (PS-b-PMMA) and polylactide acid (PLA) in acetone, on a modified silicon wafer. First, a network of cylinders with a PMMA shell and a PLA core was formed in within a continuous matrix of PS. By selectively removing PLA, 4-9 nm porous domains were created. Further PMMA removal revealed a second porosity level, with higher pores diameter and center-to-center distance.<sup>318</sup>

Another experimental work with block copolymers was done by Vayer *et al.*, where they deposited a self-assembled layer of PS-b-PLA by spin-coating. They observed the formation of a porous PS thin film with well-ordered cylindrical channels oriented perpendicularly to the surface of the film as shown in Figure 85.<sup>319</sup>

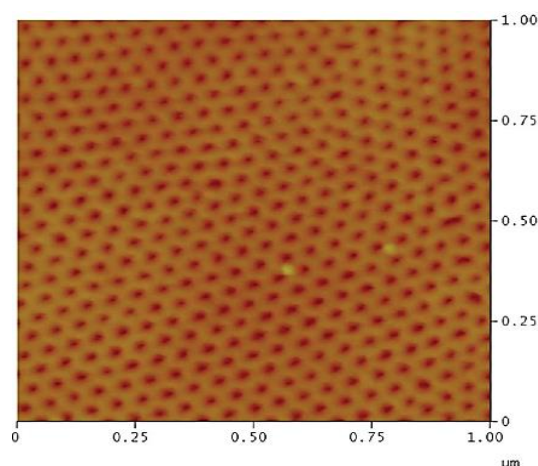


Figure 85.  $1 \mu\text{m}^2$  AFM image showing grain boundary at the surface of the porous film.<sup>319</sup>



Polymethylmethacrylate (PMMA) is commercial polymer that has a wide range of applications e.g. acrylic glass also known as Plexiglas. PMMA has also acted as hydrophilic waterproof breathable layers, which means they are a good choice for the protection of materials in water.<sup>320</sup>

PMMA was purchased from Sigma Aldrich ( $M_w = 55900$ ,  $M_n = 54000$ ,  $PDI = 1.03$ ). Thin-films of PMMA were created on a silicon substrate using spin-coating. The solution of PMMA was deposited by spin-coating, and the surface was observed by AFM imaging. Different surface and matrix morphologies of the deposition were obtained based on the concentration of PMMA and the rotational speed of the spin-coater. It was observed that surface defects in the form of pinholes appeared on the surface of films spin-coated at 8000 rpm from a 1.25% solution with a thickness of 8 nm. The deposition was either post-baked at 170°C for 60 min in an oven or left in a low vacuum chamber for a few days.<sup>321</sup>

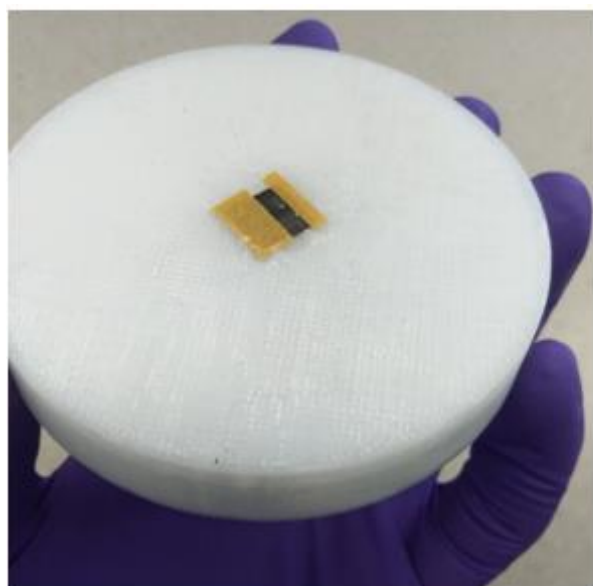
Since the procedure of synthesizing polymers to use as a protective layer for CNT thin film is complex and control of the reactions to create thin layers is almost impossible, an alternative way to create pores is required.

The process of phase inversion, also known as non-solvent induced phase separation (NIPS),<sup>322</sup> is a technique utilized for creating pores in thin polymer layers. When a water immiscible polymer solution like PMMA in toluene come into contact with water, phase inversion occurs. In this process, water occupies some areas of the surface, displacing the PMMA-toluene solution. Subsequent temperature annealing leads to the vaporization of both water and toluene, leaving behind a porous PMMA structure.<sup>323</sup> This method offers precise control over membrane structure by influencing the kinetics and thermodynamics of the phase separation process. The speed of precipitation, rates of solvent movement, and the type of demixing event during phase separation collectively determine the final porosity and structure of the membrane.<sup>324</sup>

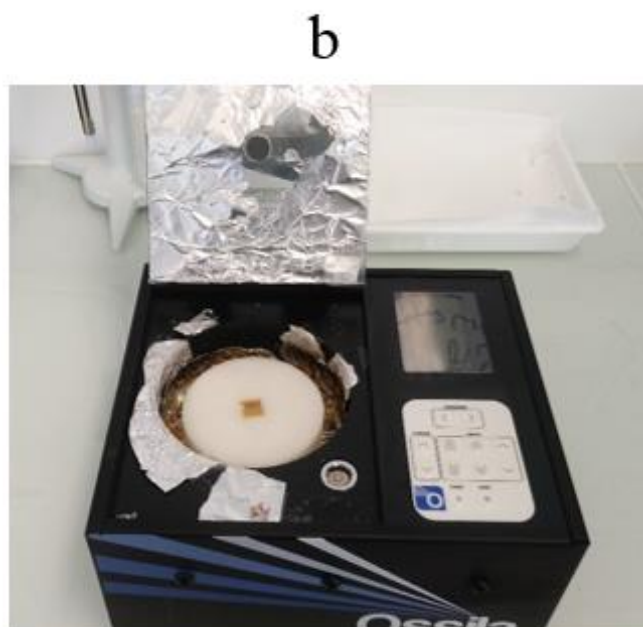
In the end, the complete process to add the protective layer can be described as the following steps:

**Preparation of PMMA Solution:** A solution of PMMA in toluene should be prepared in two steps. First, a highly concentrated solution, the mother solution, is prepared with a concentration of 175 mg/mL and should be stirred overnight. The final solution is diluted from the mother solution and has a concentration of 5 mg/ml.

**Spin-coating:** As shown in Figure 86.a, the connection pads of the chip are protected by tape to avoid the deposition PMMA over the pads. Then the chip is fixed on the holder of an Ossila spin-coater. For deposition, the machine is run for 60 seconds at the rotational speed of 1000 rpm, then 90 seconds at the speed of 3000 rpm.



a



b

Figure 86. Image of (a). placement of the taped chip on the holder, and (b) the Ossila spin-coater.

**NIPS process:** After drop-coating the PMMA solution, the chip is immersed in a solution of 5wt%  $\text{CaCl}_2$  in water for 1 minute. After removing from the solution, the tape is removed, and the chip is annealed at 80 °C for 3 hours to evaporate both solvents (water and toluene). The remaining deposition after annealing, is network of PMMA with  $\text{CaCl}_2$  salt, which can be removed by rinsing with water.

#### 4.2.1.2. Wirebonding, waterproofing and characterization method for IDEs

The next step in sensor fabrication process is to adapt the electronics for use in water. For this reason, a Printed Circuit Board (PCB) is used as an electronic bridge between the chip and the measurement Keithley devices.

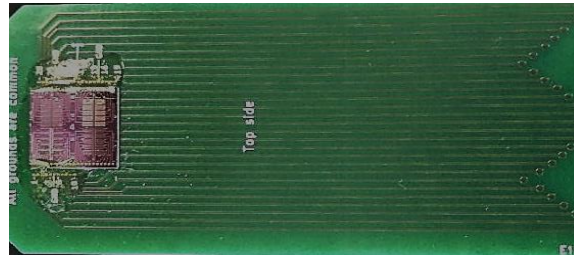


Figure 87. The PCB used to connect the chips to the measurement system.

To make the connections, first the chip is glued to the specific area on the PCB, and using a wire bonding machine connection between the pads of the chip and the pads of the PCB is made. In Figure 88, the wire bonding machine is shown as well as some examples of the connections between pads using 25 $\mu$ m diameter gold wire.

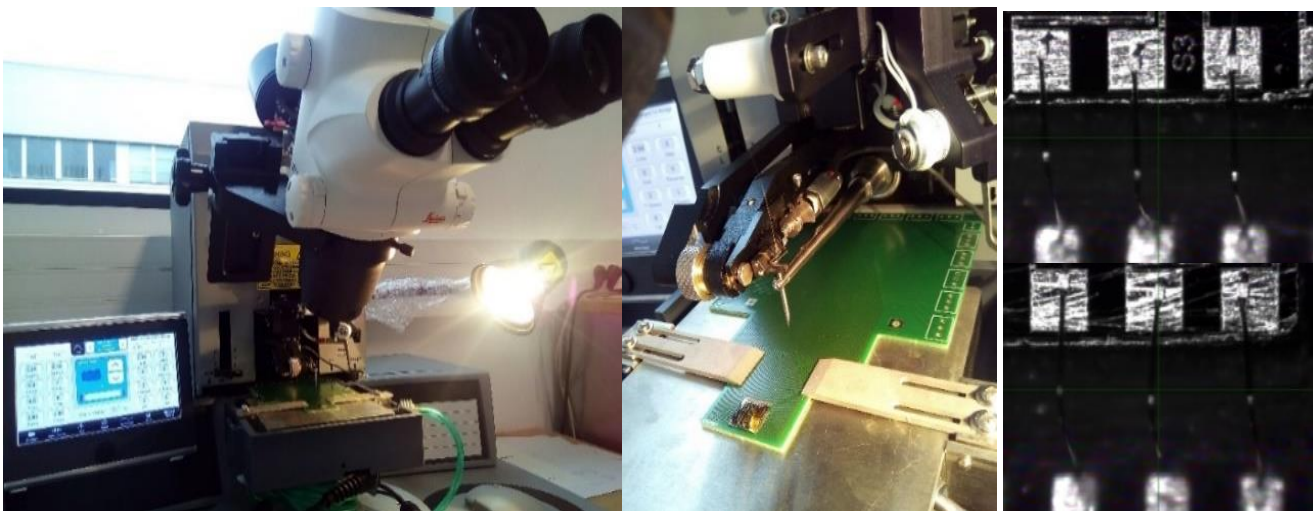


Figure 88. Wire bonding machine and the connection between the chips and the PCB.

After wire bonding, it is essential to use UV curable resin to cover the pads and the connection to conserve them against water penetration.

For characterization of the sensors, the head of the PCB where the sensor is located is immersed in a container. The container is connected to two pumps, one for circulating water, and the other for ejecting the water. The other end of the PCB is inserted to a homemade receptor wired to an Analogue Front End (AFE) which modulates the electronics of each sensor. An AFE is a component specifically designed to manage analog signals from sensors or transducers by providing functions such as amplification, filtering, and analog-to-digital conversion.<sup>325</sup> The container is a controlled system where the chemical content of water can be controlled.

#### 4.2.2. Simple electrodes on Si/Si<sub>3</sub>N<sub>4</sub> (SIN)

Figure 89 shows the structure of a chip cut from a silicon wafer with a layer of SiO<sub>2</sub> (450 nm) and Si<sub>3</sub>N<sub>4</sub> (110 nm) on top of one another. The chip is like the IDE chips, with 10 normal set of electrodes at top left. As shown in Figure 89, the CNT ink is printed on all the surface of electrodes.

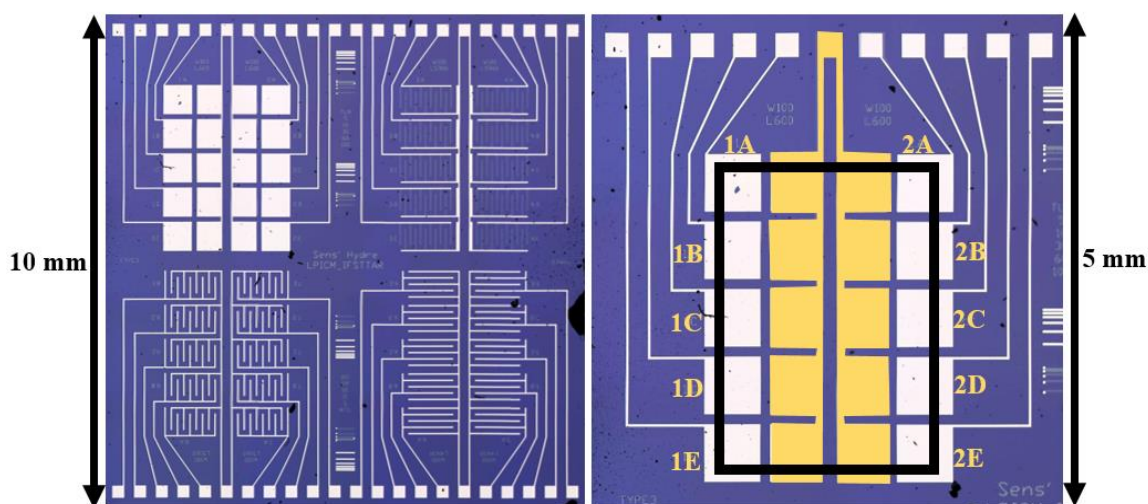


Figure 89. SIN substrates with four sections. Only the area at top left is used.

To characterize this type of sensors, a probe station is used, where the probes are placed on the pads of the chip and the electronics can be managed using a Keithley device. For the characterizations using this system, a few drops of water with known volume are placed on the CNT deposition in a way it covers the entire surface. The probing is done between pads 1A and 2E (Figure 89), which have the longest distance from one another. To change the chemical composition of the water, smaller drops of water (containing the analytes) is added on the surface, and it is homogenized by careful movements of the micropipette tip inside the drop. The concentration of the analyte in the water on the sensor can be calculated by knowing the volumes and concentrations of the added drops.

#### 4.2.3. Simple electrodes on Quartz integrated with a MicroChannel ( $\mu$ CQ)

In the design of the previous devices, a great importance has been given to the scale of the devices, which allows the acquisition of multiple sensing devices on one single chip. However, for the sake of better understanding of the phenomena that results in the sensing properties of functionalized CNTs, it is necessary to put more focus on the sensing mechanism. For this reason, new devices were designed and fabricated (Figure 90).

##### 4.2.3.1. Metal evaporation using RIBER

For the new design, a shadow mask was designed using LibreCAD software and it was fabricated at STEEC micromechanics fabrication<sup>4</sup> from 304L stainless steel with a thickness of 200  $\mu$ m and tolerance of 50  $\mu$ m. The shape and dimension of the electrodes are shown in Figure 90.a.

---

<sup>4</sup> <https://www.steec.fr/>

As discussed in the previous chapters, quartz is an interesting substrate due to its compatibility with the deposition method, the heating process, and the functionalization method. Therefore, the gold electrodes were deposited on quartz substrate using a RIBER evaporator through the designed mask. Figure 90.b shows an image of the initial device with the electrodes. The thickness of gold deposition can be controlled using the RIBER evaporator interface, and a thickness of 200 nm was chosen. It is important to note that since the adhesion of gold is not strong on quartz and glass, a thin layer of Chromium (15 nm) is first deposited using the same mask.

After the evaporation of gold electrodes, a 9\*9 mm square of the CNT ink is deposited on the electrodes as shown in Figure 90.c.

#### **4.2.3.2. Design and fabrication of microfluidic channel.**

For the characterization, a Polydimethylsiloxane (PDMS) microfluidic channel was designed and fabricated (Figure 90.d) to avoid the contact between the electrodes and the water containing the analytes. Water has been shown to significantly affect the reactivity of gold catalysts.<sup>326</sup> Observations suggest that the presence of water influences the hydrogen evolution reaction on gold electrodes, leading to oxide formation.<sup>327</sup> Therefore, protecting the contact of water and gold electrodes, could prevent oxidation of the electrodes and its impact on the sensing performance of devices.

When nitrogen is subjected to plasma, it can lead to the generation of nitrogen radicals through direct ionization of nitrogen molecules by electron impact, resulting in the formation of molecular ions and subsequent dissociative recombination with low-energy plasma electrons.<sup>328</sup> When two surfaces are exposed to plasma in nitrogen environment, their surface becomes extremely reactive and the recombination of the ions can result in their attachment. Through this process, the PDMS microchannel was attached on the chip.<sup>329</sup> The final product is illustrated in Figure 90.e. The plasma treatment was done only for 45 seconds to avoid overheating the surfaces, and then the microchannel was attached on the substrate.

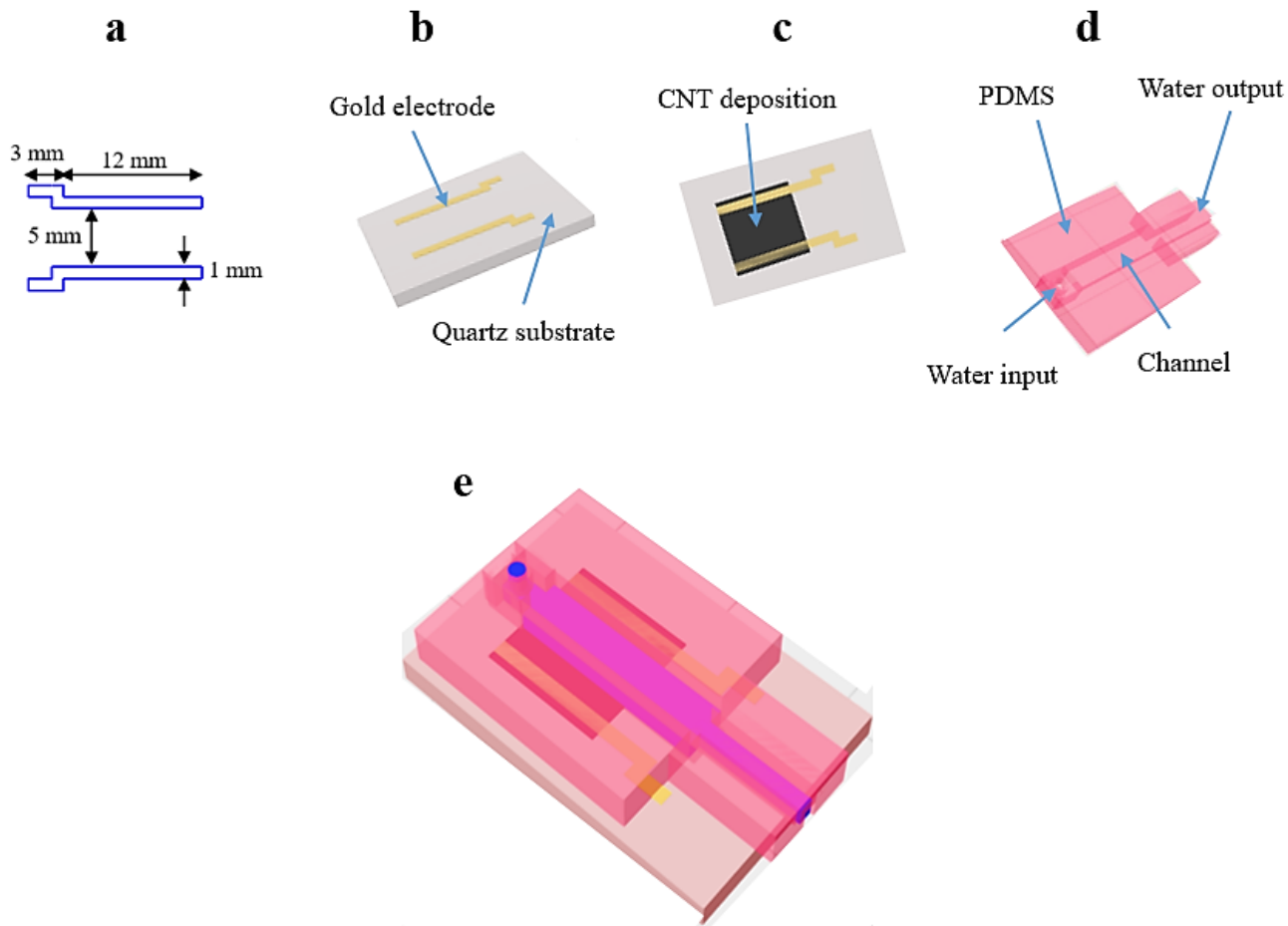


Figure 90. The design and fabrication process of  $\mu\text{CQ}$  sensing devices.

#### 4.2.3.3. Resistance study in $\mu\text{CQ}$

The resistance of the devices at each stage of the fabrication process is measured to monitor their evolution. To determine the optimal resistance range, it is crucial to consider factors such as sensitivity, response range, and noise levels. The resistance range significantly impacts the performance of these sensors.

Research by Liu<sup>330</sup> emphasizes the necessity of a sensing channel with moderate conductivity for chemiresistive sensors. Very low resistance can lead to limited sensitivity and a narrow response range, while high resistance can cause excessive noise and a low signal-to-noise ratio. Therefore, an ideal resistance range should strike a balance to ensure optimal sensor performance.



Furthermore, Khalid et al.<sup>331</sup> illustrated that the sensitivity of MWCNT-embedded sensors is influenced by the CNT content. Sensors containing 2% CNTs displayed the highest sensitivity within the tested strain range. This suggests that adjusting the CNT content can optimize the resistance range of CNT-based sensors to enhance sensitivity.

Moreover, Ishihara et al.<sup>332</sup> discussed that nanocarbon-based chemiresistive sensors exhibit responses that are 2–3 orders of magnitude lower than those of metal oxide-based sensors. They highlighted the importance of using the variation of normalized electric resistance for sensing response. This implies that selecting the resistance range for CNT-based sensors should ensure a detectable response while addressing baseline drift.

Collectively, these studies illustrate the importance of the resistance level for specific application. Therefore, this phase of monitoring is important to track the behavior of sensing devices.

In a trial to target this subject, multiple sensing devices were subjected to resistance monitoring. The resistance of devices is proportional to the volume of deposited ink. On different devices, 300, 500, 800 and 1200  $\mu\text{L}$  of the SWCNT ink was deposited. At least 10 devices were studied for each volume, and after averaging their resistance values at each stage, the results are illustrated in Figure 91.

As shown in Figure 91, for each device, the resistance has the lowest value after the ink deposition (first stage). After the heating process (second stage), the resistance of devices increases 3.9 times on average (from 3.3  $\text{k}\Omega$  to 12.7  $\text{k}\Omega$ ). This is simply due to the destruction of some of the CNTs during the necessary heating process. As a reminder, the loss of CNTs is usually due to the destruction of more defective CNTs that are more complicit in the functionalization process. Based on Figure 91, the resistance of a device, with 1200  $\mu\text{L}$  of the ink after the heating process could be similar to the resistance of a device with 400  $\mu\text{L}$  of the ink before the heating process. This indicates that due to the heating process, only almost 35% of the CNTs responsible for conductivity remain intact, illustrating that heating process has a more destruction impact on metallic CNTs.



Functionalization of CNTs has also a significant impact (1.6 times larger) on the resistance due to the introduction of insulating organic compounds. Another explanation for the reduced conductivity after functionalization is the reduced mobility of electrons in the  $\pi$  orbitals of the CNT network.

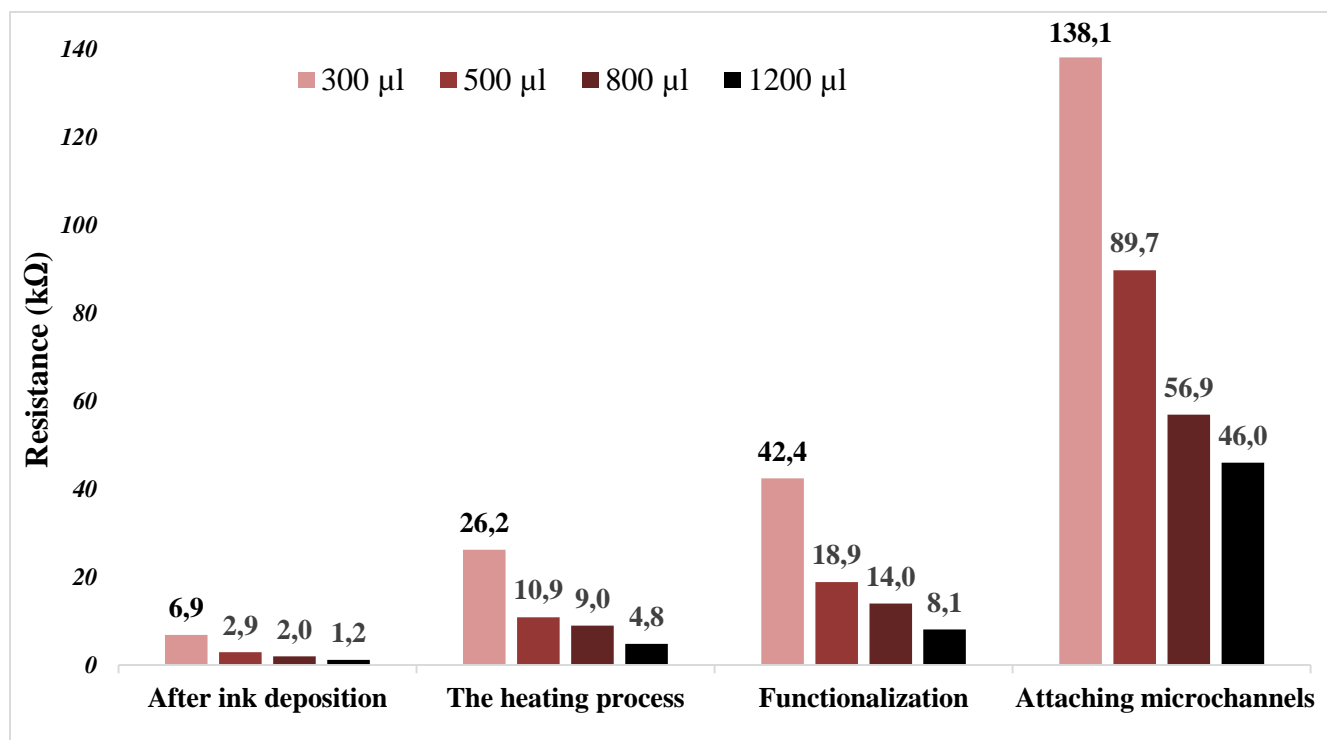


Figure 91. The evolution of resistance of devices with different steps of fabrication.

Finally, it is also very important to investigate the evolution of the resistance of the devices after the attachment of PDMS microchannel. The interaction between plasma and CNTs leads to various modifications in the properties of CNTs, affecting their structure, functionality, and applications. Plasma treatment can introduce physical and chemical defects on the surface of CNTs, such as increased oxygen content.<sup>333</sup> It is crucial to note that intense plasma treatment can also damage the CNTs due to high-energy particle bombardment.<sup>334</sup> For this reason, during the fabrication process, the CNT deposition was protected. Two small magnets with a diameter of 4 mm were placed on each side of the substrate and the CNT deposition was

protected by a small piece of paper. Despite protecting the CNT layer, the average resistance of multiple devices with different initial ink volume deposited increased 4 times.

This process is important to determine the necessary volume of initial CNT ink to obtain desired resistance.

### **4.3. Characterization of the sensing devices**

After the fabrication of different types of sensing devices (IDEs, SINs, and  $\mu$ CQs) in this section, the results of some of the characterization campaigns will be discussed. It is important to note that the characterization of different device types was not simultaneous and, in this project, the collective results of sensor and material characterization led to change the functionalization method, the CNT type and the device type. The results discussed in this section represent different characterization campaigns that led to the better understanding of the impact of CNT type, functionalization method, and the device type.

#### **4.3.1. MWCNT IDE devices to detect free chlorine.**

Chlorination of sodium hypochlorite is a well-researched topic with significant applications in various fields such as disinfection, water treatment, and chemical reactions. Sodium hypochlorite, commonly known as bleach, is a chlorine-releasing compound widely used for its disinfecting properties.<sup>335</sup> The chemical reactions involving sodium hypochlorite are intricate and can result in the formation of harmful by-products when combined with organic matter, underscoring the importance of proper handling and disposal practices.<sup>336</sup> Studies on the degradation pathways of compounds like thiuram in the presence of sodium hypochlorite have provided insights into the mechanisms involved in such reactions.<sup>337</sup>

Figure 92 illustrates the chemical structure of FF-UR conjugated polymer.<sup>338</sup> This polymer is composed of a fluorene backbone which are functionalized either with two alkyl chains to improve solubility and interaction strength with CNTs, or with two identical sensing groups, namely a urea group NH-CO-NH positioned between two phenyl groups. The polymer's ability to non-covalently functionalize CNTs is demonstrated through molecular dynamics simulations,<sup>339</sup> while its sensing capabilities are analyzed using density functional theory with an implicit solvent model.<sup>340</sup>

In essence, the formation of complexes with anions via hydrogen bonds (particularly hypochlorous ions) is expected from the urea group, while for cations, the interaction with the phenyl groups is strengthened through cation- $\pi$  interactions with the oxygen of the urea, resulting in a stronger interaction energy compared to anions, especially for  $Mg^{2+}$  and  $Na^+$ .<sup>340</sup>

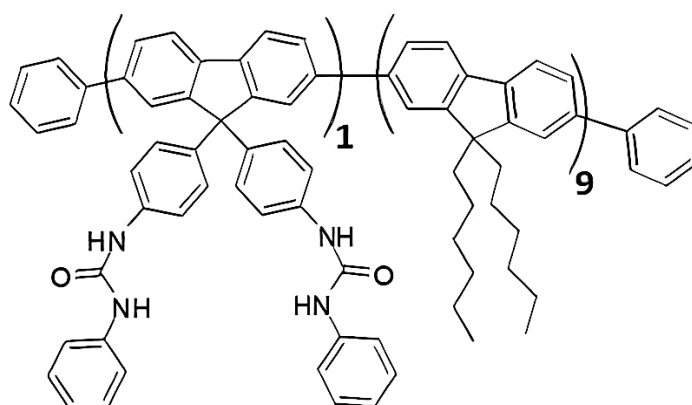
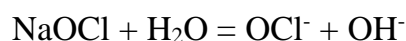
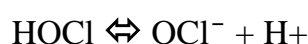


Figure 92. Chemical structure of FF-UR polymer used for the detection of free chlorine.

When hypochlorite is added to water, it also reacts to form hypochlorite ion and hydroxide:



These forms can exist together and the relative concentration of each depends on the pH of the solution and not on whether chlorine gas or bleach was added:



The pH of water significantly influences the balance between hypochlorous acid and hypochlorite ions. As the pH of a solution increases above 6, the percentage of hypochlorous acid decreases from nearly 100% to close to 0% at pH 9. Hypochlorous acid exhibits much greater bactericidal activity compared to hypochlorite, being approximately 80 times more potent. Consequently, in free residual chlorination, a higher pH leads to reduced effectiveness of the residual chlorine due to the lower presence of hypochlorous acid. This relationship is illustrated in the graph depicting the equilibrium shift with varying pH levels.<sup>341</sup>

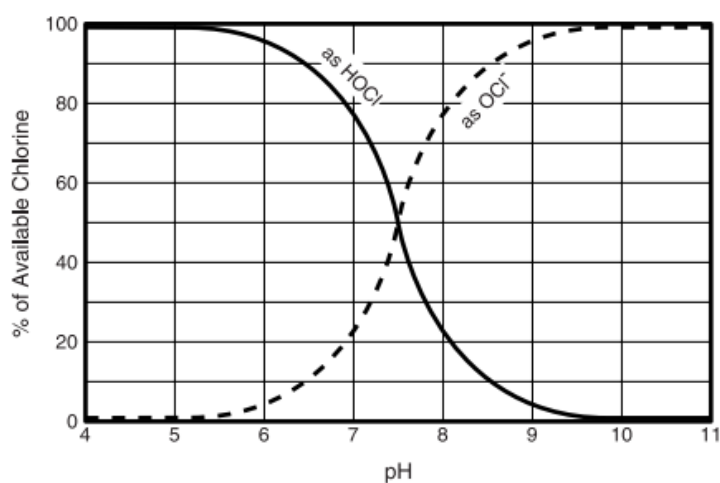


Figure 93. Relationship Between HOCl and OCl<sup>-</sup> at Various pH Values.<sup>5</sup>

As Figure 93 show, at a slightly basic pH of water, free chlorine is present as OCl<sup>-</sup> with a higher percentage compared to HOCl. This relatively small deviation from the neutral pH, makes FF-UR polymer a good receptor for OCl<sup>-</sup> with stronger interaction energy.<sup>340</sup>

Using the mixing approach of functionalization (explained in chapter 3) MWCNTs were functionalized with FF-UR polymer with a mass ratio of 1:1.5 (MWCNT: FF-UR). Table 14 represents the data of characterization of an IDE chip against the concentration of free

<sup>5</sup> <https://www.hydroinstruments.com/files/Basic%20Chemistry%20of%20Chlorination.pdf>

chlorine at pH of 8. The IDE chip contained multiple devices on some of which a pristine MWCNT ink was printed and, on the others, functionalized ink. The chip was wire bonded on a PCB and fixed inside the container with the rotational pump. 500 mL of DI water was circulated using the pump, and at certain times, the concentration of free chlorine content was increased as shown in detail in Table 14.

Sensitivity of the devices is calculated by the slope of changes between the initial and final concentrations, and as the data in Table 14 show, the more resistive a sensor, the more sensitive it gets. This implies that for more conductive films of CNT, small changes to the electronic properties, does not result in impressive sensing signals.

*Table 14. Data of characterization of sensing devices based on functionalized MWCNTs with FFUR-14 polymer.*

Time (min)	Concentration (ppm)	Resistance (kΩ)					
		Pristine devices				Functionalized devices	
		P1	P2	P3	P4	F1	F2
0	0.00	29.3	10.6	5.2	52.9	95.3	348.3
15	0.10	29.2	10.6	5.3	52.9	98.1	340.6
49	0.55	29.4	10.9	5.3	54.0	99.2	346.3
83	1.50	29.5	10.6	5.3	52.9	97.5	339.4
117	2.12	29.5	10.4	5.2	52.7	94.7	338.9
152	2.83	29.1	10.3	5.1	51.9	94.6	326.7
188	3.84	28.2	10.2	5.1	51.2	91.0	326.3
Sensitivity (kΩ/ppm)		-0.20	-0.12	-0.05	-0.49	-1.50	-5.41
Noise (kΩ)		0.06	0.02	0.01	0.10	0.32	0.59

Figure 94 summarizes the change in the normalized resistance with respect to the chlorine concentration. Both the table and the figure suggest that the resistance of the sensors increases at first for the addition of Chlorine but decreases as the chlorine concentration increases.

It should be mentioned that a constant current of 1.6  $\mu\text{A}$  was used in this characterization, and the delay between each measurement is 35 seconds.

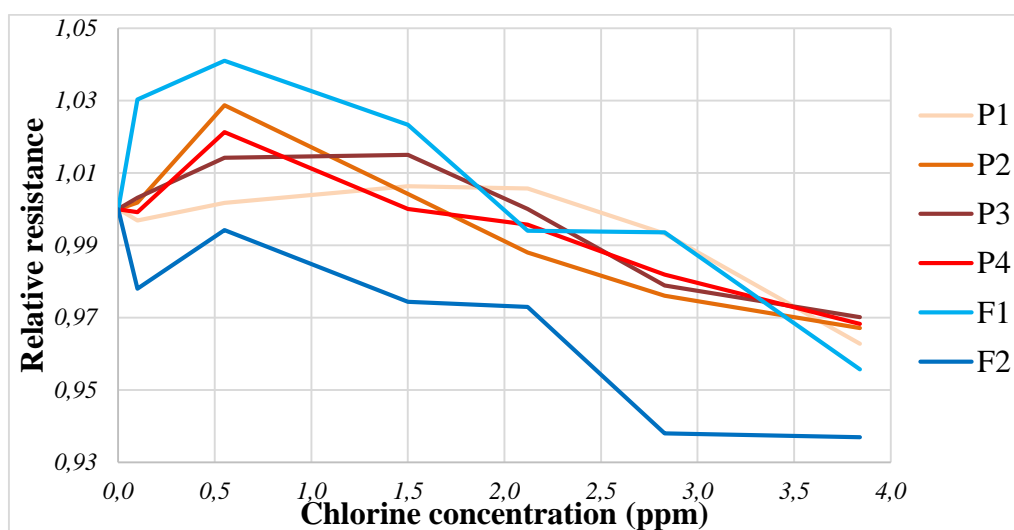


Figure 94. Response of pristine (P1, P2, P3, and P4) and functionalized (F1 and F2) IDE devices to the concentration of free chlorine in water.

The result of this characterization and similar ones using IDE devices are important in understanding the working function of these devices, the impact of different parameters like the level of resistance and the current bias, as well as the difference between the performance of devices based on pristine or functionalized MWCNT.

The results obtained here imply that the functionalization of MWCNTs do not have an important impact on the performance of the sensors in terms of sensitivity. As Figure 95 shows, the sensitivity has a linear relationship with the baseline resistance for all types of devices (pristine or functionalized). This implies that functionalization only impacts the initial resistance values, and does not result in any changes to the sensitivity.

Based on these results, it is important to tune the resistance level, and try different functionalization methods. It should be noted that the MWCNTs used in this campaign were not subject to the heating process, meaning that their functionalization could be ineffective as the ramifications of sonication, as described in the second chapter. For the rest of the project, focus will be put on other analytes that have a direct sensing mechanism instead of the sensing of free chlorine which is more complicated due to the impact of pH level.

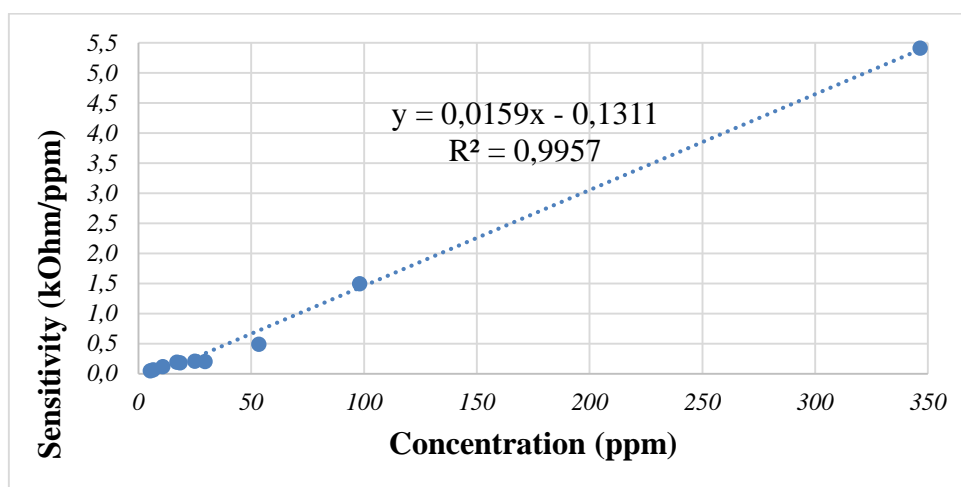


Figure 95. The relationship between the sensitivity and the baseline resistance for IDEs based on MWCNT.

### 4.3.2. Detection of pH

Analyzing the pH of drinking water is a crucial aspect of ensuring water quality and safety for consumption. Various studies have highlighted the significance of monitoring pH levels in drinking water to assess its suitability for human consumption. The World Health Organization (WHO) recommends that the pH of drinking water should fall within the range of 6.5 to 8.5.<sup>342</sup> This pH range is considered optimal for human health and indicates water that is neither too acidic nor too alkaline. Deviations from this range can impact the taste, safety, and overall quality of the water.<sup>343</sup>

Studies have shown that pH levels outside the recommended range can have adverse effects. For instance, acidic pH levels in drinking water have been associated with an increased risk of diabetes.<sup>344</sup> On the other hand, water with a pH of 9.0 to 9.5 has been found to result in higher digestion coefficients for certain components in lambs compared to water with a pH of 5.5 to 6.0.<sup>345</sup>

Monitoring pH levels in drinking water is essential for assessing water quality and ensuring it meets regulatory standards. Studies have employed various methods to analyze pH, including using standard analytical techniques,<sup>346</sup> high-performance liquid chromatography,<sup>347</sup> and spectrophotometric methods.<sup>348</sup>

In this section, the application of different sensing devices fabricated in this project for the detection of acidic and basic aqueous solutions will be discussed. Parameters like deposition method, functionalization method, the efficiency of functionalization and electronics are important to be optimized to obtain sensors to read real values of pH. On this note, the work done in this project is the efforts to understand the sensing mechanism of a pyrene-based molecule. Figure 96 shows the chemical structure of M3 molecule. The hydroxide function gets oxidized by reacting to  $H^+$  ion in water which is the indicative of pH as:  $pH = -\log [H^+]$ .

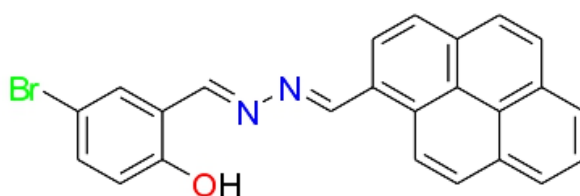


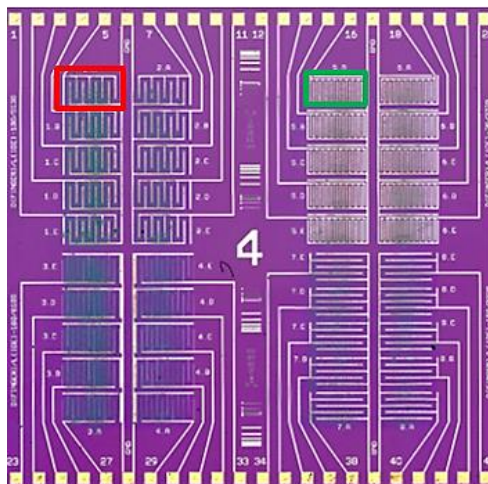
Figure 96. Chemical structure of M3, a pyrene-based molecule for the detection of water acidity.

#### 4.3.2.1. MWCNT IDE devices to detect pH

For this characterization, a single IDE chip was employed, with only two devices being printed and analyzed. The decision to print on just one device per side aimed to prevent small distances between adjacent CNT depositions, which could impact sensor functionality. Additionally, previous characterizations revealed that devices connected to the same ground



electrode exhibited similar behavior, despite differences in deposition materials (molecules or polymers). To address this, deposition was limited to specific devices connected to different ground electrodes, as shown in Figure 97.



*Figure 97. Chip used for the characterization of IDE device for the detection of pH. The device bordered in red was printed with Pristine ink, and the device in green with functionalized ink.*

The devices were functionalized with the M3 molecule using the incubation method. During incubation, one side of the chip was carefully immersed in the DMF solution containing M3 molecules while keeping the other side away from the molecule. Following the incubation process, the chip was wire bonded onto a PCB for long-term characterization, spanning over 11 days.

For the characterization, the PCB was immersed in the control container and 700 mL of DI water was circulated using the pumps. The real time pH of the circulating water was collected using an electrochemical pH sensor from Atlas scientific. For changing the pH of the circulating water, at different times, 10  $\mu\text{L}$  of HCl (1 M) or 50  $\mu\text{L}$  of NaOH (2 M) were added to the control container. It should be mentioned that a constant current of 2  $\mu\text{A}$  was used in this characterization, and the delay between each measurement is 5 seconds.

Figure 98 shows the results of this characterization for the devices with respect to the changes to the pH of the circulating water. The changes in the pH level of the circulating water are

embedded in the figure and the change in the normalized resistance of the pristine and functionalized devices are shown in the figure. The base resistance for the pristine device is 17 k $\Omega$ , and for the functionalized device is 27.8 k $\Omega$ , due to the functionalization. As Figure 98 suggests, the decrease in the pH results in a decrease in the resistance level in both type of devices, and behavior of pristine and functionalized devices seem almost identical. However, the results obtained from this characterization are interesting in drawing a full picture of the interactions of M3 molecule toward the changes in pH.

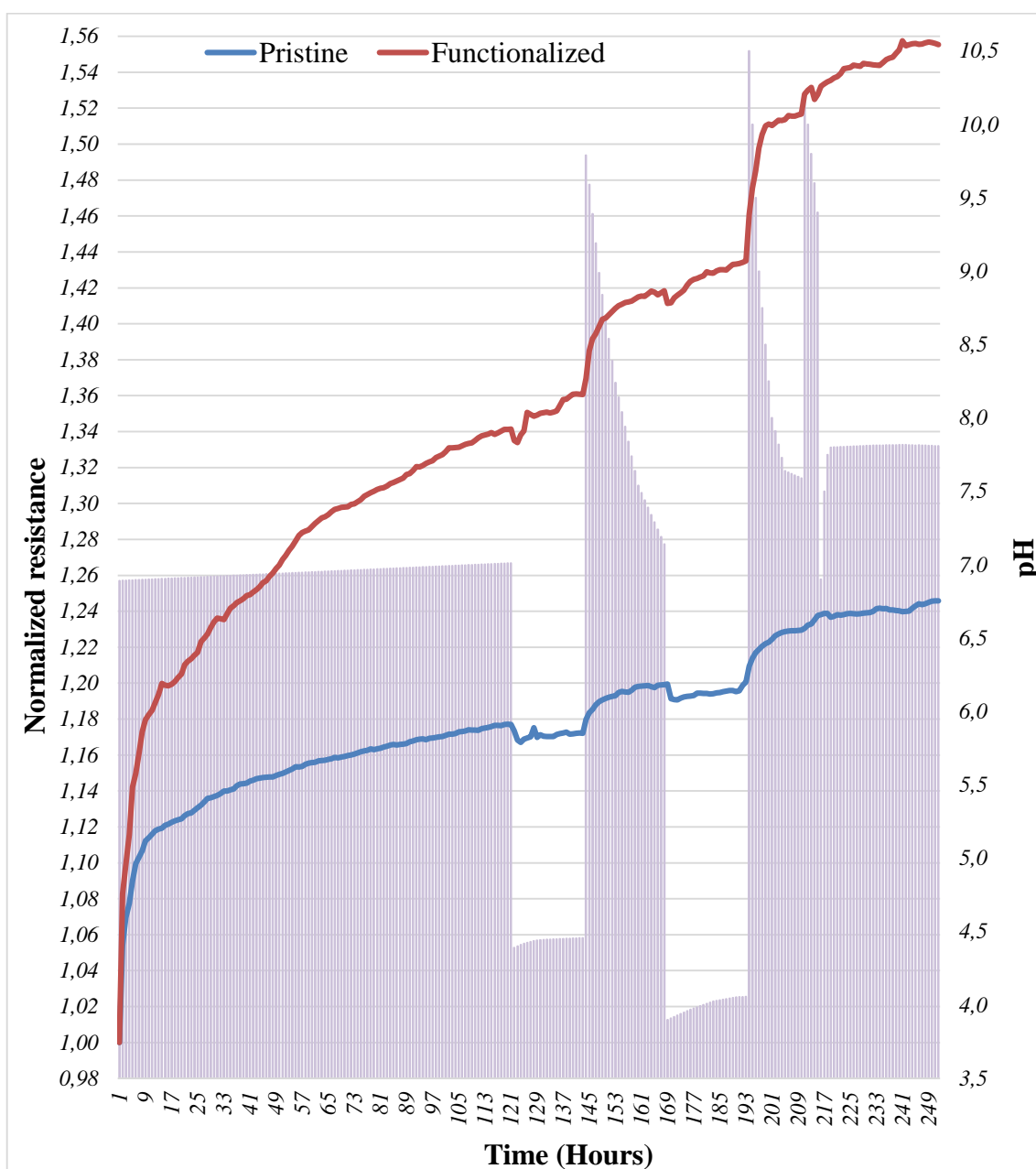


Figure 98. Result of the characterization of one IDE chip with only two printed devices.

#### 4.3.2.2. SWCNT SiN devices to detect pH

SiN devices were also used for the characterization of the response of M3 molecule to the changes in the pH of an aqueous solution. In these characterization, two changes were applied compared to the previous section.

- First, instead of MWCNTs, SWCNTs were used that due to their more important contact resistance, and lower resistivity, they are more prone to the chemical changes to their environment.
- Second, the use of SiN devices does not necessitate the wirebonding step which could harm the active material and make the results unreliable.

Using the Dimatix printer, SWCNT ink in NMP was printed on the SiN to fabricate devices. The solution of M3 molecule was prepared in THF for the incubation of the functionalized devices, and the characterization steps are summarized in Table 15. As the table shows, at different times after the start of the measurement, acidic or basic solution are added to the device.

*Table 15. The timeline of analyte addition to the SiN devices.*

<b>Time (min)</b>	<b>Action</b>
<b>40</b>	<b>+ 100 <math>\mu</math>L water</b>
<b>100</b>	<b>+ 2 <math>\mu</math>L 0.01M HCl</b>
<b>107</b>	<b>+ 2 <math>\mu</math>L 0.01M NaOH</b>
<b>118</b>	<b>+ 2 <math>\mu</math>L 0.01M HCl on the functionalized / + 2 <math>\mu</math>L 0.01M NaOH on the pristine</b>
<b>130</b>	<b>+ 2 <math>\mu</math>L 0.01M NaOH on the functionalized / + 2 <math>\mu</math>L 0.01M HCl on the pristine</b>
<b>138</b>	<b>+ 2 <math>\mu</math>L 0.01M HCl</b>
<b>147</b>	<b>+ 2 <math>\mu</math>L 0.01M NaOH on the functionalized / collecting the water from the pristine by paper</b>
<b>160</b>	<b>+ 2 <math>\mu</math>L 0.01M HCl on the functionalized / NO action to the pristine</b>

Figure 99 demonstrates the outcome of these characterizations for pristine and functionalized sensors. The presented results are averaged among three characterizations for each type of device. One important difference that outstands the other changes from the previous characterization, is the decrease in the resistance of the devices after adding water to the sensor. This outlines the importance of the CNT nature in the sensing mechanism.

Apart from the general behavior of CNT types, by looking at Figure 99, it can be noticed that the functionalization does not result in an increased amplitude of sensing, but the working function of the sensor in terms of stability and reproducibility increases. It should be mentioned that a constant current of 1  $\mu\text{A}$  was used in this characterization, and the delay between each measurement is 5 seconds.

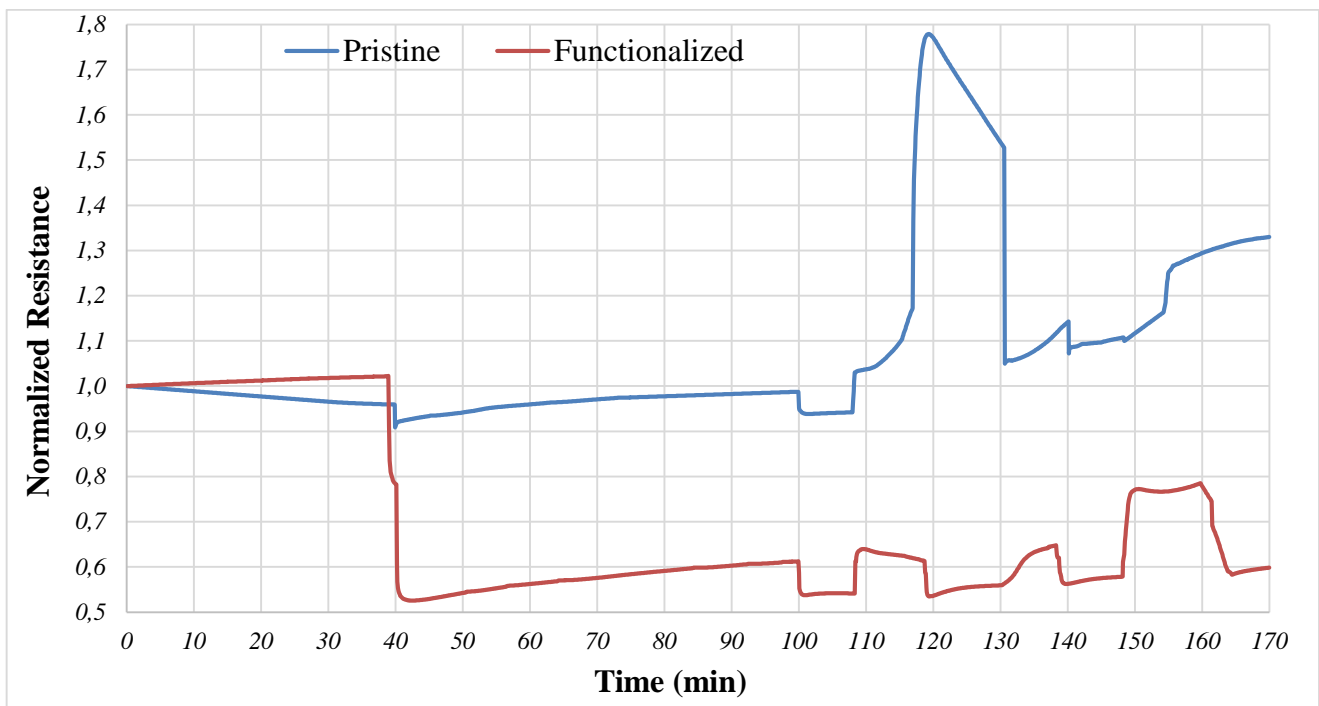


Figure 99. The results of the characterization of pristine and functionalized (with M3) SIN devices for responses against the changes in the pH of water.

As Figure 99 shows, the initial addition of water to the SWCNT devices results in the sharp decrease of the resistance values (notable in the functionalized device). However, as noticed in the previous cases (Figure 94 and Figure 98) addition of water to a deposition of MWCNTs leads to an increase in the device resistance. The decline in the conductivity of MWCNTs after contact with water may be ascribed to the interaction between water molecules and the MWCNTs, which can disrupt the formation of a conductive network within the material.<sup>349</sup> Conversely, when water is introduced to SWCNTs, it has been observed that the conductivity can actually increase. This rise in conductivity with the addition of water to SWCNTs may be attributed to the unique structure and properties of SWCNTs, which can enhance electron transport in the presence of water.

#### 4.3.3. MWCNT SiN devices to detect pH, Dissolved oxygen, and Cu (II)

In this campaign, 12 SiN devices were fabricated by printing an ink of MWCNT in NMP. As shown in Table 16, three target analytes were chosen; pH, Dissolved Oxygen (DO), and Copper (II) ions. As discussed in the previous section, M3 is a molecule that can selectively interact with H<sup>+</sup>, and as mentioned in the previous chapter, M2 molecule interacts selectively with the level of Dissolved Oxygen (DO) in water.

Table 16. SiN devices for the characterization of multiple molecules and multiple analytes.

Sensor Number	Molecule	Analyte	Initial Resistance (kΩ)
1	Pristine MWCNT	pH	11.1
2		Cu (II)	12.5
3		Dissolved Oxygen	12.7
4	M3	pH	30.9
5	(Pyrene)	Cu (II)	80.4

6		Dissolved Oxygen	59.1
7	M2 (Porphyrin)	pH	47.8
8		Cu (II)	20.1
9		Dissolved Oxygen	20.1
10	M4 (Pyrene)	pH	25.7
11		Cu (II)	24.9
12		Dissolved Oxygen	16.9

The thiourea function in M4 molecule has the properties for complexation with transition metals.<sup>350</sup> Therefore, this molecule was added in the characterization campaign for the sake of comparison and investigating the sensing properties. As a reminder, M4 molecule had the poorest degree of functionalization on the CNTs.

It should be mentioned that for all the characterizations of this section, a constant current of 1  $\mu$ A was used in this characterization, and the delay between each measurement is 10 seconds.

#### 4.3.3.1. Detection of pH

For the characterization against the pH of water, 100  $\mu$ L of DI water was added to the device at the minute 50. To change the pH of the water, drop, 6  $\mu$ L of an HCl solution of 0.01M was added to the water drop at minutes 100, 127, 150, and 189, and 6  $\mu$ L of an NaOH solution of 0.02M was added to the water drop at minutes 113, 137, 163, and 177. The times might be different for different characterization.

Figure 100 shows the results of the characterization. While the pristine device has negligible sensing toward the changes in the pH, the device incubated with M3 molecule has more sensitivity. However, the direction of the changes among the devices are the same, where

adding a base result in an increase and adding an acid result in a decrease in the resistance of the devices.

It's noteworthy that the M2 molecule has enhanced the device's sensitivity, likely due to the oxidation or reduction of the complexed palladium within its structure, as discussed in the third chapter. Conversely, when the device was incubated with the M4 molecule, it displayed no sensitivity towards acidic or basic solutions. The peak observed at minute 115 is merely noise caused by mechanical disturbance following the addition of a drop.

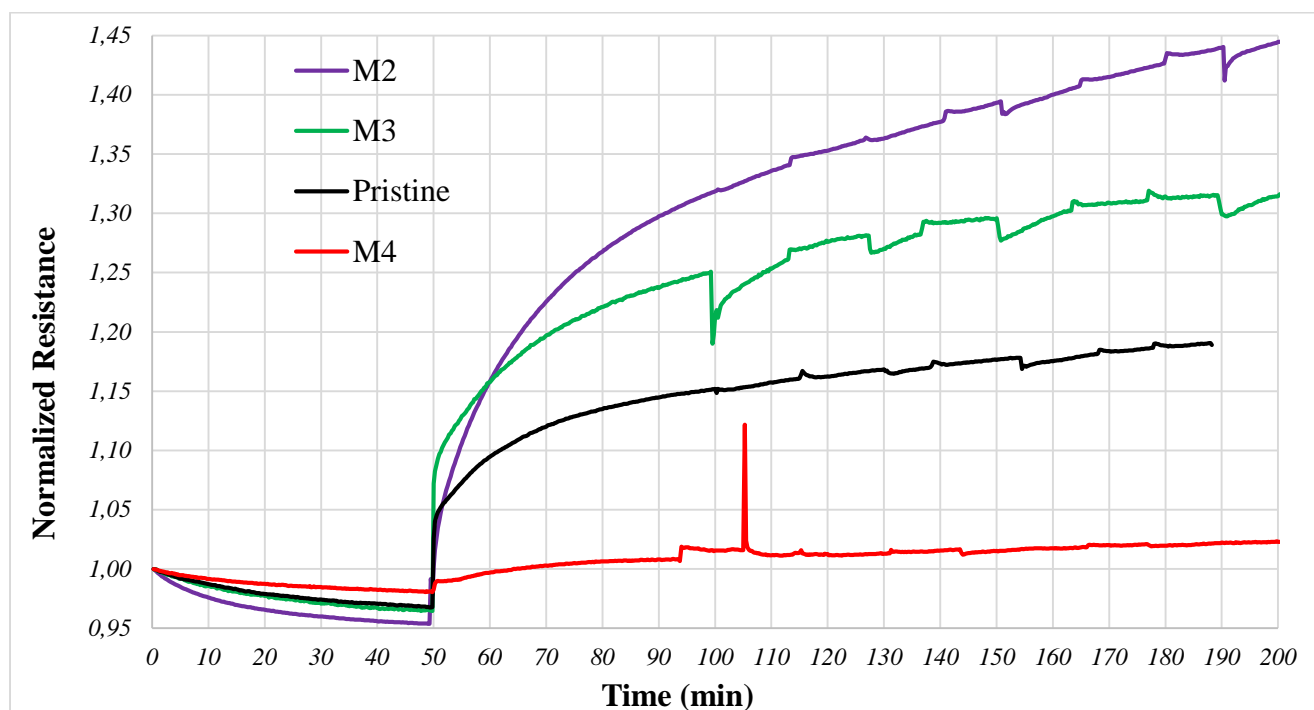


Figure 100. Results of characterization of Pristine and Functionalized sensors with M2, M3, and M4 molecules against the changes in the water pH.

#### 4.3.3.2. Detection of DO

Dissolved oxygen is an essential parameter in water quality evaluation, critical for sustaining aquatic life.<sup>351</sup> Adequate levels facilitate the oxidation of harmful compounds into beneficial

substances,<sup>352</sup> and its concentration serves as a key indicator of water quality, directly affecting aquatic respiration.<sup>353</sup> Defined as the amount of oxygen dissolved in water bodies, dissolved oxygen plays an important role in metabolic processes and ecosystem balance.<sup>354,355</sup> Studies indicate seasonal variations in surface water oxygen concentrations, typically ranging between 4.51 and 6.21 mg/L.<sup>356</sup> Maintaining optimal levels, especially in aquaculture, is vital for fish growth and survival, with recommended concentrations between 5.77 and 6.90 mg/L,<sup>357</sup> and above 5 mg/L for successful aquaculture practices.<sup>358</sup> Various factors, including temperature and fish overcrowding, can influence dissolved oxygen levels, emphasizing the need for careful monitoring in water quality assessments.<sup>359,360</sup>

Sodium sulfite ( $\text{Na}_2\text{SO}_3$ ) serves as a widely used oxygen scavenger across diverse applications, effectively reducing dissolved oxygen concentrations in solutions.<sup>361</sup> Its utility has been extensively researched, demonstrating its efficacy in eliminating oxygen from solutions, particularly in water treatment and microfluidic systems for creating hypoxic environments.<sup>361,362</sup> The concentrations employed vary depending on the application, with studies showcasing precise control over oxygen levels and notable effects on reaction kinetics.<sup>362,363</sup> Additionally, sodium sulfite exhibits potential as a growth promoter for certain organisms, further highlighting its versatility in both biological and chemical processes.<sup>364</sup>

For the characterization of the sensors against the changes in the level of DO, the sensor was kept in air for the first one hour to obtain a stabilized resistance value. After one hour, 100  $\mu\text{L}$  of a fresh solution of  $\text{Na}_2\text{SO}_3$  in DI water (100 ppm) was added on the device, and it was left for two hours.

Figure 101 shows the results of the characterization of the devices against the addition of the oxygen scavenger. For the pristine device, the resistance increases as soon as the water is dropped on the device. This is the same known behavior of the devices based on pristine MWCNT. For the case of M4 and M3 which are pyrene-based molecules, the resistance of the devices increases as well, however the increase is smaller than the case of the pristine MWCNT. This can be attributed to the fact that the presence of the molecule acts as a barrier and prohibit the interaction of water with MWCNT.



However, as Figure 101 shows, for the case of adding the oxygen scavenger on the M2-functionalized device, the resistance drops to 35% of its value immediately. This is due to the consummation of the oxygen molecules adsorbed on the M2 molecule by the  $\text{Na}_2\text{SO}_3$ . The migration of oxygen as a highly electronegative agent from the functionalized MWCNT to the solution, results in the increased conductivity of the MWCNT (+M2) network. However, since the measurement is done in air, the water drop interacts with the oxygen in air and the oxygen level is partially restored. This results in the restoration of the resistance level.

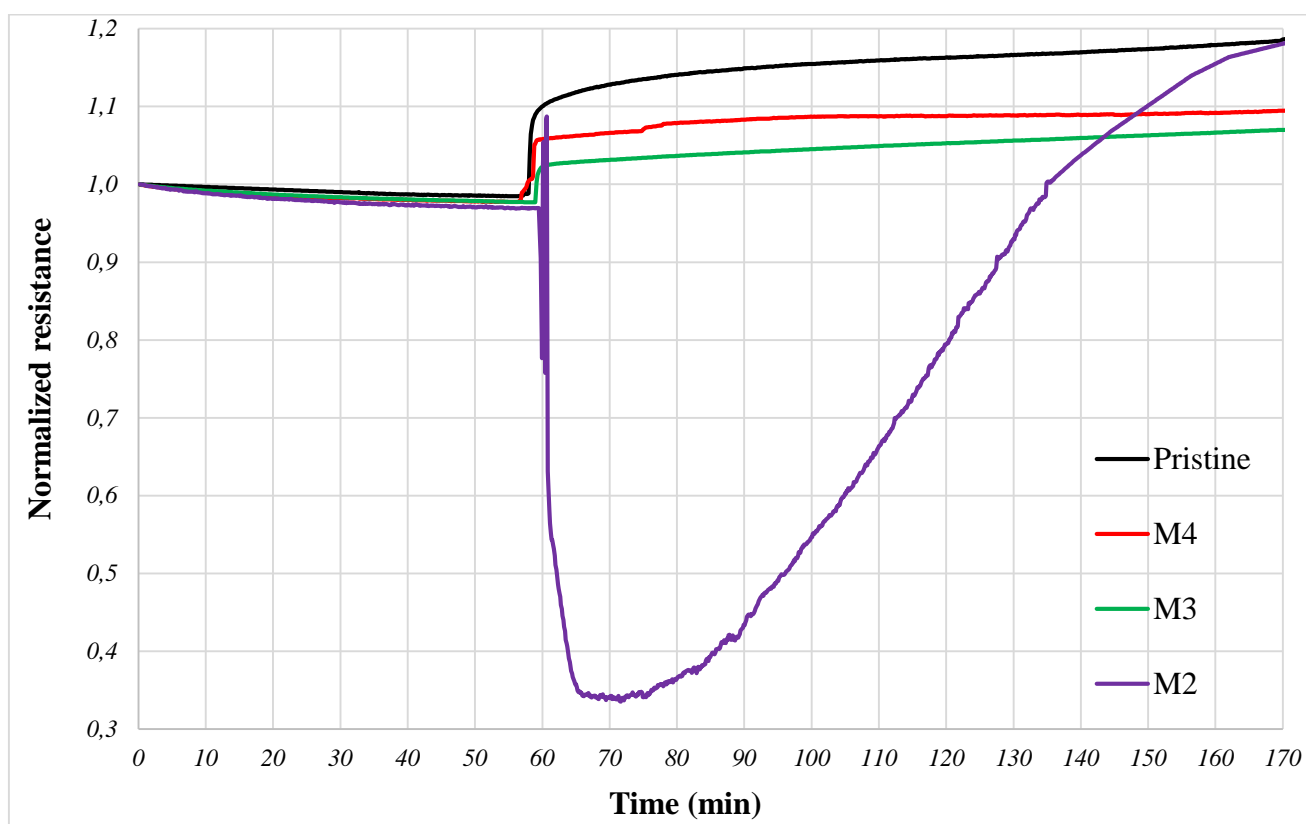


Figure 101. Results of characterization of Pristine and Functionalized sensors with M2, M3, and M4 molecules against the changes in the DO level in water.

### 4.3.3.3. Detection of Copper (II)

For this characterization, a solution of  $\text{CuCl}_2$  in DI water at the concentration of 21.3 mg/l was prepared. This concentration is equivalent to 10 ppm of the Cu (II) ion. After leaving the devices for 50 minutes in air, first 100  $\mu\text{L}$  of DI water was added on the device. After this addition, at the minutes 68, 120, 160, 200, and 300, 5  $\mu\text{L}$  of the initial solution of  $\text{CuCl}_2$  in DI water was added to the water drop. This gives an estimated concentration of 0.50, 0.97, 1.43, 1.85, and 2.26 ppm. The times could vary for different devices.

The results of this characterization are shown in Figure 102, which suggests very poor sensitivity of the fabricated devices toward the analyte. The poor sensitivity of the M4 molecule toward Cu (II) could be attributed to the low degree of functionalization, as discussed in the previous chapter.

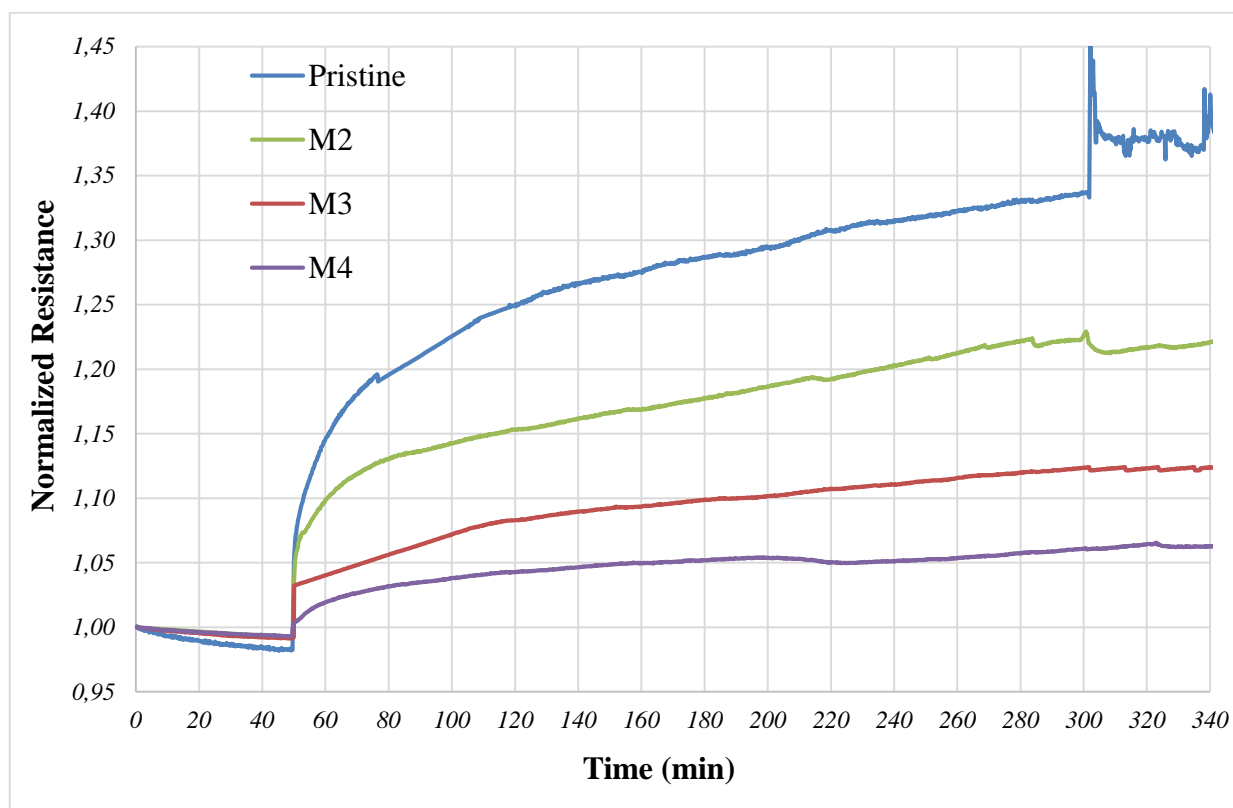


Figure 102. Results of characterization of Pristine and Functionalized sensors with M2, M3, and M4 molecules against the concentration of Cu (II) in water.

#### 4.3.4. SWCNT $\mu$ CQ devices to detect Glyphosate.

The importance of controlling the glyphosate content of water and soil was discussed in the previous chapter. As explained, M5 molecule (Figure 103 left) has shown interesting preliminary results for sensing glyphosate. In this section, the application of  $\mu$ CQ devices for the detection of the glyphosate content of water will be investigated. The chemical structure of Glyphosate is shown in Figure 103.

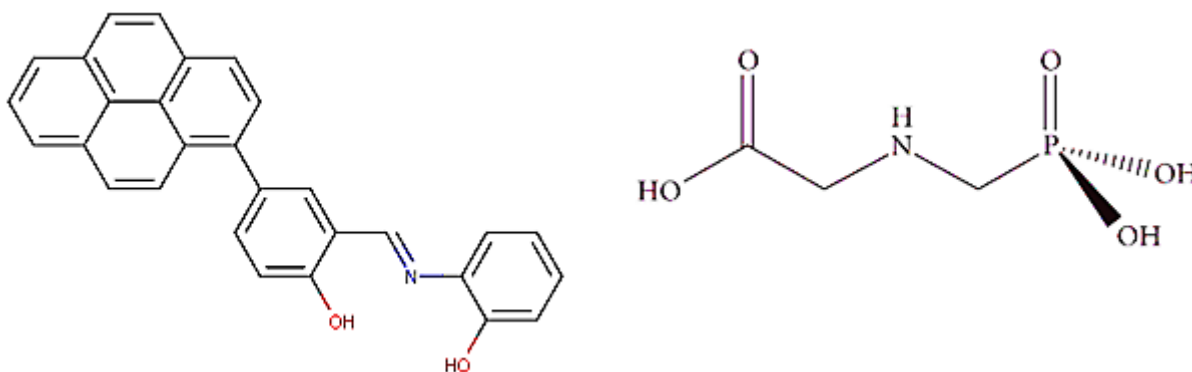


Figure 103. Reminder of the chemical structure of M5 molecule and Glyphosate.

For the device fabrication, SWCNT ink was deposited on  $\mu$ CQ chips, and the standard incubation method was applied to functionalize the devices.

To conduct the characterization, the devices were securely mounted on a surface, and the electrodes were connected to the probes of the Keithley device. A small tube was affixed to facilitate water input, while a beaker was positioned to collect the output water. The opposite end of the tube could extend outside the setup and be linked to a syringe. This configuration enabled the injection of water into the microchannel without disturbing the electrodes. Adjusting the concentration of the liquid within the microchannel was straightforward: the syringe could simply be used to introduce a new solution, displacing the previous one.

It should be noted that a constant current of 0.5  $\mu\text{A}$  was maintained throughout this characterization, with a measurement delay of 0.625 seconds between each reading. Figure 104 illustrates the results of the characterization of pristine and M5-functionalized devices against the concentration of glyphosate in DI water. The behavior of these devices is like other SWCNT-based sensors, where addition of DI water results in the decrease of resistance. However, it can be observed from the figure that while the pristine device has a random behavior but with an increasing tendency of the resistance, the resistance of the functionalized device decreases with a repeatable manner.

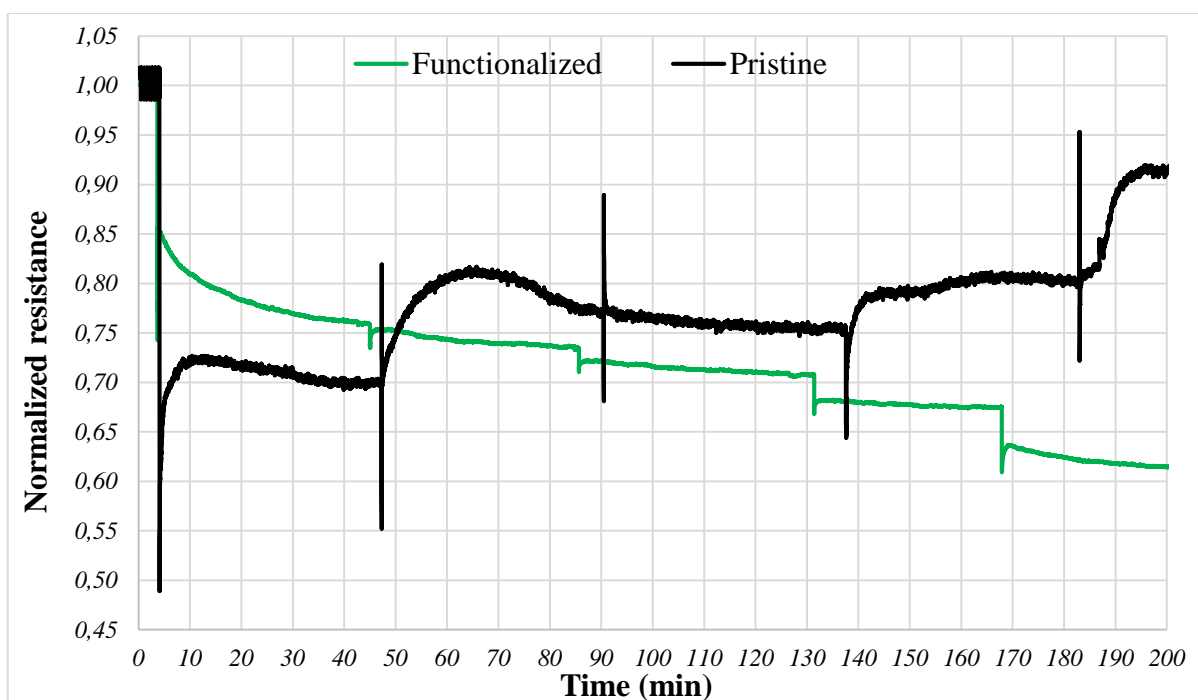


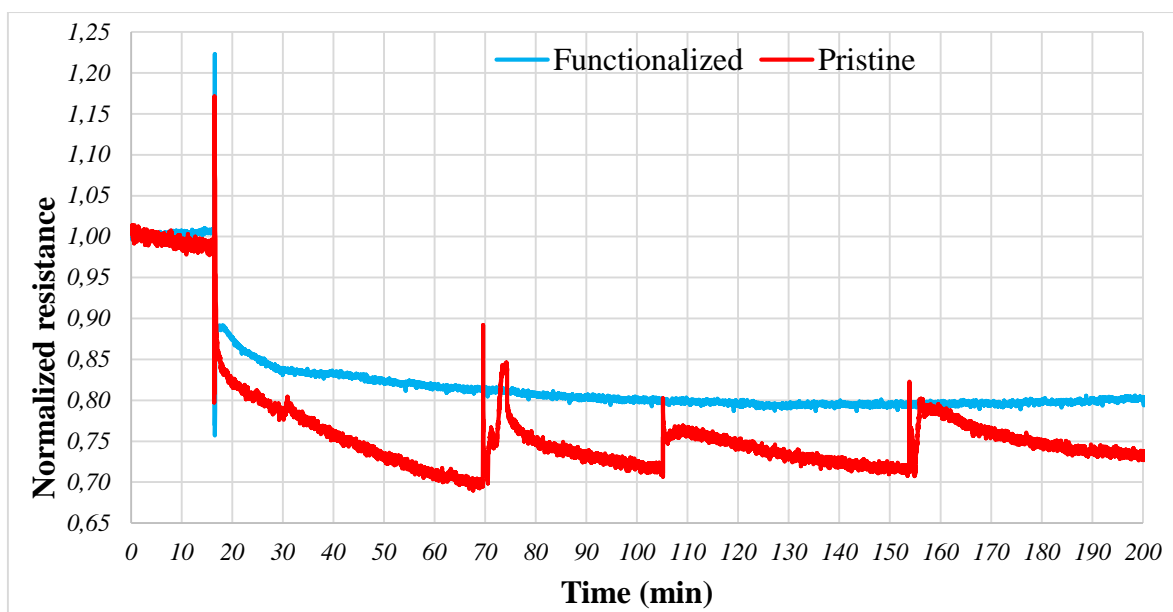
Figure 104. Results of characterization of Pristine and Functionalized with M5 molecule  $\mu\text{CQ}$  devices against the concentration of Glyphosate in water.

Since the addition of Glyphosate solution on the devices was shifted between the two sensors, **Erreur ! Source du renvoi introuvable.** clarifies the moment of each addition on both sensors.

Table 17. complementary information to Figure 104..

Solution	Time for Pristine device (min)	Time for Functionalized device (min)
DI water	4	4
[Glyphosate] = 0.5 ppb	47	45
[Glyphosate] = 20 ppb	90	85
[Glyphosate] = 300 ppb	137	131
[Glyphosate] = 1000 ppb	183	168

For the sake of comparison, pristine and M5-functionalized devices were also characterized against the concentration of copper. After the injection of DI water at the minute 16, Cu (II) solution of 0.5, 1, 3, and 5 ppm were injected at the minutes 30, 70, 105, and 155 respectively. As Figure 105 shows, while the pristine device is disturbed by the addition of Cu (II) ions, the functionalized device does not have any response to these additions. This is because the SWCNTs have been effectively covered with the M5 molecule, and they don't have any interactions with the copper ions.



*Figure 105. Results of characterization of Pristine and Functionalized with M5  $\mu$ CQ devices against the concentration of Zn(II) in water.*

#### **4.4. Conclusions on the sensing devices**

The main purpose of this chapter is evaluating the purification and functionalization of carbon nanotubes (CNTs) for their potential application in sensing devices. The results showcased here are multifaceted, with each characterization offering specific insights into various factors that influence the operational efficacy of chemiresistive sensors utilizing CNTs. Consequently, lessons were gleaned from each characterization, informing optimizations in CNT processing (particularly the heating process), CNT functionalization techniques, and the design and fabrication of sensing devices.

This iterative process led to an evolution in the characterization of sensing devices, transitioning from high-end devices (IDEs) employing untreated and inadequately functionalized CNTs, to more fundamental devices ( $\mu$ CQs) utilizing thoroughly characterized materials.

Notably, the enhanced sensitivity of CNTs towards pH variations was observed following successful functionalization with the M3 molecule. Furthermore, it was demonstrated that the functionalization of CNTs with the M2 molecule imparted selectivity towards the concentration of dissolved water. Lastly, employing  $\mu$ CQs enabled the selective examination of the response of the M5 molecule towards Glyphosate.

While the results presented in this chapter may not be revolutionary within the realm of sensor technology, they offer valuable and novel insights that can be further explored for the advancement of chemiresistive sensors leveraging CNTs.



**Institut Polytechnique de Paris**

## 5. General Conclusion

In the first section of this report, proof was provided that dealing with carbon nanotubes for sensing applications can be complex due to the nature of CNTs, their sensitivity toward their environment, and adsorption of amorphous matter. It is important to note that certain procedures must be followed as a chain of choices to be able to move on to the application of CNTs in sensors. These choices can be as delicate as the way of handling the substrates on. In the present work, the process toward developing chemiresistive sensors was designed and optimized step-by-step and the full chain of choices can be summarized below:

- Choice of the substrate: Quartz substrates due to their wettability characteristics, and their ability to resist high temperatures.
- Choice of NMP as solvent: This is a complex matter since NMP is a toxic solvent and its utilization is getting more and more restricted in Europe. However, in the scope of this project, I used very little volume of NMP, and it is due to two reasons:
  - First, the inks based on NMP are very stable and I noticed that compared to other solvents like oDCB, inks based on NMP can last and still provide homogenous depositions after 1 year. This is important, since for oDCB inks, they are not useful after 1 month, and I need to prepare another ink and using more solvent.
  - Second, in general, using Dimatix inkjet printer or even by drop casting, the required ink volume to obtain sensing devices with resistances in our optimized range is very low. Therefore, for the fabrication of 1000 sensors, only 200 ml of NMP and 15 mg of SWCNT could be enough.
- Choice of Heating process: It is necessary to choose instruments and parameters that are compatible with heating the substrates at 650°C.
- Choice of functionalization method: I perform the functionalization by incubation, because it is the only option to functionalize clean SWCNTs.
- Choice of sensing devices and characterization parameters: this topic is a perspective of this report. After successful functionalization of carbon nanotubes with engineered molecules, sensing devices can be fabricated and characterized against their respective analyte. However,





the results are too preliminary and lack repeatability, and more investigation is an aim to follow as perspectives of the work done.

## 6. Perspectives

Since the content of the present work were divided in three main chapter, the perspectives for possible future endeavors on this topic, will be provided in three subsections and are related to each chapter.

### 6.1. Perspectives on the processing CNTs

In the present work, deposition of CNT thin films from a solvent are an important aspect that shaped the chain of choices until the end. NMP and oDCB solvent were widely used and studied to develop inks that are compatible with different choices of deposition and provide a high stability of the ink over time. The question of stability is important in the quality of the deposition as well as in avoiding harmful and toxic solvent. Throughout generous volumes of these solvents were used to reach an optimized ink composition and deposition method. Once this optimized process is defined, the ink consumption for the development of CNT thin films is minimized to an estimated value of 200 mL for every square meter of CNT film.

Even though this process has a relatively low solvent waste in lab scale, applying it in more industrialized processes can result in more waste and more environmental impacts. Therefore, ink development using water as solvent is an interesting topic. Although the water-based CNT inks are well studied in the literature, but the necessity of using surfactants to disperse CNTs is a major drawback and results in a low CNT quality.

To address this issue, the thin-films from water(+surfactant)-based inks can be subjected to the heating process, ensuring the elimination of the surfactant, and acquiring high CNT thin-film quality.

## 6.2. Perspectives on the functionalization of CNTs

Like the argument of the previous section, the functionalization method described in this work is in the continuation of the commitment to the solvent-based deposition of CNTs. After different trials to find an optimal functionalization route, incubation method was chosen, which is compatible with the thin-film preparation and purification.

However, the incubation process can be a complex interaction considering the different types of conjugated bases. As a completion of the work done in this work, numerical studies on the interactions that happen at the CNT-molecule interface can provide deeper understanding of the noncovalent functionalization. Different Density functional theory (DFT) and molecular dynamics (MD) approaches can be used to simulate the infamous  $\pi$ - $\pi$  interactions in the presence of solvents used for each molecule.

As a perspective experimental work, using evaporation of thermally stable molecules to incubate CNTs in vacuum can result in extremely efficient incubations. Although this method can have limitations in terms of the choice of the molecule, it can open an interesting gate to the science of surface chemistry and noncovalent functionalization.

Experimentally study the impact of CNT chirality on their functionalization efficiency is another topic that can help understand the functionalization mechanism.

## 6.3. Perspectives on the sensors based on CNTs

Developing sensors to detect analytes in water can be a profound topic of research and development in different levels. Therefore, the perspectives for future works in both vertical and horizontal directions can be exhaustive and limitless. However, based on the experiences obtained from the present work, the following topics can be extremely interesting in probing toward real world remote sensors.

- A more profound study of the interaction chain from analyte to the electrode in a chemiresistive sensor using numerical approaches can be the subject of great amount of research. Understanding these interactions and tracking the mobility of electrons also from a quantum mechanics point of view can result in the deeper understanding of the sensing mechanisms, and the development of more efficient interfaces (analyte-molecule, molecule-CNT, CNT- CNT, CNT- metallic electrode).
- Electrochemical investigation of a system where usually a charged analyte is present in an aqueous environment, is an interesting topic. Studying the redox reactions at the level of CNT and metal can provide deep understanding of the sensing process and the electronic interactions between the CNT and the interfaced molecule. Cyclic Voltammetry (CV) in the presence of water and Electrochemical impedance Spectroscopy (EIS) studies on the devices can be subject of massive interesting research.
- Understanding the role of metallic and semiconducting CNTs in a randomly deposited network is another perspective that can help future development of CNT-based chemiresistive sensors. There is a relationship between the role of conductive CNTs in creating a resistive base and the role of semiconducting CNTs in modulating the sensitivity of sensors. This relationship is impacted by the parameters of Ohm's law, which are voltage, current and resistance. In other words, for each CNT composition with different metallic to semiconducting ratios, there is an optimum resistance value and current bias that allows the sensor to function better. Study of this topic can result in impressive advancements in the domain.

## References

- (1) Jogi, B. F.; Sawant, M.; Kulkarni, M.; Brahmkar, P. K. Dispersion and Performance Properties of Carbon Nanotubes (CNTs) Based Polymer Composites: A Review. *J. Encapsulation Adsorpt. Sci.* **2012**, *02* (04), 69–78. <https://doi.org/10.4236/jeas.2012.24010>.
- (2) Barrejón, M.; Prato, M. Carbon Nanotube Membranes in Water Treatment Applications. *Adv. Mater. Interfaces* **2022**, *9* (1), 2101260. <https://doi.org/10.1002/admi.202101260>.
- (3) Jang, S.-H.; Li, L.-Y. Self-Sensing Carbon Nanotube Composites Exposed to Glass Transition Temperature. *Materials* **2020**, *13* (2), 259. <https://doi.org/10.3390/ma13020259>.
- (4) Hinrichsen, D.; Henrylito, T. The Coming Freshwater Crisis Is Already Here, 2002. <https://www.wilsoncenter.org/sites/default/files/media/documents/publication/popwawa2.pdf>.
- (5) Ebenstein, A. The Consequences of Industrialization: Evidence from Water Pollution and Digestive Cancers in China. *Rev. Econ. Stat.* **2012**, *94* (1), 186–201. [https://doi.org/10.1162/REST\\_a\\_00150](https://doi.org/10.1162/REST_a_00150).
- (6) Chikodzi, D.; Mabhegedhe, M.; Tunha, T. K. Biomonitoring of Mucheke and Shagashe Rivers in Masvingo, Zimbabwe Using Macro-Invertebrates as Indicators of Water Quality. *J. Geosci. Environ. Prot.* **2017**, *05* (09), 221–237. <https://doi.org/10.4236/gep.2017.59016>.
- (7) Aydin, A. The Microbiological and Physico-Chemical Quality of Groundwater in West Thrace, Turkey. *Polish Journal of Environmental Studies*. 17th ed. 2007, pp 377–383.
- (8) Cho, G.; Azzouzi, S.; Zucchi, G.; Lebental, B. Electrical and Electrochemical Sensors Based on Carbon Nanotubes for the Monitoring of Chemicals in Water—A Review. *Sensors* **2021**, *22* (1), 218. <https://doi.org/10.3390/s22010218>.
- (9) Lakshmikantha, V.; Hiriyanagowda, A.; Manjunath, A.; Patted, A.; Basavaiah, J.; Anthony, A. A. IoT Based Smart Water Quality Monitoring System. *Glob. Transit. Proc.* **2021**, *2* (2), 181–186. <https://doi.org/10.1016/j.gltip.2021.08.062>.
- (10) Bhardwaj, J.; Gupta, K. K.; Gupta, R. A Review of Emerging Trends on Water Quality Measurement Sensors. In *2015 International Conference on Technologies for Sustainable Development (ICTSD)*; IEEE: Mumbai, India, 2015; pp 1–6. <https://doi.org/10.1109/ICTSD.2015.7095919>.
- (11) Kholghi Eshkalak, S.; Chinnappan, A.; Jayathilaka, W. A. D. M.; Khatibzadeh, M.; Kowsari, E.; Ramakrishna, S. A Review on Inkjet Printing of CNT Composites for Smart

Applications. *Appl. Mater. Today* **2017**, *9*, 372–386.  
<https://doi.org/10.1016/j.apmt.2017.09.003>.

- (12) Iijima, S. Helical Microtubules of Graphitic Carbon. *Nature* **1991**, *354* (6348), 56–58.  
<https://doi.org/10.1038/354056a0>.
- (13) De Volder, M. F. L.; Tawfick, S. H.; Baughman, R. H.; Hart, A. J. Carbon Nanotubes: Present and Future Commercial Applications. *Science* **2013**, *339* (6119), 535–539.  
<https://doi.org/10.1126/science.1222453>.
- (14) Lee, S.; Lim, J.; Kim, K. Fabrication of Hybrid Ladderlike Polysilsesquioxane-grafted Multiwalled Carbon Nanotubes. *J. Appl. Polym. Sci.* **2012**, *124* (5), 3792–3798.  
<https://doi.org/10.1002/app.35389>.
- (15) Xu, X.; Wang, Y.; Wang, Q.; Dong, G.; Li, W.; Li, G.; Lv, Y.; Zhang, J.; Ding, H. The Microstructures of In-Situ Synthesized TiC by Ti-CNTs Reaction in Cu Melts. *Mater. Sci.-Pol.* **2022**, *40* (1), 145–158. <https://doi.org/10.2478/msp-2022-0018>.
- (16) Carbon Nanotubes: Advanced Topics in the Synthesis, Structure, Properties and Applications. *Mater. Today* **2008**, *11* (3), 57. [https://doi.org/10.1016/S1369-7021\(08\)70021-X](https://doi.org/10.1016/S1369-7021(08)70021-X).
- (17) Khantimerov, S. M.; Togulev, P. N.; Kukovitsky, E. F.; Lyadov, N. M.; Suleimanov, N. M. Effect of Electrochemical Treatment on Electrical Conductivity of Conical Carbon Nanotubes. *J. Nanotechnol.* **2016**, *2016*, 1–5. <https://doi.org/10.1155/2016/8034985>.
- (18) Li, W.; He, W.; Chen, X.; Chen, T.; Wu, Y.; Li, C.; Zhang, X.; Yu, L.; Yang, F. Tailoring the Electrocatalytic Properties of  $Sp^2$ -Hybridized Carbon Nanomaterials with Molecule Doping. *ChemCatChem* **2022**, *14* (1), e202100684.  
<https://doi.org/10.1002/cctc.202100684>.
- (19) Dumlich, H.; Gegg, M.; Hennrich, F.; Reich, S. Bundle and Chirality Influences on Properties of Carbon Nanotubes Studied with van Der Waals Density Functional Theory. *Phys. Status Solidi B* **2011**, *248* (11), 2589–2592.  
<https://doi.org/10.1002/pssb.201100212>.
- (20) Lin, L.; Qin, L.-C.; Washburn, S.; Paulson, S. Electrical Resistance of Single-Wall Carbon Nanotubes with Determined Chiral Indices. *MRS Proc.* **2009**, *1204*, 1204-K07-06. <https://doi.org/10.1557/PROC-1204-K07-06>.
- (21) Qin, L.-C.; Liu, Z.; Zhang, Q.; Deniz, H. Determination of the Chirality of Carbon Nanotubes by Electron Diffraction. *Microsc. Microanal.* **2007**, *13* (S02).  
<https://doi.org/10.1017/S1431927607079196>.
- (22) Thrower, P. A.; Cheng, H.-M. Growth of Nanocarbons by Catalysis and Their Applications. *MRS Bull.* **2017**, *42* (11), 790–793. <https://doi.org/10.1557/mrs.2017.234>.

- (23) Belin, T.; Epron, F. Characterization Methods of Carbon Nanotubes: A Review. *Mater. Sci. Eng. B* **2005**, *119* (2), 105–118. <https://doi.org/10.1016/j.mseb.2005.02.046>.
- (24) Sinnott, S. B.; Andrews, R. Carbon Nanotubes: Synthesis, Properties, and Applications. *Crit. Rev. Solid State Mater. Sci.* **2001**, *26* (3), 145–249. <https://doi.org/10.1080/20014091104189>.
- (25) Sisto, T. J.; Zakharov, L. N.; White, B. M.; Jasti, R. Towards Pi-Extended Cycloparaphenylenes as Seeds for CNT Growth: Investigating Strain Relieving Ring-Openings and Rearrangements. *Chem. Sci.* **2016**, *7* (6), 3681–3688. <https://doi.org/10.1039/C5SC04218F>.
- (26) Bachtold, A.; Fuhrer, M. S.; Plyasunov, S.; Forero, M.; Anderson, E. H.; Zettl, A.; McEuen, P. L. Scanned Probe Microscopy of Electronic Transport in Carbon Nanotubes. *Phys. Rev. Lett.* **2000**, *84* (26), 6082–6085. <https://doi.org/10.1103/PhysRevLett.84.6082>.
- (27) Wei, L.; Lu, D.; Wang, J.; Wei, H.; Zhao, J.; Geng, H.; Zhang, Y. Highly Sensitive Detection of Trinitrotoluene in Water by Chemiresistive Sensor Based on Noncovalently Amino Functionalized Single-Walled Carbon Nanotube. *Sens. Actuators B Chem.* **2014**, *190*, 529–534. <https://doi.org/10.1016/j.snb.2013.09.017>.
- (28) Jain, N.; Negi, A. Contemporary and Looming Applications of Carbon Nanotubes. *Macromol. Symp.* **2023**, *407* (1), 2100387. <https://doi.org/10.1002/masy.202100387>.
- (29) Baughman, R. H.; Zakhidov, A. A.; De Heer, W. A. Carbon Nanotubes--the Route Toward Applications. *Science* **2002**, *297* (5582), 787–792. <https://doi.org/10.1126/science.1060928>.
- (30) Lei, J.; Ju, H. Nanotubes in Biosensing. *WIREs Nanomedicine Nanobiotechnology* **2010**, *2* (5), 496–509. <https://doi.org/10.1002/wnan.94>.
- (31) Saito, N.; Usui, Y.; Aoki, K.; Narita, N.; Shimizu, M.; Hara, K.; Ogiwara, N.; Nakamura, K.; Ishigaki, N.; Kato, H.; Taruta, S.; Endo, M. Carbon Nanotubes: Biomaterial Applications. *Chem. Soc. Rev.* **2009**, *38* (7), 1897. <https://doi.org/10.1039/b804822n>.
- (32) Haniu, H.; Saito, N.; Matsuda, Y.; Tsukahara, T.; Usui, Y.; Narita, N.; Hara, K.; Aoki, K.; Shimizu, M.; Ogihara, N.; Takanashi, S.; Okamoto, M.; Kobayashi, S.; Ishigaki, N.; Nakamura, K.; Kato, H. Basic Potential of Carbon Nanotubes in Tissue Engineering Applications. *J. Nanomater.* **2012**, *2012*, 1–10. <https://doi.org/10.1155/2012/343747>.
- (33) Uzair, M.; Arshad, M.; Abbasi, S. S.; Arshad, A.; Khattak, J. Z.; Tabassum, S.; Zakaria, U. B. Review: Biomedical Applications of Carbon Nanotubes. *Nano Biomed. Eng.* **2021**, *13* (1), 82–93. <https://doi.org/10.5101/nbe.v13i1.p82-93>.
- (34) Kam, N. W. S.; Dai, H. Carbon Nanotubes as Intracellular Protein Transporters: Generality and Biological Functionality. *J. Am. Chem. Soc.* **2005**, *127* (16), 6021–6026. <https://doi.org/10.1021/ja050062v>.

- (35) Mählich, D.; Eberhardt, O.; Wallmersperger, T. Numerical Simulation of the Mechanical Behavior of a Carbon Nanotube Bundle. *Acta Mech.* **2021**, *232* (2), 483–494. <https://doi.org/10.1007/s00707-020-02874-6>.
- (36) Jones, W. E.; Chiguma, J.; Johnson, E.; Pachamuthu, A.; Santos, D. Electrically and Thermally Conducting Nanocomposites for Electronic Applications. *Materials* **2010**, *3* (2), 1478–1496. <https://doi.org/10.3390/ma3021478>.
- (37) Dayani, Y.; Malmstadt, N. Lipid Bilayers Covalently Anchored to Carbon Nanotubes. *Langmuir* **2012**, *28* (21), 8174–8182. <https://doi.org/10.1021/la301094h>.
- (38) Huang, S.; Dai, L.; Mau, A. W. H. Patterned Growth and Contact Transfer of Well-Aligned Carbon Nanotube Films. *J. Phys. Chem. B* **1999**, *103* (21), 4223–4227. <https://doi.org/10.1021/jp990342v>.
- (39) Kausar, A. Self-Healing Polymer/Carbon Nanotube Nanocomposite: A Review. *J. Plast. Film Sheeting* **2021**, *37* (2), 160–181. <https://doi.org/10.1177/8756087920960195>.
- (40) Tune, D. D.; Flavel, B. S. Advances in Carbon Nanotube–Silicon Heterojunction Solar Cells. *Adv. Energy Mater.* **2018**, *8* (15), 1703241. <https://doi.org/10.1002/aenm.201703241>.
- (41) Ibrahim, K. S. Carbon Nanotubes-Properties and Applications: A Review. *Carbon Lett.* **2013**, *14* (3), 131–144. <https://doi.org/10.5714/CL.2013.14.3.131>.
- (42) Rahman, G.; Najaf, Z.; Mehmood, A.; Bilal, S.; Shah, A.; Mian, S.; Ali, G. An Overview of the Recent Progress in the Synthesis and Applications of Carbon Nanotubes. *C* **2019**, *5* (1), 3. <https://doi.org/10.3390/c5010003>.
- (43) Huang, Z. P.; Xu, J. W.; Ren, Z. F.; Wang, J. H.; Siegal, M. P.; Provencio, P. N. Growth of Highly Oriented Carbon Nanotubes by Plasma-Enhanced Hot Filament Chemical Vapor Deposition. *Appl. Phys. Lett.* **1998**, *73* (26), 3845–3847. <https://doi.org/10.1063/1.122912>.
- (44) Van De Burgt, Y. Laser-Assisted Growth of Carbon Nanotubes—A Review. *J. Laser Appl.* **2014**, *26* (3), 032001. <https://doi.org/10.2351/1.4869257>.
- (45) Liu, Y.; Zhang, K.; Wang, F.; Han, Y.; Li, J.; Tian, B. Horizontal Growth and Electrical-Crosstalk Simulation of CNT Interconnection. *ECS Trans.* **2014**, *60* (1), 751–756. <https://doi.org/10.1149/06001.0751ecst>.
- (46) Asakura, K.; Chun, W.-J.; Tohji, K.; Sato, Y.; Watari, F. X-Ray Absorption Fine Structure Studies on the Local Structures of Ni Impurities in a Carbon Nanotube. *Chem. Lett.* **2005**, *34* (3), 382–383. <https://doi.org/10.1246/cl.2005.382>.



- (47) Homma, Y. Carbon Nanotube Synthesis and the Role of Catalyst. In *Frontiers of Graphene and Carbon Nanotubes*; Matsumoto, K., Ed.; Springer Japan: Tokyo, 2015; pp 125–129. [https://doi.org/10.1007/978-4-431-55372-4\\_9](https://doi.org/10.1007/978-4-431-55372-4_9).
- (48) Cheung, C. L.; Kurtz, A.; Park, H.; Lieber, C. M. Diameter-Controlled Synthesis of Carbon Nanotubes. *J. Phys. Chem. B* **2002**, *106* (10), 2429–2433. <https://doi.org/10.1021/jp0142278>.
- (49) Wu, Z.-S.; Ren, W.; Gao, L.; Zhao, J.; Chen, Z.; Liu, B.; Tang, D.; Yu, B.; Jiang, C.; Cheng, H.-M. Synthesis of Graphene Sheets with High Electrical Conductivity and Good Thermal Stability by Hydrogen Arc Discharge Exfoliation. *ACS Nano* **2009**, *3* (2), 411–417. <https://doi.org/10.1021/nn900020u>.
- (50) Sari, A. H.; Khazali, A.; Parhizgar, S. S. Synthesis and Characterization of Long-CNTs by Electrical Arc Discharge in Deionized Water and NaCl Solution. *Int. Nano Lett.* **2018**, *8* (1), 19–23. <https://doi.org/10.1007/s40089-018-0227-5>.
- (51) Paladugu, M. C.; Maneesh, K.; Nair, P. K.; Haridoss, P. Synthesis of Carbon Nanotubes by Arc Discharge in Open Air. *J. Nanosci. Nanotechnol.* **2005**, *5* (5), 747–752. <https://doi.org/10.1166/jnn.2005.108>.
- (52) Bera, D.; Brinley, E.; Kuiry, S. C.; McCutchen, M.; Seal, S.; Heinrich, H.; Kabes, B. Optoelectronically Automated System for Carbon Nanotubes Synthesis via Arc-Discharge in Solution. *Rev. Sci. Instrum.* **2005**, *76* (3), 033903. <https://doi.org/10.1063/1.1857465>.
- (53) Fonseca, A.; Hernadi, K.; Piedigrosso, P.; Colomer, J.-F.; Mukhopadhyay, K.; Doome, R.; Lazarescu, S.; Biro, L. P.; Lambin, P.; Thiry, P. A.; Bernaerts, D.; Nagy, J. B. Synthesis of Single- and Multi-Wall Carbon Nanotubes over Supported Catalysts. *Appl. Phys. Mater. Sci. Process.* **1998**, *67* (1), 11–22. <https://doi.org/10.1007/s003390050732>.
- (54) Takekoshi, K.; Kizu, T.; Aikawa, S.; Kanda, M.; Nishikawa, E. Influence of Pulse Condition in the Synthesis of Carbon Nanotubes Containing Tungsten by Arc Discharge in Water. *Jpn. J. Appl. Phys.* **2012**, *51* (12R), 125102. <https://doi.org/10.1143/JJAP.51.125102>.
- (55) Cheng, Y.; Liu, C.; Cheng, H.-M.; Jiang, S. P. One-Pot Synthesis of Metal–Carbon Nanotubes Network Hybrids as Highly Efficient Catalysts for Oxygen Evolution Reaction of Water Splitting. *ACS Appl. Mater. Interfaces* **2014**, *6* (13), 10089–10098. <https://doi.org/10.1021/am500988p>.
- (56) Smagulova, G. T.; Vassilyeva, N.; Kaidar, B. B.; Yesbolov, N.; Prikhodko, N. G.; Nemkayeva, R. Synthesis of Carbon Nanotubes from High-Density Polyethylene Waste. *Eurasian Chem.-Technol. J.* **2019**, *21* (3), 241. <https://doi.org/10.18321/ectj865>.

- (57) Smagulova, G.; Yesbolov, N.; Kaidar, B.; Vassilyeva, N.; Prikhodko, N.; Mansurov, Z. Synthesis of Carbon Nanotubes from Polymer Waste; 2019. <https://doi.org/10.11159/icnfa19.154>.
- (58) Kundrapu, M.; Li, J.; Shashurin, A.; Keidar, M. A Model of Carbon Nanotube Synthesis in Arc Discharge Plasmas. *J. Phys. Appl. Phys.* **2012**, *45* (31), 315305. <https://doi.org/10.1088/0022-3727/45/31/315305>.
- (59) Karimi, M.; Solati, N.; Amiri, M.; Mirshekari, H.; Mohamed, E.; Taheri, M.; Hashemkhani, M.; Saeidi, A.; Estiar, M. A.; Kiani, P.; Ghasemi, A.; Basri, S. M. M.; Aref, A. R.; Hamblin, M. R. Carbon Nanotubes Part I: Preparation of a Novel and Versatile Drug-Delivery Vehicle. *Expert Opin. Drug Deliv.* **2015**, *12* (7), 1071–1087. <https://doi.org/10.1517/17425247.2015.1003806>.
- (60) Rosenfeld Hacoen, Y.; Popovitz-Biro, R.; Prior, Y.; Gemming, S.; Seifert, G.; Tenne, R. Synthesis of NiCl<sub>2</sub> Nanotubes and Fullerene-like Structures by Laser Ablation: Theoretical Considerations and Comparison with MoS<sub>2</sub> Nanotubes. *Phys. Chem. Chem. Phys.* **2003**, *5* (8), 1644–1651. <https://doi.org/10.1039/b211737a>.
- (61) Awais Rouf, S.; Usman, Z.; Tariq Masood, H.; Mannan Majeed, A.; Sarwar, M.; Abbas, W. Synthesis and Purification of Carbon Nanotubes. In *Carbon Nanotubes - Redefining the World of Electronics*; Kumar Ghosh, P., Datta, K., Dinkarrao Rushi, A., Eds.; IntechOpen, 2021. <https://doi.org/10.5772/intechopen.98221>.
- (62) Wu, X.; Yin, H.; Li, Q. Ablation and Patterning of Carbon Nanotube Film by Femtosecond Laser Irradiation. *Appl. Sci.* **2019**, *9* (15), 3045. <https://doi.org/10.3390/app9153045>.
- (63) Jiang, H.; Brown, D. P.; Nikolaev, P.; Nasibulin, A. G.; Kauppinen, E. I. Determination of Helicities in Unidirectional Assemblies of Graphitic or Graphiticlike Tubular Structures. *Appl. Phys. Lett.* **2008**, *93* (14), 141903. <https://doi.org/10.1063/1.2993217>.
- (64) Junghun Chae; Jain, K. Patterning of Carbon Nanotubes by Material Assisted Laser Ablation Process. *IEEE Trans. Nanotechnol.* **2010**, *9* (3), 381–385. <https://doi.org/10.1109/TNANO.2009.2029696>.
- (65) Henley, S. J.; Anguita, J. V.; Silva, S. R. P. Synthesis of Carbon Nanotubes. In *Encyclopedia of Nanotechnology*; Bhushan, B., Ed.; Springer Netherlands: Dordrecht, 2015; pp 1–9. [https://doi.org/10.1007/978-94-007-6178-0\\_54-2](https://doi.org/10.1007/978-94-007-6178-0_54-2).
- (66) Brhane, Y.; Gabriel, T. PRODUCTION, PURIFICATION AND FUNCTIONALIZATION OF CARBON NANOTUBES FOR MEDICAL APPLICATIONS. *Int. Res. J. Pharm.* **2016**, *7* (7), 19–27. <https://doi.org/10.7897/2230-8407.07780>.
- (67) Lim, S. H.; Luo, Z.; Shen, Z.; Lin, J. Plasma-Assisted Synthesis of Carbon Nanotubes. *Nanoscale Res. Lett.* **2010**, *5* (9), 1377–1386. <https://doi.org/10.1007/s11671-010-9710-2>.

- (68) Yuan, W.; Xiao, K.; Wu, X.; Wang, J.; Ma, T.; Song, H.; Huang, C. Carbon Nanotube Sponges Filled Sandwich Panels with Superior High-Power Continuous Wave Laser Resistance. *Sci. Rep.* **2022**, *12* (1), 21435. <https://doi.org/10.1038/s41598-022-25829-4>.
- (69) Boroznin, S. V. Carbon Nanostructures Containing Boron Impurity Atoms: Synthesis, Physicochemical Properties and Potential Applications. *Mod. Electron. Mater.* **2022**, *8* (1), 23–42. <https://doi.org/10.3897/j.moem.8.1.84317>.
- (70) Bardecker, J. A.; Afzali, A.; Tulevski, G. S.; Graham, T.; Hannon, J. B.; Jen, A. K.-Y. Directed Assembly of Single-Walled Carbon Nanotubes via Drop-Casting onto a UV-Patterned Photosensitive Monolayer. *J. Am. Chem. Soc.* **2008**, *130* (23), 7226–7227. <https://doi.org/10.1021/ja802407f>.
- (71) Peng, H.; Yang, Z.; Huang, S.; Liu, T. Green and Highly Efficient Functionalization of Carbon Nanotubes by Combination of 1,3-Dipolar Cycloaddition and Curtius Rearrangement Reactions. *Chin. J. Chem.* **2010**, *28* (7), 1223–1228. <https://doi.org/10.1002/cjoc.201090212>.
- (72) Chen, W.; Duan, L.; Zhu, D. Adsorption of Polar and Nonpolar Organic Chemicals to Carbon Nanotubes. *Environ. Sci. Technol.* **2007**, *41* (24), 8295–8300. <https://doi.org/10.1021/es071230h>.
- (73) Schroeder, V.; Savagatrup, S.; He, M.; Lin, S.; Swager, T. M. Carbon Nanotube Chemical Sensors. *Chem. Rev.* **2019**, *119* (1), 599–663. <https://doi.org/10.1021/acs.chemrev.8b00340>.
- (74) Yao, X.; Zhang, Y.; Jin, W.; Hu, Y.; Cui, Y. Carbon Nanotube Field-Effect Transistor-Based Chemical and Biological Sensors. *Sensors* **2021**, *21* (3), 995. <https://doi.org/10.3390/s21030995>.
- (75) Rakow, N. A.; Suslick, K. S. A Colorimetric Sensor Array for Odour Visualization. *Nature* **2000**, *406* (6797), 710–713. <https://doi.org/10.1038/35021028>.
- (76) Ovsienko, I.; Len, T.; Matzui, L.; Tkachuk, V.; Berkutov, I.; Mirzoiev, I.; Prylutsky, Y.; Tsierkezos, N.; Ritter, U. Magnetoresistance of Functionalized Carbon Nanotubes: Der Magnetoresistive Effekt von Funktionalisierten Kohlenstoffnanoröhren. *Mater. Werkst.* **2016**, *47* (2–3), 254–262. <https://doi.org/10.1002/mawe.201600482>.
- (77) Campidelli, S.; Klumpp, C.; Bianco, A.; Guldi, D. M.; Prato, M. Functionalization of CNT: Synthesis and Applications in Photovoltaics and Biology. *J. Phys. Org. Chem.* **2006**, *19* (8–9), 531–539. <https://doi.org/10.1002/poc.1052>.
- (78) Veca, L. M.; Meziani, M. J.; Wang, W.; Wang, X.; Lu, F.; Zhang, P.; Lin, Y.; Fee, R.; Connell, J. W.; Sun, Y. Carbon Nanosheets for Polymeric Nanocomposites with High Thermal Conductivity. *Adv. Mater.* **2009**, *21* (20), 2088–2092. <https://doi.org/10.1002/adma.200802317>.

- (79) Pelech, I.; Kaczmarek, A.; Pelech, R. Current-Voltage Characteristics of the Composites Based on Epoxy Resin and Carbon Nanotubes. *J. Nanomater.* **2015**, *2015*, 1–7. <https://doi.org/10.1155/2015/405345>.
- (80) Lin, Y.; Zhou, B.; Shiral Fernando, K. A.; Liu, P.; Allard, L. F.; Sun, Y.-P. Polymeric Carbon Nanocomposites from Carbon Nanotubes Functionalized with Matrix Polymer. *Macromolecules* **2003**, *36* (19), 7199–7204. <https://doi.org/10.1021/ma0348876>.
- (81) Liu, X.; Qin, Y.; Zhao, S.; Dong, J.-Y. Nanocomposites-Turned-Nanoalloys Polypropylene/Multiwalled Carbon Nanotubes- Graft -Polystyrene: Synthesis and Polymer Nanoreinforcement. *Ind. Eng. Chem. Res.* **2021**, *60* (28), 10167–10179. <https://doi.org/10.1021/acs.iecr.1c01362>.
- (82) Volponi, R.; De Nicola, F.; Spena, P. Nanocomposites for New Functionalities in Multiscale Composites. *MATEC Web Conf.* **2018**, *188*, 01027. <https://doi.org/10.1051/mateconf/201818801027>.
- (83) Chen, J.; Liu, H.; Weimer, W. A.; Halls, M. D.; Waldeck, D. H.; Walker, G. C. Noncovalent Engineering of Carbon Nanotube Surfaces by Rigid, Functional Conjugated Polymers. *J. Am. Chem. Soc.* **2002**, *124* (31), 9034–9035. <https://doi.org/10.1021/ja026104m>.
- (84) Backes, C.; Mundloch, U.; Schmidt, C. D.; Coleman, J. N.; Wohlleben, W.; Hauke, F.; Hirsch, A. Enhanced Adsorption Affinity of Anionic Perylene-Based Surfactants towards Smaller-Diameter SWCNTs. *Chem. – Eur. J.* **2010**, *16* (44), 13185–13192. <https://doi.org/10.1002/chem.201000232>.
- (85) Chen, R. J.; Bangsaruntip, S.; Drouvalakis, K. A.; Wong Shi Kam, N.; Shim, M.; Li, Y.; Kim, W.; Utz, P. J.; Dai, H. Noncovalent Functionalization of Carbon Nanotubes for Highly Specific Electronic Biosensors. *Proc. Natl. Acad. Sci.* **2003**, *100* (9), 4984–4989. <https://doi.org/10.1073/pnas.0837064100>.
- (86) Pumera, M.; Šmíd, B. Redox Protein Noncovalent Functionalization of Double-Wall Carbon Nanotubes: Electrochemical Binder-Less Glucose Biosensor. *J. Nanosci. Nanotechnol.* **2007**, *7* (10), 3590–3595. <https://doi.org/10.1166/jnn.2007.846>.
- (87) In Het Panhuis, M.; Maiti, A.; Dalton, A. B.; Van Den Noort, A.; Coleman, J. N.; McCarthy, B.; Blau, W. J. Selective Interaction in a Polymer–Single-Wall Carbon Nanotube Composite. *J. Phys. Chem. B* **2003**, *107* (2), 478–482. <https://doi.org/10.1021/jp026470s>.
- (88) Clavé, G.; Delport, G.; Roquelet, C.; Lauret, J.-S.; Deleporte, E.; Violla, F.; Langlois, B.; Parret, R.; Voisin, C.; Roussignol, P.; Jousset, B.; Gloter, A.; Stephan, O.; Filoramo, A.; Derycke, V.; Campidelli, S. Functionalization of Carbon Nanotubes through Polymerization in Micelles: A Bridge between the Covalent and Noncovalent Methods. *Chem. Mater.* **2013**, *25* (13), 2700–2707. <https://doi.org/10.1021/cm401312v>.

- (89) Das, A. K.; Mukherjee, A.; Baba, K.; Hatada, R.; Bhowmik, R.; Meikap, A. K. Current–Voltage Hysteresis Behavior of PVA-Assisted Functionalized Single-Walled Carbon Nanotube Free-Standing Film. *J. Phys. Chem. C* **2018**, *122* (51), 29094–29105. <https://doi.org/10.1021/acs.jpcc.8b08875>.
- (90) Mansukhani, N. D.; Guiney, L. M.; Wei, Z.; Roth, E. W.; Putz, K. W.; Luijten, E.; Hersam, M. C. Optothermally Reversible Carbon Nanotube–DNA Supramolecular Hybrid Hydrogels. *Macromol. Rapid Commun.* **2018**, *39* (2), 1700587. <https://doi.org/10.1002/marc.201700587>.
- (91) Thongam, D. D.; Chaturvedi, H. Functionalization of Pristine, Metallic, and Semiconducting-SWCNTs by ZnO for Efficient Charge Carrier Transfer: Analysis through Critical Coagulation Concentration. *ACS Omega* **2022**, *7* (17), 14784–14796. <https://doi.org/10.1021/acsomega.2c00193>.
- (92) Nonoguchi, Y.; Ohashi, K.; Kanazawa, R.; Ashiba, K.; Hata, K.; Nakagawa, T.; Adachi, C.; Tanase, T.; Kawai, T. Systematic Conversion of Single Walled Carbon Nanotubes into N-Type Thermoelectric Materials by Molecular Dopants. *Sci. Rep.* **2013**, *3* (1), 3344. <https://doi.org/10.1038/srep03344>.
- (93) Liu, Y.; Nitschke, M.; Stepien, L.; Khavrus, V.; Bezugly, V.; Cuniberti, G. Ammonia Plasma-Induced n-Type Doping of Semiconducting Carbon Nanotube Films: Thermoelectric Properties and Ambient Effects. *ACS Appl. Mater. Interfaces* **2019**, *11* (24), 21807–21814. <https://doi.org/10.1021/acsami.9b02918>.
- (94) Nonoguchi, Y.; Nakano, M.; Murayama, T.; Hagino, H.; Hama, S.; Miyazaki, K.; Matsubara, R.; Nakamura, M.; Kawai, T. Simple Salt-Coordinated n-Type Nanocarbon Materials Stable in Air. *Adv. Funct. Mater.* **2016**, *26* (18), 3021–3028. <https://doi.org/10.1002/adfm.201600179>.
- (95) Dwivedi, N.; Shukla, R. K. Theoretical Study of Pure/Doped (Nitrogen and Boron) Carbon Nanotubes for Chemical Sensing of Formaldehyde. *SN Appl. Sci.* **2020**, *2* (2), 262. <https://doi.org/10.1007/s42452-020-2055-2>.
- (96) Palma, M.; Wang, W.; Penzo, E.; Brathwaite, J.; Zheng, M.; Hone, J.; Nuckolls, C.; Wind, S. J. Controlled Formation of Carbon Nanotube Junctions via Linker-Induced Assembly in Aqueous Solution. *J. Am. Chem. Soc.* **2013**, *135* (23), 8440–8443. <https://doi.org/10.1021/ja4018072>.
- (97) Chen, J.; Gao, X.; Xu, D. Recent Advances in Characterization Techniques for the Interface in Carbon Nanotube-Reinforced Polymer Nanocomposites. *Adv. Mater. Sci. Eng.* **2019**, *2019*, 1–24. <https://doi.org/10.1155/2019/5268267>.
- (98) Hill, D. E.; Lin, Y.; Rao, A. M.; Allard, L. F.; Sun, Y.-P. Functionalization of Carbon Nanotubes with Polystyrene. *Macromolecules* **2002**, *35* (25), 9466–9471. <https://doi.org/10.1021/ma020855r>.

- (99) Eitan, A.; Jiang, K.; Dukes, D.; Andrews, R.; Schadler, L. S. Surface Modification of Multiwalled Carbon Nanotubes: Toward the Tailoring of the Interface in Polymer Composites. *Chem. Mater.* **2003**, *15* (16), 3198–3201. <https://doi.org/10.1021/cm020975d>.
- (100) Barrau, S.; Vanmansart, C.; Moreau, M.; Addad, A.; Stoclet, G.; Lefebvre, J.-M.; Seguela, R. Crystallization Behavior of Carbon Nanotube–Polylactide Nanocomposites. *Macromolecules* **2011**, *44* (16), 6496–6502. <https://doi.org/10.1021/ma200842n>.
- (101) Hussain, S.; Jha, P.; Chouksey, A.; Raman, R.; Islam, S. S.; Islam, T.; Choudhary, P. K. Spectroscopic Investigation of Modified Single Wall Carbon Nanotube (SWCNT). *J. Mod. Phys.* **2011**, *02* (06), 538–543. <https://doi.org/10.4236/jmp.2011.26063>.
- (102) Silva-Jara, J. M.; Manríquez-González, R.; López-Dellamary, F. A.; Puig, J. E.; Nuño-Donlucas, S. M. Semi-Continuous Heterophase Polymerization to Synthesize Nanocomposites of Poly(Acrylic Acid)-Functionalized Carbon Nanotubes. *J. Macromol. Sci. Part A* **2015**, *52* (9), 732–744. <https://doi.org/10.1080/10601325.2015.1063873>.
- (103) Weese, M. E.; Krevh, R. A.; Li, Y.; Alvarez, N. T.; Ross, A. E. Defect Sites Modulate Fouling Resistance on Carbon-Nanotube Fiber Electrodes. *ACS Sens.* **2019**, *4* (4), 1001–1007. <https://doi.org/10.1021/acssensors.9b00161>.
- (104) Montanheiro, T. L. D. A.; De Menezes, B. R. C.; Ribas, R. G.; Montagna, L. S.; Campos, T. M. B.; Schatkoski, V. M.; Righetti, V. A. N.; Passador, F. R.; Thim, G. P. Covalently  $\gamma$ -Aminobutyric Acid-Functionalized Carbon Nanotubes: Improved Compatibility with PHBV Matrix. *SN Appl. Sci.* **2019**, *1* (10), 1177. <https://doi.org/10.1007/s42452-019-1224-7>.
- (105) Zhao, F.; Qian, W.; Li, M.; Li, W.; Chen, L.; Zhong, F.; Huang, W.; Dong, C. Directly Grown Carbon Nanotube Based Hybrid Electrodes with Enhanced Thermo-Cell Performances. *RSC Adv.* **2017**, *7* (38), 23890–23895. <https://doi.org/10.1039/C7RA02264F>.
- (106) Gao, Y.; Li, L.; Tan, P.; Liu, L.; Zhang, Z. Application of Raman Spectroscopy in Carbon Nanotube-Based Polymer Composites. *Chin. Sci. Bull.* **2010**, *55* (35), 3978–3988. <https://doi.org/10.1007/s11434-010-4100-9>.
- (107) Gao, Y.; Li, J.; Liu, L.; Ma, W.; Zhou, W.; Xie, S.; Zhang, Z. Axial Compression of Hierarchically Structured Carbon Nanotube Fiber Embedded in Epoxy. *Adv. Funct. Mater.* **2010**, *20* (21), 3797–3803. <https://doi.org/10.1002/adfm.201001227>.
- (108) Mueller, A.; Vigolo, B.; McRae, E.; Soldatov, A. V. Raman Study of Inhomogeneities in Carbon Nanotube Distribution in CNT–PMMA Composites. *Phys. Status Solidi B* **2010**, *247* (11–12), 2810–2813. <https://doi.org/10.1002/pssb.201000198>.
- (109) Parra-Vasquez, A. N. G.; Behabtu, N.; Green, M. J.; Pint, C. L.; Young, C. C.; Schmidt, J.; Kesselman, E.; Goyal, A.; Ajayan, P. M.; Cohen, Y.; Talmon, Y.; Hauge, R.

H.; Pasquali, M. Spontaneous Dissolution of Ultralong Single- and Multiwalled Carbon Nanotubes. *ACS Nano* **2010**, *4* (7), 3969–3978. <https://doi.org/10.1021/nn100864v>.

- (110) Soares, B. G.; Calheiros, L. F.; Silva, A. A.; Indrusiak, T.; Barra, G. M. O.; Livi, S. Conducting Melt Blending of Polystyrene and EVA Copolymer with Carbon Nanotube Assisted by Phosphonium-based Ionic Liquid. *J. Appl. Polym. Sci.* **2018**, *135* (24), 45564. <https://doi.org/10.1002/app.45564>.
- (111) Yu, W.-J.; Liu, C.; Hou, P.-X.; Zhang, L.; Shan, X.-Y.; Li, F.; Cheng, H.-M. Lithiation of Silicon Nanoparticles Confined in Carbon Nanotubes. *ACS Nano* **2015**, *9* (5), 5063–5071. <https://doi.org/10.1021/acsnano.5b00157>.
- (112) Købler, C.; Poulsen, S. S.; Saber, A. T.; Jacobsen, N. R.; Wallin, H.; Yauk, C. L.; Halappanavar, S.; Vogel, U.; Qvortrup, K.; Møllhave, K. Time-Dependent Subcellular Distribution and Effects of Carbon Nanotubes in Lungs of Mice. *PLOS ONE* **2015**, *10* (1), e0116481. <https://doi.org/10.1371/journal.pone.0116481>.
- (113) Tsentelovich, D. E.; Ma, A. W. K.; Lee, J. A.; Behabtu, N.; Bengio, E. A.; Choi, A.; Hao, J.; Luo, Y.; Headrick, R. J.; Green, M. J.; Talmon, Y.; Pasquali, M. Relationship of Extensional Viscosity and Liquid Crystalline Transition to Length Distribution in Carbon Nanotube Solutions. *Macromolecules* **2016**, *49* (2), 681–689. <https://doi.org/10.1021/acs.macromol.5b02054>.
- (114) Siu, K. S.; Zheng, X.; Liu, Y.; Zhang, Y.; Zhang, X.; Chen, D.; Yuan, K.; Gillies, E. R.; Koropatnick, J.; Min, W.-P. Single-Walled Carbon Nanotubes Noncovalently Functionalized with Lipid Modified Polyethylenimine for siRNA Delivery *in Vitro* and *in Vivo*. *Bioconjug. Chem.* **2014**, *25* (10), 1744–1751. <https://doi.org/10.1021/bc500280q>.
- (115) Jeong, S.; Lee, J.; Kim, H.-C.; Hwang, J. Y.; Ku, B.-C.; Zakharov, D. N.; Maruyama, B.; Stach, E. A.; Kim, S. M. Direct Observation of Morphological Evolution of a Catalyst during Carbon Nanotube Forest Growth: New Insights into Growth and Growth Termination. *Nanoscale* **2016**, *8* (4), 2055–2062. <https://doi.org/10.1039/C5NR05547D>.
- (116) De Araujo, W. R.; Reddy, S. M.; Paixão, T. R. L. C. Introduction of Materials Used in Chemical Sensors. In *Materials for Chemical Sensing*; Cesar Paixão, T. R. L., Reddy, S. M., Eds.; Springer International Publishing: Cham, 2017; pp 1–5. [https://doi.org/10.1007/978-3-319-47835-7\\_1](https://doi.org/10.1007/978-3-319-47835-7_1).
- (117) Xiao, M.; Liang, S.; Han, J.; Zhong, D.; Liu, J.; Zhang, Z.; Peng, L. Batch Fabrication of Ultrasensitive Carbon Nanotube Hydrogen Sensors with Sub-Ppm Detection Limit. *ACS Sens.* **2018**, *3* (4), 749–756. <https://doi.org/10.1021/acssensors.8b00006>.
- (118) Truong, D. V.; Linh, B. T.; Kien, N. M.; Anh, L. T. L.; Tu, N. C.; Chien, N. D.; Lam, N. H. Development of NH<sub>3</sub> Gas Sensors at Room Temperature Based on Modified Carbon Nanotubes. *Mater. Trans.* **2020**, *61* (8), 1540–1543. <https://doi.org/10.2320/matertrans.MT-MN2019005>.

- (119) Arunachalam, S.; Izquierdo, R.; Nabki, F. Ionization Gas Sensor Using Suspended Carbon Nanotube Beams. *Sensors* **2020**, *20* (6), 1660. <https://doi.org/10.3390/s20061660>.
- (120) Hsu, M.; Lee, G. Carbon Nanotube-based Hot-film and Temperature Sensor Assembled by Optically-induced Dielectrophoresis. *IET Nanobiotechnol.* **2014**, *8* (1), 44–50. <https://doi.org/10.1049/iet-nbt.2013.0040>.
- (121) Zhang, X.; Xiang, D.; Zhu, W.; Zheng, Y.; Harkin-Jones, E.; Wang, P.; Zhao, C.; Li, H.; Wang, B.; Li, Y. Flexible and High-Performance Piezoresistive Strain Sensors Based on Carbon Nanoparticles@polyurethane Sponges. *Compos. Sci. Technol.* **2020**, *200*, 108437. <https://doi.org/10.1016/j.compscitech.2020.108437>.
- (122) Lee, B. Y.; Seo, S. M.; Lee, D. J.; Lee, M.; Lee, J.; Cheon, J.-H.; Cho, E.; Lee, H.; Chung, I.-Y.; Park, Y. J.; Kim, S.; Hong, S. Biosensor System-on-a-Chip Including CMOS-Based Signal Processing Circuits and 64 Carbon Nanotube-Based Sensors for the Detection of a Neurotransmitter. *Lab. Chip* **2010**, *10* (7), 894. <https://doi.org/10.1039/b916975j>.
- (123) Lee, Y.; Yoon, J.; Kim, Y.; Kim, D. M.; Kim, D. H.; Choi, S.-J. Humidity Effects According to the Type of Carbon Nanotubes. *IEEE Access* **2021**, *9*, 6810–6816. <https://doi.org/10.1109/ACCESS.2020.3048173>.
- (124) Skutin, E. D.; Podgorniy, S. O.; Podgornaya, O. T.; Kolyanichev, N. S.; Katkov, A. A. Gas Sensitivity of Polymeric Composites with Carbon Nanotubes. *J. Phys. Conf. Ser.* **2018**, *944*, 012110. <https://doi.org/10.1088/1742-6596/944/1/012110>.
- (125) Jerome, A.; Thostenson, E.; Keefe, M.; Doshi, S.; Chaudhari, A. Carbon Nanomaterial Based Multifunctional Fabrics for Characterizing Human Joint Motion. In *SAMPE 2020 / Virtual Series*; NA SAMPE, 2020. <https://doi.org/10.33599/nasampe/s.20.0159>.
- (126) Tadakaluru, S.; Thongsuwan, W.; Singjai, P. Stretchable and Flexible High-Strain Sensors Made Using Carbon Nanotubes and Graphite Films on Natural Rubber. *Sensors* **2014**, *14* (1), 868–876. <https://doi.org/10.3390/s140100868>.
- (127) Obitayo, W.; Liu, T. A Review: Carbon Nanotube-Based Piezoresistive Strain Sensors. *J. Sens.* **2012**, *2012*, 1–15. <https://doi.org/10.1155/2012/652438>.
- (128) Cullinan, M. A.; Culpepper, M. L. Noise Mitigation Techniques for Carbon Nanotube-Based Piezoresistive Sensor Systems. *MRS Proc.* **2011**, *1303*, mrsf10-1303-y10-34. <https://doi.org/10.1557/opl.2011.409>.
- (129) Cullinan, M. A.; Culpepper, M. L. Nanomanufacturing Methods for the Reduction of Noise in Carbon Nanotube-Based Piezoresistive Sensor Systems. *J. Micro Nano-Manuf.* **2013**, *1* (1), 011011. <https://doi.org/10.1115/1.4023159>.



- (130) Wu, Z.; Wei, L.; Tang, S.; Xiong, Y.; Qin, X.; Luo, J.; Fang, J.; Wang, X. Recent Progress in  $Ti_3C_2T_x$  MXene-Based Flexible Pressure Sensors. *ACS Nano* **2021**, *15* (12), 18880–18894. <https://doi.org/10.1021/acsnano.1c08239>.
- (131) Santos, A.; Amorim, L.; Nunes, J. P.; Rocha, L. A.; Silva, A. F.; Viana, J. C. A Comparative Study between Knocked-Down Aligned Carbon Nanotubes and Buckypaper-Based Strain Sensors. *Materials* **2019**, *12* (12), 2013. <https://doi.org/10.3390/ma12122013>.
- (132) Gao, C.; Guo, Z.; Liu, J.-H.; Huang, X.-J. The New Age of Carbon Nanotubes: An Updated Review of Functionalized Carbon Nanotubes in Electrochemical Sensors. *Nanoscale* **2012**, *4* (6), 1948. <https://doi.org/10.1039/c2nr11757f>.
- (133) Qu, L.; Peng, Q.; Dai, L.; Spinks, G. M.; Wallace, G. G.; Baughman, R. H. Carbon Nanotube Electroactive Polymer Materials: Opportunities and Challenges. *MRS Bull.* **2008**, *33* (3), 215–224. <https://doi.org/10.1557/mrs2008.47>.
- (134) Hu, C.; Hu, S. Carbon Nanotube-Based Electrochemical Sensors: Principles and Applications in Biomedical Systems. *J. Sens.* **2009**, *2009*, 1–40. <https://doi.org/10.1155/2009/187615>.
- (135) Viet, N. X.; Kishimoto, S.; Ohno, Y. Highly Uniform, Flexible Microelectrodes Based on the Clean Single-Walled Carbon Nanotube Thin Film with High Electrochemical Activity. *ACS Appl. Mater. Interfaces* **2019**, *11* (6), 6389–6395. <https://doi.org/10.1021/acсами.8b19252>.
- (136) Kokab, T.; Shah, A.; Khan, M. A.; Arshad, M.; Nisar, J.; Ashiq, M. N.; Zia, M. A. Simultaneous Femtomolar Detection of Paracetamol, Diclofenac, and Orphenadrine Using a Carbon Nanotube/Zinc Oxide Nanoparticle-Based Electrochemical Sensor. *ACS Appl. Nano Mater.* **2021**, *4* (5), 4699–4712. <https://doi.org/10.1021/acsanm.1c00310>.
- (137) Jin, Z.-H.; Liu, Y.-L.; Chen, J.-J.; Cai, S.-L.; Xu, J.-Q.; Huang, W.-H. Conductive Polymer-Coated Carbon Nanotubes To Construct Stretchable and Transparent Electrochemical Sensors. *Anal. Chem.* **2017**, *89* (3), 2032–2038. <https://doi.org/10.1021/acs.analchem.6b04616>.
- (138) Zhao, Q.; Guan, L.; Gu, Z.; Zhuang, Q. Determination of Phenolic Compounds Based on the Tyrosinase- Single Walled Carbon Nanotubes Sensor. *Electroanalysis* **2005**, *17* (1), 85–88. <https://doi.org/10.1002/elan.200403123>.
- (139) . B.; . S. AN AMPEROMETRIC GLUCOSE BIOSENSOR BASED ON THE IMMOBILIZATION OF GLUCOSE OXIDASE ON THE CARBON NANOTUBES MODIFIED GLASSY CARBON ELECTRODE. *Int. J. Eng. Appl. Sci. Technol.* **2019**, *4* (2), 190–196. <https://doi.org/10.33564/IJEAST.2019.v04i02.035>.
- (140) Manivel, P.; Thamilselvan, A.; Rajagopal, V.; Nesakumar, N.; Suryanarayanan, V. Enhanced Electrocatalytic Activity of Ni-CNT Nanocomposites for Simultaneous

Determination of Epinephrine and Dopamine. *Electroanalysis* **2019**, *31* (12), 2387–2396. <https://doi.org/10.1002/elan.201900201>.

- (141) Chen, S.; Qamar, A. Z.; Asefifeyzabadi, N.; Funneman, M.; Taki, M.; Elliot, L.; Kinsel, M. E.; Kinsel, G. R.; Shamsi, M. H. Hand-Fabricated CNT/AgNPs Electrodes Using Wax-on-Plastic Platforms for Electro-Immunosensing Application. *Sci. Rep.* **2019**, *9* (1), 6131. <https://doi.org/10.1038/s41598-019-42644-6>.
- (142) Wang, F.; Hu, S.; Shi, F.; Huang, K.; Li, J. A Non-Enzymatic Sensor Based on Fc-CHIT/CNT@Cu Nanohybrids for Electrochemical Detection of Glucose. *Polymers* **2020**, *12* (10), 2419. <https://doi.org/10.3390/polym12102419>.
- (143) Ding, S.; Cargill, A.; Das, S.; Medintz, I.; Claussen, J. Biosensing with Förster Resonance Energy Transfer Coupling between Fluorophores and Nanocarbon Allotropes. *Sensors* **2015**, *15* (6), 14766–14787. <https://doi.org/10.3390/s150614766>.
- (144) Lin, R. Design and Implementation of Multi-Walled Carbon Nanotube Electrodes for Electrochemical Sensors and Thermocells, Nanyang Technological University, 2018. <https://doi.org/10.32657/10356/73367>.
- (145) Pyo, J.-Y.; Cho, W.-J. High-Sensitivity pH Sensor Using Separative Extended-Gate Field-Effect Transistors with Single-Walled Carbon-Nanotube Networks. *Jpn. J. Appl. Phys.* **2018**, *57* (4S), 04FP02. <https://doi.org/10.7567/JJAP.57.04FP02>.
- (146) Naderi, A.; Tahne, B. A. Review—Methods in Improving the Performance of Carbon Nanotube Field Effect Transistors. *ECS J. Solid State Sci. Technol.* **2016**, *5* (12), M131–M140. <https://doi.org/10.1149/2.0021612jss>.
- (147) Valed Karimi, N.; Poursad, Y. Investigating the Effect of Some Parameters of the Channel on the Characteristics of Tunneling Carbon Nanotube Field-Effect Transistor. *Int. Nano Lett.* **2016**, *6* (4), 215–221. <https://doi.org/10.1007/s40089-016-0182-y>.
- (148) Imam, S.-A.; Kalam, N.; Abdullah, S. Comparative Analysis of Control Coefficients on the Performance of CNTFET Under Different Parameters. *Int. J. Nanosci.* **2016**, *15* (03), 1640005. <https://doi.org/10.1142/S0219581X16400056>.
- (149) Anantram, M. P.; Léonard, F. Physics of Carbon Nanotube Electronic Devices. *Rep. Prog. Phys.* **2006**, *69* (3), 507–561. <https://doi.org/10.1088/0034-4885/69/3/R01>.
- (150) Liu, W.; Chikkadi, K.; Lee, S.-W.; Hierold, C.; Haluska, M. Improving Non-Suspended Carbon Nanotube FET Performance by Using an Alumina Protective Layer. *Sens. Actuators B Chem.* **2014**, *198*, 479–486. <https://doi.org/10.1016/j.snb.2014.03.039>.
- (151) Park, S.; Zhang, Z.; Qi, H.; Liang, B.; Mahmood, J.; Noh, H.-J.; Hamsch, M.; Wang, M.; Wang, M.; Ly, K. H.; Wang, Z.; Weidinger, I. M.; Zhou, S.; Baek, J.-B.; Kaiser, U.; Mannsfeld, S. C. B.; Feng, X.; Dong, R. In-Plane Oriented Two-Dimensional Conjugated

Metal–Organic Framework Films for High-Performance Humidity Sensing. *ACS Mater. Lett.* **2022**, *4* (6), 1146–1153. <https://doi.org/10.1021/acsmaterialslett.2c00160>.

- (152) Zhang, Y.; Xu, M.; Bunes, B. R.; Wu, N.; Gross, D. E.; Moore, J. S.; Zang, L. Oligomer-Coated Carbon Nanotube Chemiresistive Sensors for Selective Detection of Nitroaromatic Explosives. *ACS Appl. Mater. Interfaces* **2015**, *7* (14), 7471–7475. <https://doi.org/10.1021/acsmi.5b01532>.
- (153) Liu, S. F.; Moh, L. C. H.; Swager, T. M. Single-Walled Carbon Nanotube–Metalloporphyrin Chemiresistive Gas Sensor Arrays for Volatile Organic Compounds. *Chem. Mater.* **2015**, *27* (10), 3560–3563. <https://doi.org/10.1021/acs.chemmater.5b00153>.
- (154) Liu, S. F.; Petty, A. R.; Sazama, G. T.; Swager, T. M. Single-Walled Carbon Nanotube/Metalloporphyrin Composites for the Chemiresistive Detection of Amines and Meat Spoilage. *Angew. Chem. Int. Ed.* **2015**, *54* (22), 6554–6557. <https://doi.org/10.1002/anie.201501434>.
- (155) He, M.; Croy, R. G.; Essigmann, J. M.; Swager, T. M. Chemiresistive Carbon Nanotube Sensors for *N*-Nitrosodialkylamines. *ACS Sens.* **2019**, *4* (10), 2819–2824. <https://doi.org/10.1021/acssensors.9b01532>.
- (156) Soylemez, S.; Yoon, B.; Toppare, L.; Swager, T. M. Quaternized Polymer–Single-Walled Carbon Nanotube Scaffolds for a Chemiresistive Glucose Sensor. *ACS Sens.* **2017**, *2* (8), 1123–1127. <https://doi.org/10.1021/acssensors.7b00323>.
- (157) Kwon, O. S.; Park, C. S.; Park, S. J.; Noh, S.; Kim, S.; Kong, H. J.; Bae, J.; Lee, C.-S.; Yoon, H. Carboxylic Acid-Functionalized Conducting-Polymer Nanotubes as Highly Sensitive Nerve-Agent Chemiresistors. *Sci. Rep.* **2016**, *6* (1), 33724. <https://doi.org/10.1038/srep33724>.
- (158) Bezdek, M. J.; Luo, S.-X. L.; Ku, K. H.; Swager, T. M. A Chemiresistive Methane Sensor. *Proc. Natl. Acad. Sci.* **2021**, *118* (2), e2022515118. <https://doi.org/10.1073/pnas.2022515118>.
- (159) Lutsyk, P. M.; Shankar, P.; Rozhin, A. G.; Kulinich, S. A. Surface Sensitivity of Ultrasonically Treated Carbon Nanotube Network towards Ammonia. *Surf. Interfaces* **2019**, *17*, 100363. <https://doi.org/10.1016/j.surfin.2019.100363>.
- (160) Patel, V.; Saha, D.; Kruse, P.; Selvaganapathy, P. R. Reagent-Free Hydrogen Peroxide Sensing Using Carbon Nanotube Chemiresistors with Electropolymerized Crystal Violet. *ACS Appl. Nano Mater.* **2022**, *5* (3), 3957–3966. <https://doi.org/10.1021/acsanm.1c04540>.
- (161) Basova, T. V.; Polyakov, M. S. Hybrid Materials Based on Carbon Nanotubes and Polyaromatic Molecules: Methods of Functionalization and Sensor Properties. *Macroheterocycles* **2020**, *13* (2), 91–112. <https://doi.org/10.6060/mhc200710b>.

- (162) Chinnathambi, S.; Euverink, G.-J. Manufacturing of a Nafion-Coated, Reduced Graphene Oxide/Polyaniline Chemiresistive Sensor to Monitor pH in Real-Time During Microbial Fermentation. *J. Vis. Exp.* **2019**, No. 143, 58422. <https://doi.org/10.3791/58422-v>.
- (163) Shirsat, S. M.; Bodkhe, G. A.; Sonawane, M. M.; Gawali, B. W.; Shirsat, M. D. Multivariate Analysis of a Cobalt Octaethyl Porphyrin-Functionalized SWNT Microsensor Device for Selective and Simultaneous Detection of Multiple Analytes. *J. Electron. Mater.* **2021**, *50* (10), 5780–5787. <https://doi.org/10.1007/s11664-021-09111-3>.
- (164) Zhu, R.; Azzarelli, J. M.; Swager, T. M. Wireless Hazard Badges to Detect Nerve-Agent Simulants. *Angew. Chem.* **2016**, *128* (33), 9814–9818. <https://doi.org/10.1002/ange.201604431>.
- (165) Yang, T. Optimizing Electrode Structure of Carbon Nanotube Gas Sensors for Sensitivity Improvement Based on Electric Field Enhancement Effect of Fractal Geometry. *Sci. Rep.* **2021**, *11* (1), 16675. <https://doi.org/10.1038/s41598-021-96239-1>.
- (166) Chahal, M. K.; Sumita, M.; Labuta, J.; Payne, D. T.; Hill, J. P.; Yamauchi, Y.; Nakanishi, T.; Tanaka, T.; Kataura, H.; Koga, K.; Miyamura, H.; Kon, Y.; Hong, D.; Ishihara, S. Selective Detection of Toxic C1 Chemicals Using a Hydroxylamine-Based Chemiresistive Sensor Array. *ACS Sens.* **2023**, *8* (4), 1585–1592. <https://doi.org/10.1021/acssensors.2c02720>.
- (167) Szabó, E.; Pap, Z.; Simon, G.; Dombi, A.; Baia, L.; Hernádi, K. New Insights on the Simultaneous Removal by Adsorption on Organoclays of Humic Acid and Phenol. *Water* **2016**, *8* (1), 21. <https://doi.org/10.3390/w8010021>.
- (168) Xie, Z.; Ye, C.; Li, C.; Shi, X. *Recent Progress on the Non-Point Source Pollution Research from the World and China's Perspective: A Bibliometric Analysis from 2012 to 2021*; preprint; In Review, 2022. <https://doi.org/10.21203/rs.3.rs-1395029/v1>.
- (169) Zhang, L.; Cheng, Y.; Zhou, Y.; Lu, W.; Li, J. Effect of Different Types of Anthropogenic Pollution on the Bacterial Community of Urban Rivers. *Water Environ. Res.* **2021**, *93* (8), 1322–1332. <https://doi.org/10.1002/wer.1517>.
- (170) Luo, H.; Liu, D.; Ji, D.; Huang, Y. Dissolved Oxygen Characteristics of Spring Algal Bloom in Xiangxi Bay of Three Gorges Reservoir. In *2010 4th International Conference on Bioinformatics and Biomedical Engineering*; IEEE: Chengdu, China, 2010; pp 1–4. <https://doi.org/10.1109/ICBBE.2010.5515102>.
- (171) Wei, Y.; Jiao, Y.; An, D.; Li, D.; Li, W.; Wei, Q. Review of Dissolved Oxygen Detection Technology: From Laboratory Analysis to Online Intelligent Detection. *Sensors* **2019**, *19* (18), 3995. <https://doi.org/10.3390/s19183995>.

- (172) Spatial and Temporal Variations in Physico-Chemical Parameters and Abundance of Mollusc Species in Shiroro Lake, Minna, Niger State. *Aquac. Fish. Stud.* **2022**, 3 (5). <https://doi.org/10.31038/AFS.2021353>.
- (173) Analyzing Physico - Chemical Quality Parameters of Abay River Near To Bahir Dar, Ethiopia. *Civ. Environ. Res.* **2020**. <https://doi.org/10.7176/CER/12-2-02>.
- (174) Md Zain, B. A.; Shah, M. A. M.; Pauline, O.; Bte Jafferi, N. Modelling and Simulation of Flexible Beam as Aerator to Generate Dissolved Oxygen in Water. *Appl. Mech. Mater.* **2015**, 773–774, 188–193. <https://doi.org/10.4028/www.scientific.net/AMM.773-774.188>.
- (175) Krause, J. D. Legionella and the Role of Dissolved Oxygen in Its Growth and Inhibition: A Review. *Water* **2022**, 14 (17), 2644. <https://doi.org/10.3390/w14172644>.
- (176) Huang, S. J.; Zhou, G. Q.; Tang, Y. D.; Wei, J. Investigation on Water Pollution Control of Drinking Water Source in China. *IOP Conf. Ser. Earth Environ. Sci.* **2023**, 1204 (1), 012004. <https://doi.org/10.1088/1755-1315/1204/1/012004>.
- (177) Shah, M. A.; Lee, D.-G.; Lee, B.-Y.; Hur, S. Classifications and Applications of Inkjet Printing Technology: A Review. *IEEE Access* **2021**, 9, 140079–140102. <https://doi.org/10.1109/ACCESS.2021.3119219>.
- (178) Castrejon-Pita, J. R.; Baxter, W. R. S.; Morgan, J.; Temple, S.; Martin, G. D.; Hutchings, I. M. FUTURE, OPPORTUNITIES AND CHALLENGES OF INKJET TECHNOLOGIES. *At. Sprays* **2013**, 23 (6). <https://doi.org/10.1615/AtomizSpr.2013007653>.
- (179) Sowade, E.; Polomoshnov, M.; Willert, A.; Baumann, R. R. Toward 3D-Printed Electronics: Inkjet-Printed Vertical Metal Wire Interconnects and Screen-Printed Batteries. *Adv. Eng. Mater.* **2019**, 21 (10), 1900568. <https://doi.org/10.1002/adem.201900568>.
- (180) Zhou, Y. M.; Jiang, Z. M. Study of Hybrid Printing Based on Printed Electronics. *Appl. Mech. Mater.* **2015**, 731, 316–320. <https://doi.org/10.4028/www.scientific.net/AMM.731.316>.
- (181) Liu, Q.; Le, T.; He, S.; Tentzeris, M. M. Button-Shaped Radio-Frequency Identification Tag Combining Three-Dimensional and Inkjet Printing Technologies. *IET Microw. Antennas Propag.* **2016**, 10 (7), 737–741. <https://doi.org/10.1049/iet-map.2015.0711>.
- (182) Tortorich, R. P.; Choi, J.-W. Inkjet Printing of Carbon Nanotubes. *Nanomaterials* **2013**, 3 (3), 453–468. <https://doi.org/10.3390/nano3030453>.
- (183) Zub, K.; Hoepfner, S.; Schubert, U. S. Inkjet Printing and 3D Printing Strategies for Biosensing, Analytical, and Diagnostic Applications. *Adv. Mater.* **2022**, 34 (31), 2105015. <https://doi.org/10.1002/adma.202105015>.

- (184) Tortorich, R. P.; Song, E.; Choi, J.-W. Inkjet-Printed Carbon Nanotube Electrodes with Low Sheet Resistance for Electrochemical Sensor Applications. *J. Electrochem. Soc.* **2013**, *161* (2), B3044. <https://doi.org/10.1149/2.008402jes>.
- (185) Scuratti, F.; Salazar-Rios, J. M.; Luzio, A.; Kowalski, S.; Allard, S.; Jung, S.; Scherf, U.; Loi, M. A.; Caironi, M. Charge Transport in High-Mobility Field-Effect Transistors Based on Inkjet Printed Random Networks of Polymer Wrapped Single-Walled Carbon Nanotubes. *Adv. Funct. Mater.* **2021**, *31* (5), 2006895. <https://doi.org/10.1002/adfm.202006895>.
- (186) Ko, H.; Lee, J.; Kim, Y.; Lee, B.; Jung, C.-H.; Choi, J.-H.; Kwon, O.-S.; Shin, K. Active Digital Microfluidic Paper Chips with Inkjet-Printed Patterned Electrodes. *Adv. Mater.* **2014**, *26* (15), 2335–2340. <https://doi.org/10.1002/adma.201305014>.
- (187) Zhao, Y. J.; Beisteiner, C.; Gschossmann, S.; Schagerl, M. An Inkjet-Printed Carbon Nanotube Strain Distribution Sensor for Quasi Real-Time Strain Monitoring of Lightweight Design Materials. *Adv. Sci. Technol.* **2017**, *101*, 3–8. <https://doi.org/10.4028/www.scientific.net/AST.101.3>.
- (188) Kao, H.-L.; Cho, C.-L.; Chang, L.-C.; Chen, C.-B.; Chung, W.-H.; Tsai, Y.-C. A Fully Inkjet-Printed Strain Sensor Based on Carbon Nanotubes. *Coatings* **2020**, *10* (8), 792. <https://doi.org/10.3390/coatings10080792>.
- (189) Chen, P.; Chen, H.; Qiu, J.; Zhou, C. Inkjet Printing of Single-Walled Carbon Nanotube/RuO<sub>2</sub> Nanowire Supercapacitors on Cloth Fabrics and Flexible Substrates. *Nano Res.* **2010**, *3* (8), 594–603. <https://doi.org/10.1007/s12274-010-0020-x>.
- (190) Ghaderpoori, M.; Kamarehie, B.; Jafari, A.; Ghaderpoury, A.; Karami, M. Heavy Metals Analysis and Quality Assessment in Drinking Water – Khorramabad City, Iran. *Data Brief* **2018**, *16*, 685–692. <https://doi.org/10.1016/j.dib.2017.11.078>.
- (191) Li, H.; Smith, C.; Wang, L.; Li, Z.; Xiong, C.; Zhang, R. Combining Spatial Analysis and a Drinking Water Quality Index to Evaluate Monitoring Data. *Int. J. Environ. Res. Public Health* **2019**, *16* (3), 357. <https://doi.org/10.3390/ijerph16030357>.
- (192) Liao, Y.; Zhang, C.; Zhang, Y.; Strong, V.; Tang, J.; Li, X.-G.; Kalantar-zadeh, K.; Hoek, E. M. V.; Wang, K. L.; Kaner, R. B. Carbon Nanotube/Polyaniline Composite Nanofibers: Facile Synthesis and Chemosensors. *Nano Lett.* **2011**, *11* (3), 954–959. <https://doi.org/10.1021/nl103322b>.
- (193) Darestani-Farahani, M.; Montealegre, I. M.; Gilavan, M. T.; Kirby, T.; Ravi Selvaganapathy, P.; Kruse, P. A Highly Sensitive Ion-Selective Chemiresistive Sensor for Online Monitoring of Lead Ions in Water. *Analyst* **2024**, *149* (10), 2915–2924. <https://doi.org/10.1039/D4AN00159A>.
- (194) Goh, G. L.; Agarwala, S.; Tan, Y. J.; Yeong, W. Y. A Low Cost and Flexible Carbon Nanotube pH Sensor Fabricated Using Aerosol Jet Technology for Live Cell

Applications. *Sens. Actuators B Chem.* **2018**, *260*, 227–235.  
<https://doi.org/10.1016/j.snb.2017.12.127>.

- (195) Jeon, J.-Y.; Kang, B.-C.; Ha, T.-J. Flexible pH Sensors Based on Printed Nanocomposites of Single-Wall Carbon Nanotubes and Nafion. *Appl. Surf. Sci.* **2020**, *514*, 145956. <https://doi.org/10.1016/j.apsusc.2020.145956>.
- (196) Akbar, M. A.; Sharif, O.; Selvaganapathy, P. R.; Kruse, P. Identification and Quantification of Aqueous Disinfectants Using an Array of Carbon Nanotube-Based Chemiresistors. *ACS Appl. Eng. Mater.* **2023**, *1* (11), 3040–3052. <https://doi.org/10.1021/acsaenm.3c00505>.
- (197) Langenbacher, R.; Budhathoki-Uprety, J.; Jena, P. V.; Roxbury, D.; Streit, J.; Zheng, M.; Heller, D. A. Single-Chirality Near-Infrared Carbon Nanotube Sub-Cellular Imaging and FRET Probes. *Nano Lett.* **2021**, *21* (15), 6441–6448. <https://doi.org/10.1021/acs.nanolett.1c01093>.
- (198) Lü, S. A Multi-Wall Carbon Nanotubes-Dicetyl Phosphate Electrode for the Determination of Hypoxanthine in Fish. *Anal. Sci.* **2003**, *19* (9), 1309–1312. <https://doi.org/10.2116/analsci.19.1309>.
- (199) Zhang, X.; Cao, A.; Sun, Q.; Xu, C.; Wu, D. Oxidation and Opening of Well-Aligned Carbon Nanotube Tips. *Mater. Trans.* **2002**, *43* (7), 1707–1710. <https://doi.org/10.2320/matertrans.43.1707>.
- (200) Fan, J.; Shi, Z.; Tian, M.; Wang, J.; Yin, J. Unzipped Multiwalled Carbon Nanotube Oxide/Multiwalled Carbon Nanotube Hybrids for Polymer Reinforcement. *ACS Appl. Mater. Interfaces* **2012**, *4* (11), 5956–5965. <https://doi.org/10.1021/am301623t>.
- (201) Dong, C.; Kashon, M. L.; Lowry, D.; Dordick, J. S.; Reynolds, S. H.; Rojanasakul, Y.; Sargent, L. M.; Dinu, C. Z. Exposure to Carbon Nanotubes Leads to Changes in the Cellular Biomechanics. *Adv. Healthc. Mater.* **2013**, *2* (7), 945–951. <https://doi.org/10.1002/adhm.201200430>.
- (202) *Sustainable Design and Manufacturing 2018: Proceedings of the 5th International Conference on Sustainable Design and Manufacturing (KES-SDM-18)*; Dao, D., Howlett, R. J., Setchi, R., Vlacic, L., Eds.; Smart Innovation, Systems and Technologies; Springer International Publishing: Cham, 2019; Vol. 130. <https://doi.org/10.1007/978-3-030-04290-5>.
- (203) Kim, J. Large-Scale Integrated Carbon Nanotube Gas Sensors. *J. Nanomater.* **2012**, *2012*, 1–13. <https://doi.org/10.1155/2012/741647>.
- (204) Lee, B. Y.; Sung, M. G.; Lee, J.; Baik, K. Y.; Kwon, Y.-K.; Lee, M.-S.; Hong, S. Universal Parameters for Carbon Nanotube Network-Based Sensors: Can Nanotube Sensors Be Reproducible? *ACS Nano* **2011**, *5* (6), 4373–4379. <https://doi.org/10.1021/nn103056s>.

- (205) Huang, Q.; Jiang, Y.; Duan, Z.; Yuan, Z.; Liu, B.; Zhang, Y.; Zhao, Q.; Li, Y.; Tai, H. Protrusion Microstructure-Induced Sensitivity Enhancement for Zinc Oxide–Carbon Nanotube Flexible Pressure Sensors. *ACS Appl. Electron. Mater.* **2021**, *3* (12), 5506–5513. <https://doi.org/10.1021/acsaelm.1c00930>.
- (206) Watts, P. C. P.; Lyth, S. M.; Mendoza, E.; Silva, S. R. P. Polymer Supported Carbon Nanotube Arrays for Field Emission and Sensor Devices. *Appl. Phys. Lett.* **2006**, *89* (10), 103113. <https://doi.org/10.1063/1.2345615>.
- (207) Stobinski, L.; Lesiak, B.; Kövér, L.; Tóth, J.; Biniak, S.; Trykowski, G.; Judek, J. Multiwall Carbon Nanotubes Purification and Oxidation by Nitric Acid Studied by the FTIR and Electron Spectroscopy Methods. *J. Alloys Compd.* **2010**, *501* (1), 77–84. <https://doi.org/10.1016/j.jallcom.2010.04.032>.
- (208) Dmitrović, S.; Popović, Z. P.; Damnjanović, M.; Milošević, I. Structural Model of Semi-Metallic Carbon Nanotubes: Structural Model of Semi-Metallic CNT. *Phys. Status Solidi B* **2013**, *250* (12), 2627–2630. <https://doi.org/10.1002/pssb.201300086>.
- (209) Dresselhaus, M. S.; Jorio, A.; Hofmann, M.; Dresselhaus, G.; Saito, R. Perspectives on Carbon Nanotubes and Graphene Raman Spectroscopy. *Nano Lett.* **2010**, *10* (3), 751–758. <https://doi.org/10.1021/nl904286r>.
- (210) Popov, V. N. Two-Phonon Raman Bands of Single-Walled Carbon Nanotubes: A Case Study. *Phys. Rev. B* **2018**, *98* (8), 085413. <https://doi.org/10.1103/PhysRevB.98.085413>.
- (211) Pimenta, M. A.; Dresselhaus, G.; Dresselhaus, M. S.; Cançado, L. G.; Jorio, A.; Saito, R. Studying Disorder in Graphite-Based Systems by Raman Spectroscopy. *Phys Chem Chem Phys* **2007**, *9* (11), 1276–1290. <https://doi.org/10.1039/B613962K>.
- (212) Iqbal, M. W.; Iqbal, M. Z.; Khan, M. F.; Jin, X.; Hwang, C.; Eom, J. Modification of the Structural and Electrical Properties of Graphene Layers by Pt Adsorbates. *Sci. Technol. Adv. Mater.* **2014**, *15* (5), 055002. <https://doi.org/10.1088/1468-6996/15/5/055002>.
- (213) Kwon, K. C.; Choi, K. S.; Kim, C.; Kim, S. Y. Role of Metal Cations in Alkali Metal Chloride Doped Graphene. *J. Phys. Chem. C* **2014**, *118* (15), 8187–8193. <https://doi.org/10.1021/jp500646e>.
- (214) Chiou, K.; Huang, J. Cresol-Carbon Nanotube Charge-Transfer Complex: Stability in Common Solvents and Implications for Solution Processing. *Matter* **2020**, *3* (1), 302–319. <https://doi.org/10.1016/j.matt.2020.06.010>.
- (215) Azar, N. S.; Pourfath, M. Aggregation Kinetics and Stability Mechanisms of Pristine and Oxidized Nanocarbons in Polar Solvents. *J. Phys. Chem. C* **2016**, *120* (30), 16804–16814. <https://doi.org/10.1021/acs.jpcc.6b05318>.



- (216) Clancy, A. J.; Bayazit, M. K.; Hodge, S. A.; Skipper, N. T.; Howard, C. A.; Shaffer, M. S. P. Charged Carbon Nanomaterials: Redox Chemistries of Fullerenes, Carbon Nanotubes, and Graphenes. *Chem. Rev.* **2018**, *118* (16), 7363–7408. <https://doi.org/10.1021/acs.chemrev.8b00128>.
- (217) Gao, G.; Vecitis, C. D. Electrochemical Carbon Nanotube Filter Oxidative Performance as a Function of Surface Chemistry. *Environ. Sci. Technol.* **2011**, *45* (22), 9726–9734. <https://doi.org/10.1021/es202271z>.
- (218) Liu, R.; Xu, Y.; Li, Z.; Ma, X. A Facile and Efficient Modification of CNTs for Improved Fischer–Tropsch Performance on Iron Catalyst: Alkali Modification. *ChemCatChem* **2016**, *8* (8), 1454–1458. <https://doi.org/10.1002/cctc.201501219>.
- (219) Rinaldi, A.; Frank, B.; Su, D. S.; Hamid, S. B. A.; Schlögl, R. Facile Removal of Amorphous Carbon from Carbon Nanotubes by Sonication. *Chem. Mater.* **2011**, *23* (4), 926–928. <https://doi.org/10.1021/cm103069z>.
- (220) Ferreira Oliveira, A. E.; Pereira, A. C.; Ferreira, L. F. Development of Highly Stable Conductive Multiwalled Carbon Nanotube Ink Using Covalent and Non-Covalent Functionalization for Electrochemical Sensors. *J. Electrochem. Sci. Eng.* **2021**. <https://doi.org/10.5599/jese.1134>.
- (221) Zhou, Y.; Hu, L.; Grüner, G. A Method of Printing Carbon Nanotube Thin Films. *Appl. Phys. Lett.* **2006**, *88* (12), 123109. <https://doi.org/10.1063/1.2187945>.
- (222) Loh, K. J.; Kim, J.; Lynch, J. P.; Kam, N. W. S.; Kotov, N. A. Multifunctional Layer-by-Layer Carbon Nanotube–Polyelectrolyte Thin Films for Strain and Corrosion Sensing. *Smart Mater. Struct.* **2007**, *16* (2), 429–438. <https://doi.org/10.1088/0964-1726/16/2/022>.
- (223) Shtein, M.; Pri-bar, I.; Regev, O. A Simple Solution for the Determination of Pristine Carbon Nanotube Concentration. *The Analyst* **2013**, *138* (5), 1490. <https://doi.org/10.1039/c2an36399b>.
- (224) Kim, Y. S.; Oh, J. Y.; Kim, J. H.; Shin, M. H.; Jeong, Y. C.; Sung, S. J.; Park, J.; Yang, S. J.; Park, C. R. Crucial Role of Oxidation Debris of Carbon Nanotubes in Subsequent End-Use Applications of Carbon Nanotubes. *ACS Appl. Mater. Interfaces* **2017**, *9* (20), 17552–17564. <https://doi.org/10.1021/acsami.7b00667>.
- (225) Ahmad, R.; Wolfbeis, O. S.; Hahn, Y.-B.; Alshareef, H. N.; Torsi, L.; Salama, K. N. Deposition of Nanomaterials: A Crucial Step in Biosensor Fabrication. *Mater. Today Commun.* **2018**, *17*, 289–321. <https://doi.org/10.1016/j.mtcomm.2018.09.024>.
- (226) Kang, J.; Wells, S. A.; Wood, J. D.; Lee, J.-H.; Liu, X.; Ryder, C. R.; Zhu, J.; Guest, J. R.; Husko, C. A.; Hersam, M. C. Stable Aqueous Dispersions of Optically and Electronically Active Phosphorene. *Proc. Natl. Acad. Sci.* **2016**, *113* (42), 11688–11693. <https://doi.org/10.1073/pnas.1602215113>.

- (227) Harries, R. W.; Brown, C. J.; Ogilvie, S. P.; Large, M. J.; Amorim Graf, A.; Clifford, K.; Simon, T.; Giamas, G.; Dalton, A. B.; King, A. A. K. Langmuir Films of Layered Nanomaterials: Edge Interactions and Cell Culture Applications. *J. Phys. Chem. B* **2020**, *124* (33), 7184–7193. <https://doi.org/10.1021/acs.jpccb.0c05573>.
- (228) Yang, D.; Fuadi, M. K.; Kang, K.; Kim, D.; Li, Z.; Park, I. Multiplexed Gas Sensor Based on Heterogeneous Metal Oxide Nanomaterial Array Enabled by Localized Liquid-Phase Reaction. *ACS Appl. Mater. Interfaces* **2015**, *7* (19), 10152–10161. <https://doi.org/10.1021/acsami.5b00110>.
- (229) Wei, C.; Dai, L.; Roy, A.; Tolle, T. B. Multifunctional Chemical Vapor Sensors of Aligned Carbon Nanotube and Polymer Composites. *J. Am. Chem. Soc.* **2006**, *128* (5), 1412–1413. <https://doi.org/10.1021/ja0570335>.
- (230) Uehara, S.; Kawabe, T.; Wood, P.; Tsuji, O. UV/Ozone Surface Modification for Long-Term Stable Hydrophilic Surface of Polymer Microfluidic Devices. *MRS Adv.* **2016**, *1* (11), 743–748. <https://doi.org/10.1557/adv.2016.167>.
- (231) Schutzeichel, C.; Kiriy, N.; Kiriy, A.; Voit, B. Self-Aligned Polymer Film Patterning on Microstructured Silicon Surfaces. *Macromol. Chem. Phys.* **2022**, *223* (23), 2200228. <https://doi.org/10.1002/macp.202200228>.
- (232) Samavat, S.; Lloyd, J.; O’Dea, L.; Zhang, W.; Preedy, E.; Luzio, S.; Teng, K. S. Uniform Sensing Layer of Immiscible Enzyme-Mediator Compounds Developed via a Spray Aerosol Mixing Technique towards Low Cost Minimally Invasive Microneedle Continuous Glucose Monitoring Devices. *Biosens. Bioelectron.* **2018**, *118*, 224–230. <https://doi.org/10.1016/j.bios.2018.07.054>.
- (233) Sayago, I.; Santos, J. P.; Sánchez-Vicente, C. The Effect of Rare Earths on the Response of Photo UV-Activate ZnO Gas Sensors. *Sensors* **2022**, *22* (21), 8150. <https://doi.org/10.3390/s22218150>.
- (234) Kazemi, K. K.; Zarifi, T.; Mohseni, M.; Narang, R.; Golovin, K.; Zarifi, M. H. Smart Superhydrophobic Textiles Utilizing a Long-Range Antenna Sensor for Hazardous Aqueous Droplet Detection plus Prevention. *ACS Appl. Mater. Interfaces* **2021**, *13* (29), 34877–34888. <https://doi.org/10.1021/acsami.1c07880>.
- (235) Howard, N. S.; Archer, A. J.; Sibley, D. N.; Southee, D. J.; Wijayantha, K. G. U. Surfactant Control of Coffee Ring Formation in Carbon Nanotube Suspensions. *Langmuir* **2023**, *39* (3), 929–941. <https://doi.org/10.1021/acs.langmuir.2c01691>.
- (236) Kontturi, E.; Thüne, P. C.; Niemantsverdriet, J. W. (Hans). Cellulose Model Surfaces Simplified Preparation by Spin Coating and Characterization by X-Ray Photoelectron Spectroscopy, Infrared Spectroscopy, and Atomic Force Microscopy. *Langmuir* **2003**, *19* (14), 5735–5741. <https://doi.org/10.1021/la0340394>.

- (237) Pandhi, T.; Chandnani, A.; Subbaraman, H.; Estrada, D. A Review of Inkjet Printed Graphene and Carbon Nanotubes Based Gas Sensors. *Sensors* **2020**, *20* (19), 5642. <https://doi.org/10.3390/s20195642>.
- (238) Khalate, A. A.; Bombois, X.; Scorletti, G.; Babuska, R.; Koekebakker, S.; de Zeeuw, W. A Waveform Design Method for a Piezo Inkjet Printhead Based on Robust Feedforward Control. *J. Microelectromechanical Syst.* **2012**, *21* (6), 1365–1374. <https://doi.org/10.1109/JMEMS.2012.2205899>.
- (239) Wijshoff, H. Drop Dynamics in the Inkjet Printing Process. *Curr. Opin. Colloid Interface Sci.* **2018**, *36*, 20–27. <https://doi.org/10.1016/j.cocis.2017.11.004>.
- (240) Meng, Z.; Hashishin, T.; Tamaki, J.; Kojima, K. Fabrication of Thin-Film WO<sub>3</sub> Sensors and Their Sensing Properties to Dilute NO<sub>2</sub>. In *2012 IEEE Sensors*; IEEE: Taipei, Taiwan, 2012; pp 1–4. <https://doi.org/10.1109/ICSENS.2012.6411090>.
- (241) Baba, A.; Oyanagi, R.; Mashima, T.; Ohdaira, Y.; Shinbo, K.; Kato, K.; Kaneko, F.; Jiang, G.; Advincula, R. Surface Manipulation of Precursor Carbazole Dendron Polymer Thin Films by Conducting-AFM Nanolithography. In *Extended Abstracts of the 2010 International Conference on Solid State Devices and Materials*; The Japan Society of Applied Physics: The University of Tokyo, Tokyo, Japan, 2010. <https://doi.org/10.7567/SSDM.2010.A-5-1>.
- (242) Xu, L.; Luo, X.; Qian, H.; Zheng, G.; Xian, F.; Su, J. Deposition and Characterization of Zn–Sn–O (ZSO) Thin Films with Novel Optical Properties. *Phys. Status Solidi A* **2022**, *219* (8), 2100651. <https://doi.org/10.1002/pssa.202100651>.
- (243) Et. Al., S. K. R. Structural, Optical and Morphological Properties Of Zn And Mg Co-Doped V<sub>2</sub>O<sub>5</sub> Thin Film nanostructures. *Turk. J. Comput. Math. Educ. TURCOMAT* **2021**, *12* (6), 934–940. <https://doi.org/10.17762/turcomat.v12i6.2371>.
- (244) Blattmann, C. O.; Güntner, A. T.; Pratsinis, S. E. In Situ Monitoring of the Deposition of Flame-Made Chemoresistive Gas-Sensing Films. *ACS Appl. Mater. Interfaces* **2017**, *9* (28), 23926–23933. <https://doi.org/10.1021/acsami.7b04530>.
- (245) Moonosawmy, K. R.; Kruse, P. To Dope or Not To Dope: The Effect of Sonicating Single-Wall Carbon Nanotubes in Common Laboratory Solvents on Their Electronic Structure. *J. Am. Chem. Soc.* **2008**, *130* (40), 13417–13424. <https://doi.org/10.1021/ja8036788>.
- (246) Yau, H. C.; Bayazit, M. K.; Steinke, J. H. G.; Shaffer, M. S. P. Sonochemical Degradation of N-Methylpyrrolidone and Its Influence on Single Walled Carbon Nanotube Dispersion. *Chem. Commun.* **2015**, *51* (93), 16621–16624. <https://doi.org/10.1039/C5CC06526G>.

- (247) Cheng, Q.; Debnath, S.; Gregan, E.; Byrne, H. J. Ultrasound-Assisted SWNTs Dispersion: Effects of Sonication Parameters and Solvent Properties. *J. Phys. Chem. C* **2010**, *114* (19), 8821–8827. <https://doi.org/10.1021/jp101431h>.
- (248) Tortorich, R.; Choi, J.-W. Inkjet Printing of Carbon Nanotubes. *Nanomaterials* **2013**, *3* (3), 453–468. <https://doi.org/10.3390/nano3030453>.
- (249) Fujii, S.; Honda, S.; Oka, Y.; Kuwahara, Y.; Saito, T. Dispersion of Long and Isolated Single-Wall Carbon Nanotubes by Using a Hydrodynamic Cavitation Method. *Materials* **2023**, *16* (2), 466. <https://doi.org/10.3390/ma16020466>.
- (250) Wang, R.; Hughes, T.; Beck, S.; Vakil, S.; Li, S.; Pantano, P.; Draper, R. K. Generation of Toxic Degradation Products by Sonication of Pluronic® Dispersants: Implications for Nanotoxicity Testing. *Nanotoxicology* **2013**, *7* (7), 1272–1281. <https://doi.org/10.3109/17435390.2012.736547>.
- (251) Yang, Y.; Liu, S.; Guo, K.; Chen, L.; Xu, J.; Liu, W. Effective Air Purification via Pt-Decorated N3-CNT Adsorbent. *Front. Ecol. Evol.* **2022**, *10*, 897410. <https://doi.org/10.3389/fevo.2022.897410>.
- (252) Yang, X.; Li, L.; Shang, S.; Tao, X. Water-based Amorphous Carbon Nanotubes Filled Polymer Nanocomposites. *J. Appl. Polym. Sci.* **2011**, *122* (3), 1986–1992. <https://doi.org/10.1002/app.34072>.
- (253) Singh, R.; Pantarotto, D.; McCarthy, D.; Chaloin, O.; Hoebeke, J.; Partidos, C. D.; Briand, J.-P.; Prato, M.; Bianco, A.; Kostarelos, K. Binding and Condensation of Plasmid DNA onto Functionalized Carbon Nanotubes: Toward the Construction of Nanotube-Based Gene Delivery Vectors. *J. Am. Chem. Soc.* **2005**, *127* (12), 4388–4396. <https://doi.org/10.1021/ja0441561>.
- (254) Arnett, C. M.; Marsh, C. P.; Welch, C. R.; Strano, M. S.; Han, J.-H.; Gray, J. H.; Carlson, T. A. Enzyme-Mediated Assimilation of DNA-Functionalized Single-Walled Carbon Nanotubes. *Langmuir* **2010**, *26* (2), 613–617. <https://doi.org/10.1021/la902564n>.
- (255) Miyata, Y.; Mizuno, K.; Kataura, H. Purity and Defect Characterization of Single-Wall Carbon Nanotubes Using Raman Spectroscopy. *J. Nanomater.* **2011**, *2011*, 1–7. <https://doi.org/10.1155/2011/786763>.
- (256) Kim, U. J.; Furtado, C. A.; Liu, X.; Chen, G.; Eklund, P. C. Raman and IR Spectroscopy of Chemically Processed Single-Walled Carbon Nanotubes. *J. Am. Chem. Soc.* **2005**, *127* (44), 15437–15445. <https://doi.org/10.1021/ja052951o>.
- (257) Li, Q.; Zhu, Y.; Eichhorn, S. J. Carbonized Electrospun Cellulose Composite Nanofibres Containing Silicon Carbide Nanoparticles. *Compos. Part Appl. Sci. Manuf.* **2019**, *123*, 71–78. <https://doi.org/10.1016/j.compositesa.2019.04.028>.

- (258) Tuncel, D. Non-Covalent Interactions between Carbon Nanotubes and Conjugated Polymers. *Nanoscale* **2011**, *3* (9), 3545. <https://doi.org/10.1039/c1nr10338e>.
- (259) Pathak, P.; Park, S.; Cho, H. J. A Carbon Nanotube–Metal Oxide Hybrid Material for Visible-Blind Flexible UV-Sensor. *Micromachines* **2020**, *11* (4), 368. <https://doi.org/10.3390/mi11040368>.
- (260) Woo, S.; Lee, Y.; Sunkara, V.; Cheedarala, R. K.; Shin, H. S.; Choi, H. C.; Park, J. W. “Fingertip”-Guided Noncovalent Functionalization of Carbon Nanotubes by Dendrons. *Langmuir* **2007**, *23* (23), 11373–11376. <https://doi.org/10.1021/la701968y>.
- (261) Park, S. H.; Jin, S. H.; Jun, G. H.; Jeon, S.; Hong, S. H. Enhanced Electrical Properties in Carbon Nanotube/Poly (3-Hexylthiophene) Nanocomposites Formed through Non-Covalent Functionalization. *Nano Res.* **2011**, *4* (11), 1129–1135. <https://doi.org/10.1007/s12274-011-0161-6>.
- (262) Figueira-Duarte, T. M.; Müllen, K. Pyrene-Based Materials for Organic Electronics. *Chem. Rev.* **2011**, *111* (11), 7260–7314. <https://doi.org/10.1021/cr100428a>.
- (263) Weng, Y.-Q.; Yue, F.; Zhong, Y.-R.; Ye, B.-H. A Copper(II) Ion-Selective On–Off-Type Fluoroionophore Based on Zinc Porphyrin–Dipyridylamino. *Inorg. Chem.* **2007**, *46* (19), 7749–7755. <https://doi.org/10.1021/ic061709v>.
- (264) Lee, C.-S.; Kim, J. S.; Kim, T. H. A Chemodosimeter-Modified Carbon Nanotube-Field Effect Transistor: Toward a Highly Selective and Sensitive Electrical Sensing Platform. *RSC Adv.* **2019**, *9* (49), 28414–28420. <https://doi.org/10.1039/C9RA04656A>.
- (265) Claucherty, S.; Sakaue, H. An Optical-Chemical Sensor Using Pyrene-Sulfonic Acid for Unsteady Surface Pressure Measurements. *Sens. Actuators Phys.* **2021**, *317*, 112359. <https://doi.org/10.1016/j.sna.2020.112359>.
- (266) Udhayakumari, D.; Velmathi, S.; Venkatesan, P.; Wu, S.-P. A Pyrene-Linked Thiourea as a Chemosensor for Cations and Simple Fluorescent Sensor for Picric Acid. *Anal. Methods* **2015**, *7* (3), 1161–1166. <https://doi.org/10.1039/C4AY02529F>.
- (267) Omurtag, P. S.; Alkan, B.; Durmaz, H.; Hizal, G.; Tunca, U. Indirect Functionalization of Multiwalled Carbon Nano Tubes through Non-Covalent Interaction of Functional Polyesters. *Polymer* **2018**, *141*, 213–220. <https://doi.org/10.1016/j.polymer.2018.03.017>.
- (268) Bains, G. K.; Kim, S. H.; Sorin, E. J.; Narayanaswami, V. The Extent of Pyrene Excimer Fluorescence Emission Is a Reflector of Distance and Flexibility: Analysis of the Segment Linking the LDL Receptor-Binding and Tetramerization Domains of Apolipoprotein E3. *Biochemistry* **2012**, *51* (31), 6207–6219. <https://doi.org/10.1021/bi3005285>.
- (269) Karmakar, A.; Paul, A.; Sabatini, E. P.; Guedes Da Silva, M. F. C.; Pombeiro, A. J. L. Pyrene Carboxylate Ligand Based Coordination Polymers for Microwave-Assisted

Solvent-Free Cyanosilylation of Aldehydes. *Molecules* **2021**, *26* (4), 1101. <https://doi.org/10.3390/molecules26041101>.

- (270) Sadieva, L. K.; Taniya, O. S.; Kovalev, I. S.; Kopchuk, D. S.; Zyryanov, G. V.; Rusinov, V. L.; Chupakhin, O. N. Pyrene-1-Carboxylic Acid Polyethylene Glycol Esters: Synthesis and Photophysical Studies. *Russ. Chem. Bull.* **2021**, *70* (6), 1174–1179. <https://doi.org/10.1007/s11172-021-3201-8>.
- (271) Baskaran, D.; Mays, J. W.; Zhang, X. P.; Bratcher, M. S. Carbon Nanotubes with Covalently Linked Porphyrin Antennae: Photoinduced Electron Transfer. *J. Am. Chem. Soc.* **2005**, *127* (19), 6916–6917. <https://doi.org/10.1021/ja0508222>.
- (272) Praus, P.; Kočiřová, E.; Mojzeř, P.; řtěpánek, J.; Seksek, O.; Sureau, F.; Turpin, P. *Time-resolved Microspectrofluorometry and Fluorescence Imaging Techniques: Study of Porphyrin-mediated Cellular Uptake of Oligonucleotides*. *Ann. N. Y. Acad. Sci.* **2008**, *1130* (1), 117–121. <https://doi.org/10.1196/annals.1430.007>.
- (273) Martín, M. T.; Prieto, I.; Camacho, L.; Möbius, D. Partial Stacking of a Water-Soluble Porphyrin in Complex Monolayers with Insoluble Lipid. *Langmuir* **1996**, *12* (26), 6554–6560. <https://doi.org/10.1021/la960695a>.
- (274) Liu, Z.; Yasserli, A. A.; Loewe, R. S.; Lysenko, A. B.; Malinovskii, V. L.; Zhao, Q.; Surthi, S.; Li, Q.; Misra, V.; Lindsey, J. S.; Bocian, D. F. Synthesis of Porphyrins Bearing Hydrocarbon Tethers and Facile Covalent Attachment to Si(100). *J. Org. Chem.* **2004**, *69* (17), 5568–5577. <https://doi.org/10.1021/jo049439q>.
- (275) Balakumar, A.; Lysenko, A. B.; Carcel, C.; Malinovskii, V. L.; Gryko, D. T.; Schweikart, K.-H.; Loewe, R. S.; Yasserli, A. A.; Liu, Z.; Bocian, D. F.; Lindsey, J. S. Diverse Redox-Active Molecules Bearing O-, S-, or Se-Terminated Tethers for Attachment to Silicon in Studies of Molecular Information Storage. *J. Org. Chem.* **2004**, *69* (5), 1435–1443. <https://doi.org/10.1021/jo034944t>.
- (276) Francisco, A. P.; Botequim, D.; Prazeres, D. M. F.; Serra, V. V.; Costa, S. M. B.; Laia, C. A. T.; Paulo, P. M. R. Extreme Enhancement of Single-Molecule Fluorescence from Porphyrins Induced by Gold Nanodimer Antennas. *J. Phys. Chem. Lett.* **2019**, *10* (7), 1542–1549. <https://doi.org/10.1021/acs.jpcclett.9b00373>.
- (277) Carcel, C. M.; Laha, J. K.; Loewe, R. S.; Thamyongkit, P.; Schweikart, K.-H.; Misra, V.; Bocian, D. F.; Lindsey, J. S. Porphyrin Architectures Tailored for Studies of Molecular Information Storage. *J. Org. Chem.* **2004**, *69* (20), 6739–6750. <https://doi.org/10.1021/jo0498260>.
- (278) Shaikh, A. J.; Rabbani, F.; Sherazi, T. A.; Iqbal, Z.; Mir, S.; Shahzad, S. A. Binding Strength of Porphyrin–Gold Nanoparticle Hybrids Based on Number and Type of Linker Moieties and a Simple Method To Calculate Inner Filter Effects of Gold Nanoparticles Using Fluorescence Spectroscopy. *J. Phys. Chem. A* **2015**, *119* (7), 1108–1116. <https://doi.org/10.1021/jp510924n>.

- (279) Borggaard, O. K.; Gimsing, A. L. Fate of Glyphosate in Soil and the Possibility of Leaching to Ground and Surface Waters: A Review. *Pest Manag. Sci.* **2008**, *64* (4), 441–456. <https://doi.org/10.1002/ps.1512>.
- (280) Feltracco, M.; Barbaro, E.; Morabito, E.; Zangrando, R.; Piazza, R.; Barbante, C.; Gambaro, A. Assessing Glyphosate in Water, Marine Particulate Matter, and Sediments in the Lagoon of Venice. *Environ. Sci. Pollut. Res.* **2022**, *29* (11), 16383–16391. <https://doi.org/10.1007/s11356-021-16957-x>.
- (281) Kuckhoff, T.; Landfester, K.; Zhang, K. A. I.; Ferguson, C. T. J. Photocatalytic Hydrogels with a High Transmission Polymer Network for Pollutant Remediation. *Chem. Mater.* **2021**, *33* (23), 9131–9138. <https://doi.org/10.1021/acs.chemmater.1c02180>.
- (282) Motta, E. V. S.; Raymann, K.; Moran, N. A. Glyphosate Perturbs the Gut Microbiota of Honey Bees. *Proc. Natl. Acad. Sci.* **2018**, *115* (41), 10305–10310. <https://doi.org/10.1073/pnas.1803880115>.
- (283) Abdul-Aziz, O. I.; Gebreslase, A. K. Emergent Scaling of Dissolved Oxygen (DO) in Freshwater Streams Across Contiguous USA. *Water Resour. Res.* **2023**, *59* (2), e2022WR032114. <https://doi.org/10.1029/2022WR032114>.
- (284) Ahmed, M. H.; Lin, L.-S. Dissolved Oxygen Concentration Predictions for Running Waters with Different Land Use Land Cover Using a Quantile Regression Forest Machine Learning Technique. *J. Hydrol.* **2021**, *597*, 126213. <https://doi.org/10.1016/j.jhydrol.2021.126213>.
- (285) Diaz, R. J.; Rosenberg, R. Spreading Dead Zones and Consequences for Marine Ecosystems. *Science* **2008**, *321* (5891), 926–929. <https://doi.org/10.1126/science.1156401>.
- (286) Diaz, R. J. Overview of Hypoxia around the World. *J. Environ. Qual.* **2001**, *30* (2), 275–281. <https://doi.org/10.2134/jeq2001.302275x>.
- (287) Conlon, P.; Yang, C. J.; Wu, Y.; Chen, Y.; Martinez, K.; Kim, Y.; Stevens, N.; Marti, A. A.; Jockusch, S.; Turro, N. J.; Tan, W. Pyrene Excimer Signaling Molecular Beacons for Probing Nucleic Acids. *J. Am. Chem. Soc.* **2008**, *130* (1), 336–342. <https://doi.org/10.1021/ja076411y>.
- (288) Van Hameren, R.; Van Buul, A. M.; Castriciano, M. A.; Villari, V.; Micali, N.; Schön, P.; Speller, S.; Monsù Scolaro, L.; Rowan, A. E.; Elemans, J. A. A. W.; Nolte, R. J. M. Supramolecular Porphyrin Polymers in Solution and at the Solid–Liquid Interface. *Nano Lett.* **2008**, *8* (1), 253–259. <https://doi.org/10.1021/nl072563f>.
- (289) Zhang, Y.; Yuan, S.; Zhou, W.; Xu, J.; Li, Y. Spectroscopic Evidence and Molecular Simulation Investigation of the  $\pi$ – $\pi$  Interaction Between Pyrene Molecules and Carbon Nanotubes. *J. Nanosci. Nanotechnol.* **2007**, *7* (7), 2366–2375. <https://doi.org/10.1166/jnn.2007.412>.

- (290) Qu, L.; Martin, R. B.; Huang, W.; Fu, K.; Zweifel, D.; Lin, Y.; Sun, Y.-P.; Bunker, C. E.; Harruff, B. A.; Gord, J. R.; Allard, L. F. Interactions of Functionalized Carbon Nanotubes with Tethered Pyrenes in Solution. *J. Chem. Phys.* **2002**, *117* (17), 8089–8094. <https://doi.org/10.1063/1.1510745>.
- (291) Zhang, H.; Bork, M. A.; Riedy, K. J.; McMillin, D. R.; Choi, J. H. Understanding Photophysical Interactions of Semiconducting Carbon Nanotubes with Porphyrin Chromophores. *J. Phys. Chem. C* **2014**, *118* (22), 11612–11619. <https://doi.org/10.1021/jp503273d>.
- (292) Koyama, T.; Sugiura, J.; Koishi, T.; Ohashi, R.; Asaka, K.; Saito, T.; Gao, Y.; Okada, S.; Kishida, H. Excitation Energy Transfer by Electron Exchange via Two-Step Electron Transfer between a Single-Walled Carbon Nanotube and Encapsulated Magnesium Porphyrin. *J. Phys. Chem. C* **2020**, *124* (35), 19406–19412. <https://doi.org/10.1021/acs.jpcc.0c06766>.
- (293) Campos-Roldán, C. A.; Ramos-Sánchez, G.; Gonzalez-Huerta, R. G.; Vargas García, J. R.; Balbuena, P. B.; Alonso-Vante, N. Influence of  $sp^3$ – $sp^2$  Carbon Nanodomains on Metal/Support Interaction, Catalyst Durability, and Catalytic Activity for the Oxygen Reduction Reaction. *ACS Appl. Mater. Interfaces* **2016**, *8* (35), 23260–23269. <https://doi.org/10.1021/acsami.6b06886>.
- (294) Fang, Z.; Li, L.; Dixon, D. A.; Fushimi, R. R.; Dufek, E. J. Nature of Oxygen Adsorption on Defective Carbonaceous Materials. *J. Phys. Chem. C* **2021**, *125* (37), 20686–20696. <https://doi.org/10.1021/acs.jpcc.1c06741>.
- (295) Hertmanowski, R.; Chrzumnicka, E.; Martyński, T.; Bauman, D. Self-Aggregates Formation of 3,4,9,10-Tetra-(n-Alkoxy-Carbonyl)-Perylenes in Langmuir–Blodgett Films. *J. Lumin.* **2007**, *126* (2), 323–332. <https://doi.org/10.1016/j.jlumin.2006.07.027>.
- (296) Tamesue, S.; Abe, S.; Mitsumata, T.; Tsubokawa, N.; Yamauchi, T. Photo-Triggered Microgel Aggregation Using *o*-Nitrobenzaldehyde as Aggregating Power Source. *J. Polym. Sci. Part Polym. Chem.* **2016**, *54* (10), 1317–1322. <https://doi.org/10.1002/pola.27985>.
- (297) Massolo, E.; Benaglia, M. Stereoselective Organocascades: From Fundamentals to Recent Developments. *Phys. Sci. Rev.* **2023**, *8* (3), 405–440. <https://doi.org/10.1515/psr-2018-0096>.
- (298) Ryu, J.; Han, M. Improvement of the Mechanical and Electrical Properties of Polyamide 6 Nanocomposites by Non-Covalent Functionalization of Multi-Walled Carbon Nanotubes. *Compos. Sci. Technol.* **2014**, *102*, 169–175. <https://doi.org/10.1016/j.compscitech.2014.07.022>.
- (299) Parra, E. J.; Rius, F. X.; Blondeau, P. A Potassium Sensor Based on Non-Covalent Functionalization of Multi-Walled Carbon Nanotubes. *The Analyst* **2013**, *138* (9), 2698. <https://doi.org/10.1039/c3an00313b>.



- (300) Giroud, F.; Minter, S. D. Anthracene-Modified Pyrenes Immobilized on Carbon Nanotubes for Direct Electroreduction of O<sub>2</sub> by Laccase. *Electrochem. Commun.* **2013**, *34*, 157–160. <https://doi.org/10.1016/j.elecom.2013.06.006>.
- (301) Sun, B.; Dreger, Z. A.; Gupta, Y. M. High-Pressure Effects in Pyrene Crystals: Vibrational Spectroscopy. *J. Phys. Chem. A* **2008**, *112* (42), 10546–10551. <https://doi.org/10.1021/jp806382x>.
- (302) Coates, J. Interpretation of Infrared Spectra, A Practical Approach. In *Encyclopedia of Analytical Chemistry*; Meyers, R. A., Ed.; Wiley, 2000. <https://doi.org/10.1002/9780470027318.a5606>.
- (303) Paulat, F.; Praneeth, V. K. K.; Näther, C.; Lehnert, N. Quantum Chemistry-Based Analysis of the Vibrational Spectra of Five-Coordinate Metalloporphyrins [M(TPP)Cl]. *Inorg. Chem.* **2006**, *45* (7), 2835–2856. <https://doi.org/10.1021/ic0510866>.
- (304) Reuillard, B.; Le Goff, A.; Holzinger, M.; Cosnier, S. Non-Covalent Functionalization of Carbon Nanotubes with Boronic Acids for the Wiring of Glycosylated Redox Enzymes in Oxygen-Reducing Biocathodes. *J Mater Chem B* **2014**, *2* (16), 2228–2232. <https://doi.org/10.1039/C3TB21846E>.
- (305) Isshiki, Y.; Nishino, T.; Fujii, S. Electronic Structure and Transport Properties of Single-Molecule Junctions with Different Sizes of  $\pi$ -Conjugated System. *J. Phys. Chem. C* **2021**, *125* (6), 3472–3479. <https://doi.org/10.1021/acs.jpcc.0c05478>.
- (306) Zhao, Y.-L.; Stoddart, J. F. Noncovalent Functionalization of Single-Walled Carbon Nanotubes. *Acc. Chem. Res.* **2009**, *42* (8), 1161–1171. <https://doi.org/10.1021/ar900056z>.
- (307) Abdel Hamid, Z.; Abdul Azum, A.; Abdel Mouez, F.; Abdel Rehim, S. Synthesis and Characterization of Carbon Nanostructures from Green Oil Using Thermal Pyrolysis Process. *Int. Conf. Chem. Environ. Eng.* **2016**, *8* (13), 421–441. <https://doi.org/10.21608/iccee.2016.35136>.
- (308) Bouanis, F. Z.; Bensifia, M.; Florea, I.; Mahouche-cherghi, S.; Carbonnier, B.; Grande, D.; Léonard, C.; Yassar, A.; Pribat, D. Non-Covalent Functionalization of Single Walled Carbon Nanotubes with Fe-/Co-Porphyrin and Co-Phthalocyanine for Field-Effect Transistor Applications. *Org. Electron.* **2021**, *96*, 106212. <https://doi.org/10.1016/j.orgel.2021.106212>.
- (309) Simmons, T. J.; Bult, J.; Hashim, D. P.; Linhardt, R. J.; Ajayan, P. M. Noncovalent Functionalization as an Alternative to Oxidative Acid Treatment of Single Wall Carbon Nanotubes with Applications for Polymer Composites. *ACS Nano* **2009**, *3* (4), 865–870. <https://doi.org/10.1021/nn800860m>.
- (310) An Account of Several New Instruments and Processes for Determining the Constants of a Voltaic Circuit. *Abstr. Pap. Print. Philos. Trans. R. Soc. Lond.* **1843**, *4*, 469–471. <https://doi.org/10.1098/rspl.1837.0240>.

- (311) Xia, D.; Xue, Q.; Xie, J.; Chen, H.; Lv, C.; Besenbacher, F.; Dong, M. Fabrication of Carbon Nanoscrolls from Monolayer Graphene. *Small* **2010**, *6* (18), 2010–2019. <https://doi.org/10.1002/sml.201000646>.
- (312) Bondavalli, P.; Gorintin, L.; Feugnet, G.; Lehoucq, G.; Pribat, D. Selective Gas Detection Using CNTFET Arrays Fabricated Using Air-Brush Technique, with Different Metal as Electrodes. *Sens. Actuators B Chem.* **2014**, *202*, 1290–1297. <https://doi.org/10.1016/j.snb.2014.06.064>.
- (313) Heinze, S.; Tersoff, J.; Martel, R.; Derycke, V.; Appenzeller, J.; Avouris, Ph. Carbon Nanotubes as Schottky Barrier Transistors. *Phys. Rev. Lett.* **2002**, *89* (10), 106801. <https://doi.org/10.1103/PhysRevLett.89.106801>.
- (314) Tongay, S.; Schumann, T.; Hebard, A. F. Graphite Based Schottky Diodes Formed on Si, GaAs, and 4H-SiC Substrates. *Appl. Phys. Lett.* **2009**, *95* (22), 222103. <https://doi.org/10.1063/1.3268788>.
- (315) Jiang, Y.; Wang, P.; Lin, L. Characterizations of Contact and Sheet Resistances of Vertically Aligned Carbon Nanotube Forests with Intrinsic Bottom Contacts. *Nanotechnology* **2011**, *22* (36), 365704. <https://doi.org/10.1088/0957-4484/22/36/365704>.
- (316) Lee, S.; Park, H.; Paine, D. C. A Study of the Specific Contact Resistance and Channel Resistivity of Amorphous IZO Thin Film Transistors with IZO Source–Drain Metallization. *J. Appl. Phys.* **2011**, *109* (6), 063702. <https://doi.org/10.1063/1.3549810>.
- (317) Jackson, E. A.; Hillmyer, M. A. Nanoporous Membranes Derived from Block Copolymers: From Drug Delivery to Water Filtration. *ACS Nano* **2010**, *4* (7), 3548–3553. <https://doi.org/10.1021/nn1014006>.
- (318) Nguyen, T.-H.; Vayer, M.; Sinturel, C. PS-b-PMMA/PLA Blends for Nanoporous Templates with Hierarchical and Tunable Pore Size. *Appl. Surf. Sci.* **2018**, *427*, 464–470. <https://doi.org/10.1016/j.apsusc.2017.08.160>.
- (319) Vayer, M.; Nguyen, T. H.; Grosso, D.; Boissiere, C.; Hillmyer, M. A.; Sinturel, C. Characterization of Nanoporous Polystyrene Thin Films by Environmental Ellipsometric Porosimetry. *Macromolecules* **2011**, *44* (22), 8892–8897. <https://doi.org/10.1021/ma201497z>.
- (320) Tehrani-Bagha, A. R. Waterproof Breathable Layers – A Review. *Adv. Colloid Interface Sci.* **2019**, *268*, 114–135. <https://doi.org/10.1016/j.cis.2019.03.006>.
- (321) Semaltianos, N. G. Spin-Coated PMMA Films. *Microelectron. J.* **2007**, *38* (6–7), 754–761. <https://doi.org/10.1016/j.mejo.2007.04.019>.
- (322) Teixeira, J.; Cardoso, V. F.; Botelho, G.; Morão, A. M.; Nunes-Pereira, J.; Lanceros-Mendez, S. Effect of Polymer Dissolution Temperature and Conditioning Time on the

Morphological and Physicochemical Characteristics of Poly(Vinylidene Fluoride) Membranes Prepared by Non-Solvent Induced Phase Separation. *Polymers* **2021**, *13* (23), 4062. <https://doi.org/10.3390/polym13234062>.

- (323) Bicy, K.; Rouxel, D.; Poncot, M.; Royaud, I.; Bourson, P.; Chapron, D.; Kalarikkal, N.; Thomas, S. Interfacial Tuning and Designer Morphologies of Microporous Membranes Based on Polypropylene/Natural Rubber Nanocomposites. *J. Appl. Polym. Sci.* **2021**, *138* (41), 51208. <https://doi.org/10.1002/app.51208>.
- (324) Willott, J. D.; Nielen, W. M.; De Vos, W. M. Stimuli-Responsive Membranes through Sustainable Aqueous Phase Separation. *ACS Appl. Polym. Mater.* **2020**, *2* (2), 659–667. <https://doi.org/10.1021/acspm.9b01006>.
- (325) Ng, K. A.; Chan, P. K. A CMOS Analog Front-End IC for Portable EEG/ECG Monitoring Applications. *IEEE Trans. Circuits Syst. Regul. Pap.* **2005**, *52* (11), 2335–2347. <https://doi.org/10.1109/TCSI.2005.854141>.
- (326) Valdés, H.; Molina, L. M.; Alonso, J. A. Water Adsorption and Dissociation on Gold Catalysts Supported on Anatase-TiO<sub>2</sub>(101). *Appl. Surf. Sci.* **2019**, *487*, 244–252. <https://doi.org/10.1016/j.apsusc.2019.04.249>.
- (327) Burch, R. Gold Catalysts for Pure Hydrogen Production in the Water–Gas Shift Reaction: Activity, Structure and Reaction Mechanism. *Phys Chem Chem Phys* **2006**, *8* (47), 5483–5500. <https://doi.org/10.1039/B607837K>.
- (328) Menshakov, A. I.; Bryukhanova, Yu. A. Influence of Parameters of the Discharge with a Self-Heating Hollow Cathode and a Sectional Anode on the Activation Degree of a Vapor-Gas Medium. In *8th International Congress on Energy Fluxes and Radiation Effects*; Crossref, 2022; pp 1061–1066. <https://doi.org/10.56761/EFRE2022.C4-P-021601>.
- (329) Xia, Y.; Whitesides, G. M. Soft Lithography. *Angew. Chem. Int. Ed.* **1998**, *37* (5), 550–575. [https://doi.org/10.1002/\(SICI\)1521-3773\(19980316\)37:5<550::AID-ANIE550>3.0.CO;2-G](https://doi.org/10.1002/(SICI)1521-3773(19980316)37:5<550::AID-ANIE550>3.0.CO;2-G).
- (330) Liu, J.; Tan, F.; Xing, Y.; Zhang, Q.; Zhao, Z.; Wang, X.; Wang, Y.; Zhao, H. Label-Free Chemiresistive Sensors Based on Self-Assembled Ti<sub>3</sub>C<sub>2</sub>T<sub>x</sub> MXene Films for Monitoring of Microcystin-LR in Water Samples. *Environ. Sci. Technol.* **2023**, *57* (41), 15432–15442. <https://doi.org/10.1021/acs.est.3c05791>.
- (331) Khalid, H. R.; Jang, D.; Abbas, N.; Haider, M. S.; Bukhari, S. N. A.; Mirza, C. R.; Elboughdiri, N.; Ahmad, F. Electrical Stability and Piezoresistive Sensing Performance of High Strain-Range Ultra-Stretchable CNT-Embedded Sensors. *Polymers* **2022**, *14* (7), 1366. <https://doi.org/10.3390/polym14071366>.
- (332) Ishihara, S.; Bahuguna, A.; Kumar, S.; Krishnan, V.; Labuta, J.; Nakanishi, T.; Tanaka, T.; Kataura, H.; Kon, Y.; Hong, D. Cascade Reaction-Based Chemiresistive Array for

Ethylene Sensing. *ACS Sens.* **2020**, *5* (5), 1405–1410. <https://doi.org/10.1021/acssensors.0c00194>.

- (333) Yang, D.-Q.; Sacher, E. Strongly Enhanced Interaction between Evaporated Pt Nanoparticles and Functionalized Multiwalled Carbon Nanotubes via Plasma Surface Modifications: Effects of Physical and Chemical Defects. *J. Phys. Chem. C* **2008**, *112* (11), 4075–4082. <https://doi.org/10.1021/jp076531s>.
- (334) Ruelle, B.; Peeterbroeck, S.; Godfroid, T.; Bittencourt, C.; Hecq, M.; Snyders, R.; Dubois, P. Selective Grafting of Primary Amines onto Carbon Nanotubes via Free-Radical Treatment in Microwave Plasma Post-Discharge. *Polymers* **2012**, *4* (1), 296–315. <https://doi.org/10.3390/polym4010296>.
- (335) Halfhide, D. E.; Gannon, B. W.; Hayes, C. M.; Roe, J. M. Wide Variation in Effectiveness of Laboratory Disinfectants against Bacteriophages. *Lett. Appl. Microbiol.* **2008**, *47* (6), 608–612. <https://doi.org/10.1111/j.1472-765X.2008.02474.x>.
- (336) Borges, T. J.; Moretti, L. K.; Silva, M. M. N.; Tondo, E. C.; Pereira, K. S. *Salmonella* Sensitivity to Sodium Hypochlorite and Citric Acid in Washing Water of Lettuce Residues. *J. Food Saf.* **2020**, *40* (2), e12748. <https://doi.org/10.1111/jfs.12748>.
- (337) Kodama, S.; Yamamoto, A.; Ohto, M.; Matsunaga, A. Major Degradation Pathway of Thiuram in Tap Water Processed by Oxidation with Sodium Hypochlorite. *J. Agric. Food Chem.* **1999**, *47* (7), 2914–2919. <https://doi.org/10.1021/jf9813440>.
- (338) Zucchi, G.; Lebental, B.; Loisel, L.; Ramachandran, S.; Flores, A.; Wang, Xinyang; Mallesham, G.; Bodelot, L. Chemical sensors based on carbon nanotubes functionalised by conjugated polymers for analysis in aqueous medium. WO/2018/189479. <https://patentscope.wipo.int/search/en/detail.jsf?docId=WO2018189479>.
- (339) Benda, R.; Zucchi, G.; Cancès, E.; Lebental, B. Insights into the  $\pi - \pi$  Interaction Driven Non-Covalent Functionalization of Carbon Nanotubes of Various Diameters by Conjugated Fluorene and Carbazole Copolymers. *J. Chem. Phys.* **2020**, *152* (6), 064708. <https://doi.org/10.1063/1.5133634>.
- (340) Robert Benda; Thomas Vezin; Bérengère Lebental. Prediction of the Interaction Strength of an Urea-Based Probe towards Ions in Water by Means of DFT/PCM Calculations. *J. Comput. Aided Mol. Des.* **2021**.
- (341) Clarkson, R.; Podlich, H.; Savage, N.; Moule, A. A Survey of Sodium Hypochlorite Use by General Dental Practitioners and Endodontists in Australia. *Aust. Dent. J.* **2003**, *48* (1), 20–26. <https://doi.org/10.1111/j.1834-7819.2003.tb00004.x>.
- (342) Akhtar, F.; Ahmed, M.; Akhtar, M. N. Drinking, Tap and Canal Water Quality Analysis for Human Consumption: A Case Study of Nawabshah City, Pakistan. *Mehran Univ. Res. J. Eng. Technol.* **2021**, *40* (2), 392–398. <https://doi.org/10.22581/muet1982.2102.13>.

- (343) Rana, A.; Jillani, S. M. S.; Alhooshani, K. Water Quality Characterization Using ASTM Methods in an Undergraduate Advanced Instrumental Analysis Laboratory Course. *J. Chem. Educ.* **2021**, *98* (9), 2919–2926. <https://doi.org/10.1021/acs.jchemed.0c01097>.
- (344) Winkler, C.; Mollenhauer, U.; Hummel, S.; Bonifacio, E.; Ziegler, A.-G. Exposure to Environmental Factors in Drinking Water: Risk of Islet Autoimmunity and Type 1 Diabetes – The BABYDIAB Study. *Horm. Metab. Res.* **2008**, *40* (08), 566–571. <https://doi.org/10.1055/s-2008-1073165>.
- (345) Galyean, M. L.; Morrical, D. G.; Hayes, R.; Caton, J. The Influence of Dietary Nitrogen Source and Drinking Water pH on Growth, Digestibility, and Nitrogen Metabolism in Lambs Fed a High Roughage Diet. *J. Range Manag.* **1983**, *36* (1), 31. <https://doi.org/10.2307/3897976>.
- (346) García-Ávila, F.; Ramos- Fernández, L.; Pauta, D.; Quezada, D. Evaluation of Water Quality and Stability in the Drinking Water Distribution Network in the Azogues City, Ecuador. *Data Brief* **2018**, *18*, 111–123. <https://doi.org/10.1016/j.dib.2018.03.007>.
- (347) Chen, S.; Liu, L. Simultaneous Species Analysis of Arsenic, Selenium, Bromine, and Iodine in Bottled Drinking Water and Fruit Juice by High-Performance Liquid Chromatography-Inductively Coupled Plasma Mass Spectrometry. *Anal. Sci.* **2021**, *37* (9), 1241–1246. <https://doi.org/10.2116/analsci.20P399>.
- (348) BezgiN, E.; Eryücel, C. O.; Tuncel, Z. Physicochemical Properties of Both Drinking and Domestic Waters in Çorum. *Int. J. Sci. Lett.* **2019**, *1* (1), 42–55. <https://doi.org/10.38058/ijsl.594005>.
- (349) Tarawneh, M. A.; Ali, A. M.; Ahmad, S. H.; Yu, L. J. Influence of Multiwalled Carbon Nanotubes Content on Thermal Conductivity of Polyactic Acid/Liquid Natural Rubber Nanocomposite. *World J. Eng.* **2016**, *13* (1), 1–5. <https://doi.org/10.1108/WJE-02-2016-005>.
- (350) Adhikari, S.; Hussain, O.; Phillips, R. M.; Kaminsky, W.; Kollipara, M. R. Synthesis, Structural and Chemosensitivity Studies of Arene d<sup>6</sup> Metal Complexes Having N-phenyl-N'-(Pyridyl/Pyrimidyl)Thiourea Derivatives. *Appl. Organomet. Chem.* **2018**, *32* (6), e4362. <https://doi.org/10.1002/aoc.4362>.
- (351) Yasin, M.; Ketema, T.; Bacha, K. Physico-Chemical and Bacteriological Quality of Drinking Water of Different Sources, Jimma Zone, Southwest Ethiopia. *BMC Res. Notes* **2015**, *8* (1), 541. <https://doi.org/10.1186/s13104-015-1376-5>.
- (352) Olayinka, O. O.; Adewusi, A. A.; Olarenwaju, O. O.; Aladesida, A. A. Concentration of Polycyclic Aromatic Hydrocarbons and Estimated Human Health Risk of Water Samples Around Atlas Cove, Lagos, Nigeria. *J. Health Pollut.* **2018**, *8* (20), 181210. <https://doi.org/10.5696/2156-9614-8.20.181210>.

- (353) Haifa, S.; Assad, A.; Naser, H.; Fares, R. M. Modeling the Water Quality of the Middle Section of the Northern Great River (Dissolved Oxygen and Water Temperature) Using WASP8 Model. *IOP Conf. Ser. Earth Environ. Sci.* **2023**, *1252* (1), 012062. <https://doi.org/10.1088/1755-1315/1252/1/012062>.
- (354) Rahmi, I.; Arfiati, D.; Musa, M.; Karimah, K. Dynamics of Physics and Chemistry of Vanamei Shrimp (*Litopenaeus Vannamei*) Pond Water with Semi Biofloc System. *J. Penelit. Pendidik. IPA* **2023**, *9* (1), 249–256. <https://doi.org/10.29303/jppipa.v9i1.2528>.
- (355) Gustinasari, K.; Hermana, J.; Pandebesie, E. S. Water Bodies Quality along Paddy Field in Karang Ploso Sub District, Malang City, Indonesia. *E3S Web Conf.* **2019**, *125*, 04007. <https://doi.org/10.1051/e3sconf/201912504007>.
- (356) Shefat, S.; Chowdhury, M.; Haque, F.; Hasan, J.; Salam, M.; Shaha, D. Assessment of Physico-Chemical Properties of the Pasur River Estuarine Water. *Ann. Bangladesh Agric.* **2021**, *24* (1), 1–16. <https://doi.org/10.3329/aba.v24i1.51932>.
- (357) Hanafie, A.; Biyatmoko, D.; Fatmawati, .; Arida Fauzana, N. Growth Performance and Survival of Climbing Perch (*Anabas Testudineus* Bloch) Raised in Conventional and Bioflocs System. *Asian J. Fish. Aquat. Res.* **2023**, 14–37. <https://doi.org/10.9734/ajfar/2023/v21i2530>.
- (358) Layugan, E. A.; Tabasin, J. P. B.; Alejos, M.; Pidoy, L. E.; Rabajante, J. F.; Babaran, R. P. Site Selection for New Green Mussel Culture Area Expansion in Buguey Estuary, Cagayan, Philippines. *agriRxiv* **2018**, 2018, 20203217318. <https://doi.org/10.31220/osf.io/3nb6w>.
- (359) Kikuchi, R.; Ferreira, C. S. S.; Gerardo, R. Climatic Factors Affecting Water Quality under Natural Conditions: A Field Survey of a Local Reservoir. *Int. J. Environ. Clim. Change* **2023**, *13* (5), 422–430. <https://doi.org/10.9734/ijecc/2023/v13i51787>.
- (360) Najm, H. H.; Al-Shwany, T. M. K. A. Evaluation of Some Physical, Chemical and Bacteriological Characteristics of Fish Ponds in Kirkuk City. *Int. J. Health Sci.* **2022**, 13253–13273. <https://doi.org/10.53730/ijhs.v6nS1.8318>.
- (361) Sudha, N. R.; Varaprasad, D.; Riazunnisa, K.; Chandrasekhar, T.; Prasanna, V. A.; Reddy, P. R. Effects of Oxygen Scavengers (Sodium Sulfite, Sodium Bisulfite, Sodium Dithionite, and Sodium Metabisulfite) on Growth and Accumulation of Biomass in the Green Alga *Asterarcys Quadricellulare*. *J. Appl. Biol. Biotechnol.* **2022**, 136–140. <https://doi.org/10.7324/JABB.2022.100418>.
- (362) Lam, S. F.; Shirure, V. S.; Chu, Y. E.; Soetikno, A. G.; George, S. C. Microfluidic Device to Attain High Spatial and Temporal Control of Oxygen. *PLOS ONE* **2018**, *13* (12), e0209574. <https://doi.org/10.1371/journal.pone.0209574>.



- (363) Kwon, S. J.; Bard, A. J. Analysis of Diffusion-Controlled Stochastic Events of Iridium Oxide Single Nanoparticle Collisions by Scanning Electrochemical Microscopy. *J. Am. Chem. Soc.* **2012**, *134* (16), 7102–7108. <https://doi.org/10.1021/ja300894f>.
- (364) Wang, Y. Enhanced Coenzyme Q10 Yield by Blocking Hopanoids Pathway. *Adv. Biotechnol. Microbiol.* **2017**, *3* (2). <https://doi.org/10.19080/AIBM.2017.03.555610>.

**Titre :** Fonctionnalisation non covalente de nanotubes de carbone avec de nouveaux ligands aromatiques conjugués pour la détection sélective des polluants de l'eau.

**Mots clés :** Impression jet d'encre, Capteurs chimiques résistifs, Fonctionnalisation non covalente, Microscopie électronique, Capteurs multi paramètres, Qualité de l'eau

**Résumé :** La nanotechnologie a apporté des contributions significatives à la résolution des problèmes mondiaux, notamment en améliorant l'accès à l'eau potable. Avec le changement climatique qui aggrave la qualité de l'eau, des solutions innovantes sont nécessaires. Les capteurs nanotechnologiques permettent une analyse à distance de la qualité de l'eau, essentielle pour la gestion de crise. Ce travail se concentre sur l'utilisation des nanotubes de carbone (CNT) en tant que nanomatériaux bidimensionnels pour améliorer la fiabilité des dispositifs résistifs. Un nouveau processus de purification a été introduit pour éliminer les impuretés amorphes, améliorant ainsi l'efficacité des dépôts de CNT à base de solvants. Cette approche vise à rétablir la confiance dans des méthodes rentables et évolutives, tout en répondant

aux préoccupations concernant la mauvaise qualité et la forte teneur en matières amorphes. Dans la phase expérimentale, les CNT ont été étudiés pour leurs capacités électroniques et chimiques, aboutissant à la création de nanohybrides avec des molécules conjuguées via une fonctionnalisation  $\pi$ - $\pi$  non covalente. Après avoir comparé plusieurs méthodes, celle de l'incubation a été retenue pour ses résultats prometteurs et sa compatibilité avec le traitement en film mince. Les nanohybrides ont montré de bonnes performances, et les dispositifs résistifs intégrés ont donné des résultats préliminaires prometteurs pour l'analyse de la qualité de l'eau, ouvrant la voie à des développements futurs dans ce domaine.

**Title:** Noncovalent functionalization of carbon nanotubes with new conjugated aromatic ligands for selective detection of water pollutants.

**Keywords:** Inkjet Printing, Chemiresistive chemical sensors, Noncovalent functionalization, Electronic microscopy, Multiparameter sensors, Water quality

**Abstract:** Nanotechnology has made significant contributions to solving global issues, particularly by improving access to clean water. With climate change worsening water quality, innovative solutions are required. Nanotechnological sensors enable remote water quality analysis, critical for crisis management. This work focuses on carbon nanotubes (CNT) as two-dimensional nanomaterials to enhance the reliability of resistive devices. A new purification process was introduced to remove amorphous impurities, improving the efficiency of CNT-based solvent deposition processes. This approach aims to restore confidence in cost-effective and scalable methods while addressing concerns about poor quality and high amorphous content. In the experimental phase, CNTs were studied for their

electronic and chemical capabilities, leading to the creation of nanohybrids with conjugated molecules through non-covalent  $\pi$ - $\pi$  functionalization. After comparing various non-covalent functionalization methods, the incubation method was selected for its promising results and compatibility with the thin-film process developed earlier. The resulting nanohybrids were integrated into thin films, which demonstrated high electronic and chemical performance. These films were further incorporated into different resistive device concepts and tested against various analytes in water. Although the results are preliminary, they show promise for advancing water quality sensor development.